
# Characterisation of the Cellular Response to Defective Translational Termination

**By Athanasios Ploumakis**

**A thesis submitted to the College of Medical and Dental Sciences, the University of Birmingham, for the degree of DOCTOR OF PHILOSOPHY**

**Institute of Cancer and Genomic Sciences**

**College of Medical and Dental Sciences**

**University of Birmingham**

**September 2017**

# Abstract

Enzymatic hydroxylation of varied cellular substrates is catalyzed by the 2-oxoglutarate and Fe(II) dependent 2-oxoglutrate (OG) oxygenase group of proteins. These enzymes control gene expression, from epigenetics to splicing and translation. The 2OG oxygenase JMJD4 has been shown to catalyse the hydroxylation of the eukaryotic omnipotent termination factor 1 (eRF1), and is essential for optimal translational termination. In this thesis, we expand on previous work by examining two further potential binding partners of JMJD4, GTF2I and TCP1-γ. Subsequently, we find that depletion of JMJD4 and eRF1 is associated with growth reduction in cancer cell lines in 2D and 3D. The transcriptomic changes in response to eRF1 depletion are then assessed by RNA-Seq. Among the potential pathways identified, downstream targets of the transcription factor ATF4 were most prominent. Upregulation of ATF4 and its downstream targets was validated in an eRF1 rescue system and the contribution of specific subdomains of eRF1 to the transcriptional response assessed, indicating multiple arms of the unfolded protein response being upregulated downstream of defective translational termination. The implications of our findings and their relevance in wider biological and disease contexts, including cancer, is finally discussed.

# Acknowledgments

This work would have been impossible without the help of my supervisor, Dr. Mathew L. Coleman. Dr Coleman has been a constant pillar of support, providing helpful advice, scientific insights and suggestions as well as being a good friend. I would also like to thank the other members of the Tumour Oxygenase Group that have come and gone over the years: Helen Smith for her support and advice when I started; Charlotte Eaton and Charlotte Hall for being excellent labmates and great people; and Dr. Zhuang for our interesting discussions. Many thanks also go to Dr. Robert Hollows for his help with analyzing the RNA-Seq data included in this thesis.

I would also like to thank Dr. Claire Davies and Dr. Andrew Philp for acting as my assessors during the annual progress reviews. Their suggestions and criticisms have been instrumental in the development and maturation of this work.

I would furthermore like to extend thanks to my family for their patience in those four years. Doing a PhD is lonely work, and their encouragement and support are greatly appreciated.

Finally, I would like to thank my funding bodies, BBSRC and GlaxoSmithKline, for providing me with the resources to perform this research, as well as my industrial supervisor, Dr. Sarah J. Hopkins, for her time and support.

# Declaration

I hereby declare that the contents of this thesis are my own work, unless otherwise stated in the figure legend or in the main body of the text. Specifically:

The proteomic screen shown in Figure 2.1 was performed by Dr. Mathew L. Coleman (Nuffield Department of Medicine, University of Oxford; currently the Institute of Cancer and Genomic Sciences, University of Birmingham).

Analysis of the RNA-Seq to obtain the lists of upregulated and downregulated transcripts was performed by Dr. Robert Hollows (Institute of Cancer and Genomic Sciences, University of Birmingham). The relevant material is included in figures 4.3, 4.4, 4.5 and 4.10.

Figures 1.1, 1.2 and 1.3 were published in the following scientific review:

**Athanasios Ploumakis**, Mathew L. Coleman, OH, the Places You'll Go! Hydroxylation, Gene Expression, and Cancer, ***Molecular Cell***, Volume 58, Issue 5, 2015, Pages 729-741

Contributions by others and third party material are acknowledged where appropriate in the text.

# Table of Contents

# List of Figures

# Abbreviations

(Asterisks indicate alphanumerical identifiers covering multiple proteins with that prefix)

| | |
|---|---|
| 2OG | 2-Oxoglutarate |
| ASNS | Asparagine Synthase |
| ATF4 | Activating Transcription Factor 4 |
| BYDV | Barley Yellow Dwarf Virus |
| CBS | Cystathionine β-Synthase |
| COL* | Collagen * |
| CTH | Cystathionine γ-Lyase |
| DDIT3 | DNA Damage Inducible Transcript 3 |
| DDIT4 | DNA Damage Inducible Transcript 4 |
| DMOG | Dimethyl-oxalylglycine |
| ECM | Extracellular Matrix |
| eIF2α | Eukaryotic Initiation Factor 2, Subunit α |
| eRF1 | Eukaryotic translation termination factor 1 |
| GTF2I | General Transcription Factor 2I |
| HEMK2 | HemK Methyltransferase Family Member 2 |
| IGF4BP | Insulin-like growth factor-binding protein 4 |
| ITG* | Integrin * |
| JMJD4 | Jumonji Domain Containing 4 |
| LAM* | Laminin * |
| NOG | N-Oxalylglycine |
| RNA-Seq | RNA Sequencing (Whole Transcriptome Shotgun Sequencing) |
| RPL* | Large Ribosomal Subunit Protein |
| RPS* | Small Ribosomal Subunit Protein |
| RT-qPCR | Real Time Quantitative PCR |
| SECISBP2 | Selenocysteine Insertion Sequence Binding Protein 2 |
| shFF3 | Control shRNA |

| | |
|---|---|
| siCtrl | Control siRNA |
| TCP1-γ | T-Complex 1-γ Protein |
| TMV | Tobacco Mosaic Virus |
| TRIB3 | Tribbles Pseudokinase 3 |
| Trm112 | TRNA Methyltransferase 112 Homolog |

# CHAPTER 1: Introduction

## 1.1 Preface:

The research described in this Thesis centres around two main axes: Investigation of the binding partners and cellular effects of the 2-oxoglutarate (2OG) oxygenase JMJD4, and studies of the cellular responses to functional defects in its substrate, the eukaryotic translational termination factor eRF1. Therefore, this Introduction is divided into two sections: The first gives an overview of 2OG oxygenases and their role in gene expression, with a focus on 2OG oxygenases involved in protein translation. The second provides a general description of protein synthesis and its control, with a special emphasis on translational termination and the factors involved.

## 1.2 Overview of the discovery, structure and catalytic mechanisms of 2OG Oxygenases

2-Oxoglutarate (2OG) oxygenases, also referred to as 2OG-dioxygenases, are a diverse class of ~70 enzymes characterised by their capacity to perform two electron oxidation of their substrate. Originally identified as catalysing collagen hydroxylation in the extracellular matrix (reviewed in (Loenarz and Schofield, 2011)), 2OG oxygenases are now known to also be involved in every step of the gene expression pathway, from epigenetic modifications of DNA to protein synthesis. Importantly, with respect to this Thesis, they also catalyse the hydroxylation of targets involved in protein synthesis, including ribosomal proteins and translation factors (Figure 1.2) (reviewed in (Ploumakis and Coleman, 2015)).

2OG oxygenase activity is dependent on 2OG, Fe(II) and oxygen availability, while some enzymes also require reducing agents such as ascorbate (Reviewed in (Johansson et al., 2014). 2OG, also known as α-ketoglutarate, is a key intermediate in

the Tricarboxylic Acid (TCA) cycle, produced by the decarboxylation of D-isocitrate by the enzyme isocitrate dehydrogenase and sequentially converted to succinyl-CoA by the α-ketoglutarate dehydrogenase enzyme (Akram, 2014). The activity of 2OG oxygenases is generally not modulated by signaling targeting the enzyme itself (e.g. phosphorylation) but may be modified by modulation of co-factor availability, in particular oxygen, discussed in detail in section 1.3.3, and the level of expression within the cell (Pollard et al., 2008). That 2OG oxygenase activity may be regulated by the levels of 2OG in the cell, providing a link to the TCA cycle, has been proposed in the past and there is some evidence that certain oxygenases may detect changes in amino acid availability through changes in the concentration of 2OG (Duran et al., 2013). Availability of Fe(II) may also play a role in modulating the activity of some 2OG oxygenases, since Fe(II) supplementation is sufficient to promote hydroxylase activity *in vitro* (Knowles et al., 2003). Additionally, chaperones PCBP1&2, the iron chaperones for ferritin, are also responsible for carrying Fe(II) to the active site of the 2OG oxygenases PHD1-3, potentially integrating them into the system of cellular control of iron availability (Nandal et al. 2009).

Due to their wide range of substrates, 2OG oxygenases affect numerous processes from extracellular matrix remodelling, epigenetic modifications, oxygen sensing, development and cellular proliferations. This series of functions may also be closely entwined with their involvement in tumorigenesis, from the level of escaping growth suppression, to metastasis (reviewed in (Ploumakis and Coleman, 2015)). Indeed, numerous 2OG oxygenases are genetically altered and deregulated in a variety of cancers. Finally, specific 2OG oxygenases are associated with a plethora of other diseases, including developmental disorders most commonly affected by the epigenetic level of 2OG influence and metabolism (Johansson et al., 2014).

*Structure and Catalysis*

Members of the 2OG oxygenase superfamily all share the same catalytic motif found in the cupin superfamily of proteins, referred to as the double stranded β-helix (DSBH) fold and also known as the double Greek key motif, "jelly roll" fold, or Jumonji C (JmjC) domain. This fold is composed of 8 antiparallel β-sheets that create a barrel-like structure which forms the active site of the enzyme (Figure 1.1B). Within the DSBH domain resides an Fe(II) binding site, the iron being coordinated by a moderately conserved His-Xxx-Asp/Glu...His motif. Additional binding sites for 2OG and the substrate are also present but tend to be more variable in sequence (Clifton, I.J. et al, 2006). The 2OG in the active site is further stabilised by interaction with the Fe(II) ion being coordinated in a bidentate manner through the ketone and C1 carboxyl group of the 2OG (Figure 1.1C) (McDonough et al., 2010), while at least one Lysine/Arginine residue is used to bind the C5 carboxyl (Tarhonskaya et al., 2014). Beyond the defining active site, 2OG oxygenases exhibit a variety of additional domains. For example, members of the histone lysine demethylase family possess CxxC type Zinc Fingers (as in KDM2A and KDM2B), Tudor (JMJD2A-D) and/or ARID (KDM5A-D, also mediated by ARID5 in KDM7C) domains, which are typically required for interaction with nucleic acids and chromatin (Johansson et al., 2014).

The catalytic cycle is initiated by 2OG binding, leading to the formation of a ternary oxygenase–2OG–substrate complex. This enables oxygen to bind followed by oxidative decarboxylation of 2OG, resulting in an oxo-Fe(IV) species which readily oxidises substrates in a 2-electron oxidation, thus yielding reduced Fe(II), succinate and the oxidised substrate (Aik et al., 2012) (Figure 1.1D). Compared to heme-iron hydroxylases such as P450, the less rigid catalytic site of 2OG oxygenases results in

an increased rate of oxidative modification by oxygen radical by-products of the reaction, which along with loss or oxidation of the iron at the catalytic site is one of the main reasons these enzymes have not been synthesised as catalysts on a larger scale (Mantri et al., 2012b). Whether these oxidative self-modifications play any important biological role is uncertain; however auto-modification of the JmjC domain JMJD6 hydroxylase has been observed in human cell cultures (Mantri et al., 2012a) and occurs on lysine residues, in agreement with known activity.

Selectivity in substrate binding in 2OG oxygenases appears to be in large part conferred by both the architecture and polarity of the active site, as well as targeting by the non-catalytic domains. For the former, lysine demethylases (KDMs, examined more comprehensively in section 1.3.2) generally exhibit a deeper and narrower substrate binding pocket compared to the protein hydroxylases, along with hydrophobic regions near the active site (Horton et al., 2010). Demethylases targeting trimethylated residues (e.g. KDM4/KDM6 family members) tend to exhibit more open substrate binding sites closer to the surface of the protein, alongside larger hydrophobic patches, which would be excluded from the binding sites of KDMs primarily targeting mono- or di-methylated residues. (Ng et al., 2007). In contrast, hydroxylases rely primarily on main chain hydrogen bonds for stabilising the substrate in the active site, and can be stereoselective as a result (Elkins et al., 2003). With regard to the role of the additional domains to substrate specificity, most of the work has been once again performed on KDMs. For instance, the lysine demethylase activity of KDM7B is strongly dependent on binding of the KDM7B PHD domain to H3K4Me3 histones (Horton et al., 2010). In a similar fashion, the tRNA hydroxylase TYW5 is proposed to bind tRNAs via a positively charged patch formed by the C-terminal α-helices near its dimerization domain (Kato et al., 2011a). JMJD6, another

2OG oxygenase targeting RNA, also exhibits a positively charged surface patch near its dimerization domain, indicating that this architecture may represent a common strategy for targeting the enzymes to RNA substrates (Hong et al., 2010a). Generally, phylogenetically related 2OG oxygenases will tend to bind to their substrates in similar manners. A comparison of the structure of the ribosomal oxygenases MINA53 and NO66 for instance reveals highly similar binding approaches, consisting of a combination of extensive hydrogen bonding between the substrate and the DSBH domain, reinforced by hydrophobic contacts with additional domains (Chowdhury et al., 2014a).

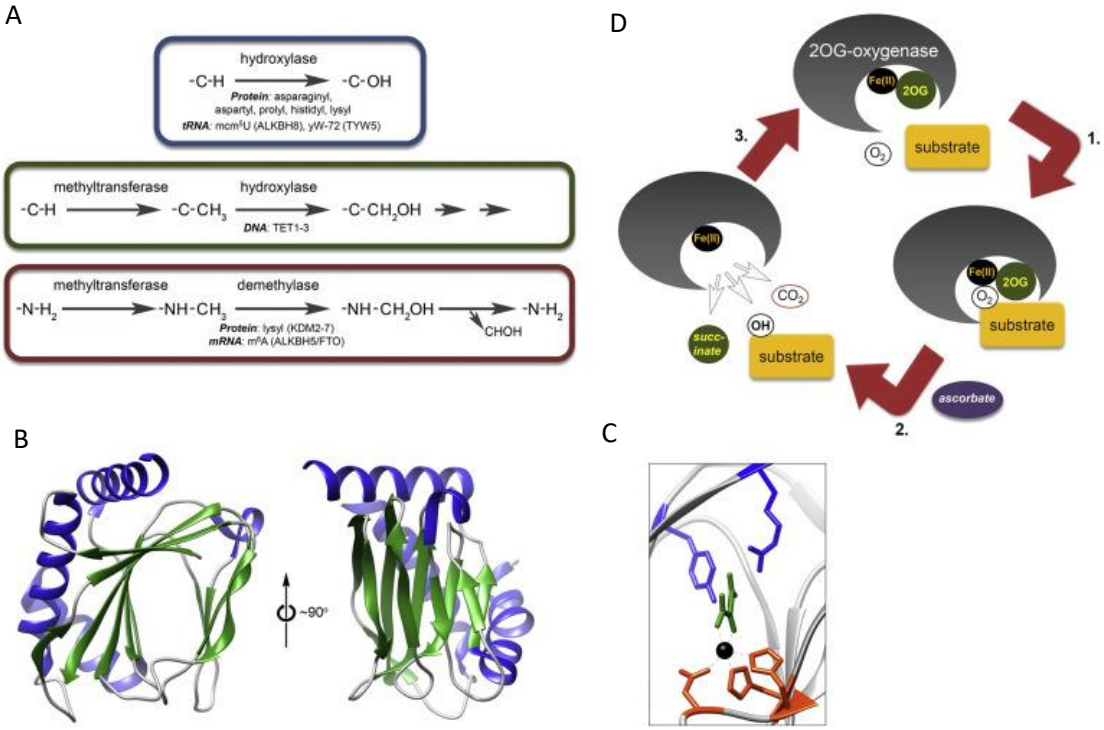


**Figure 1.1: 2OG Oxygenases catalyse the addition of hydroxyl group to a plethora of substrates:** A) Types of reactions catalyzed by 2OG Oxygenases. These include hydroxylation of nucleic acid and protein substrates as well as demethylation of the other nucleic acid targets through an intermediate hydroxymethyl step. B) Structural features of the 2OG Oxygenase catalytic domain. The double-stranded β helix (DSBH, green) is assembled in a barrel-like structure which allows ligation of 2OG, oxygen and the substrate in the fairly wide catalytic site. C) Coordination of the essential $Fe^{2+}$ in the generic 2OG catalytic site. $Fe^{2+}$ (Black) is bound by 2 Histidine residues and an Asp/Glu residue (all in orange), while 2OG (Green) is bound by a Tyrosine and Arginine residue (in blue). D) Pictorial diagram of the 2OG catalytic cycle. Ascorbate is only required by some 2OG oxygenases such as the collagen prolyl hydroxylases not discussed here. Structural images in (B) and (C) are derived from PDB: 3OUJ using Chimera. Figure reproduced from (Ploumakis and Coleman, 2015).

## 1.3 2OG Oxygenases and gene expression

2OG oxygenases have been shown to be involved at every step of the gene expression pathway, from DNA, to histones, to RNA splicing control, tRNA modification and finally translation control (Figures 1.2/3). An overview of the major points of control is provided below, divided into the specific elements of gene expression control that are affected.

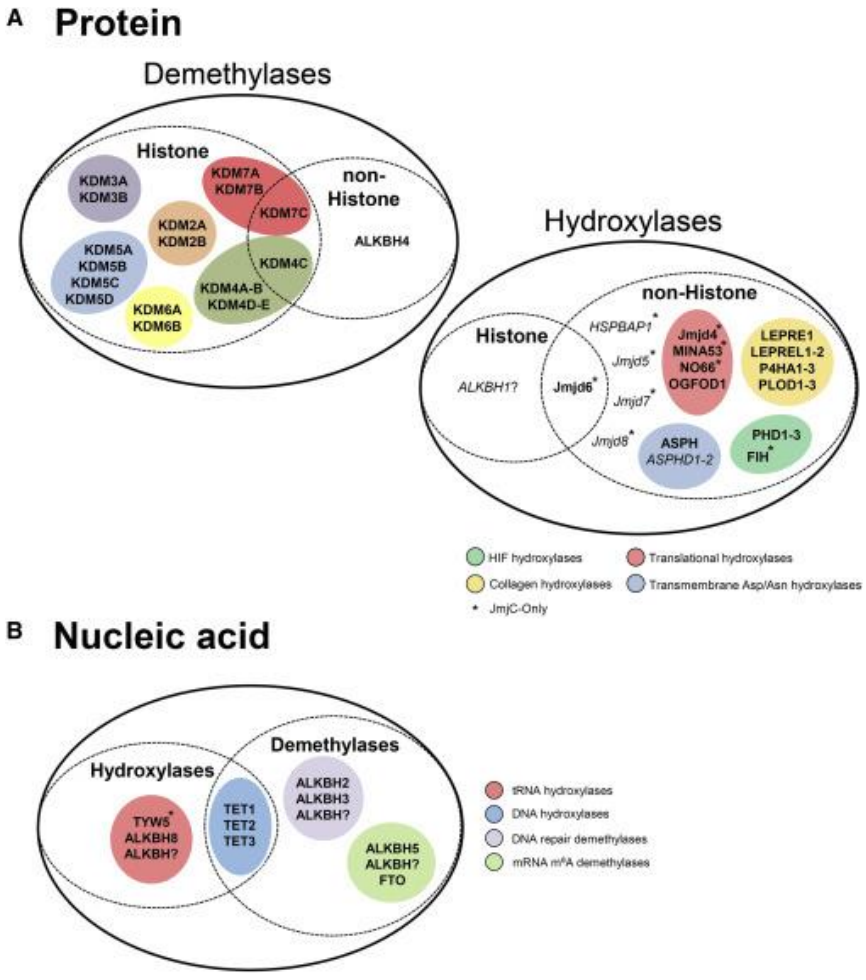


**Figure 1.2: Substrate based classification of 2OG oxygenases:** A) Numerous protein substrates are targeted by 2OG oxygenases. The main two reaction types are hydroxylation and demethylation. Enzyme names are written in light italic font if the corresponding substrate is uncertain or unknown. B) 2OG oxygenases that target nucleic acids. JmjC-only 2OG oxygenases are marked with an asterisk. Certain enzyme classes are ommited. Figure reproduced from (Ploumakis and Coleman, 2015).

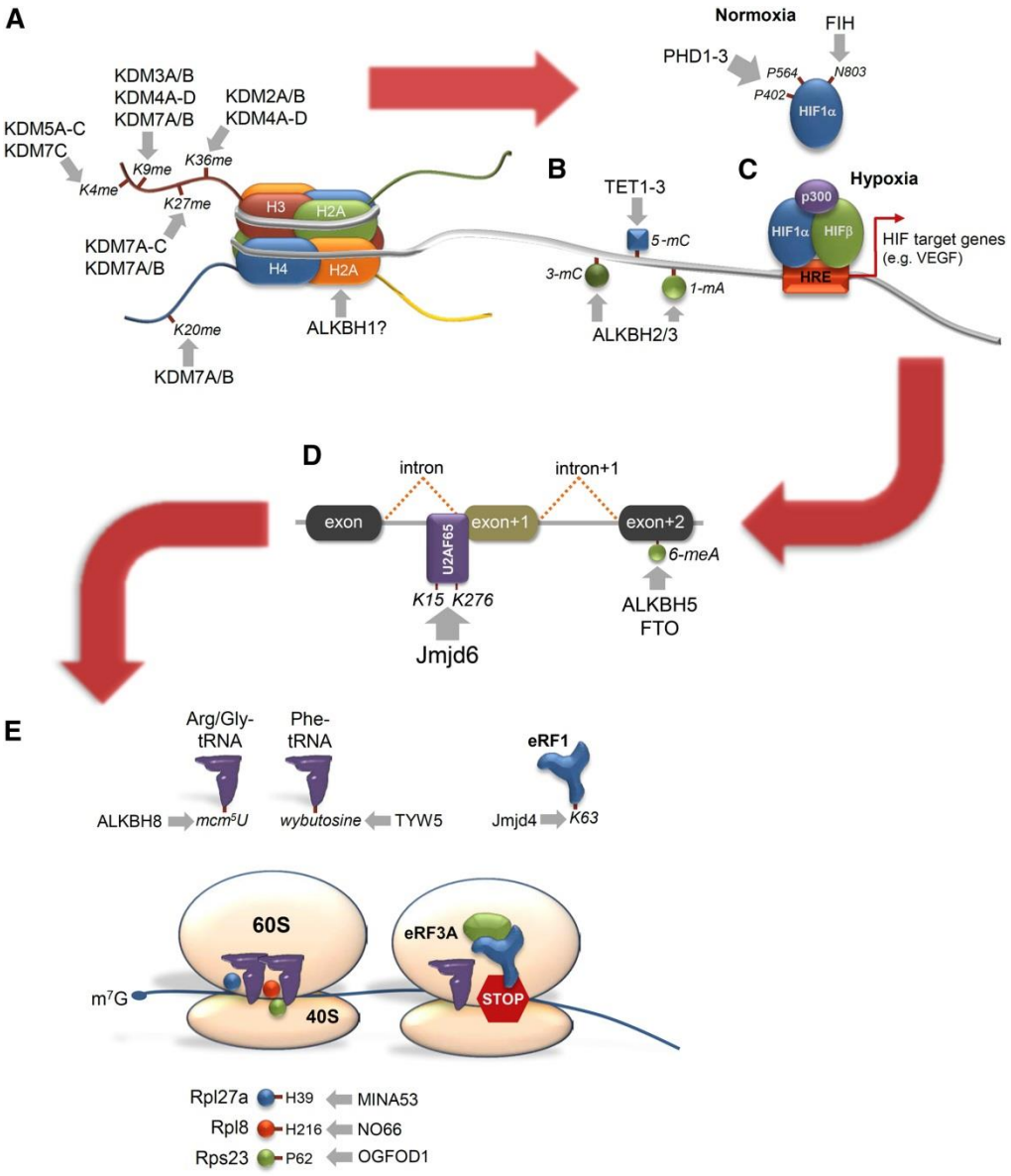


**Figure 1.3: Regulation of gene expression by 2OG Oxygenases**. A) JmjC histone demethylases. "?" indicate possible but not confirmed activity. B) Oxidation of DNA modifications by 2OG oxygenases. TET enzymes hydroxylate 5-methylcytosine (5-mC) in CpG islands. ALKBH2/ALKBH3 demethylate alkylated cytosine (3-methylcytosine, 3-meC) and adenosine (1-methyladenosine, 1-meA). C) Regulation of the hypoxic response through 2OG oxygenases and the Hypoxia Inducible Factor (HIF) D) 2OG oxygenases affect RNA demethylation and alternative splicing. E) 2OG oxygenase mediated control of translation. $m^7G$ = 7-methylguanosine cap. Figure reproduced from (Ploumakis and Coleman, 2015).

### 1.3.1 DNA Hydroxylation and Demethylation

DNA targeting 2OG oxygenases are a functional paraphyletic group of nucleotide hydroxylases composed of members of the TET (TET1-3) and ALKBH (ALKBH1-8, as well as the highly related FTO protein families) (Figure 1.3B). The TET dioxygenase family is structurally characterised by the presence of a large insertion in the DBSH domain, splitting into a central and a C-terminal section (Tahiliani et al., 2009a), while the ALKBH family is somewhat more varied, sharing an AlkB domain and additional structures in the more functionally derived ALKBH8 and FTO.

*TET Family*

Cytosine methylation is an important epigenetic modification with consequences in the binding affinity of transcription factors to DNA (Yin et al., 2017). TET1 catalyses three known hydroxylation reactions in the methylcytosine demethylation pathway: the hydroxylation of 5-methylcytosine (5mC) to 5-hydroxymethylcytosine (5hmC) and subsequently also 5hmC into 5-formylcytosine (5fC) as well as 5fC to 5-carboxylcytosine (5caC) (Tahiliani et al., 2009b). The exact step during which cytosine demethylation occurs is debated. It may be either following 5hmC deamination into 5-hydroxymethyluracil and subsequent removal by the AID/APOBEC base excision repair pathway (Guo et al., 2011) or by sequential conversion to 5caC and removal by the Thymine DNA Glycosylase (TDG), with *in vitro* and *in vivo* evidence pointing to the latter (Kohli and Zhang, 2013).

TET2 and 3 appear to share similar catalytic activity to TET1 and exhibit 5mC, 5hmC and 5fC dioxygenase activities at TET1 proximal kinetics and apparently serve the

same physiological roles *in vivo* (Ko et al., 2010, He et al., 2011b). Intriguingly however, TET2 and 3 appear to directly bind to and promote the activity of O-GlcNAc transferase (OGT), responsible for catalyzing the O-linked GlcNacation of Ser and Thr residues (Chen et al., 2013b). OGT activity in mammals has been linked to insulin sensitivity and energy metabolism (Yang et al., 2008b), it is a modulator of the AKT pathway (Yang et al., 2008a) and is crucial during murine embryogenesis and development, including sustained embryonic stem cell maintenance (Shafi et al., 2000).

TET enzymes also appear to play a significant role in cancer. A potential role in cancer as a tumour suppressor has been described for TET1, as downregulation of TET1 mediated demethylation is essential for KRAS driven transformation (Wu and Brenner, 2014), while overexpression leads to inhibition of migration and invasion in cancer cell lines (Park et al., 2016) and renal carcinoma (Fan et al., 2015) and inhibits colon cancer growth (Neri et al., 2015). However, its role may be more nuanced, as it appears to act as a co-activator of the hypoxia-induced epithelial-mesenchymal transition (Tsai et al., 2014). It was also recently shown that tumour hypoxia results in DNA hypermethylation through a reduction in TET1/3 activity, with important implication for hypoxia driven tumourigenesis (Thienpont et al., 2016).

*ALKB Family*

ALKB is a protein family with 9 homologues in humans, ALKBH1-8 and FTO, and was originally described as human orthologues of the E. coli Alkb DNA alkylation repair enzyme, responsible for the dealkylation of 1-methyladenosine and 3-methylcytosine of ssDNA (Sedgwick, 2004).

Of these, ALKBH2 and 3 have been established as significant dealkylation enzymes in mice and human models, with different substrate specificities. ALKBH2 shows 3-methylcytosine (3-meC) and 1-methyladenine (1-meA) activity in dsDNA at more than twice the level for ssDNA, while the opposite holds true for ALKBH3 (Duncan et al., 2002). Overall, ALKBH2 is the more efficient of the two, while also having demonstrated the capacity to repair 1-ethenoadenine adducts *in vitro* (Lee et al., 2005a, Ringvoll et al., 2008). Nevertheless dealkylation is remarkably rapid, with both enzymes acting close to the diffusion limit (Lee et al., 2005b). ALKBH2 promotes transcription of the rRNA genes through its dealkylase activity and associates with DNA repair proteins Ku70 and Ku80 (Li et al., 2013). ALKBH2 and 3 expression have been associated with a number of cancers, including aggressive urothelial carcinoma (Fujii et al., 2013) (Shimada et al., 2012), glioblastoma (Johannessen et al., 2013) and prostate malignancies (Koike et al., 2012).

The other members of the ALKB family have different activities, described in the following section where appropriate.

### 1.3.2 Histone Demethylases

Modification of the N-terminal tails of histone proteins represents a major level of gene expression regulation that is distinct from DNA demethylation. Histone tails are targeted by a large variety of different modifications, among which methylation is accepted to be extremely important. The methylation marks themselves are dynamic and influence the recruitment of transcriptional regulators in highly specific manners. For instance, although H3K9 methylation in the promoter is typically associated with transcriptional repression, and is considered one of the defining traits of heterochromatin, H3K9 di- and tri-methylation in the coding region has been discovered in actively transcribed genes (Vakoc et al., 2005). The JMJD (Jumonji C Domain containing) family of ~20 hydroxylases (also known as Lysine Demethylases, KDMs) forms, along with the unrelated lysine-Specific Demethylases (LSDs) the two known families of histone demethylases that are responsible for reversing these modifications (Klose et al., 2006) (Figure 1.3A). Demethylation is achieved *via* hydroxylation of the carbon of the methyl residue, creating an unstable hydroxymethyl intermediate which decomposes into formaldehyde (Figure 1.4) (Berry and Janknecht, 2013a). The specific reaction catalysed by JMJD proteins allows them to also demethylate tri-methyl lysines, an inaccessible target for LSD demethylases (Black et al., 2012) and potentially methylated arginine residues (Kooistra and Helin, 2012a).

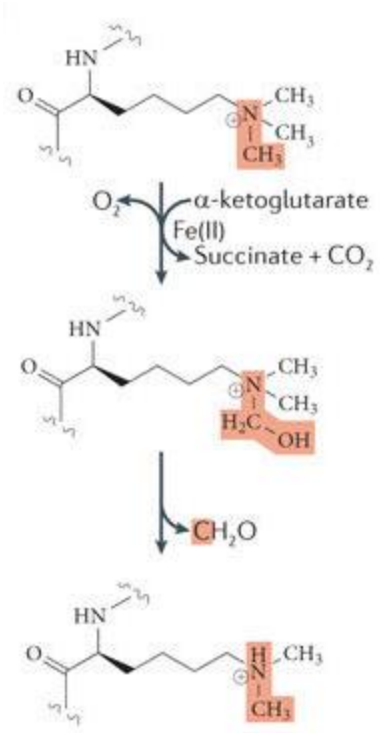


**Figure 1.4: The catalytic mechanism of JMJC histone demethylases**. Tri-methyl lysine is presented as an example. Hydroxylation of the methyl carbon creates an unstable hydroxymethyl intermediate, which decomposes into formaldehyde ($CH_2O$), demethylating the residue. The methyl group available for demethylation and the lysine side chain amine are highlighted in red. Figure adapted from (Kooistra and Helin, 2012b).

JMJC lysine demethylases are grouped into six distinct subfamilies (KDM2-7), based on sequence homology and structural similarity, though significant overlap exists on their activities and substrates (Kooistra and Helin, 2012b). JMJC lysine demethylases have been implicated in a wide range of cellular activities, including but not limited to establishing transcriptionally permissive chromatin microenvironments, influencing cell fate during differentiation, DNA replication and cell division, and resetting the germline (Dimitrova et al., 2015). As a result, changes in the lysine methylation status brought about by changes in the activity of JMJC lysine demethylases have been associated with numerous disease states, including, most prominently, cancer (Dhar et

al., 2014) (He et al., 2011a) (reviewed in (Ploumakis and Coleman, 2015, Johansson et al., 2014)). JMJC lysine demethylases have been shown to possess both oncogenic and tumour suppressor functions, depending on the specific enzyme and cancer type in question (Berry and Janknecht, 2013b) (Van der Meulen et al., 2014, Kandoth et al., 2013) (Hu et al., 2001) (Kim et al., 2012).

Beyond the JMJC lysine demethylases, an additional 2OG oxygenase, JMJD5, also known as KDM8, has been putatively identified as a histone demethylase targeting dimethylated H3K36, despite lacking any known histone interacting domains. Notably, one of its binding sites is the coding region of the Cyclin A1 ORF, implying that JMJD5 is an important cell cycle regulator. This role has been recapitulated by the discovery that JMJD5 is overexpressed in a range of tumors and JMJD5 loss of function mutations lead to cell cycle arrest in breast cancer cell lines (Hsia et al., 2010). Nevertheless, the role of JMJD5 as a histone demethylase has recently been disputed on the basis of new biochemical assays *in vivo* (Youn et al., 2012) and the elucidation of its crystal structure. The latter displays greater structural homology with non-histone protein hydroxylases and RNA hydroxylases, suggesting those as alternative roles for JMJD5 (Del Rizzo et al., 2012, Wang et al., 2013).

### 1.3.3 Oxygen Sensing and Transcription Factor Mediated Effects

*Control of the Hypoxic Response through Hydroxylation of HIF*

One of the most well-known and studied examples of hydroxylase-mediated gene expression control is the regulation of the Hypoxia Inducible Factor (HIF) abundance and activity. HIF is a heterodimeric member of the PER-ARNT-SIM (PAS) subfamily

of the basic helix-loop-helix (bHLH) family of transcription factors, composed of two structurally related α and β subunits. There are three known isoforms of the α subunit, HIF1α and 2α, which share significant sequence homology (Zhao et al., 2015), and HIF3α, which lacks a transactivation domain (Gu et al., 1998). Under physiological oxygenation levels, HIF1α is hydroxylated at conserved proline residues (P402 and P564 in *H. sapiens*) by the oxygen-dependent prolyl hydroxylases PHD1-3 (also known as EGLN1-3) (Figure 1.3C). Prolyl hydroxylation at these sites results in the proteasomal degradation of HIF1α through the creation of a recognition motif for the von-Hippel Lindau (pVHL) E3 ubiquitin ligase subunit (Shen and Kaelin, 2013), which marks it for degradation. The β subunit is instead constitutively expressed (Ratcliffe, 2013). During limited oxygen availability, otherwise known as hypoxia, PHD activity is reduced, resulting in reduced HIF1α degradation and increased abundance. However, functional activation of HIF activity is further dependent on the loss of hydroxylation by a fourth HIF hydroxylase, the Factor Inhibiting HIF (FIH). During normoxia, FIH hydroxylates a conserved asparaginyl residue in the crucial C-terminal transactivation domain, preventing it from binding to the crucial transcriptional co-activator p300/CBP (reviewed in (Lisy and Peet, 2008)). During hypoxia, loss of this modification allows HIF to recruit p300/CBP, thus enabling its function as a transcription factor. HIF1-dependent transcriptional expression in turn regulates itself, through a negative feedback loop involving the induction of PHD2 and PHD3 (EGLN3) (Epstein et al., 2001a) (Jaakkola and Rantanen, 2013). An additional negative feedback loop exists in the form of HIF3α splicing, which can produce a HIF3 variant, termed IPAS, that modulates HIF1 activity in a dominant negative manner (Makino et al., 2001, Makino et al., 2002, Makino et al., 2007).

The downstream transcriptional targets of HIF expression cover a vast range of responses related to the hypoxic response, including more than 500 unique binding sites identified in the human genome by Chip-Seq (Schodel et al., 2013), including both promoter as well as distal regulatory elements such as enhancers. In functional terms, the HIF-mediated transcription program is involved in numerous cellular processes, including metabolism, epigenetics, cell fate determination, apoptosis, migration and angiogenesis (Ratcliffe, 2013, Shen and Kaelin, 2013). Perhaps unsurprisingly, this widespread involvement has also made HIF and important target in a number of diseases, including cancer. In tumours, HIF activation is often found to contribute to tumour development either through activation as a result of hypoxic conditions in the tumour, or as a result of a pseudo hypoxic state brought about by increased HIF1α stabilisation, for example by reduced expression or activity of PHD1-3 and FIH (Ratcliffe, 2013, Shen and Kaelin, 2013, Semenza, 2010, Semenza, 2003). Notably, in at least one type of cancer, clear renal cell carcinoma, protein coding mutations often lead to loss of VHL activity (Gerlinger et al., 2014), resulting in direct activation of the HIF pathway and driving spontaneous ccRCC formation in mouse models (Wang et al., 2014).

HIF2α is highly similar to HIF1α in terms of structure and has been shown to be regulated in the same manner by oxygen availability through PHD1-3 and FIH hydroxylation (reviewed in (Schofield and Ratcliffe, 2004)). However, unlike the ubiquitous HIF1α, HIF2α is only expressed in specific tissues and developmental stages (Patel et al., 2010). Additionally, the downstream targets of HIF2α appear to differ to an extent from HIF1α. For instance, HIF1α and HIF2α exhibit opposing roles in Vascular Endothelial Growth Factor (VEGF) expression in mononuclear phagocytes (Eubank et al., 2011) and unlike HIF1α, enhanced HIF2α expression

during human trophoblast differentiation suppresses transcription of the placental growth factor (PGF) (Epstein et al., 2001b). The role and regulation of HIF3α is less well understood. It retains one of the PHD hydroxylation sites and multiple splice variants of it are targeted by pVHL, targeting them for proteolytic degradation (Maynard et al., 2003) and as discussed, some splice variants negatively regulate HIF1α (and likely HIF2α) activity (Makino et al., 2007). A specific role in signaling in adipose tissue has been proposed for HIF3α (Heidbreder et al., 2007, Pfeiffer et al., 2016).

*Non-Enzymatic Transcriptional Control through JARID2*

Beyond their activity in modifying transcription factors, 2OG oxygenases can also possess intrinsic transcription factor activity, as exemplified by the first identified member of the JMJC group, JARID2 (a member of the KDM5 subfamily). The JmjC domain of JARID2, despite the presence of an intact DSBH fold, lacks apparent 2OG oxygenase activity due to mutation of key residues in the iron and 2OG binding sites (Pasini et al., 2010). Nevertheless, the protein plays an important role in murine Embryonic Stem (ES) cell differentiation by mediating DNA binding to the developmentally crucial Polycomb Repressive Complex 2 (PRC2), via direct interaction with its SUZ12 core component (Pasini et al., 2010). A recent study (Kaneko et al., 2014) has also identified long non-coding RNAs (lncRNAs) from the developmentally significant imprinted Dlk1-Dio3 locus as JARID2 binding partners. Finally, JARID2 appears to be essential for cancer stem cell maintenance in bladder cancer (Zhu et al., 2017).

### 1.3.4 RNA Modification

*Splicing Control by JMJD6*

Originally thought to be a phosphatidylserine receptor involved in apoptotic phagocytosis (Bose et al., 2004), JMJD6 was later found to act as a 5-lysyl hydroxylase of spliceosome components U2AF/U2AF65 and LUC7L2, affecting spliceomorph choice in a subset of pre-mRNAs (Webby et al., 2009) (Figure 1.3D). Interestingly, it would appear that lysine hydroxylation of spliceosome components by JMJD6 only partially accounts for its activity and JMJD6 may also determine splicing events through non-enzymatic means (Yi et al., 2017). An additional function has been proposed for JMJD6 as a histone arginine demethylase targeting H3R2me (histone 3, Arginine 2 methylation) and H4R3me (Chang et al., 2007), with some further evidence for single stranded RNA hydroxylase activity (Hong et al., 2010b). However, both of these assignments appear not to represent the primary roles *in vivo* (Webby et al., 2009). Additionally, JMJD6 overexpression is associated with poor prognosis in breast cancer (Lee et al., 2012).

*Demethylation of $N^6$-Methyladenosine*

Adenosine methylation to $N^6$-methyladenosine (6-meA), catalysed by the $N^6$-adenosine methyltransferase complex (Bokar et al., 1997), is a highly evolutionarily conserved nucleotide modification, encountered from viruses (Beemon and Keith, 1977) to eukaryotes (Zhong et al., 2008, Wei and Moss, 1977). It primarily affects mRNA, where it is the most common post-transcriptional modification, found in 25%

of all transcripts, typically located in the 5′ UTR or in the proximity of the stop codon (reviewed in (Yue et al., 2015)). This modification has been found to be dynamic and reversible by two identified 2OG oxygenases, ALKBH5 and the Fat Mass and Obesity associated protein (FTO) (Figure 1.3D).

In contrast to ALKBH2/3 (discussed above), ALKBH5 exhibits 6-meA RNA demethylase activity, and appears to be crucial in murine spermatogenesis (Zheng et al.). Despite the similarity to FTO (discussed below), ALKBH5 does not appear to play a significant role in metabolic disorders (Shen et al., 2015). Interestingly, ALKBH5 has been shown to be a target of HIF, adding an further layer of complexity to the regulation of gene expression by 2OG oxygenases (Thalhammer et al., 2011).

Another member of the ALKB family, FTO, has been established as a 6-meA demethylase with additional *in vitro* DNA 3-methylthymine and 3-methyluridine ssRNA demethylase activity (Gerken et al., 2007)(Jia et al., 2011). Nevertheless, recent evidence indicates that FTO preferentially demethylates $N^6$,2′-*O*-dimethyladenosine ($m^6A_m$,containing an additional methylation at the 2'-hydroxyl position of the ribose), a modification that is generally observed adjacent to the m7-methylguanosine cap of mRNA, where it has a major role in regulating mRNA stability (Mauer et al., 2017). FTO appears to play an important role in regulating energy intake and is a likely genetic factor for obesity and associated co-morbidities (Fredriksson et al., 2008) (Do et al., 2008) (Jacobsson et al., 2008)**.** Interestingly, FTO may also have a role in cancer, acting as an oncogene promoting cell transformation and tumorigenesis in types of acute myeloid leukemia (Li et al., 2017). Furthermore, FTO variants have also been associated with increased risk of breast cancer (Garcia-Closas et al., 2013) and melanoma (Iles et al., 2013).

### 1.3.5 Roles of Hydroxylases in Protein Synthesis

Translation represents one of the major targets of gene expression control by 2OG oxygenases and ribosomal oxygenases are potentially the phylogenetically oldest oxygenase class (Chowdhury et al., 2014b). 2OG oxygenases have been shown to catalyse the hydroxylation of factors involved in every step of translation, from ribosomal subunit proteins (Ge et al., 2012a) to the eukaryotic termination factor eRF1 (Feng et al., 2014b) (Figure 1.3E). The dependence of 2OG oxygenases on 2OG, Fe(II), and oxygen presents a unique junction for the integration of energy availability, the redox state of the cell, and oxygen availability to mechanisms of translational control (reviewed in (Ploumakis and Coleman, 2015)). In terms of pathology, the tumour microenvironment may be associated with limitations in all three of these cofactors, perhaps explaining the upregulation of translational oxygenases in several cancer types as a necessary adaptive response (Zhuang et al., 2015).

*tRNA Hydroxylation*

Post transcriptional modification of tRNAs has been postulated to enable tRNA folding and translation fidelity (El Yacoubi et al., 2012). Thus far, three 2OG oxygenases which hydroxylate tRNA have been discovered: TYW5, ALKBH8 and ALKBH1.

TYW5 is a homodimeric tRNA hydroxylase involved in the generation of the hypermodified guanosine-derived base wybutosine (yB), found in position 37 of tRNA(Phe). Specifically, it catalyses one of the steps in the pathway, the conversion of 7-(a-amino-a-carboxypropyl)wyosine (yW-72) to undermodified hydroxywybutosine (OHyW*) (Kato et al., 2011b).

ALKBH8 is composed of a JMJC domain and a predicted methyltransferase domain. Uniquely, within the ALKBH family, the methyltransferase domain of ALKBH8 catalyses the methylation of 5-carboxymethyl uridine to 5-methylcarboxymethyl uridine in the wobble position in the anticodon loop Glu- and Arg-tRNA's (Fu et al., 2010a). An ALKBH8 truncation mutant that lacks the methyltransferase domain is capable of hydroxylating methoxycarbonylmethyluridine to 5-methoxycarbonylhydroxymethyluridine (Fu et al., 2010b), though this activity has not been confirmed for the full-length protein. Interestingly, ALKBH8 is overexpressed in urothelial carcinomas where it appears to promote cell survival, similar to other members of the ALKBH family (Shimada et al., 2009).

ALKBH1 was recently shown to catalyse the demethylation of *N1*-methyladenosine ($m^1A$) in the stem loop structure of tRNAs, the only enzyme known to be able to reverse this type of modification. ALKBH1-mediated $m^1A$ demethylation appears to play a role in coupling nutrient status with translational control, as glucose deprivation results in elevated ALKBH1 levels, leading to increased m1A tRNA demethylation and an attenuation of polysome translation (Liu et al., 2016). Additionally, ALKBH1 appears to catalyse *N5*-methylcytosine (m5C) demethylation in the wobble position of the anti-codon stem loop of the mitochondrial initiator methionine tRNA (Haag et al., 2016). Finally, a potential role for ALKBH1 in DNA demethylation has been suggested due to it exhibiting 3-methylcytosine and 1-methyladenosine dioxygenase on ssDNA *in vitro*. However, the potential physiological relevance of these activities is unclear (Westbye et al., 2008).

*Ribosomal Oxygenases*

In humans, the large ribosomal subunit is modified by two oxygenases, Nucleolar Protein 66 (NO66) and the Myc Induced Nuclear Antigen (MINA53), which catalyse the C3 H216 hydroxylation of ribosomal protein Rpl8 and the C3 hydroxylation of Rpl27a H39, respectively (Ge et al., 2012a). Structurally, both share high sequence homology and are closely related to the bacterial homologue ycfD, an arginine hydroxylase of the 50S ribosomal subunit Rpl16 (Ge et al., 2012b, Chowdhury et al., 2014c).

Recent structural studies have indicated that the Rpl8 hydroxylase activity of NO66 is dependent on its homooligomerisation into a tetramer, recognising the consensus sequence motif NHxH (Wang et al., 2015). An additional role has been suggested for NO66 as a histone demethylase targeting H3K4me1, 3 and to a lesser extent H3K4me2 as well as H3K36me2 and me3 as its substrates (Sinha et al., 2010b). Within this context, NO66 has been proposed to bind to and inhibit the osteoclast-specific transcription factor Osterix (OSX) (Sinha et al., 2010a), resulting in defects in osteoclast differentiation in histone demethylase activity dependent manner (Tao et al., 2013). However, this role has been disputed on functional and structural grounds (Chowdhury et al., 2014b). NO66 is likely pro-tumorigenic, as it is often overexpressed in non-small cell lung cancer, the most common form of lung cancer (Suzuki et al., 2007b). It is further associated with increased metastatic potential in invasive colorectal cancer (Nishizawa et al., 2017), while ectopic expression of NO66 leads to an increased proliferation phenotype (Suzuki et al., 2007a).

As with NO66, a potential role for MINA53 as a histone lysyl demethylase targeting H3K9me has been proposed (Lu et al., 2009, Chen et al., 2013a), but without *in vivo*

evidence. In terms of physiology, MINA53 appears to play a significant role in the immune response by acting as a determinant of Th2 T cell bias, a genetic trait that increases the likelihood of allergies and autoimmune disorders, as well as affecting pathogen susceptibility (Okamoto et al., 2009). In this context, Th2 T cell bias appears to be mediated through suppression of Interleukin-4 (IL4) expression, in turn caused by MINA53 binding to the IL4 promoters in an IL4 and NFAT dependent manner (Okamoto et al., 2009). Despite its role in immunity, it is difficult to establish MINA53 as a prognostic marker, as its pattern of overexpression is inconsistent and associated with poor prognosis in renal cell carcinoma (Ishizaki et al., 2007), favourable prognosis in early stage lung cancer (Komiya et al., 2010) and poor prognosis in breast cancer (Thakur et al., 2014).

The final ribosomal oxygenase known in humans is OGFOD1, which catalyses the trans-3 hydroxylation of Pro62 of the 40S ribosomal subunit protein Rps23 (Singleton et al., 2014a). Rps23 hydroxylation by homologues of OGFOD1 (e.g. Tpa1p in *S. cerevisieae*) is conserved across eukaryotes, though in basal eukaryotes 3,4-dihydroxyproline appears to be the final product (Loenarz et al., 2014). The trans-3 prolyl hydroxylation of Rps23 by OGFOD1 or its Tpa1p homologue appears to be significant in controlling translational termination efficiency, as knockdown of Tpap1 results in changes in stop codon readthrough (Loenarz et al., 2014). Whether an increase or decrease in stop codon readthrough occurs appears to be dependent on the termination context and specifically on the nucleotide following the stop codon. The hydroxylated Proline and its surrounding sequence are likely extremely important in translation, as all the Proline mutational variants are lethal in yeast (Loenarz et al., 2014). OGFOD1 is necessary for optimal growth across a range of human cell lines in an activity dependent manner and its knockdown results in the formation of stress

granules and translational arrest (Singleton et al., 2014b). Finally, OGFOD1 may play a role in cancer, as it is frequently overexpressed in breast cancer tissues and associated with poor prognosis (Kim et al., 2015).

### 1.3.6 The Termination Factor Hydroxylase JMJD4

JMJD4, investigated later in this Thesis, is a 52.5 kDa JMJC 2OG oxygenase sharing ~34% sequence homology with JMJD6. In the first comprehensive study of JMJD4 (Feng et al, 2014), potential targets and binding partners of JMJD4 were identified by generation of a catalytically inactive mutant substituting H189A at the Fe(II) binding site of JMJD4, followed by affinity purification and mass spectrometry, and comparison to wild-type JMJD4 data. Despite the high sequence homology with JMJD6, none of the latter's binding partners were identified. Instead, the major activity dependent JMJD4 interactors were found to be the eukaryotic omnipotent termination factor eRF1 and its binding partner eRF3a (discussed later in the introduction), with stoichiometric evidence indicating that JMJD4 specifically interacts with eRF1. *In vitro* and *in vivo* experiments further demonstrated that JMJD4 specifically catalyses the C-4 lysyl hydroxylation of K63 on eRF1. K63 of eRF1 resides within a conserved 'NIKS' sequence motif, which participates in stop codon recognition during translational termination (for a further analysis on the NIKS motif and eRF1 please section 1.4.4 of this introduction). Interestingly, JMJD4 is the only known 2OG lysyl hydroxylase capable of catalysing a C-4 hydroxylation; all other reported lysyl hydroxylases target the C-5 carbon. The catalytic activity of JMJD4 is dependent as with other 2OG oxygenases of its family, on Fe(II), 2OG and molecular oxygen. Despite the dependence on oxygen, JMJD4 maintains high levels of activity even under severe hypoxia ($\leq$1% $O_2$), indicating it is likely not a physiological oxygen sensor.

JMJD4 was further found to be abundantly expressed in several mouse tissues, including brain, heart, lung, liver, kidney and testes, with an exclusively cytoplasmic distribution. JMJD4 mediated eRF1 hydroxylation has over 90% abundance in immortalized cell lines and mouse tissues and is essential for optimal termination. Knockdown of JMJD4 in multiple cell lines resulted in an increase in translational termination readthrough, where the translating ribosome proceeds past the normal stop codon, resulting in an extended C-terminus. This data was further validated by the finding that in an *in vitro* system hydroxylated eRF1 was more efficient at releasing stalled termination complexes than the unmodified version, at all three stop codons (Feng et al., 2014b). While the mechanism by which JMJD4 hydroxylation confers increased termination efficiency to eRF1 is not yet well understood, it is hypothesized to occur likely via an interaction between the hydroxylated lysine in the NIKS motif and the uridine in the first nucleotide of a stop codon (Chavatte et al., 2002). The mechanism of stop codon recognition by eRF1 and the contribution of the K63 hydroxylation in that is explored in greater detail in section 1.4.4 (eRF1).

The physiological role that JMJD4 might play has not been established as well. Attempts to describe the *in vivo* importance of JMJD4 have only occurred recently (Yoo et al., 2016b). In this study, JMJD4 knockout mice were generated to assess developmental and other phenotypes. In contrast to the study by Feng *et al*, expression of JMJD4 was found to be sporadic and concentrated primarily in the eyes and gut. Additionally, overall JMJD4 expression appears to decrease as cells become increasingly differentiated, overall suggesting a specialized or limited developmental role. Embryonic Stem Cell (ESC) colonies derived from these mice exhibited a normal level of proliferation and appeared to be indistinguishable from WT ESC colonies. Finally, JMJD4 -/- homozygous mice develop apparently normally, without

demonstrating growth retardation or reduction in viability, indicating that JMJD4 is dispensable for embryonic development in mice. Nevertheless, the aforementioned study only verified knockout of JMJD4 in the affected mice and ESC colonies at the transcript rather than protein level. Additionally, the level of JMJD4 activity in the mice tissues or whether an increase in translational readthrough occurred was not tested for.

Profiling of the global gene expression in response to JMJD4 knockdown in mice has also been recently performed (Hu and Imbalzano, 2016), but without any attendant data analysis. Due to difficulties in accessing the dataset, the data contained where not analysed further in this Thesis. Finally, a possible mechanism of JMJD4 regulation was proposed by (Zhang et al., 2017), reporting that knockdown of the miR-370 miRNA in porcine induced Pluripotent Stem Cells (piPISCS) results in an increase in JMJD4 expression, part of more general upregulation of development associated genes. Finally, no work has been performed on the disease relevance of JMJD4. However, using publicly available datasets, evidence for a potential involvement in cancer can be found, and is presented in section 3.2 of this Thesis.

## 1.4 Translation

### 1.4.1 Overview of Translation

Translation is the process by which proteins are synthesised, consisting of the sequential addition of single amino acids at the end of a growing polypeptide chain and is catalysed by a large protein and ribonucleic acid complex known as the ribosome. Translation can be conceptually divided into its initiation, elongation and termination stages. In a mechanism shared by prokaryotes and eukaryotes, a mature, translation competent ribosome is assembled from two distinct subunits, a large and small one, at the site of an initiation codon on mRNA, with the aid of initiation Factors (eIFs in eukaryotes). Aminoacyl tRNA synthetases load tRNAs with specific aminoacids dependent on their anti-codon loop sequence. The ribosome has three tRNA binding sites, the aminoacyl site (A), the peptidyl site (P) and the exit site (E), located in an E-P-A sequence relative to the mRNA orientation. The aminoacyl groups of charged tRNAs are then added to the growing polypeptide chain based on the Watson-Crick base pairing of the mRNA codons and the tRNA anti-codon loop and elongation continues in a GTP dependent manner. Termination of translation is the result of a stop codon in the mRNA, which causes the recruitment of a Release Factor (RF1 and 2 in prokaryotes, eRF1 in eukaryotes), allowing release of the polypeptide chain. The process by which this protein synthesis occurs and is regulated is widely covered in literature and beyond the scope of this Thesis; therefore, a brief overview of translational initiation and elongation is provided, followed by a more in-depth look into the process of termination.

### 1.4.2 Translation Initiation

Translational initiation is the process of assembly of translation competent 80S ribosomes so that the start codon in mRNA is paired with an initiator Methionine-loaded Met-tRNA (Met-tRNA$^{Met}_i$) at the P-site of the ribosome, through their codon:anti-codon loop base pairing. The first step of translation initiation is the formation of the 43S preinitiation complex, composed of the 40S subunit, the eIF2-GTP-Met-tRNA$^{Met}_i$ ternary complex, eIF1, eIF1A and potentially eIF5 (Jackson et al., 2010). The 43S complex subsequently attaches to the modified 5'- methylguanosine cap of mRNA and recruits eIF4A, eIF4B and eIF4F, resulting in the loss of the local mRNA tertiary structure (Sonenberg and Hinnebusch, 2009). The 43S complex then scans along the 5' untranslated region (5'-UTR) (Pestova and Kolupaeva, 2002), until it encounters an initiator codon. To guarantee fidelity of translation it is necessary to ensure that partial binding of the anti-codon loop of Met-tRNA$^{Met}_i$ with the 5'UTR does not occur. For this reason, the initiator methionine codon (AUG, highlighted in bold below) is typically presented in an optimal recognition sequence, GCC(A/G)CC**AUG**G (Kozak, 1991). Fidelity of initiation is enhanced by eIF1, which increases selectivity for correct initiation contexts and decomposes ribosomes assembled at Met codons that are in a poor sequence context (Pestova and Kolupaeva, 2002). Binding and commitment to the initiator Met codon is mediated by eIF2 in a GTP-dependent manner, resulting in the formation of the 48S complex. Hydrolysis of GTP is caused by eIF2γ aided by eIF5 and eIF5B binding to eIF2β. The latter is predicted to occur by either eIF5 acting as a classic GTPase Activator Protein and providing an arginine finger (Paulin et al., 2001), or by de-repressing eIF2γ GTPase activity (Marintchev and Wagner, 2004). eIF2 GTP hydrolysis subsequently participates in the displacement of the eIFs and allows binding of the 60S subunit and

consequently permits translational elongation to begin. (Jackson et al., 2010). A schematic of the process of translation initiation can be found in Figure 1.5.

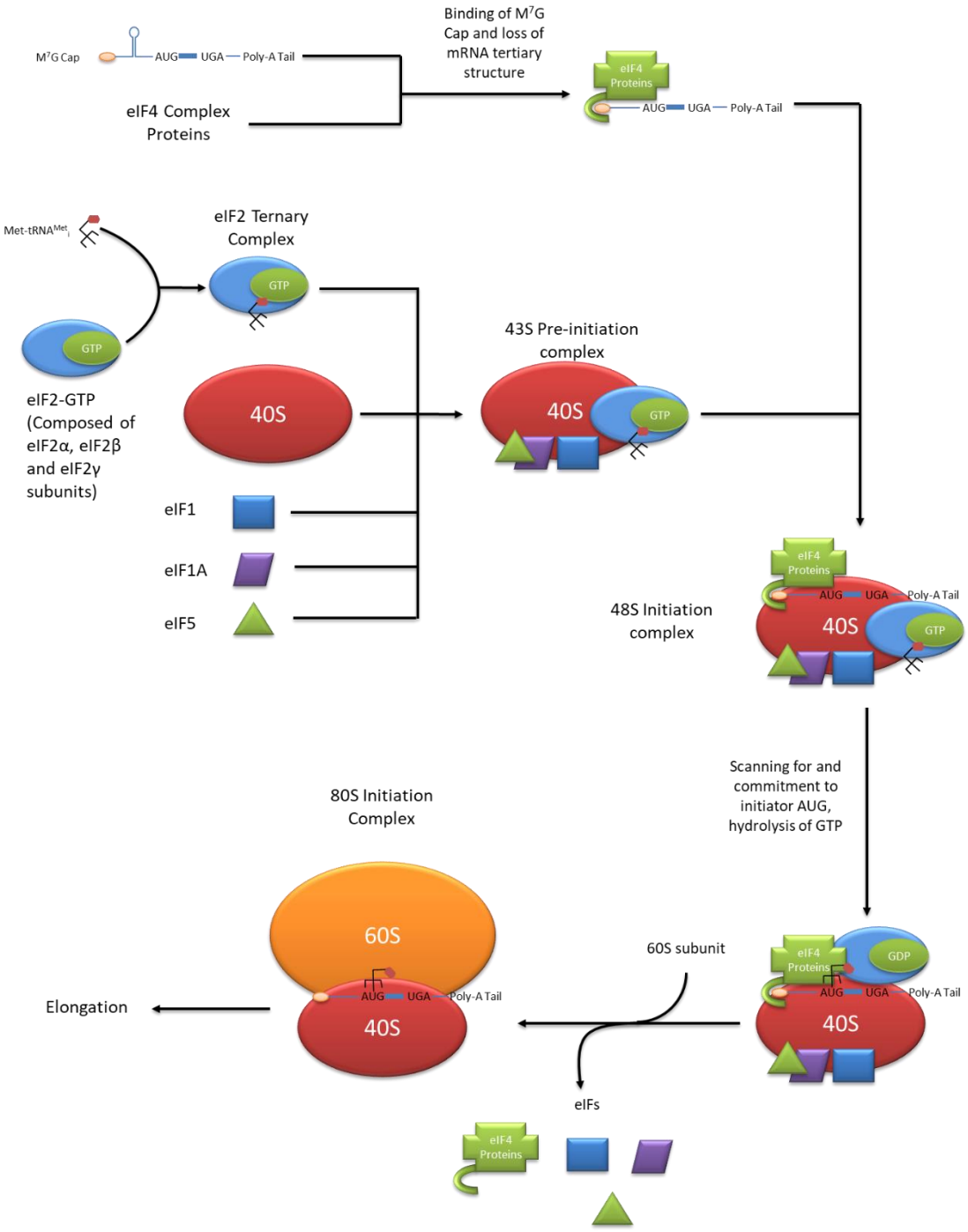


**Figure 1.5: The process of eukaryotic translation initiation**. Binding of eIF1, eIF1A and eIF5 to the 40S ribosomal subunit results in the formation of the 43S pre-initiation complex, which then recruits the eIF4 complex bound mRNA, forming the 48S initiation complex. The mRNA is scanned for an initiation codon in an optimal context, and the choice committed to via hydrolysis of the eIF2 bound GTP. This results in the dissociation of the initiation factors and recruitment of the 60S subunit, forming the 80S initiation complex, allowing translation elongation to begin. Individual components not to scale.

### 1.4.3 Translational Elongation

Following translational initiation, the Met-RNA$^{Met}_{i}$ is base paired to the mRNA start codon and located at the P-site of the 80S ribosome. The subsequent codon in a 5'-3'direction is then open to the A site. Binding of a cognate aminoacyl-tRNA to that codon is mediated by the eukaryotic elongation factor 1A (eEF1A), which directs aminoacyl tRNAs to the A site in a GTP dependent manner. In the event of a base pair match, GTP hydrolysis occurs by eEF1A, which dissociates from the translating complex (Dever and Green, 2012). Accommodation of the aminoacyl-tRNA at the A site is rapidly followed by peptide bond formation with the P-site peptidyl tRNA, through the Peptidyl Transferase Centre (PTC) of the large (60S) subunit, so that the polypeptide chain is now bound only to the tRNA at the A site. The latter is almost universally conserved among eukaryotes and prokaryotes and is composed in large part by ribosomal RNA (rRNA), with crucial roles in the catalysis of the reaction. Following peptide bond formation, the small and large ribosomal subunits move relative to each other, so that the tRNAs previously at the P- and A-sites are now in a hybrid P/E and A/P configuration respectively. Specifically, the acceptor arms containing the aminoacid groups are moved to the E and P sites, while the anti-codon loops remain in the P and A sites. This hybrid state is stabilised by GTP binding through the eukaryotic Elongation Factor 2 (eEF2). The latter acts as a translocase, pushing the peptidyl-tRNA into the P-site and the deacylated tRNA into the E-site, freeing the A-site for another round of elongation (Rodnina and Wintermeyer, 2009, Dever and Green, 2012). It is currently not clear whether release of the deacylated tRNA at the E-site is coupled to eEF1A mediated binding of a new aminoacyl-tRNA at the A site as an allosteric effect, or whether it occurs earlier (Nierhaus, 1990, Chen et al., 2011). A schematic of this process is presented in Figure 1.6.

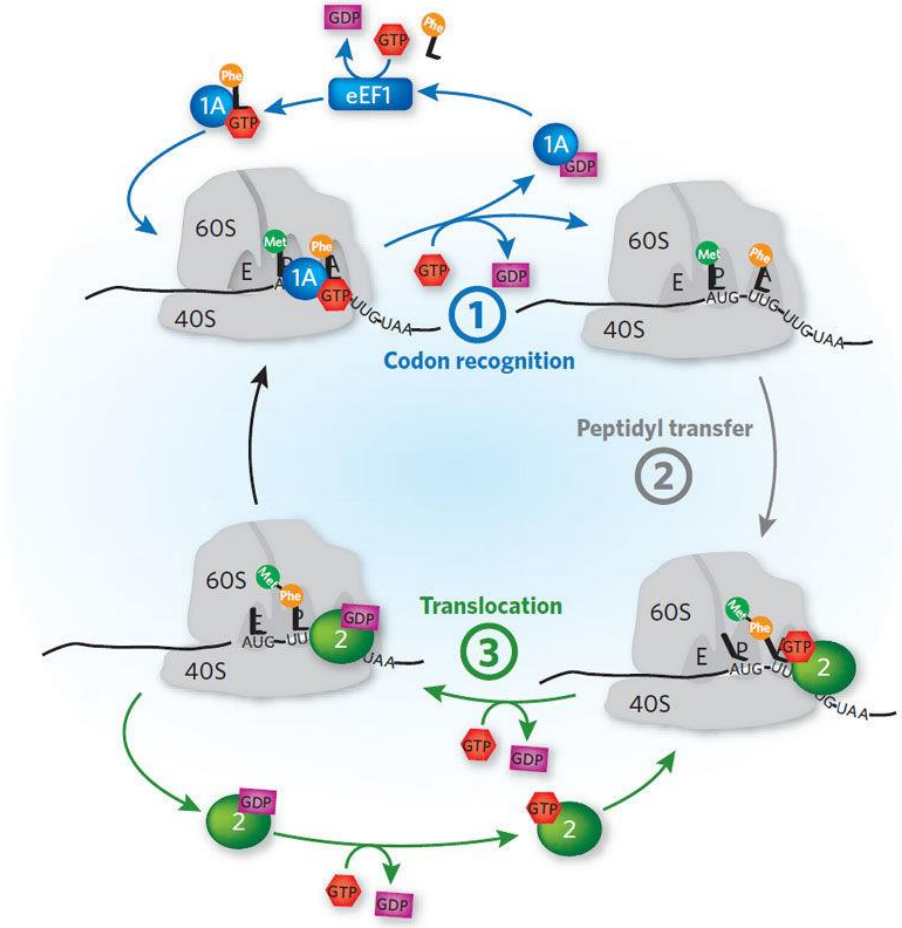


**Figure 1.6: The eukaryotic translational elongation cycle**. eEF1A delivers the aminoacyl-tRNA to the 80S ribosomal A-site. There, if the aminoacyl-tRNA anticodon loop is cognate to the triplet in the codon loop, GTP hydrolysis occurs and eEF1A is released. Peptidyl transfer of the aminoacyl-tRNA in the A position then occurs by peptide bond formation to the ribosomal PTC. Subsequently, ratcheting of the ribosome causes the two aminoacyl tRNAs to adopt hybrid positions, which ribosomal translocation across the mRNA causes to shift to the E and P positions respectively, accompanied by GTP hydrolysis and eEF2 dissociation. (Figure adapted from (Schneider-Poetsch et al., 2010))

### 1.4.4 Translational Termination

Translational termination occurs when a stop codon (UGA, UAA or UGA) enters the A site of a translating ribosome. In both bacteria and eukaryotes, this process is controlled by Class I and II 'release factors', which acts as either a tRNA mimic or as a GTPase, respectively, and function cooperatively (Zhouravleva et al., 1995). In eukaryotic organisms, the class I release factor is eRF1 and the class II is eRF3a. In bacteria these are referred to as RF1/2 and RF3, respectively (Atkinson et al., 2008). Of these, eRF1 is the major focus of study in this Thesis.

*eRF1*

Encoded by the ETF1 gene, eRF1 (also known as TB3-1) is a protein which in eukaryotes acts as an omnipotent termination factor, i.e. is able to decode all three UGA, UAA and UAG termination codons (Goldstein et al., 1970, Konecki et al., 1977). eRF1 is a functional counterpart of eubacterial RF1 and RF2 but unrelated in primary structure and with significant differences in secondary and tertiary structure (Figure 1.7). However, it exhibits 30% pairwise sequence identity with archaeal RFs, indicating the presence of two distinct protein families with convergent function and characteristics (Vestergaard et al., 2001).

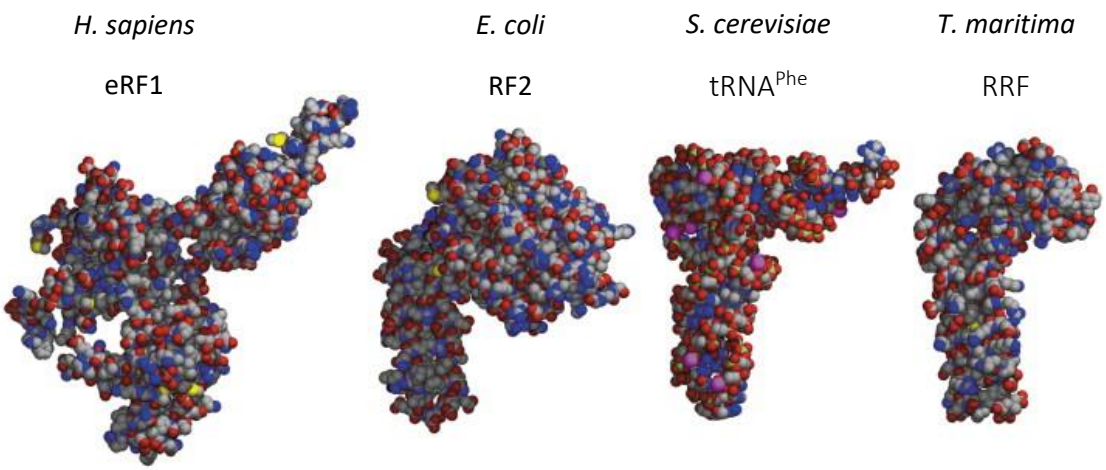


**Figure 1.7**: **Eukaryotic, eubacterial and archaebacterial translation Release Factors are not structurally similar:** Corey-Pauling-Koltun-type molecular representations of translation Release Factors across the domains of life, including a typical charged tRNA structure for comparison (figure adapted from (Vestergaard et al., 2001))

As discussed, termination of protein biosynthesis is signalled by the presence of an in-frame stop codon. eRF1 recognises the stop codon and causes the peptidyl transferase centre of the ribosome to hydrolyse the amide bond between the peptidyl-tRNA site and the polypeptide (Song et al., 2000). Termination efficiency can vary among sequences, and in *S. cerevisiae* and *E. coli* it has been shown to be affected by the bases flanking the stop codon with a specific bias towards the 3' base in the latter (Bonetti et al., 1995, Poole et al., 1995, Mottagui-Tabar et al., 1998).

The crystal structure of eRF1 was determined at 2.8Å in 2000 by Song *et al* (Song et al., 2000) and was shown to be composed of three approximately equally sized domains in an approximate 'Y' shape, in contrast to the tRNA and bacteria RF 'L' shape, demonstrating that eRF1 is not as dependent on molecular mimicry as its prokaryotic counterparts. In general, it would appear that each of the three domains of eRF1 is broadly associated with a different function: Domain 1 (N-terminal) is responsible for conferring stop codon specificity (Frolova et al., 2000, Inagaki et al.,

2002), domain 2 (Middle) mimics the tRNA acceptor arm and is responsible for peptidyl bond hydrolysis leading to release of the polypeptide (Song et al., 2000, Seit-Nebi et al., 2001b) and domain 3 (C-terminal) mediates eRF3a binding (Nakamura and Ito, 1998, Kononenko et al., 2008, Cheng et al., 2009) (Figure 1.8)**.**

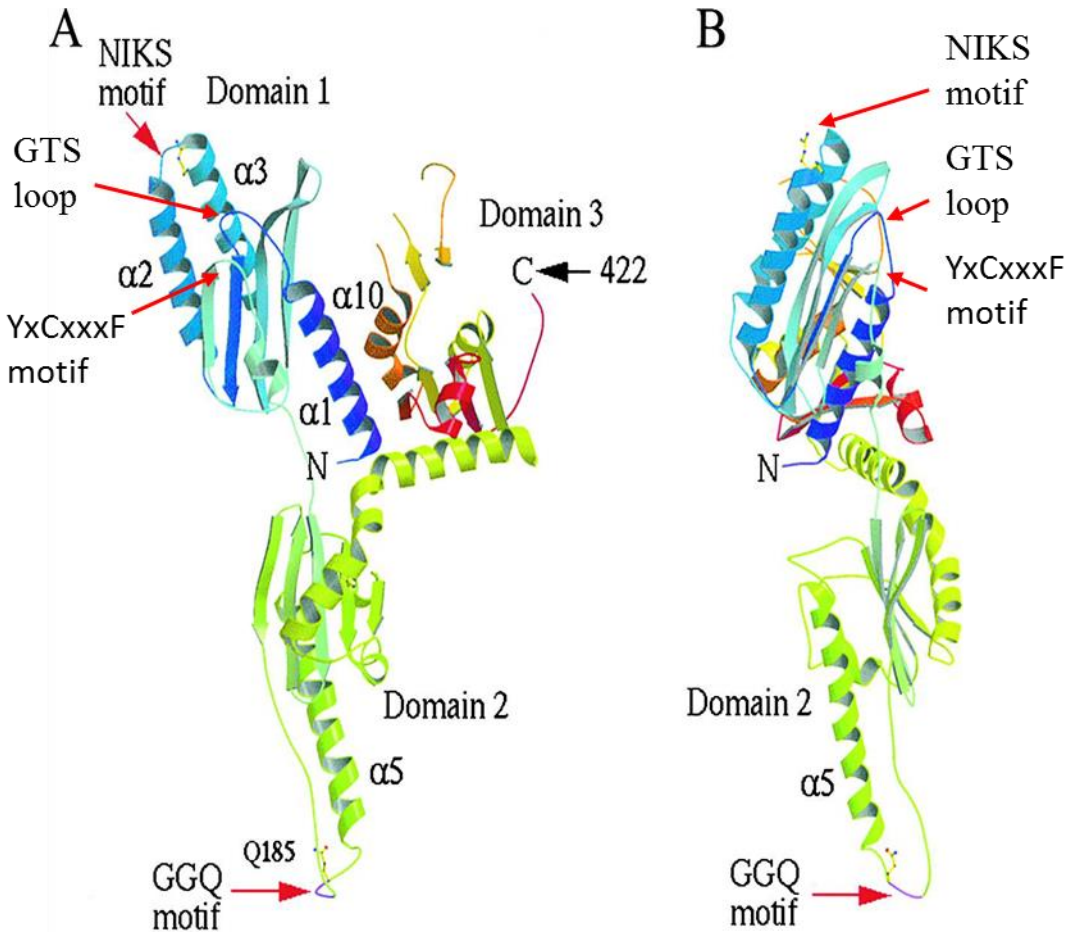


**Figure 1.8**: **Domains and structural features of the eukaryotic Termination Factor eRF1.** A) Ribbon diagram of *H. sapiens* eRF1. The protein is composed of three domains, outlined in blue, green and orange respectively. The conserved NIKS and GGQ motifs are indicated by arrows. B) Orthogonal view of the same (Figure adapted from (Song et al., 2000)).

Domain 2 exhibits one particular sequence of great importance, the 'GGQ' motif, which is found within the conserved GRGGQS sequence context, in turn located within a turn connecting the N-terminus of the α-5 helix with a β-strand, forming a GGQ minidomain (Song et al., 2000). The GGQ sequence motif is universally conserved among all eubacteria, archaebacterial and eukaryotic release factors (Frolova et al., 1999, Song et al., 2000). Mutations abolish the peptidyl-tRNA hydrolysis activity during termination, indicating that it is likely essential for the hydrolytic activity of the ribosomal peptidyl transferase centre. Specifically, mutation of the two glycine residues (G183 and G184 in *H. sapiens*) causes complete loss of all release factor activity, with mutant eRF1 competing with wild type for the ribosome binding sites in *in vitro* assays and displaying a dominant negative phenotype. However, mutations in the GGQ motif do not appear to affect the ability of eRF1 to stimulate eRF3 GTPase activity (Frolova et al., 1999). Additionally, mutations within the broader minidomain context that do not affect the GGQ sequence directly generally result in wild type phenotypes (Song et al., 2000). A proposed mechanism by which the GGQ motif functions in peptidyl-tRNA hydrolysis is that the amide nitrogen on the Gln residue plays a crucial role by coordinating a water molecule, which performs a nucleophilic attack on the peptidyl-tRNA ester (in a manner similar to the nucleophilic attack by the amino group of the aminoacyl-tRNA during normal elongation) (Song et al., 2000). The Glutamine on GGQ undergoes N-5 methylation in yeast and metazoa by the methyltransferase HEMK2 in complex with its obligate biding partner Trm112 (Figaro et al., 2008). Though the function of the methylation is yet unknown, deletion of HEMK2 results in growth defects in yeast (Polevoda et al., 2006) and early embryonic lethality in mice (Liu et al., 2010).

Domain 1 contains three conserved sequences of interest: the NIKS motif, the YxCxxxF motif and the GTS loop, all of which have been linked to stop codon specificity (Bulygin et al., 2010, Cheng et al., 2009). The Tyrosine (Y125 in *H. sapiens* eRF1) in the YxCxxxF motif is invariant and along with another highly conserved residue, E55, has been shown to be involved in the formation of hydrogen bonding networks with the stop codon and each other (Kolosov et al., 2005). Mutant eRF1 terminating at UGA stop codons only has been shown to exhibit different positioning of the GTS loop, suggesting that it too participates in conferring specificity to stop codons (Wong et al., 2012).

The primary contribution to stop codon recognition by eRF1 is likely mediated by the NIKS motif, based on a 3.5-3.8Å Cryoelectron Microscopy (Cryo-EM) structure of the stalled eukaryotic termination complex (Brown et al., 2015). eRF1 is able to decipher between stop and sense codons by exploiting the architecture of the local rRNA and mRNA sequences (Figure 1.9). Specifically, nucleotide A1825 of the 18S ribosomal RNA is rotated during binding of eRF1, causing it to stack on positions 2 and 3 of the codon bases. As a result, base G626 of the 18S rRNA can stabilise the base in the 4$^{th}$ position, securing it within the A-site of the ribosome. This results in an overall compaction of the mRNA conformation, resulting in a hydrogen bonding network between the codon, the 18S rRNA and the NIKS motif of eRF1 in which only uridine can be accommodated in the +1 position. More specifically, an additional hydrogen bond can form between the uracil carbonyl groups and the main chain carbonyl of N61 since the N61 and K63 side chains are now within hydrogen-bonding distance. In this context, JMJD4-mediated C4 hydroxylation of K63 is thought to permit the formation of an additional interaction with the mRNA phosphate backbone, thus optimising hydrogen bonding through the C5 aminogroup. (Brown et al., 2015).

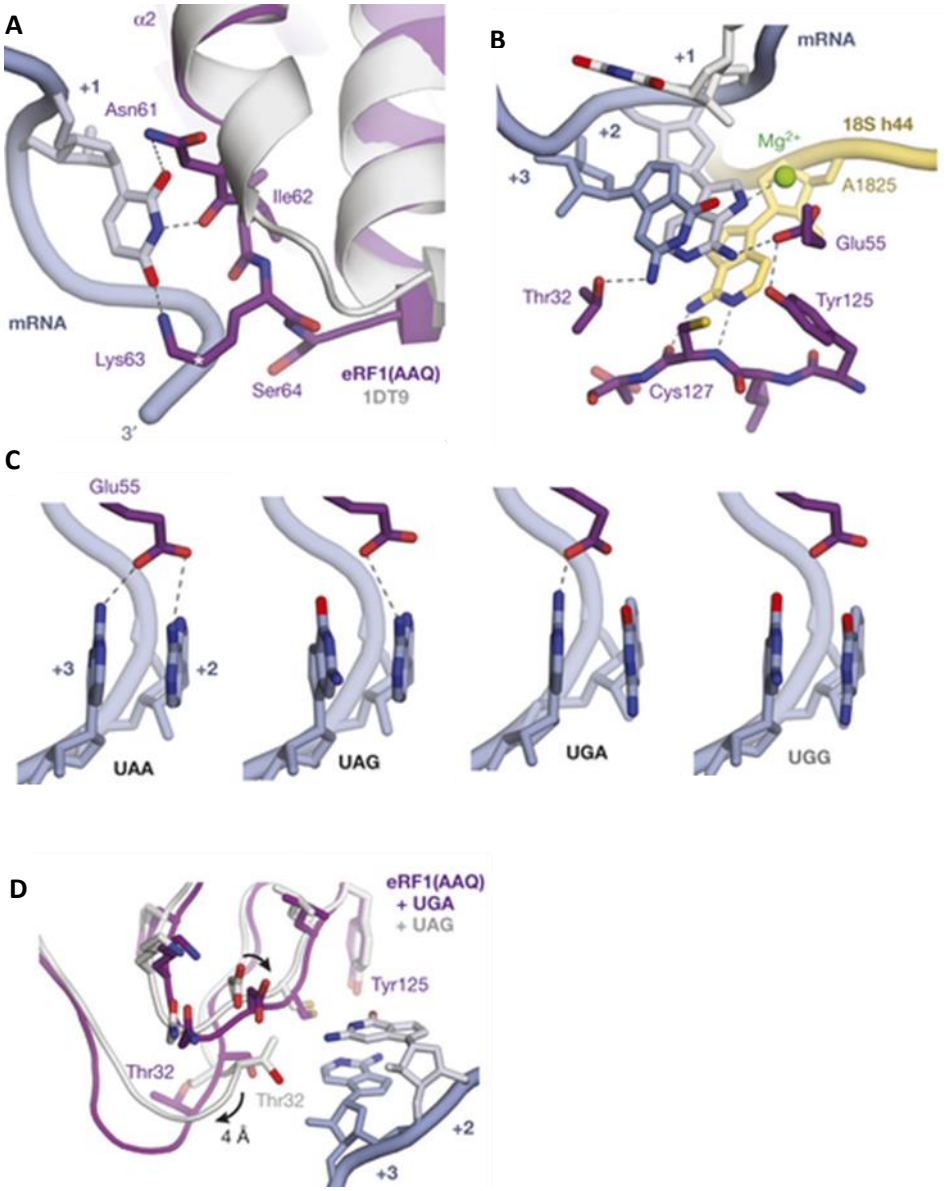


**Figure 1.9: Interaction networks conferring specificity of stop-codon recognition during translational termination**. A) eRF1 K63 permits bonding with the +1 Uridine in stop codons. JMJD4 mediated hydroxylation of K63 occurs at C4 (white asterisk) and would permit hydrogen bonding to the mRNA backbone, stabilising the interaction. Ribosome bound AAQ-eRF1 in purple, eRF1 crystal structure in light grey. B) The stop codon proposed interaction network between AAQ-eRF1, the stop codon (UAG) and 18S rRNA. eRF1 in purple, stop codon in slate, rRNA in yellow. C) Model for stop codon discrimination based on hydrogen bonding of eRF1 Glu55. Hydrogen bonding to all three stop codons is possible, but not to the UGG sense codon. D) Response of eRF1 conformation to different stop codons. UGA bound AAQ-eRF1 in purple, UAG bound AAQ-eRF1 in white. Figure adapted from (Brown et al., 2015).

Furthermore, the NIKS motif lines the top of the stop codon forming extensive hydrogen bond networks with it, the YxCxxxF motif participates in stabilising the flipped A1825 and forms the middle part of the pocket, and Thr32 of the GTS loop is responsible for closing the binding pocket near position 3 of the stop codon (Brown et al., 2015). Stop codon specificity is then granted through the interactions of these motifs with the codon. Hydrogen bonding by K63 of the NIKS motif selectively allows only codons initiating with a Uracil to bind, while the local rRNA architecture necessary to accommodate eRF1 and mRNA in the site would preclude purines due to size and cytosine would be destabilised. In the second position, stacking between A1825 and position 3 of the stop codon as well as Tyr of the YxCxxxF motif favours purines. Based on this model, E55 derived electrostatic interactions should reduce guanosine affinity for the site and favour adenine (Brown et al., 2015). The study used UAA(A) as the stalled stop codon, which may account for the decoding architecture specifically favouring adenine in position 2, given that E55 could adopt any rotameric conformation and ease the energy barrier for guanine. Finally, the third position in a UNR turn must always be a purine and position 4 stacks with G626 of the 18S RNA, stabilising the whole structure. (Brown et al., 2015).

*eRF3a*

eRF3a is a class 2 release factor which is not codon specific and enforces GTP dependence on this process, accelerating peptide release and increasing termination efficiency (Alkalaeva et al., 2006, Eyler and Green, 2011). In contrast to its prokaryotic counterparts, eRF3 GTPase activity requires the presence of eRF1 (Frolova et al., 1996). Binding of GTP-eRF3 to the termination complex likely occurs following binding of eRF1, as GTP-eRF3 exhibits significantly lower constant of dissociation when in the presence of the eRF1: ribosome complex (Pisareva et al., 2006), with eRF1 acting as a dissociation inhibitor. Overexpression of eRF1 is enough to promote efficient translational termination in the absence of eRF3a (Frolova et al., 1994), however *S. cerevisiae* viability is eRF3a dependent (Stansfield et al., 1995).

### 1.4.5 Aberrant Translation in Cancer

A role for translation in cancer has been indicated since the early days of cancer molecular biology. Specifically, cancer cells had been noted to exhibit increased rates of global protein synthesis (Johnson et al., 1976) along with increased ribosome abundance (Zetterberg et al., 1995) and recruitment of mRNAs unique to tumour cells in the polyribosomal assemblies (Getz et al., 1976).

Further work has concentrated primarily on the regulation of translation initiation in cancer. One of the best examined factors in that regard is the $m^7$G-cap binding eIF4 complex, whose abundance is rate limiting for translation (Gingras et al., 1999). Of the proteins participating in the complex, two have been specifically pinpointed as cancer relevant: eIF4e and eIF4g. Overexpression of eIF4e is by itself sufficient to reduce the doubling time and relieve contact inhibition in cell cultures and is associated with increased activity of the GTPase Activating Protein (GAP) Ras, a known oncogene (Kevil et al., 1996). Additionally, eIF4e expression is upregulated by the MYC oncogene (Rosenwald et al., 1999) and is required for MYC dependent transformation of primary mouse fibroblasts (Lazaris-Karatzas and Sonenberg, 1992). In accordance to its observed role *in vitro*, eIF4e expression is increased in breast, head and neck, colon and ovarian carcinoma (Li et al., 1997, Sorrells et al., 1999, Rosenwald et al., 1999, Noske et al., 2008). Similarly, eIF4g has been shown to be upregulated in squamous cell carcinoma, inflammatory breast cancer and naso-pharyngeal carcinoma (Brass et al., 1996, Silvera et al., 2009) (Tu et al., 2010).

Another initiation factor which has received interest with regards to its role in cancer is eIF3. Several of the subunits of eIF3 have been shown to be overexpressed in a number of malignancies, including breast, colon, prostate and lung (Chen and Burger,

2004, Goh et al., 2011, Pincheira et al., 2001). *In vitro*, ectopic overexpression of specific eIF3 subunits has been shown to promote cell growth and malignant transformation, while overexpression of others curtails cell proliferation (Zhang et al., 2007). The reason for this difference is not as of yet understood. However, it is notable that eIF3 has been recently shown to be capable of binding to mRNA transcripts of genes associated with cell cycling, growth, and differentiation. These include the proliferation regulators c-Jun and BTG1, and eIF3 can either activate or repress their translation depending on the type of RNA stem loop binding it (Lee et al., 2015).

Overexpression of the translation initiation factor eIF5A has also been observed in lung, pancreatic, colorectal and ovarian tumours and is associated with poor prognosis (Mathews and Hershey, 2015). Furthermore, induced overexpression of EIF5A has been shown to promote metastasis and tissue invasion via upregulating expression of the genes Metastasis Associated protein 1 (MTA1) and Matrix Metalloproteinase 2 (MMP2) in colorectal and gastric and liver cancer respectively (Zhu et al., 2012, Meng et al., 2015, Wang et al., 2014). eIF5A physiologically undergoes hypusination, a posttranslational modification that is catalyzed by deoxyhypusine synthase (DHS) and deoxyhypusine hydroxylase (DOHH) (Rossi et al., 2014, Landau et al., 2010) and is necessary for eIF5A to associate with ribosomes (Jao and Chen, 2006, Saini et al., 2009). Pharmacological obstruction of hypusination and knockdown of eIF5A has been shown to result in reduction of cell proliferation, motility and invasiveness (Memin et al., 2014, Zhu et al., 2012) as well as tumour growth *in vivo* (Fujimura et al., 2014).

Nevertheless, there are some evidence that the upregulation of eIFs in cancer is more complex than a shift to increased translation initiation, as indicated by the pattern of

eIF6 expression, eIF6 binds to free 60S ribosomal subunits and prevents their association with 40S subunits, effectively preventing translation from initiating (Miluzio et al., 2009). Surprisingly however, eIF6 is also upregulated in a variety of cancers, including acute promyelocytic leukemia, head and neck carcinomas, ovarian serous carcinomas and colorectal (Harris et al., 2004, Rosso Md et al., 2004, Flavin et al., 2008, Sanvito et al., 2000).

Another example of conflicting activities for a translation initiation factor is eIF2. Phosphorylation of the eIF2 subunit eIF2α by the kinase PERK results in a generally cytoprotective phenotype (Koromilas, 2015). However, the type, severity, and duration of the cellular stress can result in a pro-apoptotic phenotype (Koromilas and Mounir, 2013). Increased levels of PERK activity promote cancer cell survival but inhibit progression through the cell cycle, resulting in a quiescent tumour phenotype (Ranganathan et al., 2008). At the same time, PERK mediated phosphorylation of eIF2a is required for tumour growth and angiogenesis under hypoxia (Bi et al., 2005). Ectopic overexpression of a non-phosphorylatable S51A mutant promotes malignant transformation of NIH 3T3 cells (Donze et al., 1995), however inhibition of dephosphorylation results in sensitisation of cells to apoptosis (Teng et al., 2014).

Other than eIFs, a surprising new mechanism by which the process of translation can contribute to tumorigenesis and maintenance of cancer is by modulation the abundancies of specific tRNAs. Specifically, tRNAGluUUC and tRNAArgCCG have been characterized as promoting breast cancer metastasis by promoting translation of mRNA transcripts enriched for these codons, in this case EXOSC2 and GRIPA1 (Goodarzi et al., 2016). This would be in accordance with previous studies in mice, where substitution of rare codons with synonymous mutations in the KRAS oncogene reduced tumour prevalence following carcinogen exposure (Pershing et al., 2015).

In addition to the above, evidence has arisen over the years that mutations in ribosomal components, or modifiers thereof, have the capacity to promote tumourigenesis. An example of this is the X-linked Dyskeratosis Congenita (XDC), resulting in the inactivation of the conserved dyskerin enzyme, which catalyses the post transcriptional pseudouridylation of specific uridines in ribosomal RNA (rRNA) (Heiss et al., 1998). Among other pathophysiologies, XDC is associated with an increased malignancy risk, which has been linked to defects in translation of specific mRNAs, specifically including p53 mRNA, even though the overall volume of translation remains unperturbed (Montanaro et al., 2010). Furthermore, differential expression of specific ribosomal proteins has been observed in colorectal cancer, although this could be attributed to extra-ribosomal functions (Lai and Xu, 2007). With regard to the ribosomal RNA (rRNA) components of the ribosome, aggressively malignant cells have displayed increased synthesis of 45S pre-rRNA, with activation of an alternative pre-mRNA synthetic pathway containing a 43S precursor and enhanced post-transcriptional methylation of specific sites located in the 28S rRNA. Additionally, these changes in nucleolar appearance are associated with reduced translation efficiency of a number of mRNAs, prominently including p53 (Belin et al., 2009).

Changes in appearance and activity of the nucleolus, the site of ribosome biogenesis, have also been noted. Nucleolar hypertrophy and upregulation of ribosome production are common, though not universal, features of neoplastic cells (Derenzini and Trere, 1991) and nucleolar hypertrophy is considered a marker of poor prognosis (Derenzini et al., 2004). However significant variability in this attribute may be seen even within the same tumour, with the nucleolar changes strongly correlated with the number of proliferating cells within the tumour and the rapidity of cell division, attributes that

vary greatly among tumours (Derenzini and Trere, 1991). The increase in nucleolar size and ribosomal production rate is thought to be the result of changes in the activity of multiple well characterized oncogenes and tumour suppressor genes, including MYC, p53 and the Retinoblastoma Protein (pRb). For example, wild type p53 binds to the selectivity Factor 1 (SL1) protein, hindering the formation of the UBF-SL1 complex necessary for RNA polymerase I recruitment to the rRNA gene promoter and resulting in repression of RNA Pol I and reduced rRNA expression (Zhai and Comai, 2000). In contrast, c-Myc binds to consensus elements in the promoters of genes coding for rRNA and recruits SL1, enhancing transcription by RNA Pol I (Arabi et al., 2005).

There has been very little work on a potential role for translation termination and the associated factors in cancer. Certain alleles of eRF3a are found at higher frequencies among the breast cancer patient population compared to average, but those mutations are not associated with any apparent changes in termination efficiency (Malta-Vacas et al., 2009a). Additionally, while eRF3a levels are increased in a number of tumour types, this is not associated with changes in the total volume of translation in the cell (Malta-Vacas et al., 2009b). A potential role has been described for eRF1 as a tumour suppressor gene in acute myeloid leukemia (Dubourg et al., 2002). However this is unlikely to be true, as loss of the eukaryotic termination factor results in lethality (Blanchet et al., 2015). Finally, no role in cancer has been described for JMJD4 thus far.

## 1.5 Aim and Scope of this Thesis

As summarised through this Introduction, 2OG oxygenases have been implicated in a wide variety of fundamental cellular processes, and throughout the gene expression pathway. In general, the 2OG oxygenases involved in such processes have been relatively well characterised, their physiological relevance realised and, in several cases, a role in disease elucidated. In contrast, our understanding of the physiological importance of JMJD4 and its potential role in disease was far less clear. Similarly, compared to the processes of translational initiation and elongation, our understanding of termination is relatively poor, particularly with respect to cell biology, physiology and disease. Therefore, as part of this Thesis we intend to broaden our understanding of JMJD4 and its known binding partners, and to characterise the response of cells to defective translational termination. To this end, in Chapter 2, following previous work, we attempt to identify a potential novel interactor and target of JMJD4. In Chapter 3, the effects of JMJD4, HEMK2 and eRF1 on cell proliferation are examined. In Chapter 4, the transcriptional effects of defective translational termination are examined and potential pathways identified. Finally, in Chapter 5, the most promising of these transcriptional pathways are evaluated and their mechanism of regulation investigated.

# CHAPTER 2: Investigating Novel Binding Partners of JMJD4

## 2.1 Introduction

As described in the Introduction, JMJD4 was originally identified as a C-4 lysyl hydroxylase that targets K63 within the NIKS motif of the eukaryotic termination factor, eRF1 (Feng et al., 2014a). The proteomic screen which led to the discovery of eRF1 as a substrate of JMJD4 compared the binding of proteins co-immunoprecipitated from HEK293T cells overexpressing WT JMJD4 with a catalytically inactive H189A JMJD4, thus yielding a list of activity-dependent interactors (Figure 2.1). Other than eRF1, and its binding partner eRF3A, the screen identified several other candidate activity-dependent binding proteins, albeit at generally lower abundance (M. L. Coleman, personal communication). Of these, the General Transcription factor 2I (GTF2I, also known as TFII-I) was of interest and explored further here in this Chapter as a potential JMJD4 substrate.

| Protein | Description | Number of Peptides | Spectral Count |
|---|---|---|---|
| IPI00552715 | CCT3 T-complex protein 1 subunit gamma isoform c | 46 | 2 |
| IPI00103471 | GTF2I General transcription factor II-I, isoform 2 | 87 | 2 |
| IPI00429191 | ETF1 Eukaryotic peptide chain release factor subunit 1 (eRF1) | 33 | 206 |
| IPI00909083 | GSPT1 eukaryotic peptide chain release factor GTP-binding subunit ERF3A isoform 2 | 32 | 79 |
| IPI00031617 | C6orf125 Uncharacterized protein C6orf125 | 2 | 2 |
| IPI00647163 | TCEAL4 Isoform 2 of Transcription elongation factor A protein-like 4 | 3 | 5 |
| IPI00015671 | TUBAL3 Isoform 1 of Tubulin alpha chain-like 3 | 7 | 2 |
| IPI00219889 | UQCC Isoform 2 of Ubiquinol-cytochrome c reductase complex chaperone CBP3 homolog | 2 | 2 |
| IPI00001684 | ZNF180 Zinc finger protein 180 | 2 | 1 |
| IPI00011374 | FAM76A Isoform 4 of Protein FAM76A | 2 | 1 |
| IPI00219114 | DCTN1 Isoform p135 of Dynactin subunit 1 | 4 | 3 |
| IPI00549766 | FAM40A Isoform 1 of Protein FAM40A | 3 | 6 |
| IPI00297723 | RBM6 RNA-binding protein 6 | 4 | 2 |
| IPI00305698 | GGCX Vitamin K-dependent gamma-carboxylase | 3 | 2 |
| IPI00296909 | PARP4 Poly [ADP-ribose] polymerase 4 | 3 | 1 |

**Figure 2.1: List of potential activity dependent JMJD4 interacting proteins**. To identify potential JMJD4 substrates HEK293T cells stably expressing Empty Vector (EV) control, WT FLAG-JMJD4 or H189A FLAG-JMJD4 were subjected to immunoprecipitation using α-FLAG beads. The immunoprecipitates subsequently underwent tryptic cleavage and analysed using Liquid Chromatography-Mass Spectrometry (LC-MS/MS). The proteomic hits were cross-referenced with the human UniProt database through the use of the Mascot search engine. Since the H189A mutation ablates the iron binding site of JMJD4 and consequently its catalytic activity, proteins which bind to WT but not the H189A JMJD4 should be JMJD4 substrates. The list shown is of those proteins identified in the WT JMJD4 expressing cells alone. Spectral Count is the total number of fragmentation spectra that map to peptides of a given protein and can be used as a semiquantitative measure of protein abundance (reviewed in (Lundgren et al, 2010)). Experiment performed by Dr Mathew L. Coleman.

GTF2I is a 112kDa multifunctional transcription factor with 4 recorded isoforms that is involved in a rare developmental disorder known as Williams-Beuren syndrome, and is likely also involved in B-cell development via NF-kB regulation and c-Myc upregulation (Ashworth and Roy, 2007, Novina et al., 1999). GTF2I isoforms are not equivalent in role and in fact the nuclear localisation of isoforms 2 and 4 is mutually exclusive as they display opposing functions (Novina et al., 1999). Additionally, GTF2I has been shown to be a significant factor in embryonic heart and craniofacial development, at least partly through regulation of the TGFRII and VEGFR signal transduction cascades (Roy, 2012). GTF2I has been identified in the past to interact with the C-terminus of the breast and ovarian cancer associated Breast Cancer Type 1 susceptibility protein (BRAC1) (Tanikawa et al., 2011), making it of interest with respect to its potential association with JMJD4, which is upregulated in breast cancer (see Chapter 3). Here we test GTF2I as an activity-dependent JMJD4 interactor in order to investigate whether it, and by extension the other candidates presented in Figure 2.1, are potentially novel JMJD4 substrates.

## 2.2 Results

### 2.2.1 Subcellular distribution of JMJD4 and GTF2I

GTF2I is reported to be present in both the cell nucleus and the cytoplasm in an isoform specific manner (Roy, 2012). To examine which isoform JMJD4 would potentially interact with and hydroxylate, several cell lines were fractionated into cytoplasmic and nuclear samples and then Western Blotted for JMJD4, GTF2I as well as nuclear (histone H3) and cytoplasmic (tubulin) marker proteins. In all cell lines, JMJD4 was found to be exclusively cytoplasmic (Figure 2.2A). Bioinformatic analysis of predicted nuclear-associated sequences for JMJD4 further indicated that JMJD4 is likely to be restricted to the cytoplasm (Figure 2.2B). In contrast, the major pool of GTF2I was in the nuclear compartment of HeLa, A549, and SW620 cells. Interestingly, GTF2I was restricted to the cytoplasm of HEK293T cells (Figure 2.2A), which was the cell line in which the potential JMJD4:GTF2I association was first detected. This might suggest that, if physiologically relevant, JMJD4:GTF2I binding could be restricted to cell lines or tumours with cytoplasmic localisation of GTF2I.

A

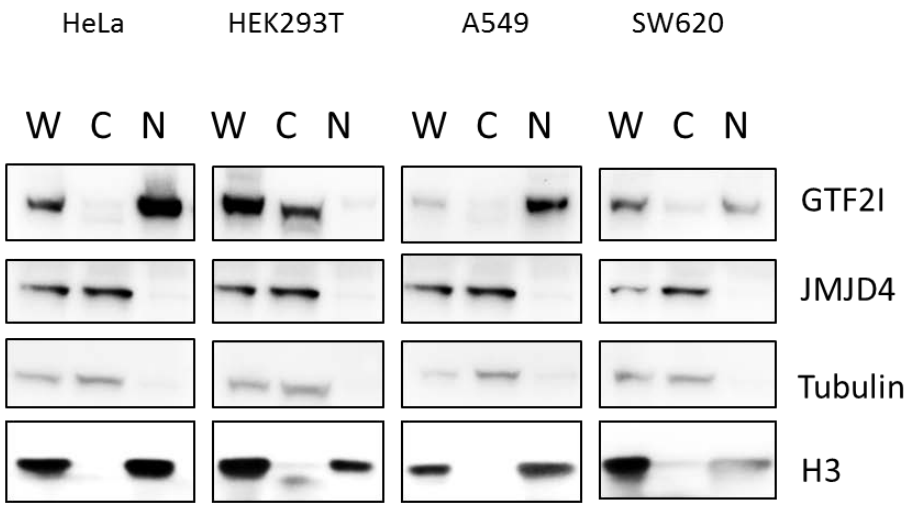


B

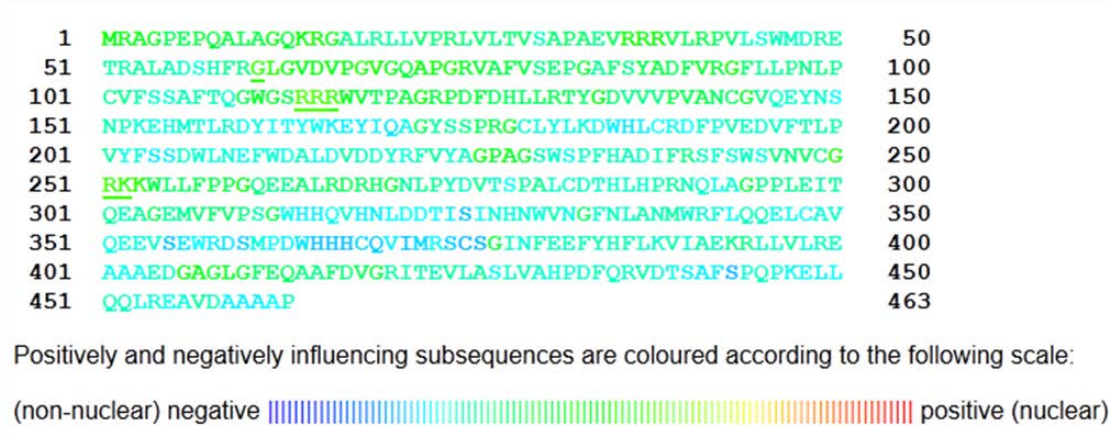


**Figure 2.2: JMJD4 and GTF2I subcellular distribution**: **A**: Cellular Fractionation of HeLa, HEK293T, A549 and SW620 followed by Western Blot of the whole cell lysate, the cytoplasmic and the nuclear fractions against JMJD4 and GTF2I. Tubulin is used as a marker of cytoplasmic material and histone H3 as a nuclear marker. (W=Whole cell Lysate, C=Cytoplasmic Fraction, N=Nuclear Fraction). **B**: NucPred prediction of the likelihood of nuclear localisation of JMJD4 based on its sequence (Brameier et al., 2007).

### 2.2.2 Examination of the GTF2I-JMJD4 association

Following the assessment of JMJD4 and GTF2I localisation, we proceeded to examine whether an interaction between the two proteins could be confirmed. Therefore, we initially attempted to replicate the conditions of the proteomic screen which identified GTF2I as a candidate substrate. Consequently, HEK293T FLAG-tagged wild type JMJD4 (WT-JMJD4) and catalytically inactive JMJD4 (H189A JMJD4) cell lines were analysed (cells provided by Dr Mathew L. Coleman) in a co-immunoprecipitation (IP) experiment. The cells were lysed and underwent immunoprecipitation using an α-FLAG antibody to precipitate JMJD4, followed by western blotting using an α-GTF2I antibody. Importantly, we found that we could detect a weak interaction between GTF2I and WT, but not H189A, JMJD4, under conditions in which the reported eRF1 interaction was also detected (Figure 2.3). Unfortunately however, we found that this interaction was unreliable and not detected in subsequent repetitions of the same experiment.

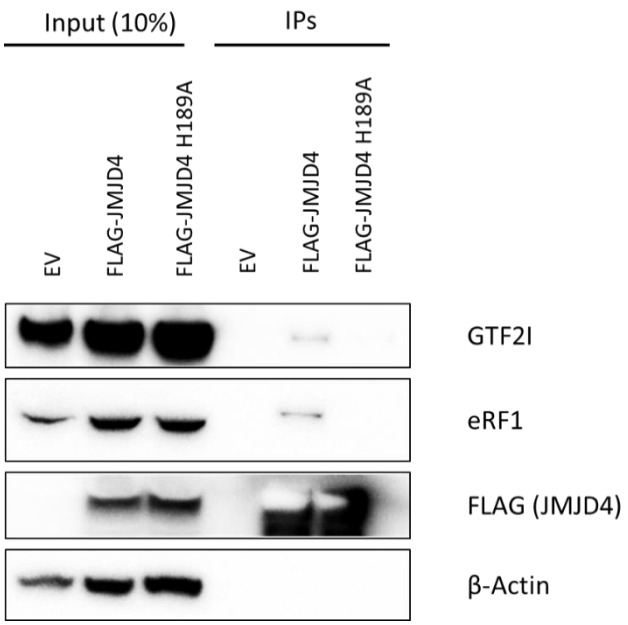


**Figure 2.3: Potential GTF2I and FLAG-JMJD4 interaction.** Assessment of endogenous GTF2I binding to EV, FLAG-JMJD4 and FLAG-JMJD4 H189A. The cells were lysed and subjected to α-FLAG (JMJD4) pulldown, prior to western blotting. 'Input' denotes whole cell extract (10%) prior to immunoprecipitation. This result suggests an interaction, which was not however found to be reliably reproducible.

The lack of reproducibility led us to consider whether the interaction might be weaker and/or more transient than eRF1. A cell permeable pan-2OG oxygenase inhibitor Dimethyloxalylglycine (DMOG) has been shown to stabilise the interaction of substrates with some 2OG-oxygenases (Rose et al., 2011). Therefore, we tested whether treating cells with DMOG enabled a JMJD4:GTF2I interaction to be detected. However, even in this context we were unable to detect an association between endogenous GTF2I and FLAG-JMJD4 (Figure 2.4).

As discussed earlier, different GTF2I isoforms have different subcellular distributions and properties. We considered the possibility that a JMJD4 interaction could be isoform specific, and that overexpression of GTF2I could enable an interaction to be reliably detected. Therefore, we proceeded to test binding of JMJD4 to both isoform 2

as well as full length GTF2I. Due to difficulties in cloning full-length *H. sapiens* GTF2I, *M. musculus* full length GTF2I was used instead. *M. musculus* GTF2I is highly similar to the human version, differing at only three of 998 residues and was therefore considered a reliable substitute.

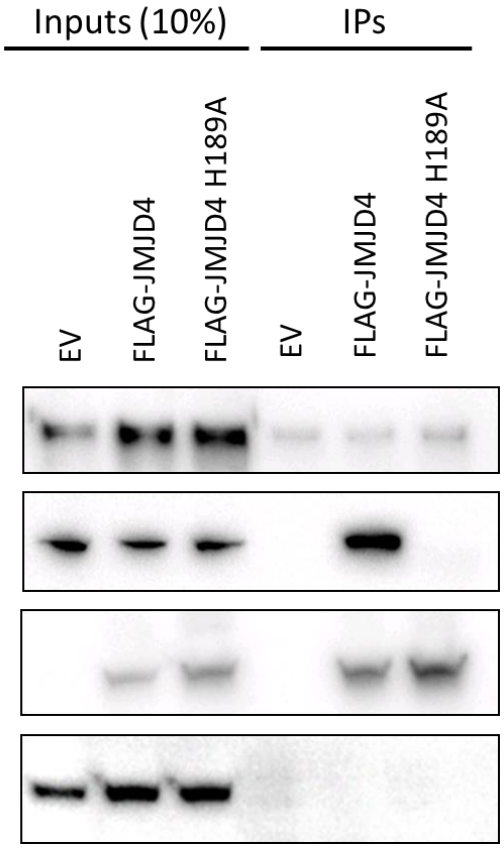


**Figure 2.4: DMOG treatment does not induce binding of GTF2I to JMJD4.** HEK293T EV, WT-JMJD4 and H189A JMJD4 cells were treated with 1 mM of the cell permeable 2OG Oxygenase inhibitor DMOG for 12h, after which they were lysed and used in α-FLAG IP. The known JMJD4 substrate eRF1 is used as a positive control. Any binding of GTF2I is non-specific.

HEK293T FLAG-JMJD4 cells were transfected with pCDNA3 'empty vector' (EV), a pCDNA3 plasmid expressing *M. musculus* full-length V5-Tagged GTF2I or a pCDNA3 plasmid expressing isoform 2 of the *H. sapiens* V5-Tagged GTF2I. The cells were allowed to rest for 48h, after which they were lysed and subjected to α-FLAG pulldown, followed by western blotting. Unfortunately however, even under those conditions, no interaction was observed with either GTF2I isoform (Figure 2.5).

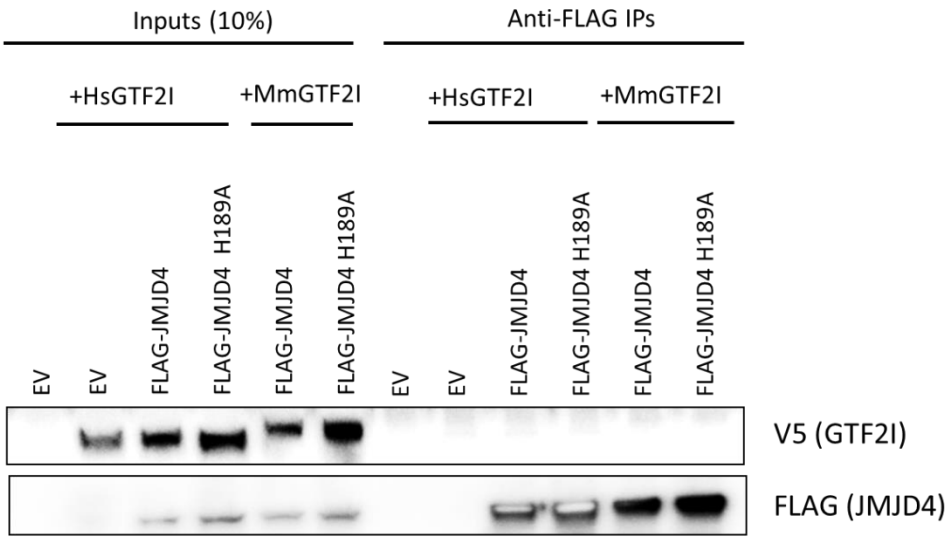


**Figure 2.5: No interaction of overexpressed GTF2I and FLAG-JMJD4.** Human isoform 2 (HsGTF2I) and full-length mouse GTF2I (MmGTF2I) were transfected into HEK293T EV, WT-JMJD4 or H189A-JMJD4 expressing cells, while one sample of HEK293T EV cells received no transfection and served as a negative control. The cells were lysed and subjected to α-FLAG pulldown and blotted for V5 (GTF2I) and FLAG (JMJD4). 'Input' denotes whole cell extract (10%) prior to immunoprecipitation. No binding is suggested by the data.

Next, we repeated the same experiment in an independent panel of JMJD4 stable cell lines where the JMJD4 protein was tagged with the HA epitope, rather than FLAG. Following 72h of transfection, cells were lysed and cell extracts immunoprecipitated

using anti-HA antibodies prior to western blotting. However, under these conditions we still failed to detect a JMJD4:GTF2I interaction (Figure 2.6).

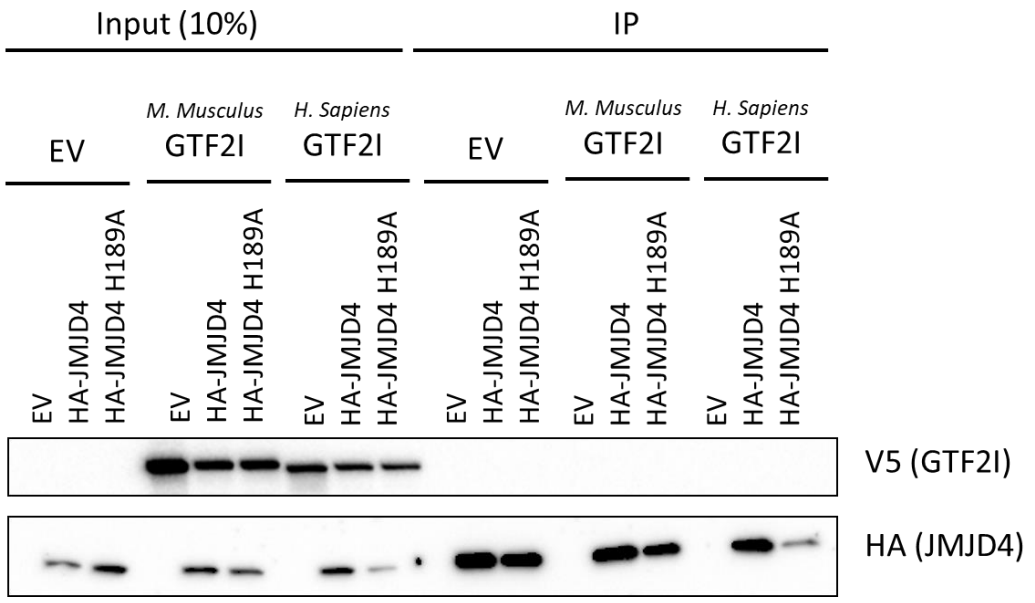


**Figure 2.6: Lack of GTF2I and HA-JMJD4 interaction.** pCDNA3 Empty Vector (EV), pCDNA3 HA-JMJD4 and pCDNA3 HA-JMJD4 H189A cells were transfected with either EV pCDNA3, pCDNA3 expressing *M. musculus* full length GTF2I, or pCDNA3 expressing *H. sapiens* GTF2I isoform 2. After 48h the cells were lysed and the lysate underwent α-HA pulldown. 'Input' denotes whole cell extract (10%) prior to immunoprecipitation. HA-JMJD4 shows no consistent interaction with V5-GTF2I

For hydroxylase substrates that are modified to >90% in the steady state, the pool of unhydroxylated material available for enzyme interaction is limited, which might prevent reliable detection. Therefore, we considered whether an interaction with JMJD4 might be more detectable using a pool of unhydroxylated GTF2I. To test this, we used an *in vitro* transcription/translation system to generate V5-tagged full length mouse GTF2I and isoform 2 of HsGTF2I. Importantly, these proteins were synthesised in the presence of the non-hydrolysable 2OG competitive inhibitor N-Oxalylglycine (NOG), in order to prevent hydroxylation by the endogenous rabbit JMJD4 (as described in Feng et al, 2014). Samples were then incubated with FLAG-

JMJD4 in the presence of NOG to potentiate enzyme: substrate interactions. Although GTF2I was detected in the FLAG-JMJD4 immunoprecipitates (Figure 2.7), it was also present in control MmGTF2I samples without FLAG-JMJD4, indicating non-specific pulldown. Overall, therefore, no interaction between JMJD4 and GTF2I could be reliably detected, despite using a variety of *in vitro* and *in vivo* approaches. Taken together these data suggest that GTF2I is unlikely to be a *bona fide* JMJD4 substrate.

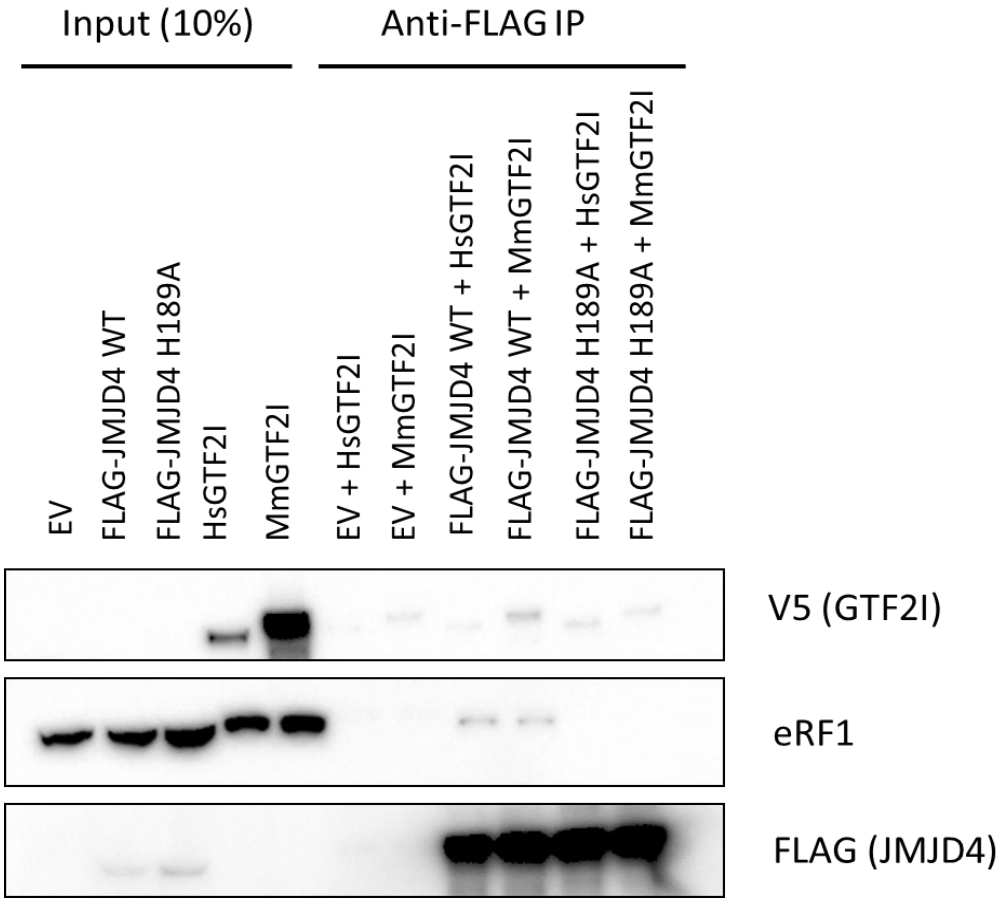


**Figure 2.7: Examination of GTF2I and FLAG-JMJD4 using an *in vitro* Transcription/Translation (IVTT) system.** HsGTF2I and MmGTF2I correspond to the IVTT preparations using *Homo sapiens* isoform 2 and *Mus musculus* full length GTF2I respectively. Samples of HsGTF2I and MmGTF2I were incubated with whole cell lysate from EV, WT and H189A HEK293T in the presence of NOG and then FLAG-IP was performed. 'Input' denotes whole cell extract (10%) prior to immunoprecipitation. Any binding of GTF2I is non-specific.

### 2.2.3 Mass spectrometry fails to identify JMJD4-dependent hydroxylation sites on GTF2I

Parallel to the interaction experiments described in section 2.2.2, we attempted to directly examine GTF2I for post-translational modifications using mass spectrometry. To this end, HEK293T EV and FLAG-JMJD4 cells were each transfected with either empty vector plasmid, or *H. sapiens* V5-GTF2I. After 24h the cells were harvested and immunoprecipitated overnight using α-V5 beads and purified immunocomplexes electrophoresed in a polyacrylamide gel. The relevant band was excised (Figure 2.7A) and submitted for mass spectrometry at the Target Discovery Institute, University of Oxford.

Prior to mass spectrometry, samples underwent in-solution digest using either Trypsin or Elastase. Because these two proteases have different cleavage specificities this approach reduces the possibility that any modified peptides are not detected because of incomplete sequence coverage. The method of mass spectrometric analysis of the peptides was similar to that previously reported (Savitski and Savitski, 2010). In this approach, standard database identification of peptides is followed by a search for peptides of similar mass/charge (m/z) ratio and likely similar composition. These peptides are likely to be modified and the specific modification can be determined assuming high mass accuracy of peptide fragment measurements. Unmodified peptides were specifically compared against likely modified ones for four specific post-translational modifications: carbamidomethylation (+57.02 m/z), deamidation (+0.98 m/z) ubiquitination (+114.04 m/z) and hydroxylation (+15.99 m/z ratio). Of these, only potential hydroxylation sites will be discussed.

A

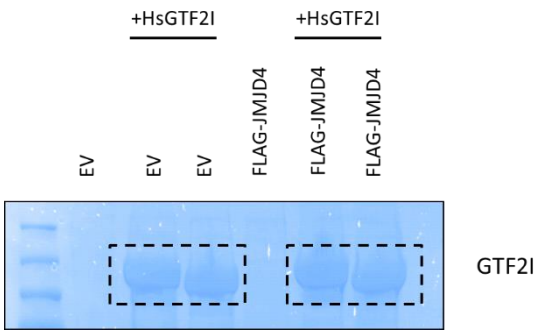


B

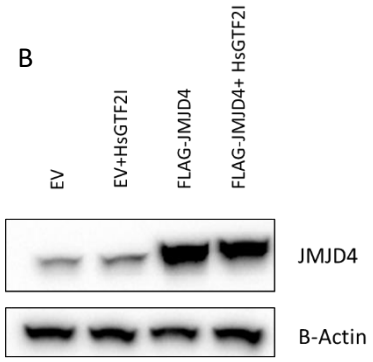


C

| Accession | -10lgP | Coverage (%) | #Peptides | #Unique | PTM | Avg. Mass | Description |
|---|---|---|---|---|---|---|---|
| P78347\|GTF2I_HUMAN | 271.56 | 95 | 944 | 943 | Y | 112416 | General transcription factor II-I |
| P04264\|K2C1_HUMAN | 139.94 | 51 | 52 | 41 | N | 66039 | Keratin, type II cytoskeletal |
| P35527\|K1C9_HUMAN | 132.1 | 48 | 36 | 36 | Y | 62064 | Keratin, type I cytoskeletal |
| Q9UNI1\|CELA1_HUMAN | 104.3 | 42 | 21 | 21 | Y | 27798 | Chymotrypsin-like elastase family member 1 |
| Q66K89\|E4F1_HUMAN | 96.14 | 28 | 25 | 25 | Y | 83496 | Transcription factor E4F1 |

D


**Figure 2.8: Mass spectrometric analysis of post translational modifications of GTF2I.** HEK293T EV and WT-JMJD4 cells were transfected with isoform 2 of *H. sapiens* GTF2I for 24h. Subsequently the proteins were IPed, separated on a standard polyacrylamide gel and the band corresponding to GTF2I in size submitted for mass spectrometry. A) Coomassie gel of samples analysed via mass spectrometry. Excised bands are indicated. B) Western Blot validation of JMJD4 expression in the cell extracts prior to IP C) Table of top 5 identified proteins in mass spectrometry sample. -10logP indicates the probability of correct assignment. Coverage (%) is the percent of the total protein length for which corresponding peptides were found. #Peptides indicates the number of total peptides assigned to the protein in question. #Unique indicates the number of peptides which can be uniquely assigned to that protein. PTM indicates if post translational modifications were found in any of the uniquely assigned peptides. D) Representative example of post-translational modification search in *H. sapiens* GTF2I using mass spectrometry. The sequence of GTF2I is indicated via single letter code, with the corresponding matched peptides in blue. Post-translational modifications are indicated on their likely position on the peptide.

A

| | HEK293T EV | | | HEK293T FLAG-JMJD4 | | | |
|---|---|---|---|---|---|---|---|
| **Residue** | Peptides Modified | Peptides Total | Relative Abund. | Peptides Modified | Peptides Total | Relative Abund. | Fold Change |
| ***K94*** | *5* | *20* | *0.25* | *5* | *16* | *0.31* | *1.25* |
| **N100** | 6 | 24 | 0.25 | 9 | 25 | 0.36 | 1.44 |
| **K140** | 8 | 58 | 0.14 | 5 | 27 | 0.19 | 1.34 |
| **D144** | 11 | 48 | 0.23 | 10 | 25 | 0.40 | 1.75 |
| **N355** | 8 | 30 | 0.27 | 8 | 29 | 0.28 | 1.03 |
| **K456** | 4 | 38 | 0.11 | 3 | 25 | 0.12 | 1.14 |
| **K561** | 4 | 50 | 0.08 | 5 | 43 | 0.12 | 1.45 |

B

| | HEK293T EV | | | HEK293T FLAG-JMJD4 | | | |
|---|---|---|---|---|---|---|---|
| **Residue** | Peptides Modified | Peptides Total | Relative Abund. | Peptides Modified | Peptides Total | Relative Abund. | Fold Change |
| ***K35*** | *3* | *10* | *0.30* | *2* | *6* | *0.33* | *1.11* |
| ***K94*** | *5* | *20* | *0.25* | *5* | *16* | *0.31* | *1.25* |
| **N100** | 6 | 24 | 0.25 | 9 | 25 | 0.36 | 1.44 |
| **R101** | 16 | 30 | 0.53 | 10 | 28 | 0.36 | 0.67 |
| **N252** | 7 | 20 | 0.35 | 6 | 21 | 0.29 | 0.82 |
| **N355** | 8 | 30 | 0.27 | 8 | 29 | 0.28 | 1.03 |
| **N565** | 13 | 50 | 0.26 | 7 | 44 | 0.16 | 0.61 |
| **R567** | 11 | 43 | 0.26 | 5 | 33 | 0.15 | 0.59 |
| **N727** | 3 | 9 | 0.33 | 4 | 8 | 0.50 | 1.50 |
| **P808** | 12 | 20 | 0.60 | 9 | 17 | 0.53 | 0.88 |
| **D907** | 3 | 7 | 0.43 | 1 | 3 | 0.33 | 0.78 |
| **P996** | 10 | 29 | 0.34 | 6 | 25 | 0.24 | 0.70 |

**Figure 2.9: Potential hydroxylation sites in *H. sapiens* GTF2I identified by unbiased mass spectrometry in the Elastase digested HEK293T and HEK293T FLAG-JMJD4 samples.** The GTF2I hydroxylation sites for HEK293T EV and HEK293T FLAG-JMJD4 cells were identified and the modified as well as total peptides for each of the sites counted and used to calculate a crude measure of PTM abundance (denoted as Relative Abundance (*Relative Abund.*) here). *Relative Abundance=Peptides Modified/Peptides Total* detected for those peptides in which the specific residue in question was included. *Fold Change=Relative Abundance FLAG-JMJD4/EV*. A) Table of the GTF2I residues exhibiting an increase in hydroxylation (Tryptic Digest). A lower limit of 4 modified peptides detected was set for consideration. B) Table of the GTF2I residues exhibiting the greatest basal hydroxylation. A lower limit of 25% modification in the EV cells was set for the residues to be considered. Lysyl residues in italics.

A

| Residue | HEK293T EV | | | HEK293T FLAG-JMJD4 | | | |
|---|---|---|---|---|---|---|---|
| | Peptides Modified | Peptides Total | Relative Abund. | Peptides Modified | Peptides Total | Relative Abund. | Fold Change |
| ***K171*** | *5* | *28* | *18* | *5* | *23* | *22* | *1.22* |
| **N355** | 6 | 15 | 40 | 6 | 13 | 46 | 1.15 |
| **R462** | 4 | 26 | 15 | 5 | 26 | 19 | 1.25 |
| **P808** | 6 | 11 | 55 | 5 | 9 | 56 | 1.02 |
| **P889** | 9 | 19 | 47 | 11 | 21 | 52 | 1.11 |
| **P996** | 4 | 11 | 36 | 6 | 14 | 43 | 1.18 |

B

| Residue | HEK293T EV | | | HEK293T FLAG-JMJD4 | | | |
|---|---|---|---|---|---|---|---|
| | Peptides Modified | Peptides Total | Relative Abund. | Peptides Modified | Peptides Total | Relative Abund. | Fold Change |
| ***K35*** | *2* | *3* | *0.67* | *2* | *3* | *0.67* | *1.00* |
| ***K92*** | *2* | *7* | *0.29* | *3* | *10* | *0.30* | *1.05* |
| ***K94*** | *2* | *4* | *0.50* | *2* | *4* | *0.50* | *1.00* |
| **P137** | 3 | 9 | 0.33 | 2 | 8 | 0.25 | 0.75 |
| **D227** | 3 | 11 | 0.27 | 3 | 10 | 0.30 | 1.10 |
| **N355** | 6 | 15 | 0.40 | 6 | 13 | 0.46 | 1.15 |
| **D471** | 3 | 9 | 0.33 | 4 | 10 | 0.40 | 1.20 |
| **P655** | 7 | 16 | 0.44 | 6 | 17 | 0.35 | 0.81 |
| **N727** | 4 | 10 | 0.40 | 4 | 11 | 0.36 | 0.91 |
| **P808** | 6 | 11 | 0.55 | 5 | 9 | 0.56 | 1.02 |
| **P889** | 9 | 19 | 0.47 | 11 | 21 | 0.52 | 1.11 |
| **P901** | 3 | 11 | 0.27 | 3 | 12 | 0.25 | 0.92 |
| **D907** | 6 | 12 | 0.50 | 4 | 13 | 0.31 | 0.62 |
| **P996** | 4 | 11 | 0.36 | 6 | 14 | 0.43 | 1.18 |

**Figure 2.10: Potential hydroxylation sites in *H. sapiens* GTF2I identified by unbiased mass spectrometry in the Trypsin digested HEK293T and HEK293T FLAG-JMJD4 samples.** The GTF2I hydroxylation sites for HEK293T EV and HEK293T FLAG-JMJD4 cells were identified and the modified as well as total peptides for each of the sites counted and used to calculate a crude measure of PTM abundance (denoted as Relative Abundance (*Relative Abund.*) here). *Relative Abundance=Peptides Modified/Peptides Total* detected for those peptides in which the specific residue was included. *Fold Change=Relative Abundance FLAG-JMJD4/EV*. A) Table of the GTF2I residues exhibiting an increase in hydroxylation (Tryptic Digest). A lower limit of 4 modified peptides detected was set for consideration. B) Table of the GTF2I residues exhibiting the greatest basal hydroxylation. A lower limit of 25% modification in the EV cells was set for the residues to be considered. Lysyl residues in italics.

Following mass spectrometry, the potential hydroxylation sites were compared between the EV and FLAG-JMJD4 overexpressing cells. We predicted that any site showing partial modification in HEK293T EV cells should be more completely modified in the HEK293T FLAG-JMJD4 cells. Specifically, based on previous examples, overexpression of the candidate substrate results in 10-25% hydroxylation on a physiological site (e.g. Feng *et al*, 2014), with overexpression of the 2OG oxygenase increasing the prevalence of the modification to >90%. Accurate quantification of peptide modification usually relies on comparing the abundance of eluted peptides by liquid chromatography MS (LC-MS), which requires detailed analyses of raw data. However, for the purposes of quickly screening the data for candidate hydroxylation sites we used a crude measure of modified peptide abundance by comparing the number of times the modified and unmodified peptides were sequenced in each sample, which we express here as an approximate percentage. Although a large number of such sites could be identified in the elastase digest data (Figure 2.9), only two of these sites, R101 and P808, appeared to be >50% hydroxylated in either of the samples tested. Neither of these however showed an increase in hydroxylation during overexpression of FLAG-JMJD4 and both are residues atypical of JMJD4, which is a lysyl hydroxylase. The greatest increases in apparent hydroxylation were observed at D144 and K561, which however still exhibited low relative abundance, at 40% and 12% modified/unmodified peptides under JMJD4 overexpression. Furthermore, neither of these sites replicate under tryptic digest of the sample (Figure 2.10A).

The fold increase in hydroxylation of specific GTF2I residues was even more modest in the trypsin treated samples (Figure 2.10). This dataset included three peptides with over 50% hydroxylation: K35, K94, and P808 as before. The greatest increase

observed is in R462, where hydroxylation apparently increased by just 25% (Figure 2.10A). However, none of these sites experienced a significant increase in hydroxylation upon overexpression of JMJD4. Overall, our mass spectrometry analysis failed to identify an abundant and reliable JMJD4-dependent hydroxylation site that warranted further investigation. Together with the negative interaction data presented above we therefore conclude that GTF2I is unlikely to represent a *bona fide* JMJD4 substrate.

### 2.2.4 JMJD4 potentially binds to the TCP-1 chaperone

During the course of the interaction experiments described above, we routinely observed a prominent Ponceau-staining band specifically co-precipitating with FLAG-JMJD4 in an activity-*independent* manner, i.e. binding was detected equally to both the wild type and the H189A mutant. Coomassie staining of batch-scale FLAG-JMJD4 immunoprecipitates identified two major bands, located at ~50 and ~65 kDa (Figure 2.11A). These bands were excised, washed and subject to trypsinolysis prior to LC-MS/MS based identification. The 50 kDa band was confirmed as full length JMJD4, as expected. Interestingly, the 65 kDa band contained subunits of T-complex protein 1 (TCP-1), a member of the Chaperonin Containing TCP-1 Complex (CCT) (Figure 2.11). One of the most abundant CCT subunits in the WT and H189A expressing HEK293T cells was TCP1-γ, which was also detected in the original JMJD4 proteomic screen (Figure 2.1).

A

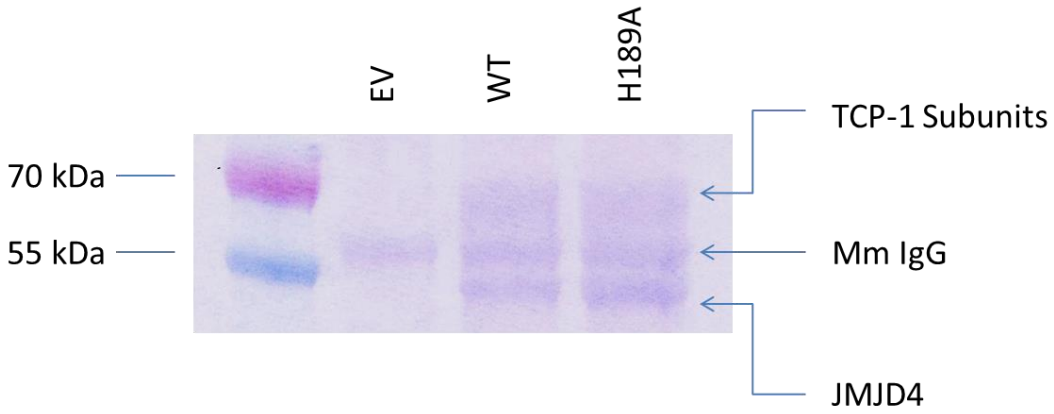


B

| Accession | Description | Score | Coverage |
|---|---|---|---|
| P17987 | T-complex protein 1 subunit alpha OS [TCPA_HUMAN] | 18.51 | 11.87 |
| P49368 | T-complex protein 1 subunit gamma OS [TCPG_HUMAN] | 17.81 | 13.94 |
| B7ZAR1 | T-complex protein 1 subunit epsilon [B7ZAR1_HUMAN] | 159 | 12.52 |
| B4DQH4 | T-complex protein 1 subunit theta OS [B4DQH4_HUMAN] | 6.11 | 11.37 |
| B7Z712 | 60 kDa heat shock protein, mitochondrial OS [B7Z712_HUMAN] | 5.55 | 15.82 |

C

| Accession | Description | Score | Coverage |
|---|---|---|---|
| Q99832 | T-complex protein 1 subunit gamma OS [TCPG_HUMAN] | 428.58 | 62.98 |
| P17987 | T-complex protein 1 subunit alpha OS [TCPA_HUMAN] | 3534 | 73.02 |
| P48643 | T-complex protein 1 subunit epsilon OS [TCPE_HUMAN] | 345.17 | 77.63 |
| P78371 | T-complex protein 1 subunit beta OS [TCPB_HUMAN] | 331.98 | 68.41 |
| P49368 | T-complex protein 1 subunit eta OS [TCPH_HUMAN] | 325.02 | 64.22 |

**Figure 2.11: Overexpressed FLAG-JMJD4 co-immunoprecipitates with T-complex proteins, including TCP1-γ.** A) Coomassie gel of immunoprecipitate following polyacrylamide gel electrophoresis. The Mm IgG band corresponds to the anti-FLAG antibody used for the IP. The FLAG-JMJD4 is visible at the bottom. The TCP-1 band is composed of multiple subunits, listed in the tables B&C. B) Table of top 5 proteins identified by LC-MS/MS in the 65kDa band of WT-JMJD4 overexpressing cells. Score is short for Binomial Peptide Score, a peptide score based on the cumulative binomial probability that the observed match is a random event. The value of the Binomial Peptide score heavily depends on the data scored, but usually scores above 50 indicate a good match. Coverage indicates the percentage protein sequence covered by peptides unique to the protein. C) Table of top 5 proteins identified by LC-MS/MS in the 65kDa band of H189A-JMJD4 overexpressing cells.

In order to independently confirm binding of TCP1-γ to JMJD4, HEK293T EV, WT-JMJD4 and H189A JMJD4 cells were lysed and subjected to α-FLAG pulldown, followed by Western Blotting. We observed that TCP1-γ co-immunoprecipitates with FLAG-tagged JMJD4 in both WT and H189A-JMJD4 (Figure 2.12A), confirming the previous observation that TCP1-γ appears to interact with JMJD4 in an activity-independent manner.

Next, we wished to determine whether endogenous TCP1-γ also interacts with the endogenous JMJD4 enzyme. We aimed to immunoprecipitate endogenous JMJD4 using a previously validated monoclonal antibody. However, it was not known whether this JMJD4 antibody was capable of successfully co-precipitating TCP1-γ. Therefore, we first immunoprecipitated JMJD4 from cell extracts derived from stable FLAG-JMJD4 cells where the interaction was shown to exist previously. As a negative control, one set of samples from the EV cells was immunoprecipitated using beads coated with an anti-p53 antibody. In those samples no JMJD4 pulldown should be observed. Although the anti-JMJD4 antibody was able to immunoprecipitate some TCP1-γ in complex with FLAG-JMJD4 (Figure 2.12B), the level of JMJD4 enrichment was modest compared to that observed by anti-FLAG immunoprecipitation (Figure 2.12A). The amount of co-purified TCP1-γ was correspondingly lower. Immunoprecipitation from EV cells purified a minor amount of endogenous JMJD4, and no TCP1-γ was detected. As expected, a similar experiment conducted in extracts from cells treated with DMOG failed to improve the outcome, with no detectable JMJD4:TCP1-γ interaction (Figure 2.12C). Although the current results may not be consistent with a strong and constitutive endogenous JMJD4:TCP1-γ interaction, it cannot be ruled out that the anti-JMJD4 antibody, in addition to being relatively inefficient at immunoprecipitation, may also (partially)

interfere with the interaction. However, considering these uncertainties, and the lack of a more positive and reliable endogenous interaction with the currently available reagents, it was decided not to pursue this further.

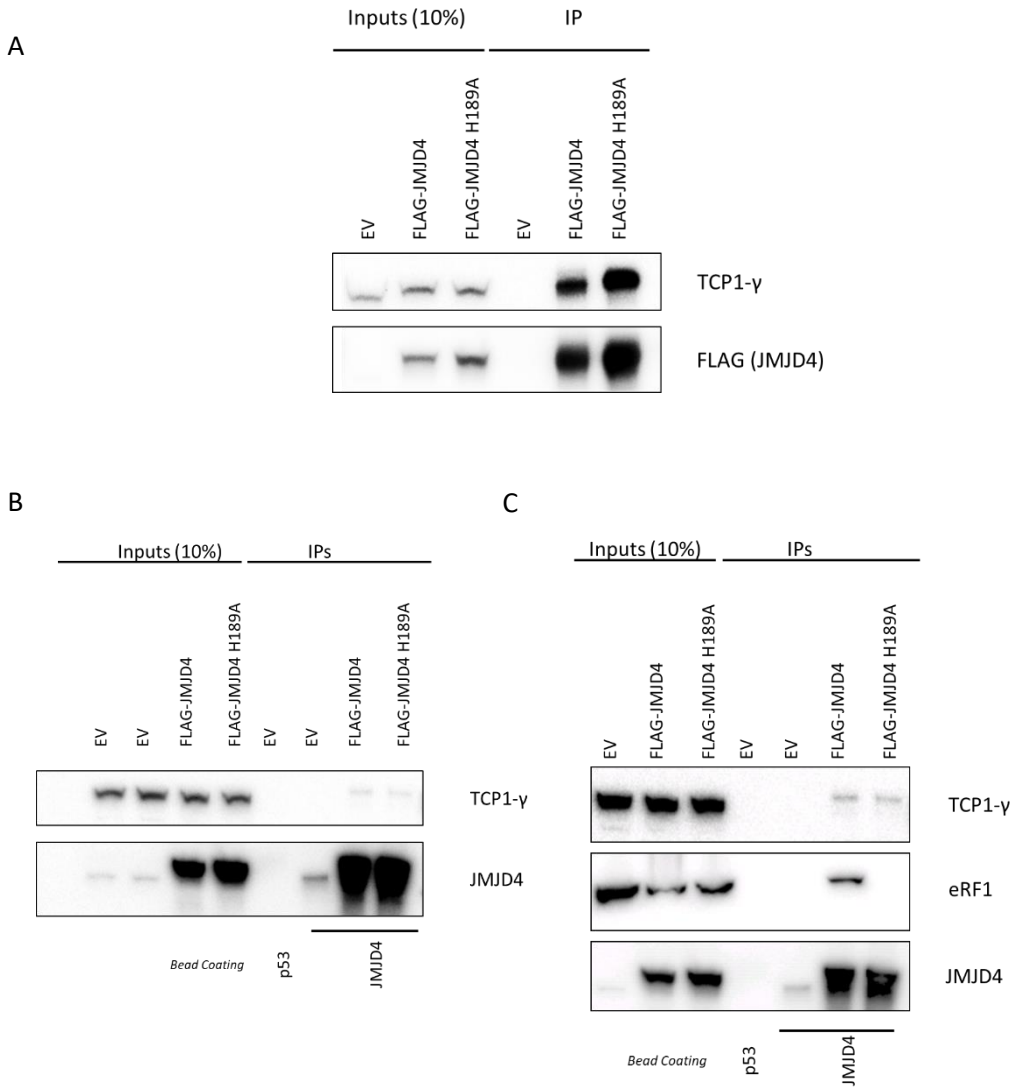


**Figure 2.12: TCP1-γ binds to overexpressed but not endogenously expressed JMJD4.** A) Western Blot of immunoprecipitate following polyacrylamide gel electrophoresis. TCP1-γ binds to overexpressed JMJD4. B) Co-IP of TCP1-γ. HEK293T EV, WT-JMJD4, or H189A JMJD4 cells were lysed and subject to pulldown using α-JMJD4 or α-p53 (negative control) coated beads. The immunocomplexes were subsequently electrophoresed and blotted for using α-JMJD4 and α-TCP1-γ antibodies. No significant binding of TCP1-γ to endogenous JMJD4 can be found. C) Co-IP of TCP1-γ under DMOG. HEK293T EV, WT-JMJD4, or H189A JMJD4 cells were treated with 1 mM of the cell permeable 2OG oxygenase inhibitor DMOG before being lysed lysed and subject to pulldown using α-JMJD4 or α-p53 (control) coated beads in buffer which contained the 2OG-Oxygenase inhibitor NOG. No significant binding of TCP1-γ to endogenous JMJD4 can be found.

## 2.3 Discussion

In this series of experiments, we attempted to discover novel proteins interacting with JMJD4. As such, we have demonstrated that FLAG-JMJD4 is co-immunoprecipitated with subunits of the TCP-1 complex, principally alpha, gamma, epsilon and theta. Significantly, the proteomic screen which identified eRF1 also identified the TCP-1 subunit gamma, although as an activity-dependent interactor (Figure 2.1), which was not observed in subsequent experiments. The TCP-1 subunits combine to form heteroligomeric rings composed of 8 subunits which are then stacked on top of each other to form the CCT complex. The CCT complex acts as an ATP dependent protein chaperone, whose activity is essential for the folding of highly expressed cytoskeletal proteins such as actin and tubulin (Brackley and Grantham, 2009). The protein folding capacity of the TCP-1 chaperone makes it possible that the observed association is the result of an overabundance of misfolded FLAG-JMJD4 from the expression constructs used. Indeed, JMJD4 has been predicted to have significant structural disorder (Figure 2.2B), making it possible that association with the chaperone is necessary for JMJD4 activity by stabilising its conformation. Furthermore, the apparently stoichiometric nature of the interaction with overexpressed JMJD4 (Figure 2.12A), under conditions in which JMJD4 is known to be active (Feng et al., 2014a) and interacting with its substrate eRF1 (Figure 2.4 and 2.12C), may be consistent with a physiologically relevant interaction. Interestingly, isolated JMJD4 only has modest activity *in vitro* (Dr Mathew Coleman, Personal Communication). Therefore, it is interesting to speculate that JMJD4 requires an obligate binding partner for activity. We are interested in the possibility that such a function could be mediated by the TCP-1 complex. This would not be the first time that such an interaction was

observed; the TCP-1 complex and the PHD3 hydroxylase have been previously shown to interact, with a possible role in regulating PHD3 function and enzyme targeting (Masson et al., 2004). Nevertheless, an endogenous interaction between JMJD4 and TCP1-γ could not be confirmed (Figures 2.12B&C). However, it remains possible that endogenous JMJD4 interacts with TCP1-γ but that the signal strength was consistently too low to detect, potentially due to the limitations of currently available reagents. Even if TCP1-γ only binds to overexpressed JMJD4 however, this activity could become significant under conditions where endogenous JMJD4 expression is significantly upregulated, as is the case in several tumour types, as analysed in the next chapter.

At the beginning of this Chapter we characterised GTF2I as a candidate JMJD4 substrate. We investigated an interaction between the two proteins by immunoprecipitation, using stable HA- or FLAG-tagged JMJD4 cell lines and under a range of conditions including both endogenous and overexpressed GTF2I and *in vitro* experiments. However, we were unable to reliably detect an interaction in any of the models used. Therefore, we conclude that, despite its identification in a former proteomics screen, GTF2I cannot be supported as a substrate of JMJD4. Consistent with this conclusion, GTF2I and JMJD4 localisation and protein expression appear to be largely independent of each other (Figure 2.2). Furthermore, mass spectrometry analysis of GTF2I post-translational modifications failed to identify any convincing JMJD4-dependent hydroxylation sites. Several residues were detected with apparently high levels of JMJD4-*independent* hydroxylation however, the most prominent of which, P808, was shared between the tryptic and elastase digest preparations. It is possible that this site is hydroxylated, perhaps by a related enzyme with prolyl hydroxylase activity. The modification site surrounding P808 (FIIKKP) is quite

dissimilar to the LxxLAP sequence recognised by the well characterised HIF prolyl hydroxylases PHD1-3 (Huang et al., 2002) and also the poly-Pro or PPG sequences preferred by collagen prolyl hydroxylases (Myllyharju, 2003), indicating that neither of these gene families are likely to catalyse this hydroxylation.

Here in this Chapter we have examined two potential new JMJD4 interactors, GTF2I and TCP1-γ. Although the known interaction of eRF1 with JMJD4 was also observed here, neither GTF2I nor TCP1-γ could be confirmed as physiologically relevant substrates or interactors. Possessing a single substrate is not impossible among 2OG-oxygenases. As discussed in the Introduction, some other closely related oxygenases involved in translation (e.g. NO66) have thus far only been reported to have a single substrate. While it is possible that other JMJD4 targets exist, it may be less likely that they are as abundant or as physiologically relevant as eRF1. Therefore, we switched our focus to examining the role of JMJD4 and eRF1 in growth control and cancer, and to exploring the cellular response to defective translational termination.

# CHAPTER 3: The role of JMJD4 and eRF1 in cell growth and stop codon readthrough

## 3.1 Introduction

The process of translation is fundamental in gene expression and as such it plays a major role in cell growth and a variety of diseases. With respect to cancer, research has primarily focused on the deregulation of translational initiation and elongation (Spilka et al., 2013), particularly the role of the elongation Initiation Factors (eIFs) in driving tumour growth (Dong and Zhang, 2006). While initiation and elongation have been widely examined however, the role and effects of translational termination and associated factors have been relatively poorly characterised. Studies in yeast indicate a role for the yeast orthologue of eRF1, Sup45p, in growth and invasion (Petrova et al., 2015). Furthermore, depletion of the eRF1 associated factor eRF3A in HCT116 cells has been shown to result in G1 cell cycle arrest (Chauvin et al., 2007). Whether eRF1 depletion induces a similar phenotype in human cells is not known. However, knockdown of the eRF1 glutamine methyltransferase HEMK2 results in a moderate reduction of growth *in vitro* and mouse embryonic lethality *in vivo*, consistent with important roles in cellular homeostasis and embryonic development (Liu et al., 2010). Whether other important eRF1 post-translational modifiers and regulators, such as JMJD4, also regulate normal growth and development is unclear. Furthermore, whether these factors support tumourigenesis, similar to initiation and elongation factors, is not known. Specifically, no work has been performed regarding any potential importance of JMJD4 in cancer.

Here, we wished to explore the potential role of eRF1 and JMJD4 in cancer, by assessing alterations and deregulated expression in cancer databases, and the effect of their inhibition on tumour cell growth. Subsequently, we engineered cell line models for conditional shRNA-mediated knockdown of JMJD4 and eRF1. These models were validated by first confirming the reported effects of eRF1 and JMJD4 depletion on translational termination (Feng et al., 2014a). We then applied these models to explore the role of eRF1 and JMJD4 in the growth of tumour cell lines in both 2D and 3D assays, and extend our findings into independent cell lines, knockdown approaches and termination assays. Finally, we establish a new cell model of inducible siRNA-resistant eRF1 mutants in order to perform structure-function analyses of eRF1 in tumour cell growth.

## 3.2 Results

### 3.2.1 Cancer Bioinformatics

To begin to explore the potential importance of translational termination in cancer, we initially examined the prevalence of amplifications, deletions and mutations in genes encoding eRF1 and its modifier JMJD4, using the tumour sequencing database cBioPortal (Gao et al., 2013). We find that significant amplification of eRF1 was only detected in two studies, Neuroendocrine Prostate Cancers (NEPC; 15%) and Clear Cell Renal Carcinomas (ccRCC, 5-14% depending on the study) (Figure 3.1A), suggesting that amplification of the eRF1 gene is not a common occurrence in all cancer types. To explore whether eRF1 expression may be deregulated by other mechanisms we next explored its mRNA levels in normal versus cancer samples using the Oncomine database (Rhodes et al., 2004). Interestingly, a statistically significant, but modest, increase in eRF1 mRNA levels was observed in a wide variety of tumour types (see Figure 3.2 for examples). Next, we undertook similar analyses for JMJD4, observing JMJD4 gene amplification in a variety of tumour types, including breast (4-14%, depending on the study stage), liver (12%), lung (8%) and uterine (5%) (Figure 3.1A). Furthermore, JMJD4 mRNA was frequently elevated in a variety of cancer types (Figure 3.3). Overall, these data indicate that deregulated expression of eRF1 and JMJD4 may be relatively common in cancer. To explore whether this deregulation might impact on tumour survival, we used the KMPlot database (Szasz et al., 2016) to identify any associations between eRF1 and JMJD4 mRNA levels and patient prognosis.

A

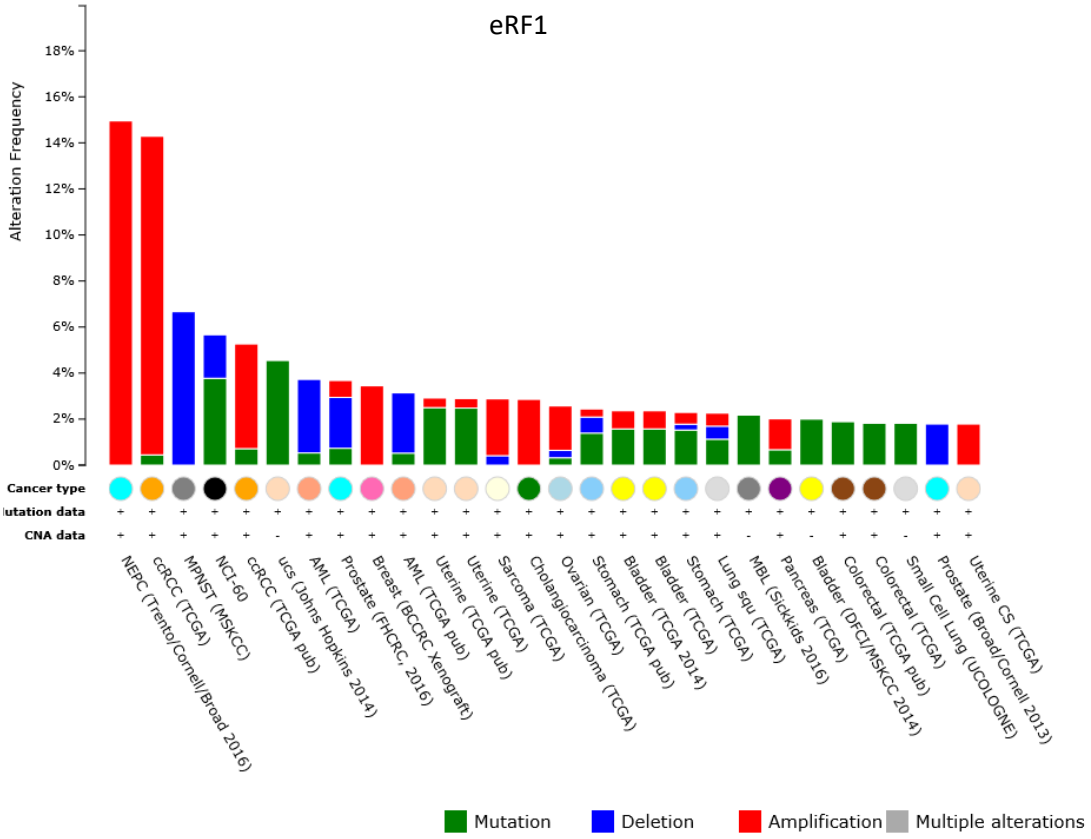


B

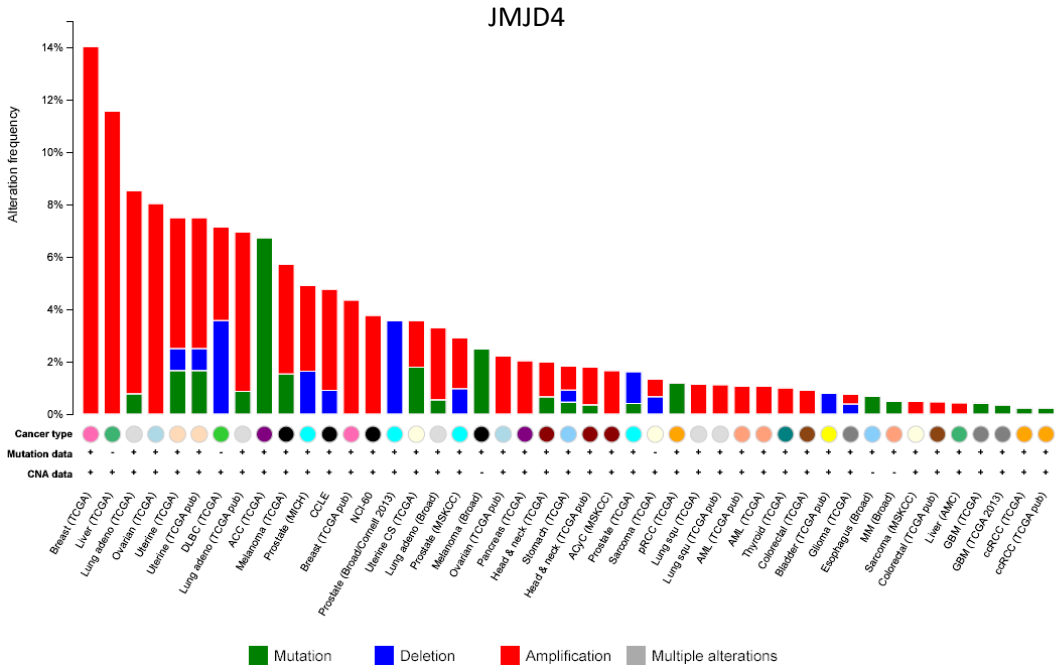


**Figure 3.1: Cancer Genomics of eRF1 and its modifier JMJD4**. A) eRF1 is amplified by up to 14% in NEPC and Kidney Renal Cell Clear Carcinoma (ccRCC). B) JMJD4 is amplified by up to 14% in a number of cancers, principally breast, liver and lung adenocarcinoma Data obtained through cBioPortal (Gao et al., 2013).

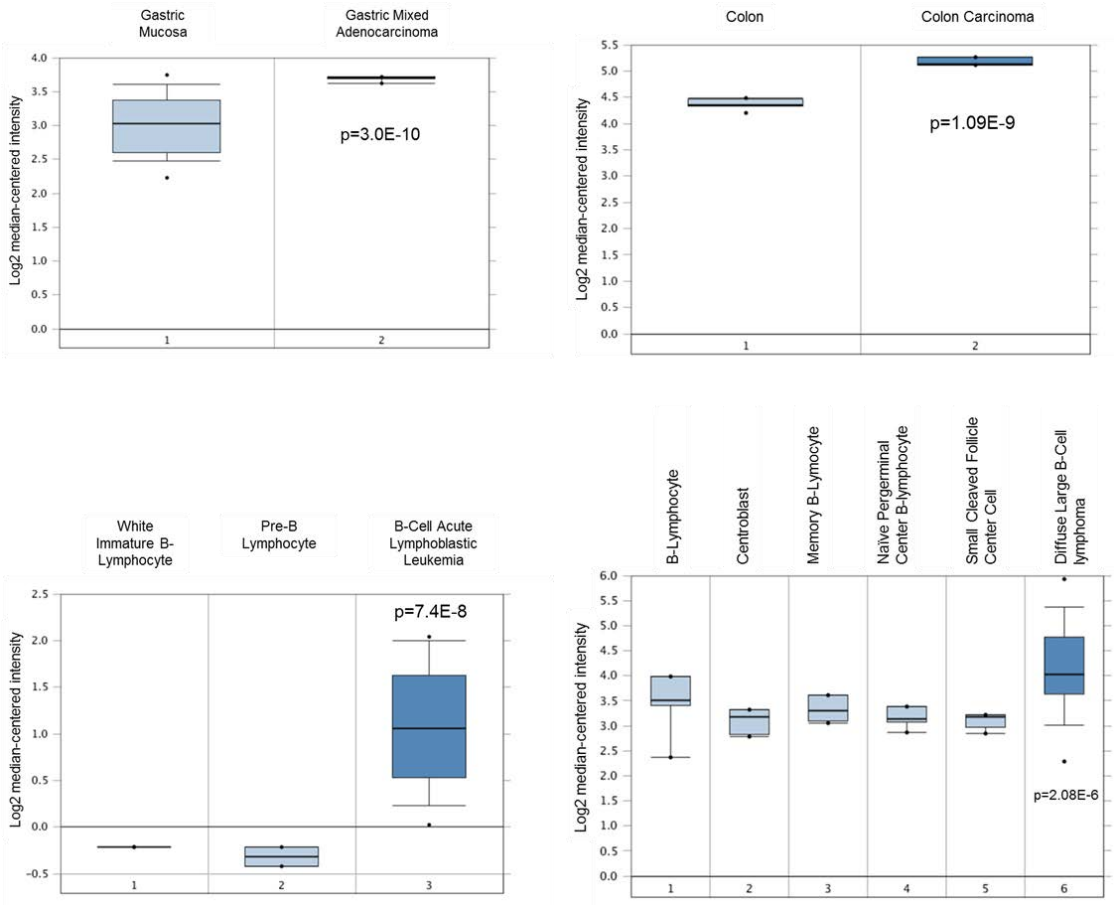


**Figure 3.2: Bioinformatics of eRF1 mRNA expression in tumours.** eRF1 transcript abundance can be shown to be significantly increased in adenocarcinoma, colon carcinoma, B cell lymphoplastic leukemia and Diffuse Large B Cell Lymphoma compared to healthy tissues. p=Probability that there is no difference between the populations by two-tailed Student's t-test. Analysis through ONCOMINE (Rhodes et al., 2004).

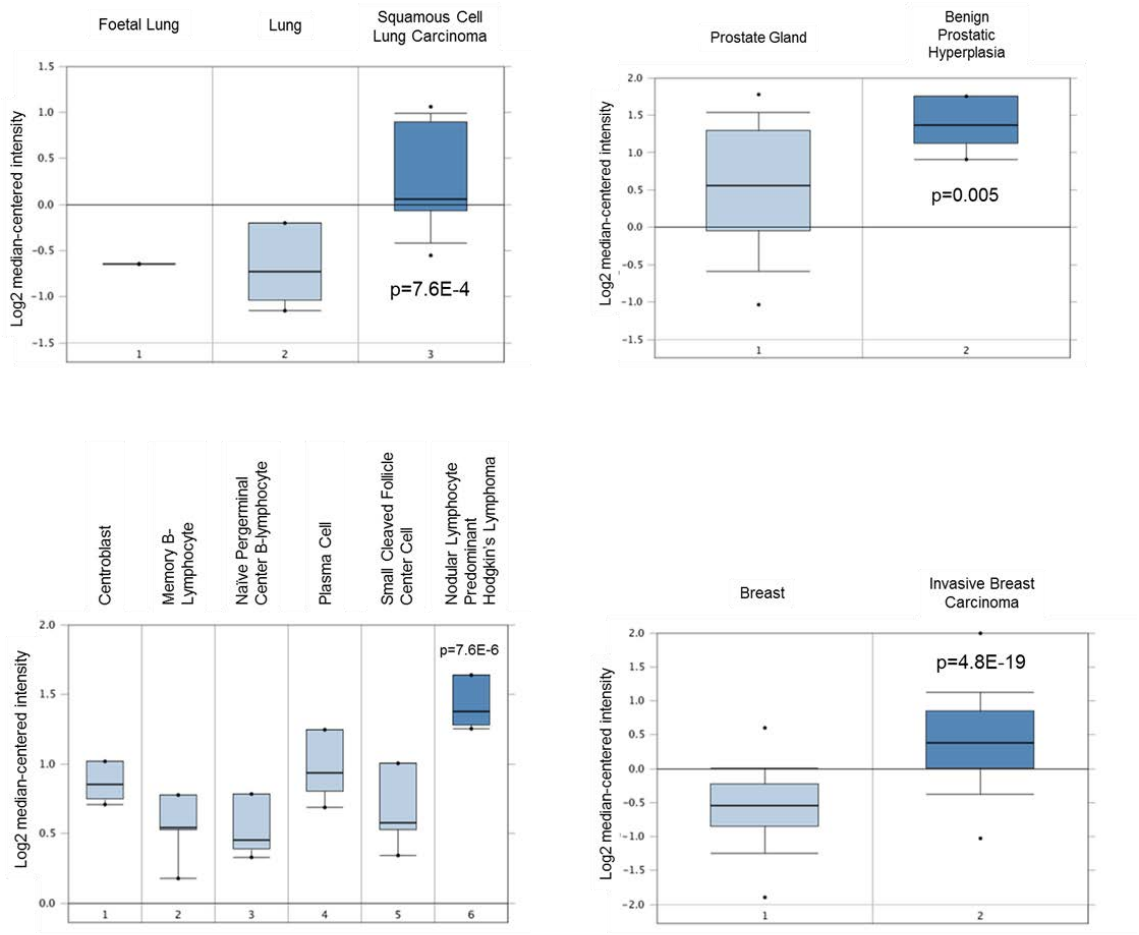


**Figure 3.3: Bioinformatics of JMJD4 mRNA expression in tumours.** JMJD4 transcript abundance can be shown to be significantly increased in squamous cell lung carcinoma, benign prostatic hyperplasia, Hodgkin's lymphoma and invasive breast carcinoma compared to healthy tissue. p=Probability that there is no difference between the populations by two-tailed Student's t-test. Analysis through ONCOMINE (Rhodes et al., 2004).

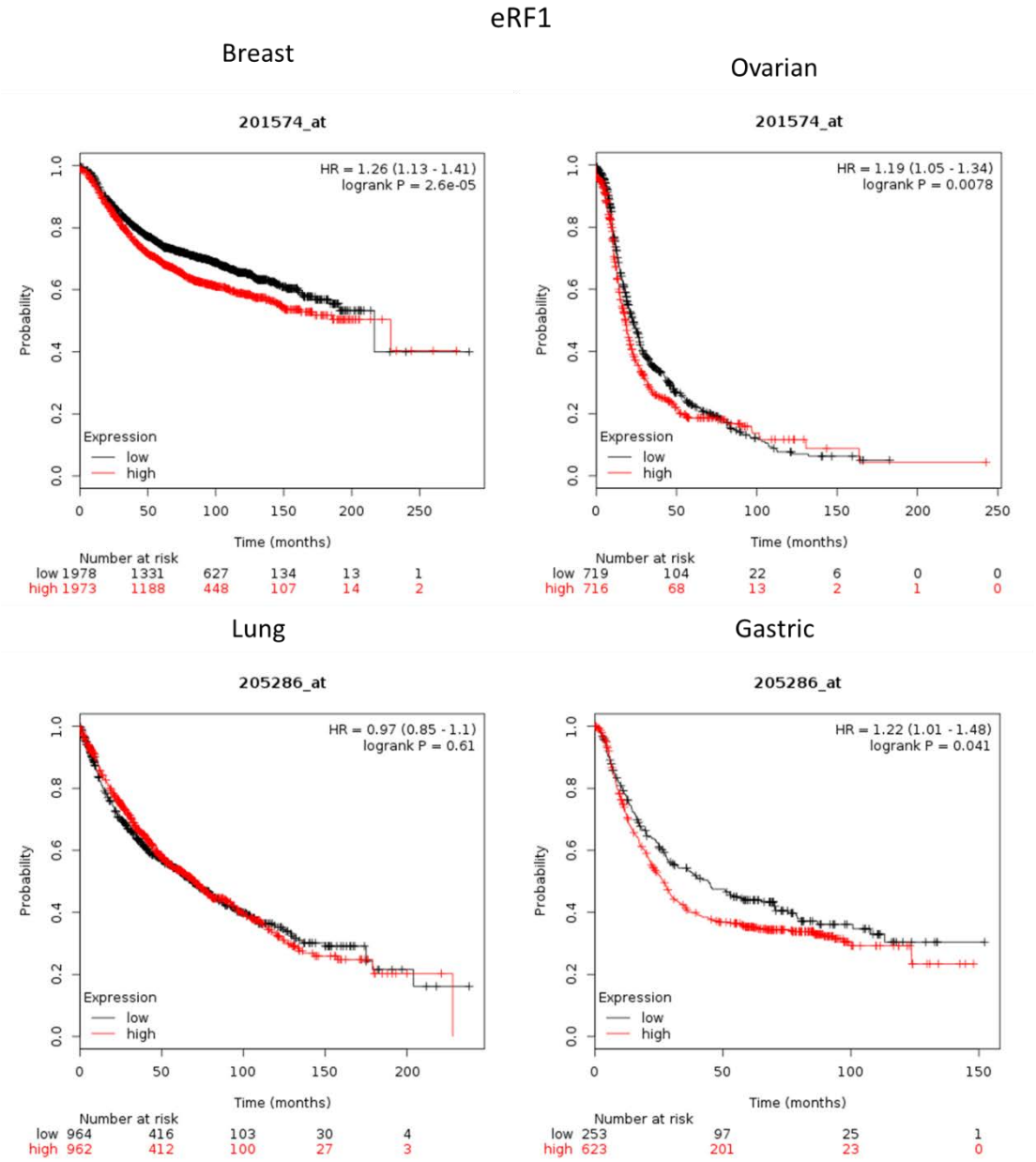


**Figure 3.4: Kaplan-Meier Survival analysis of eRF1 mRNA expression in Breast, Ovarian, Lung, and Gastric cancers.** The probe identifier is located atop each plot. HR=Hazard Ratio, the ratio at which survival is modified by amplification of the corresponding gene in each cancer type. Logrank P= Probability that the difference between the two groups is significant using the log-rank non-parametric hypothesis test for survival distribution. Probability refers to the percentage probability of survival. Patient numbers in each curve are found below each blot. Analysis via the Kaplan Meier Plotter (Szasz et al., 2016)

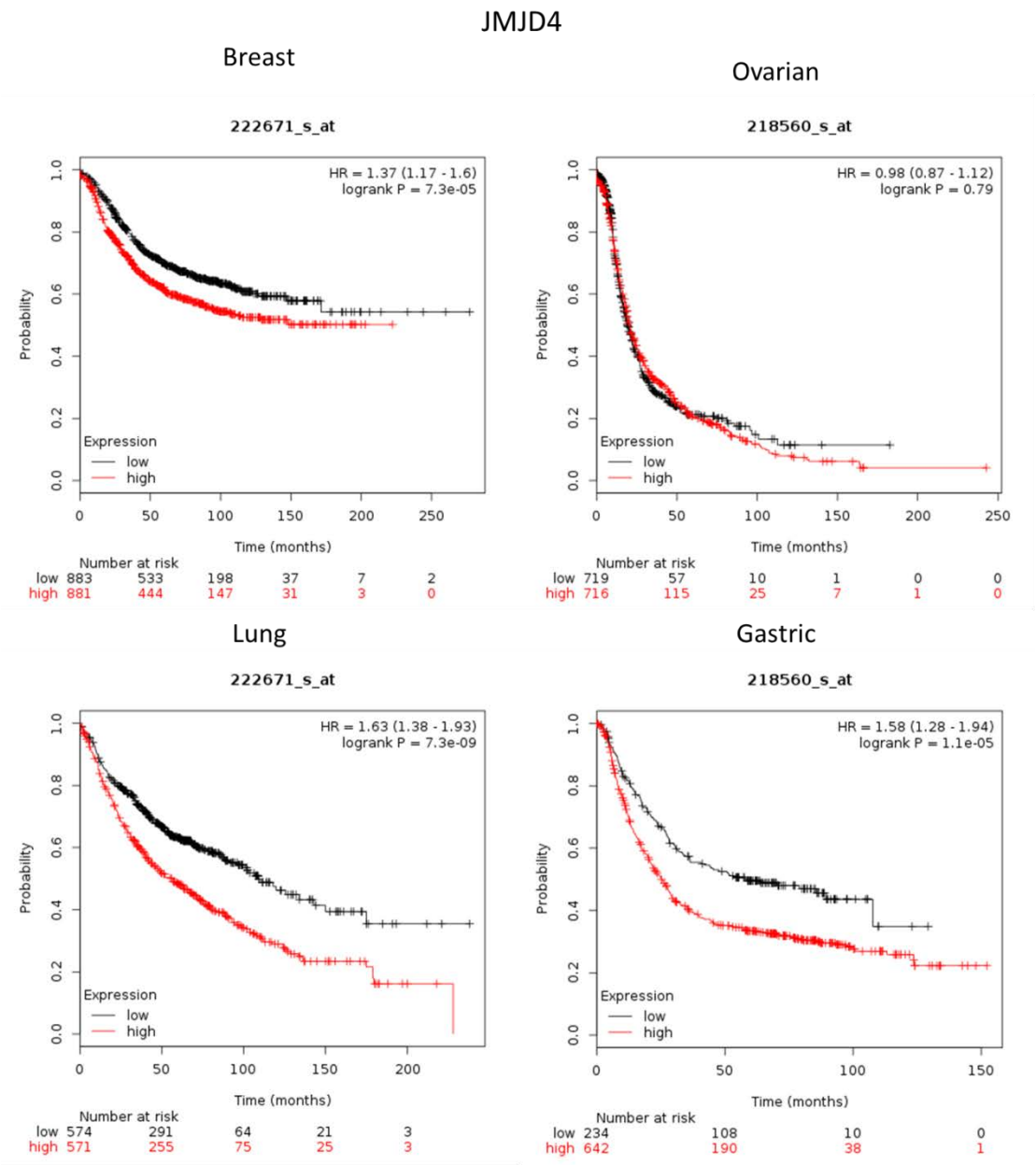


**Figure 3.5: Kaplan-Meier Survival analysis of JMJD4 mRNA expression in Breast, Ovarian, Lung, and Gastric cancers.** The probe identifier is located atop each plot. HR=Hazard Ratio, the ratio at which survival is modified by amplification of the corresponding gene in each cancer type. Logrank P= Probability that the difference between the two groups is significant using the log-rank non-parametric hypothesis test for survival distribution. Probability refers to the percentage probability of survival. Patient numbers in each curve are found below each blot. Analysis via the Kaplan Meier Plotter (Szasz et al., 2016)

Based on the Kaplan-Meier survival analysis in four different cancers (Figure 2.4), eRF1 mRNA overexpression is associated with a worse prognosis in breast, ovarian and gastric cancer. Furthermore, JMJD4 mRNA overexpression is associated with a 37-63% increase in patient mortality in Breast, Lung and Gastric cancers (Figure 2.5). Overall, the combined genomic, expression and prognostic data suggest that eRF1 and JMJD4 may support tumourigenesis. In light of this, we therefore aimed to directly test the role of JMJD4 and eRF1 in cancer cell proliferation using *in vitro* cell line models.

### 3.2.2 Engineering tumour cell lines with Doxycycline-inducible JMJD4 and eRF1 shRNA

In order to characterise of the consequences of JMJD4 and eRF1 loss-of-function, a series of cell lines capable of conditional shRNA knockdown were previously generated (by Dr Tianshu Feng, Coleman lab) and characterised and applied in detail here. A conditional system was chosen in order to avoid any potential selection pressures against cells with constitutive JMJD4/eRF1 knockdown. The commercially available lentiviral vector pTRIPZ (Figure 3.6) was utilised for this. This vector features a tetracycline inducible promoter, allowing expression of downstream sequences conditional to induction with tetracycline or one of its derivatives (e.g. doxycycline). Three prime to the promoter lies the coding sequence of Red Fluorescent Protein (RFP), followed by a site allowing cloning of shRNA sequences.

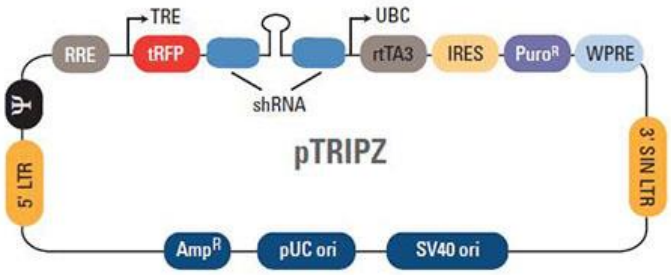


| Vector Element | Utility |
|---|---|
| TRE | Tetracycline-inducible promoter |
| tRFP | TurboRFP reporter for visual tracking of transduction and shRNA expression |
| shRNA | microRNA-adapted shRNA (based on miR-30) for gene knockdown |
| UBC | Human ubiquitin C promoter for constitutive expression of rtTA3 and puromycin resistance genes |
| rtTA3 | Reverse tetracycline-transactivator 3 for tetracycline-dependent induction of the TRE promoter |
| Puro$^R$ | Puromycin resistance permits antibiotic-selective pressure and propagation of stable integrants |
| IRES | Internal ribosomal entry site allows expression of rtTA3 and puromycin resistance genes in a single transcript |
| 5' LTR | 5' long terminal repeat |
| 3' SIN LTR | 3' self-inactivating long terminal repeat for increased lentivirus safety |
| Ψ | Psi packaging sequence allows viral genome packaging using lentiviral packaging systems |
| RRE | Rev response element enhances titer by increasing packaging efficiency of full-length viral genomes |
| WPRE | Woodchuck hepatitis posttranscriptional regulatory element enhances transgene expression in the target cells |

**Figure 3.6: Schematic diagram of the pTRIPZ vector**. Initiation of RFP and shRNA expression by doxycycline requires binding of the rtTA3 transactivator which is constitutively expressed via the *H.sapiens* Ubiquitin C promoter (UBC) but is only functional in the presence of a tetracycline, in this case Doxycyline (Figure derived from the Dharmacon website, http://dharmacon.gelifesciences.com/shrna/tripz-lentiviral-shrna/).

Addition of doxycycline would therefore allow the expression of a silencing shRNA against the transcript of interest and also permit visual tracking through RFP expression. The pTRIPZ vector also includes constitutive expression (driven by a ubiquitin promoter) of the reverse tetracycline-transactivator protein rtTA3 (for doxycycline-mediated gene expression) and a Puromycin resistance cassette to enable antibiotic selection.

For the generation of inducible shRNA cell lines, U2OS human bone Osteosarcoma-derived epithelial cells were chosen because of prior detailed characterisation with respect to translational termination and protein synthesis (Dr Tianshu Feng PhD thesis and Feng *et al*, 2014).

The following U2OS cell lines were previously generated by transduction of lentiviral particles carrying the following pTRIPZ vectors: 1) pTRIPZ containing a non-targeting control shRNA sequence referred to as shFF3, 2) pTRIPZ containing an shRNA against JMJD4 (to achieve acceptable knockdown it was necessary to screen clones (data not shown), resulting in the generation of two lines designated shJMJD4#2 and #11), and 3) pTRIPZ containing an shRNA against eRF1 and referred to as sheRF1.

To confirm the validity of these stable cell lines we first treated them with a range of doxycycline concentrations for 72 hours prior to assessing RFP levels by fluorescence microscopy and target knockdown by western blot. As expected, robust RFP expression was observed in all of the cell lines and in a dose-dependent manner for shFF3 and the shJMJD4 cell lines (Figures 3.7 & 3.8). Importantly, we confirmed doxycycline dose-dependent knockdown of eRF1 and JMJD4 in parallel samples, in the absence of altered expression of control proteins including β-actin for eRF1 and β-actin and a JMJD4-related hydroxylase (MINA53) for JMJD4. It was concluded that a common dose of 1-2 μg $ml^{-1}$ Doxycycline was able to induce efficient knockdown across all three cell lines (Figure 3.9). The two clones of shJMJD4 both show reduced levels of JMJD4 even in the absence of doxycycline stimulation, likely a result of "leaky expression" of a highly efficient shRNA, as did sheRF1 to a lesser extent.

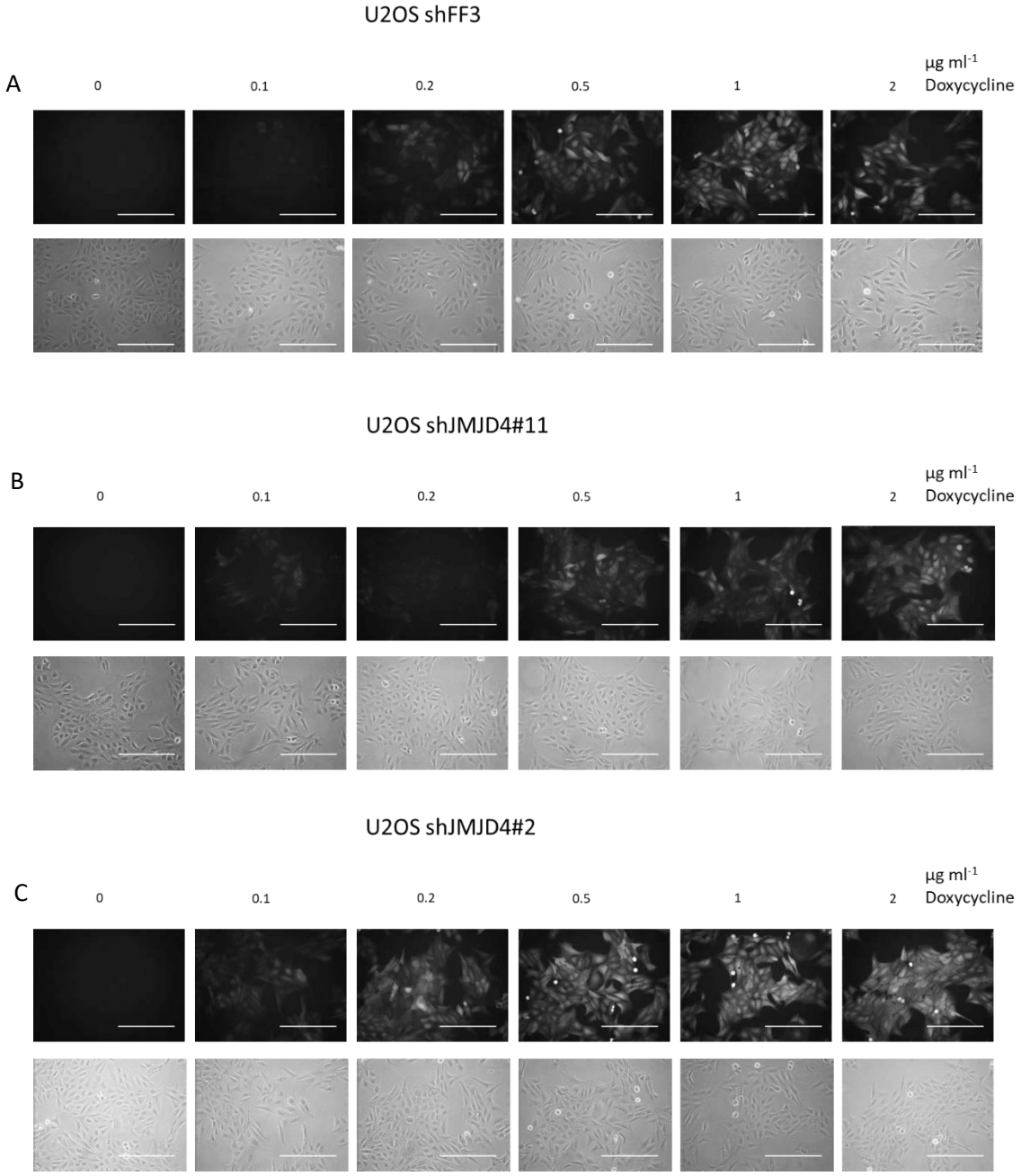


**Figure 3.7: Characterisation of RFP expression in stable cell lines expressing inducible shRNA**. U2OS cells were stably transduced with pTRIPZ containing the desired shRNA insert using lentivirus. pTRIPZ contains RFP in the same Open Reading Frame (ORF) as the shRNA insert which can be used to assess the extent of efficiency of transduction. In every image set, top is red fluorescence at 588nm (RFP emission maximum), bottom is brightfield of the same position in the plate. RFP expression is ubiquitous and appears to plateau at 1 µg ml$^{-1}$ Doxycycline after 72h. A) U2OS expressing the non-targeting sequence shFF3 B) U2OS shJMJD4 clone #11, and C) U2OS shJMJD4 #2. Scale bar is 200 µm. Magnification under a 10x objective.

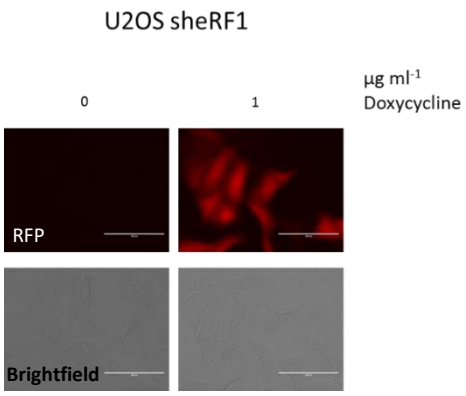


**Figure 3.8: Characterisation of RFP expression in a stable cell line expressing inducible shRNA against eRF1**. U2OS cells were stably transduced with pTRIPZ containing the desired shRNA insert using lentivirus. pTRIPZ contains RFP in the same Open Reading Frame (ORF) as the shRNA insert which can be used to assess the extent of efficiency of transduction. In every image set, top is red fluorescence at 588nm (RFP emission maximum), bottom is brightfield of the same position in the plate. RFP expression is ubiquitous following induction with 1 µg $ml^{-1}$ Doxycycline after 72h. Scale bar is 100 µm. Magnification under a 20x objective.

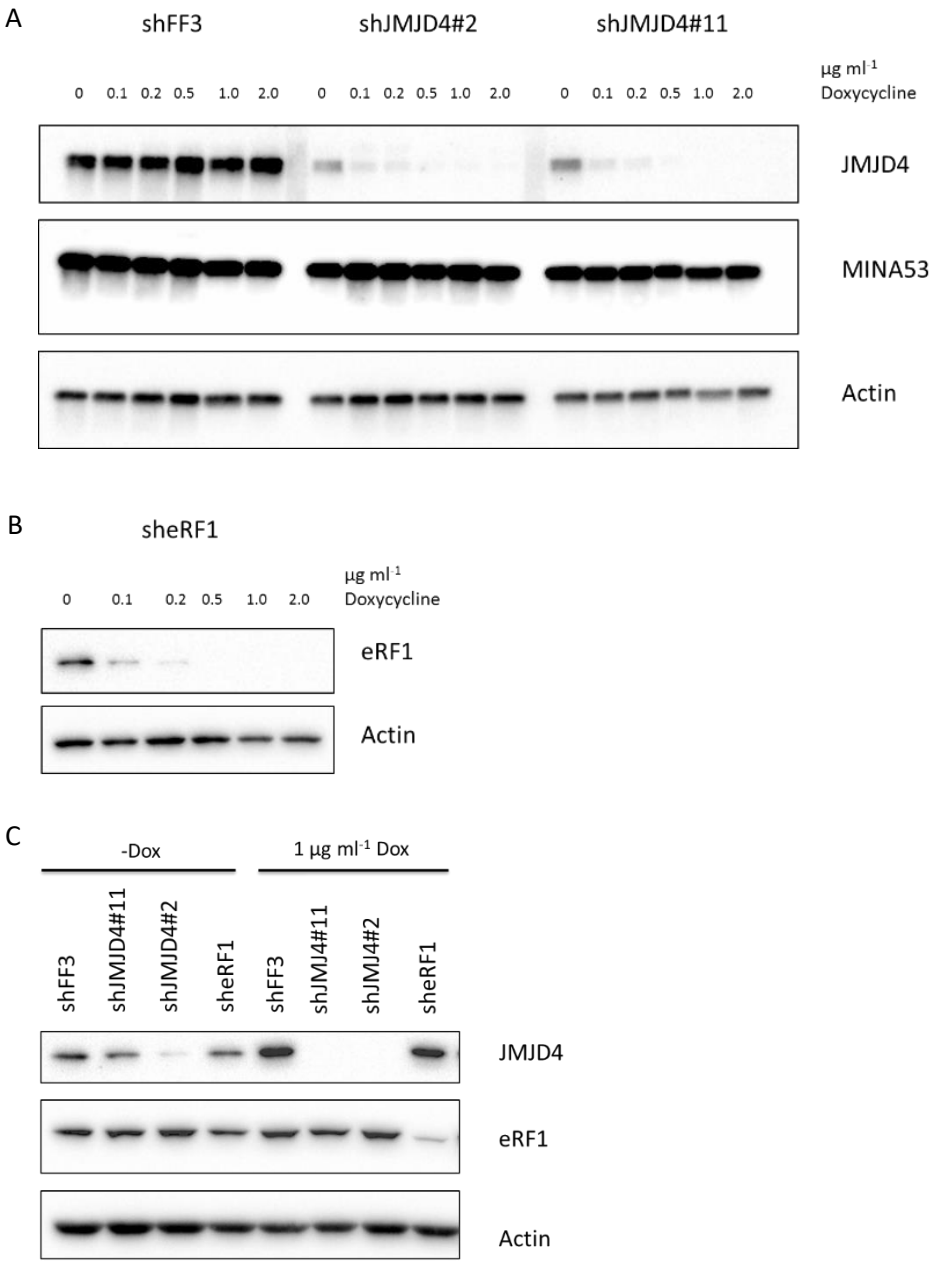


**Figure 3.9**: **Validation of shRNA mediated knockdown of JMJD4 and eRF1 in the inducible cell lines generated.** A) Western Blot of the inducible shJMJD4 cell line clones and the non-targeting sequence shFF3. Both shJMJD4#2 and shJMJD4#11 exhibit dose responsive knockdown of JMJD4. Both clones exhibit a basal level of JMJD4 knockdown, likely due to leaky expression even in the absence of doxycycline stimulation. The knockdown is specific, as demonstrated by lack of knockdown in the related 2OG oxygenase MINA53. B) Western Blot of the inducible sheRF1 cell line, showing dose dependent knockdown of eRF1 in response to doxycycline. C) Western Blot of the shRNA knockdown for all cell lines, comparing uninduced cells to induced with 1 µg $ml^{-1}$ doxycycline. This experiment was performed separately from 3.9A&B. Samples were taken following 72h of doxycycline treatment for all blots.

### 3.2.3 Knockdown of eRF1 or JMJD4 in conditional U2OS shRNA cell models promotes stop codon readthrough

Prior to characterising the role of eRF1 and JMJD4 in growth using the models described above, we first determined whether the level of knockdown achieved was sufficient to cause termination defects similar to those reported previously using siRNA (Feng et al., 2014a). In order to achieve this, a stop codon readthrough assay was employed using the U2OS shRNA knockdown cell lines shFF3, shJMJD4#2&#11 and sheRF1, as follows. Translational termination activity was measured in cells using an established dual luciferase luciferase based assay based on the p2luc vector (Figure 3.10A) (Grentzmann et al., 2000). This vector contains in-frame Firefly and *Renilla* Luciferase sequences separated by a polylinker insertion window, under the control of an SV40/T7 promoter. If a sequence containing no stop codons is inserted in the polylinker insertion window then both Firefly and *Renilla* Luicferase will be expressed at the same ratio as a fused protein connected by a short linker sequence. The sequence used in the following assays for this purpose is derived from a Tobacco Mosaic Virus termination site, with the stop codon (UAG) subsitituted for a Gln (CAG) and referred to as 'TMVR'.

Should a sequence containg a stop codon be introduced into the polylinker insertion window, only *Renilla* luciferase will be expressed because translation is halted prior to the Firefly luciferase sequence (assuming maximal termination efficiency). The only event in which Firefly luciferase is translated in the presence of a prior stop codon in the linker sequence is termination efficiency is impaired, and the ribosome reads through the stop codon, resulting in a fused *Renilla*-Firefly luciferase. Therefore, reduced translational termination efficiency and increased stop codon readthrough can be measured by an increase in Firefly relative to *Renilla* luciferase

activity. The *Renilla* and Firefly luciferases possess different substrate requirements and inhibitors specific to each luciferase exist, allowing the experimental deconvolution of the signals, despite the signal being in both cases luminescence. Initially, the activity of Firefly activity is assayed by addition of a reagent mix containing luciferin, ATP and $Mg^{2+}$. Subsequently, the *Renilla* luciferase substrate coelenterazine is added along with a Firefly luciferase inhibitor, allowing for the specific measurement of the *Renilla* luminescence.

In order to measure specific changes in translational termination, several controls are required. Firstly, the Firefly/*Renilla* ratio of a treatment group with a p2luc vector containing a stop codon (e.g. 'TMV TGA') is divided by the Firefly/*Renilla* ratio of the matched treatment group of cells transfected with a p2luc vector containing a sense codon (TMVR). This controls for potential technical differences between groups, such as the level of transfection efficiency. Secondly, this value is further divided by the Firefly/*Renilla* ratio of the cells which have received no treatment (control cells) to derive the 'Fold-increase' in translational readthrough in response to the treatment of interest (in this case shRNA knockdown). This process is schematicaly depicted in Figure 3.10B.

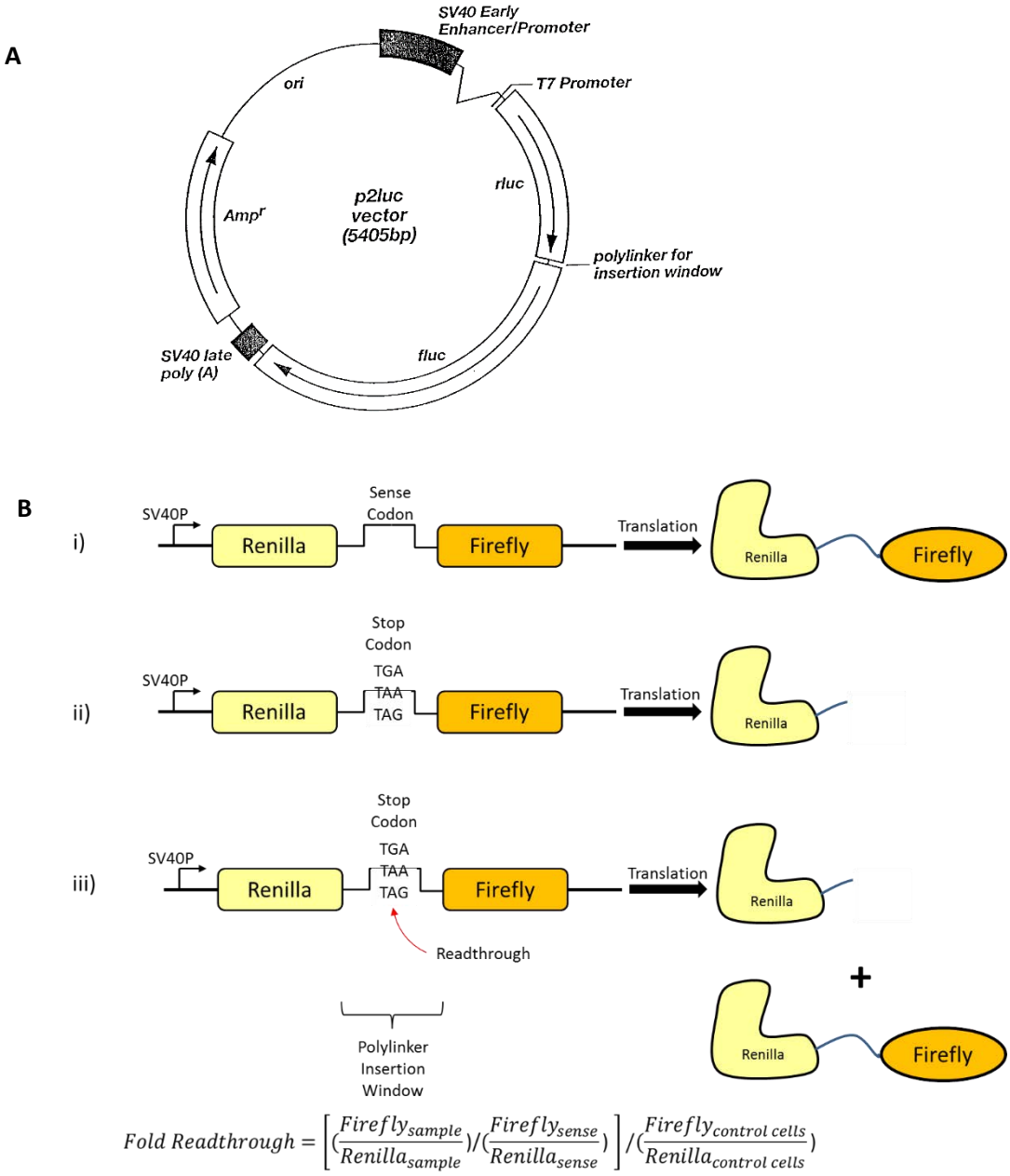


**Figure 3.10: Schematic diagram of p2luc vector and mechanism of the translational readthrough assay.** A) Schematic Diagram of the p2luc vector (adapted from Grentzmann *et al*, 2002) B) Operation of a translational readthrough assay and calculation of the Fold Readthrough parameter. i) In the presence of a sense codon, the translation products of p2luc will always be both *Renilla* and Firefly Luciferases linked by a short sequence. This plasmid is referred to as TMVR and represents the maximal activity of Firefly that can be achieved in a certain experiment. ii) If a stop codon is present in the linker sequence only *Renilla* Firefly should be expressed. iii) In the presence of translational readthrough, the stop codon may be skipped, allowing translation to continue. This leads to a mixed population of *Renilla* and *Renilla* + Firefly luciferases, the relative ratio of which can be used to determine the fold readthrough.

To assess the level of translational readthrough following eRF1 or JMJD4 knockdown, U2OS shRNA cells were treated with 2 μg $ml^{-1}$ Doxycycline for 72h before transfection with p2luc containing either one of the following three different termination contexts (or a corresponding control sequence containing a sense codon). The termination context sequences used were A) The tobacco mosaic virus (TMV) with the wild type termination codon UAG substituted with UGA, B) CFW1282*, a nonsense mutation found in cystic fibrosis patients and C) the Barley Yellow Dwarf virus termination sequence (BYDV), utilizing UAG as the stop codon. Multiple sequences were selected in order to test the robustness of the termination phenotype in diverse sequence contexts. After harvesting cell extracts 72h post transfection, samples were analysed for stop codon readthrough as described above and in the Materials and Methods.

Consistent with loss of eRF1 function, shRNA-mediated eRF1 knockdown results in a significant increase in translational readthrough in all three stop codon contexts. Consistent with previous observations (Unpublished Doctoral Thesis, Feng 2014 and Feng et al, 2014), JMJD4 knockdown also induced context-independent stop codon readthrough although, as expected, to a lesser extent than that observed with eRF1 (which was particularly evident in the context of TMV). Overall, these data indicate that both the sheRF1 and shJMJD4 systems demonstrate a replicable stop codon readthrough phenotype, thereby validating their use in subsequent experiments.

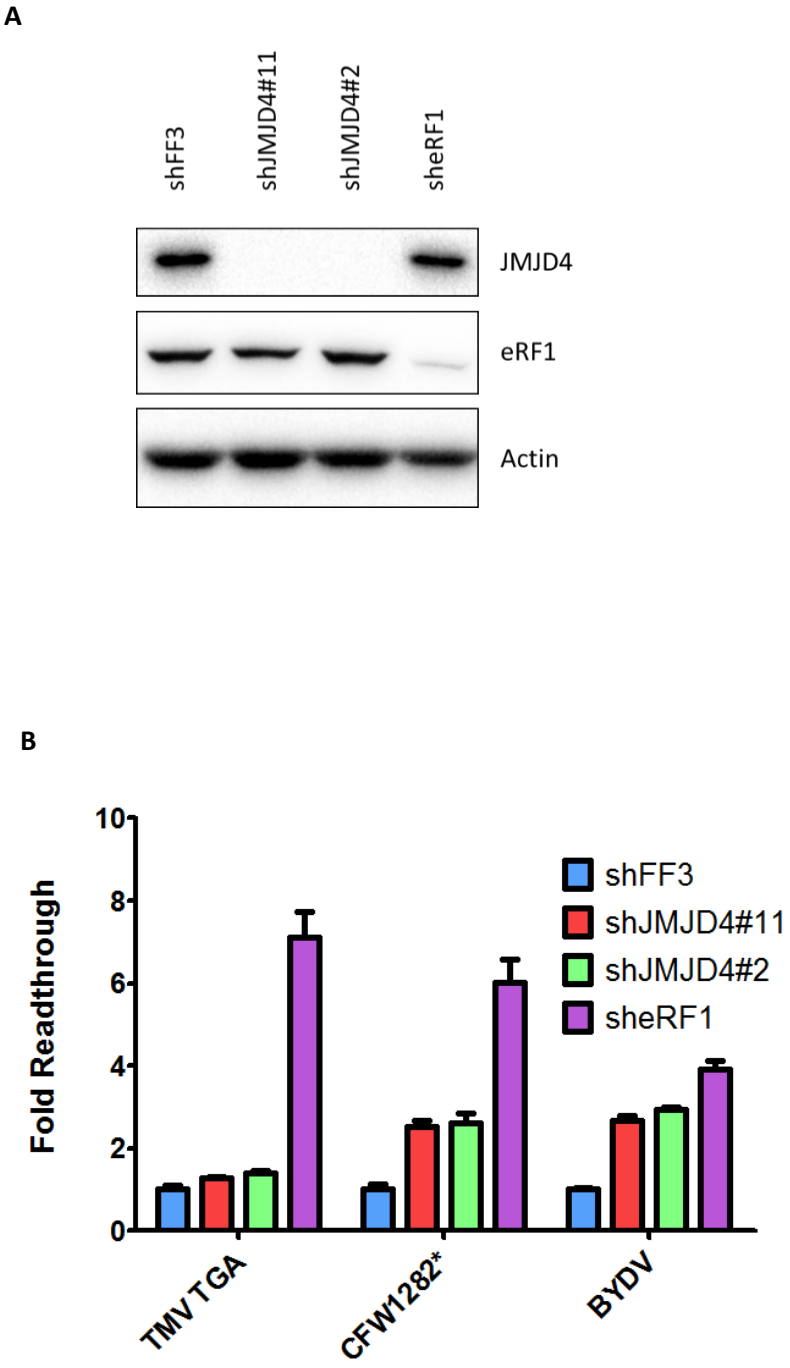


**Figure 3.11: Knockdown of JMJD4 and eRF1 results in an increase in the level of translational readthrough**. A) Western Blot validating knockdown of JMJD4 and eRF1 at the protein level. B) The sequences shown here were the Tobacco Mosaic Virus with the wild-type termination codon TAG substituted for TGA (TMV TGA), the cystic fibrosis mutation CFW1282* and the Barley Yellow Dwarf Virus termination sequence (BYDV), known to exhibit readthrough. Cells were treated with doxycycline for 72h. n=3 ± Standard Deviation

### 3.2.4 JMJD4 and eRF1 are required for normal cellular proliferation

Having confirmed that our shRNA knockdown models induce the anticipated functional consequences we wished to determine whether these changes might be associated with altered cell proliferation.

Two-dimensional cell proliferation was assayed using both MTS and CyQuant assays. MTS (3-(4,5-dimethylthiazol-2-yl)-5-(3-carboxymethoxyphenyl)-2-(4-sulfophenyl)-2H-tetrazolium) is a tetrazolium salt, which in the presence of phenazine methosulfate (PMS) can be metabolised by NAD(P)H-dependent cellular oxidoreductases into coloured formazan salts. These salts absorb at 490nm, which can then be used as a measure of cell number (Mosmann, 1983) (Cory et al., 1991). Because the MTS approach requires there to be no indirect changes in mitochondrial content and/or metabolic rate, we also used a second independent approach: The CyQuant Assay utilizes a dye that binds directly to DNA to quantify cell number by DNA content.

U2OS shFF3, sheRF1 and shJMJD4 clones #2 and #11 were subjected to 72h of 2 μg $ml^{-1}$ Doxycycline treatment and subsequently transferred into 96 well plates for growth assays over a period of 5 days. Interestingly, we find that shRNA-mediated knockdown of eRF1 results in near complete cessation of growth using both assays. The effect observed under JMJD4 knockdown is less dramatic, but is more prominent in clone shJMJD4#2, perhaps reflecting increased knockdown efficiency (we note that clone #2 displays lower levels of JMJD4 even in the absence of doxycycline, Figure 3.9). Importantly, the growth curves between the MTS and CyQuant assays were quite similar, indicating that NAD(P)H oxidoreductase activity within the cells is not affected by eRF1 or JMJD4 knockdown, validating the use of MTS assays in future 2D growth experiments.

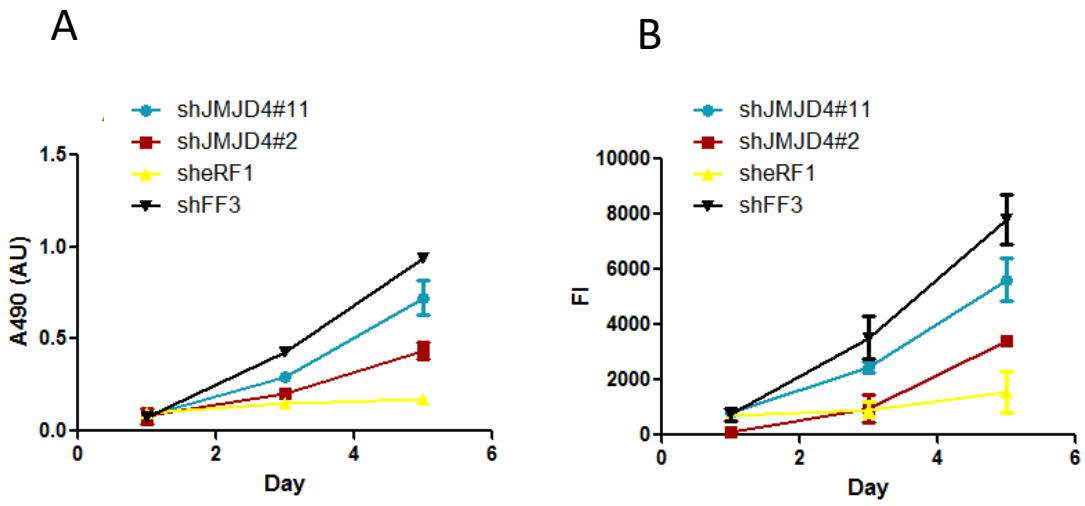


**Figure 3.12: JMJD4 and eRF1 knockdown restricts 2D growth in U2OS cells**. U2OS shFF3, shJMJD4#2&11 and sheRF1 cells were treated with 1 µg $ml^{-1}$ doxycycline for 5 days. A) U2OS shJMJD4#11, shJMJD4#2, sheRF1 and shFF3 cells were induced with Doxycycline and then their growth measure using MTS+PMS over 5 days. B) As before, however growth was measured using the DNA binding Dye CyQuant. FI=Fluorescence Intensity (Arbitrary Units) emission at 520 nm. For A&B n=4 ± Standard Deviation

Next, we sought to determine whether the requirements for eRF1 and JMJD4 in 2D growth extend into more relevant cancer cell growth assays. Tumour cells acquire the ability to grow in an anchorage-independence manner, and *in vitro* assays that mimic such conditions can be used to assess the transformation potential of cells. For example, the growth of tumour cell colonies in low percentage agar ('soft-agar' assay) is thought to reliably predict growth rate in xenograft tumour experiments (Pavelic et al., 1980). Therefore, shFF3, sheRF1 and shJMJD4#2 and #11 were treated with 1 μg $ml^{-1}$ doxycycline for 72h, then seeded into liquid noble agar and their growth measured five days later using Alamar Blue, a detection reagent operating on a similar principle to MTS. Colonies were also imaged using phase contrast microscopy.

The results for three-dimensional growth largely reflect the two-dimensional results discussed previously, with eRF1 knockdown resulting in the greatest reduction in growth, followed by shJMJD4#2 and shJMJD4#11. The results can be visually confirmed in the light microscopy images, where reduced growth can be seen in shJMJD4 #2 and #11 colonies, with effectively no colonies visible in the sheRF1 group.

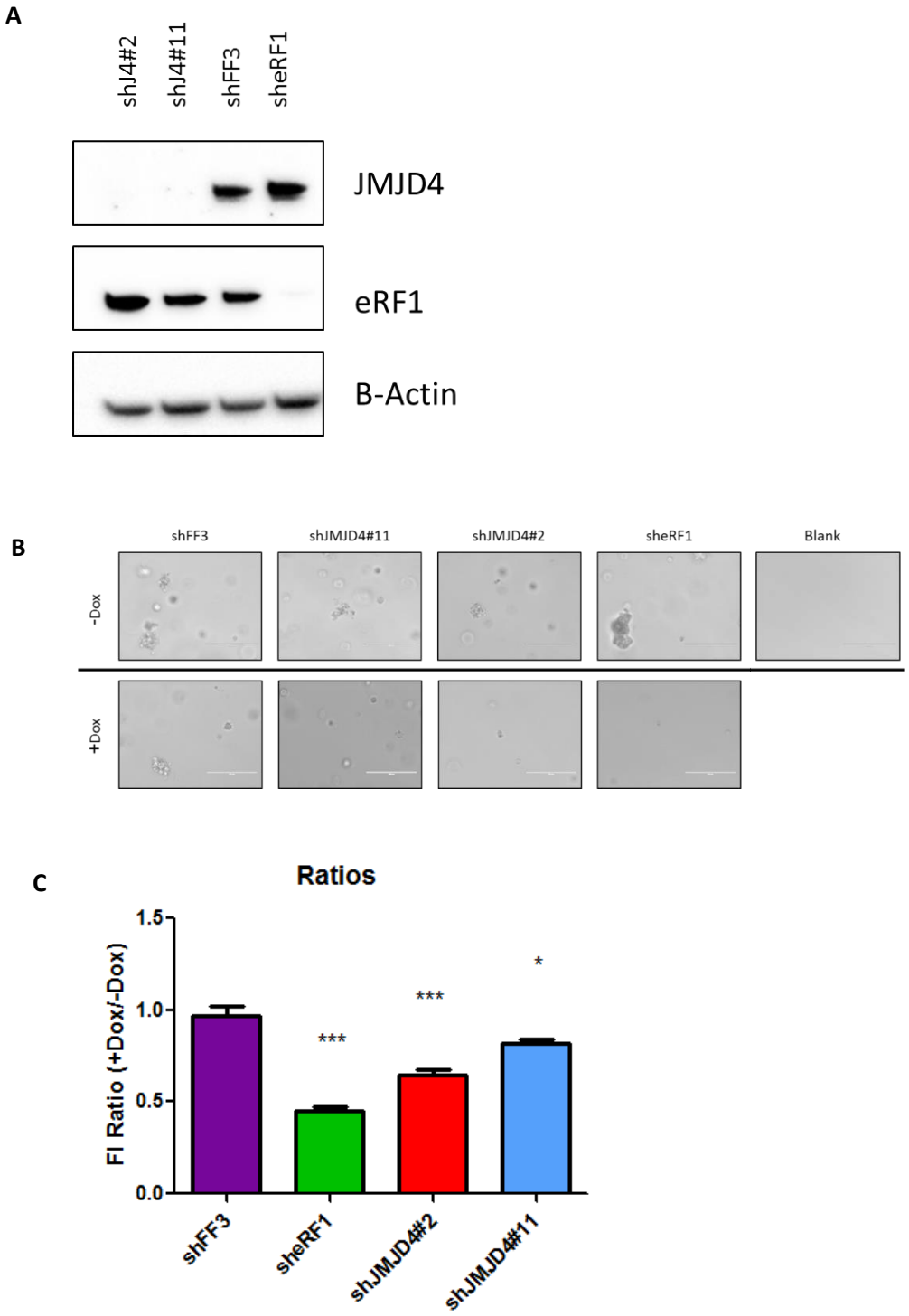


**Figure 3.13: Knockdown of JMJD4 and eRF1 curtails 3-dimensional anchorage independent growth in stable inducible U2OS cells**. Cells were seeded in noble agar and after 7 days their growth assessed using Alamar Blue. A) Western Blot confirmation of knockdown following 72h of Doxycycline treatment. B) Visual appearance of colonies inside representative wells. C) Mean Fluorescence Intensity (FI) Ratio of samples treated with Doxycycline over untreated. n=6 ± Standard Deviation *, **, *** =0.5, 0.1 and 0.01 confidence levels respectively. Student's two-tailed t-test.

### 3.2.5 shRNA knockdown of JMJD4 or eRF1 does not overtly alter cell cycle distribution

Following the observation that an increase in translational readthrough upon JMJD4/eRF1 depletion was accompanied by a reduction in growth in 2D and 3D, we considered the possibility that this might be due to the activation of a specific cell cycle phase checkpoint. In order to test this, U2OS shJMJD4#2, #11, sheRF1 and shFF3 were treated with and without 1 μg $ml^{-1}$ Doxycycline for 72h before analysis by western blot (to confirm knockdown, Figure 3.14A), MTS growth assay (to confirm reduced growth, Figure 3.14B) and flow cytometry, as follows. Cells were trypsinised, fixed with cold ethanol and stained with Propidium Iodide (PI), a DNA binding stain. Consequently, cells at G1 have the lowest PI signal, cells at G2 the highest (barring multinucleate cells) and cells in the S phase should possess a continuum of values between the two peaks. Following staining, cells were analysed using Flow Cytometry gated on the live cell population using FACS-DIVA software. The distribution of the cells by cell cycle phase was determined using Watson fitting on the Flow Cytometry Suite FlowJo and presented as Sub-G1, G1, S, G2 and super-G2 populations.

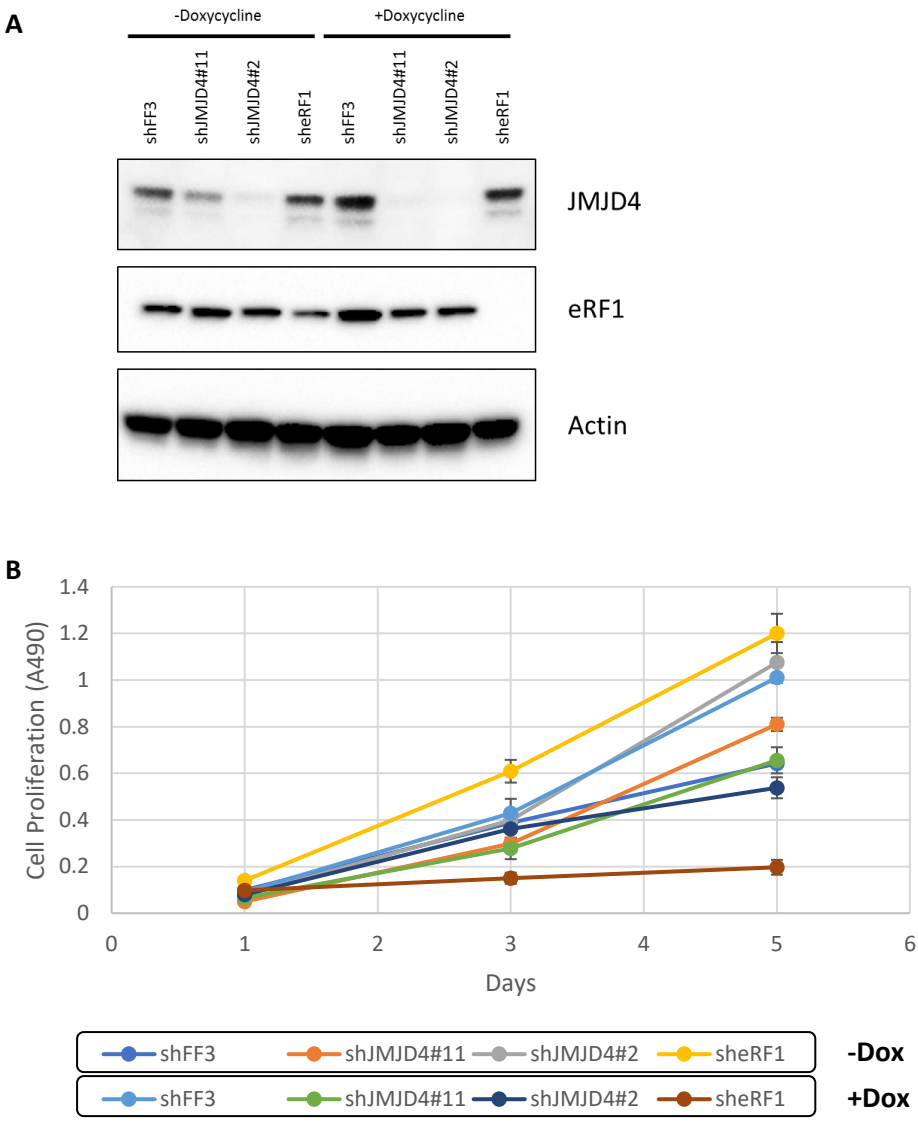


**Figure 3.14A & B: Restriction of growth by JMJD4 and eRF1 is not associated with changes in the cell cycle profile**. U2OS shFF3, shJMJD4#11, shJMJD4#2 and sheRF1 cells were induced with 1 µg $ml^{-1}$ doxycycline for 72h to knockdown their respective targets and then fixed. The cell cycle profile was then assessed using the DNA binding dye propidium iodide. A) Western Blot validation of eRF1 and JMJD4 knockdown B) Comparison of cell growth by MTS over 5 days (n=3, ± Standard Deviation

(Figure continued next page)

**C**

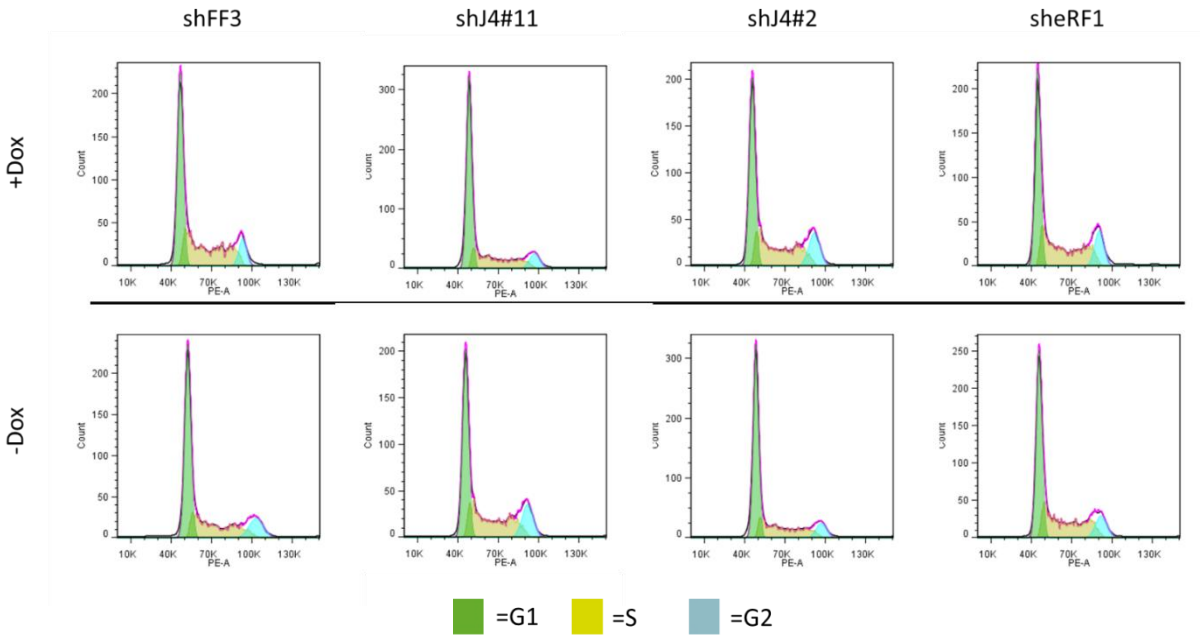


**D**

| | -Dox | | | | +Dox | | | |
|---|---|---|---|---|---|---|---|---|
| | **shFF3** | **sheRF1** | **sh2** | **sh11** | **shFF3** | **sheRF1** | **sh2** | **sh11** |
| G1 | 46.86 | 45.81 | 51.38 | 45.99 | 54 | 48.97 | 57.62 | 59.41 |
| S | 39.82 | 38.97 | 32.86 | 36.95 | 30.37 | 37.43 | 22.88 | 28.55 |
| G2 | 9.26 | 14.23 | 20.12 | 15.36 | 12.98 | 11.65 | 17.89 | 9.22 |
| Sub G1 | 1.6 | -2.02 | -6.96 | 0.54 | 2.15 | 0.47 | -0.18 | 2.09 |
| Super G2 | 1.4 | 2.14 | 1.51 | 0.8 | 0.14 | 0.91 | 1.43 | 0.41 |

**E**

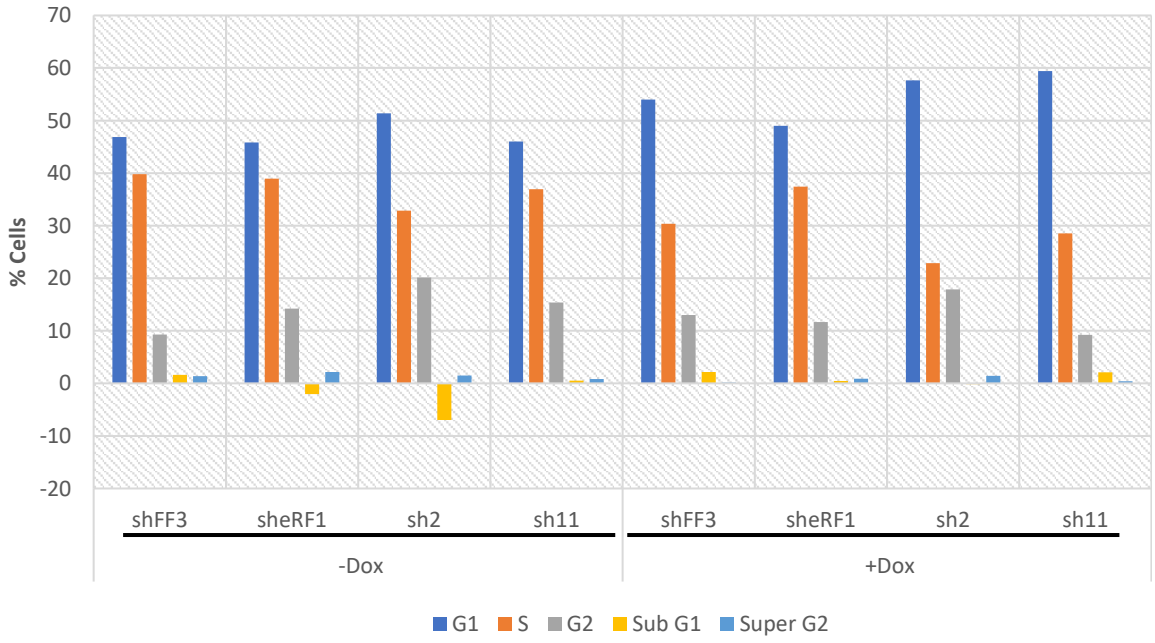

**Figure 3.14C, D & E (previous page): Restriction of growth by JMJD4 and eRF1 is not associated with changes in the cell cycle profile**. U2OS shFF3, shJMJD4#11, shJMJD4#2 and sheRF1 cells were induced with 1 μg $ml^{-1}$ doxycycline for 72h to knockdown their respective targets and then fixed. The cell cycle profile was then assessed using the DNA binding dye propidium iodide. C) Histograms of the cell cycle profiles with prediction of area covered by each cell cycle phase. Green=G1, Yellow=S, Cyan=G2) D) Table of estimated percentage of cells in each part of the cell cycle calculated by FACS-DIVA. Negative values are calculation artifacts and indicate non-existent populations. E) Histogram representation of the data in D. n=2.

In all cases, sub-G1 and super-G2 cells constituted less than 3% of the populations and were thus not depicted on the graphs for visual clarity. Any negative values in those populations arise due to the calculation algorithm deducting the overlap of populations from the reported value, causing small population whose distribution is predicted to lie entirely within a larger one to be estimated as negative. These values should be regarded as being in effect zero. The majority of the cells in the samples examined are found in G1 phase. However, no obvious difference in the cell cycle distribution was observed between cell lines or following doxycycline treatment (Figure 3.14C**)**. The subtle variations observed are disproportionately small compared to the observed reductions in growth (Figures 2.14B&C**)**. These data would suggest that reduced growth following eRF1 and JMJD4 knockdown may not be associated with the activation of a single cell cycle checkpoint. Rather, it would appear that the transition through each cell cycle phase may be slowed, rather than paused or stopped. Importantly, this type of proliferative block is not unprecedented, as discussed later.

### 3.2.6 Validation of growth phenotypes using an alternative cell line and knockdown system

Thus far, the effects of JMJD4 and eRF1 knockdown on growth have been tested on U2OS cells using an inducible shRNA system. In order to determine whether the effects observed were cell line and intervention-specific, we aimed to extend our findings using an siRNA approach in an additional cell line. In this experiment HeLa cells were twice transfected with 25 nM siRNA against JMJD4, eRF1 or a non-targeting control sequence (universal negative control #1). The siRNAs used were different to the one resulting from the processed hairpin in the U2OS shJMJD4 and sheRF1 cells. Following the second siRNA treatment the cells were trypsinised and transfected with p2luc reporter plasmids containing the termination sequences TMV TGA, TMV TAA, or the control plasmid TMVR. The samples were subsequently harvested 72h post-transfection along with protein samples, which confirmed successful knockdown **(**Figure 3.15A**)**.

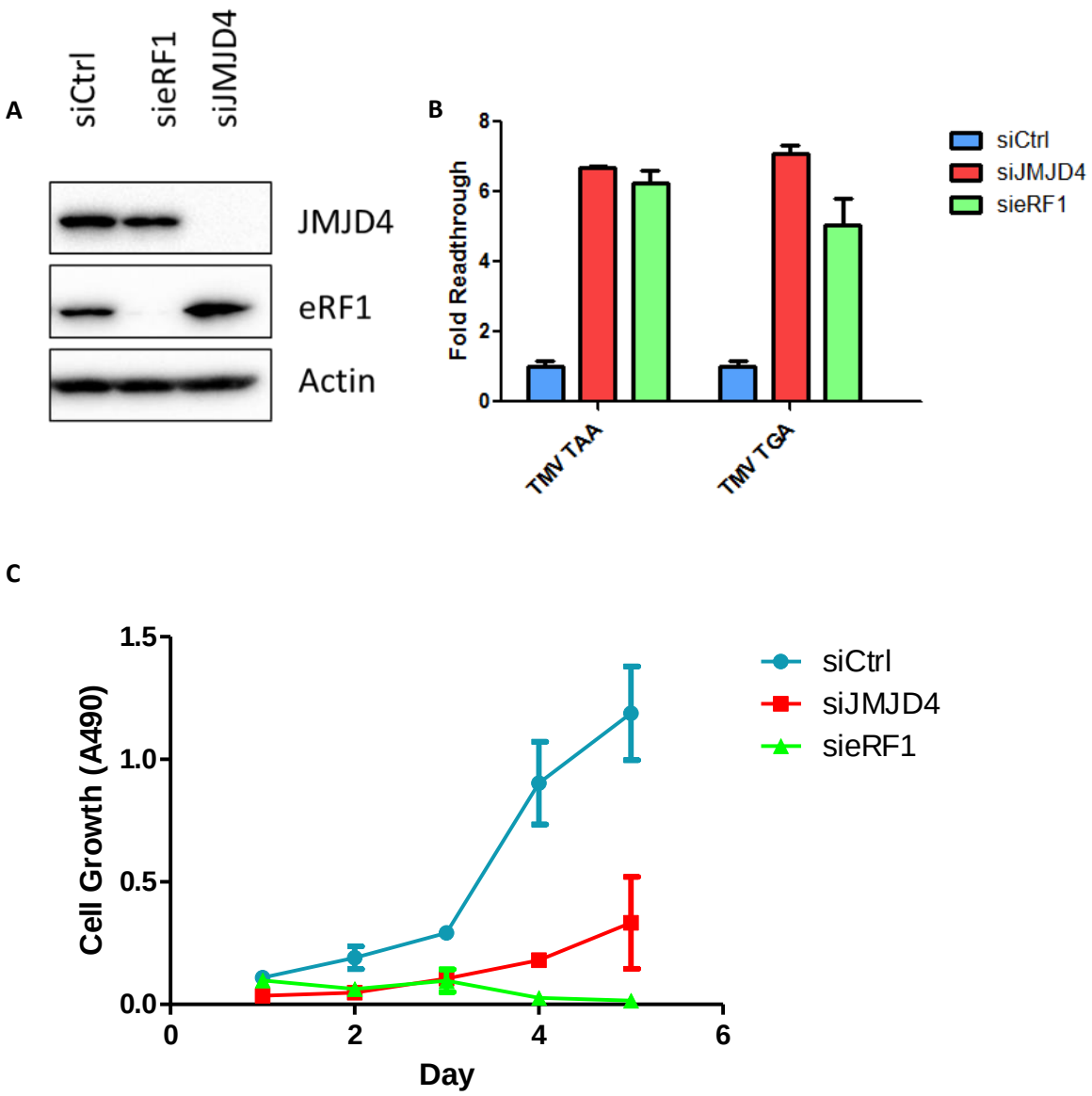


**Figure 3.15: siRNA Knockdown of JMJD4 and eRF1 recapitulates the shRNA growth phenotype**. HeLa cells were treated with siRNA against JMJD4, eRF1 or a non-targeting sequence. After 48h they were transferred to either 12 well plates for translational readthrough assay or 96 well plates and their 2D growth measured using MTS+PMS over 5 days. A) Western Blot validation of JMJD4 and eRF1 knockdown at 72h after the first siRNA transfection B) HeLa cells treated with siRNA against JMJD4, eRF1 or a non-targeting sequence were transfected with p2luc plasmids containing the Tobacco Mosaic Virus termination context, with the stop codon either the TAA or TGA. C) Cell proliferation was assayed by MTS over a period of 5 days. n=3 ± Standard Deviation

In 3.15A, an apparent increase in eRF1 upon knockdown of JMJD4 was not reproducible in other experiments. Knockdown of eRF1 by siRNA in HeLa cells resulted in comparable levels of stop codon readthrough (Figure 3.15B) to the shRNA data obtained in U2OS cells (Figure 3.11B). Interestingly however, stop codon readthrough caused by JMJD4 siRNA was substantially higher than with shRNA, and in the same range as eRF1 knockdown. This, along with the observation that shJMJD4#2 results in increased translational readthrough and reduced growth, may suggest that extremely good knockdown of JMJD4 may be necessary to elicit full growth responses and translational termination defects. Alternatively, the increased stop codon readthrough observed compared to the inducible JMJD4 shRNA cells may be due to the leaky knockdown in the latter, resulting in increased basal stop codon readthrough and thus a smaller dynamic range. Additionally, such an effect may have been also caused by habituation of the shRNA cells to leaky expression, leading to a reduction in stop codon readthrough due to potential compensatory mechanisms. Importantly however, the termination defects observed following eRF1 and JMJD4 knockdown in this model were also associated with reduced growth potential. Similar to the U2OS shRNA results, eRF1 knockdown caused a strong cytostatic effect, while knockdown of JMJD4 reduced the growth rate of HeLa cells. In both cases however the effects appear to be more pronounced than in the inducible shRNA cell lines, with evidence of cytotoxicity in the sieRF1 samples past day 4 of knockdown (as evidenced by a reduction in A490 absorbance). An apparent increase in eRF1 in the siJMJD4 treated cells in Figure 3.15A is stochastic.

### 3.2.7 HEMK2 knockdown leads to a reduction in growth and an increase in translational readthrough

Having observed that JMJD4 depletion is associated with both translational termination and growth phenotypes, we aimed to confirm whether another known eRF1 modifier, the glutamine methyltransferase HEMK2, might play a similar role. To that end, U2OS cells were transfected with either control or HEMK2 siRNA, followed by analyses of protein knockdown, stop codon readthrough and growth. Although commercially available HEMK2 antibodies do not perform well in western blotting (Figure 3.16A), it was possible to confirm knockdown of HEMK2 protein 72 hours post-transfection of siRNA. Under these conditions, HEMK2 knockdown resulted in a modest increase in translational readthrough, consistent with a role in promoting eRF1 activity (Liu et al., 2010). Similar to JMJD4 and eRF1, siRNA knockdown of HEMK2 also induced a significant growth deficit (Figure 3.16C).

JMJD4 and eRF1 are required for normal cell growth, and their expression may be deregulated and associated with poor prognosis in cancer (section 3.2.1). Therefore, having confirmed a role for HEMK2 in cell growth, we next asked whether HEMK2 expression was also deregulated and associated with prognosis in cancer. The cBioPortal database indicates that the HEMK2 gene is not commonly amplified, with only breast cancer patient xenograft samples (30%), neuroendocrine prostate cancers (14%) and typical prostate cancers (5%) showing evidence of amplification (Figure 3.17). However, similar to other termination factors eRF1 and JMJD4, HEMK2 mRNA appears to be upregulated in a variety of cancer types (Figure 3.18).

Interestingly, although overexpression of HEMK2 mRNA was only associated with reduced survival in breast cancer (Figure 3.19), a trend towards worse prognosis was observed in breast, lung and gastric cancer patients with tumours expressing increased mRNA levels of the HEMK2 co-activator Trm112 (Figure 3.20).

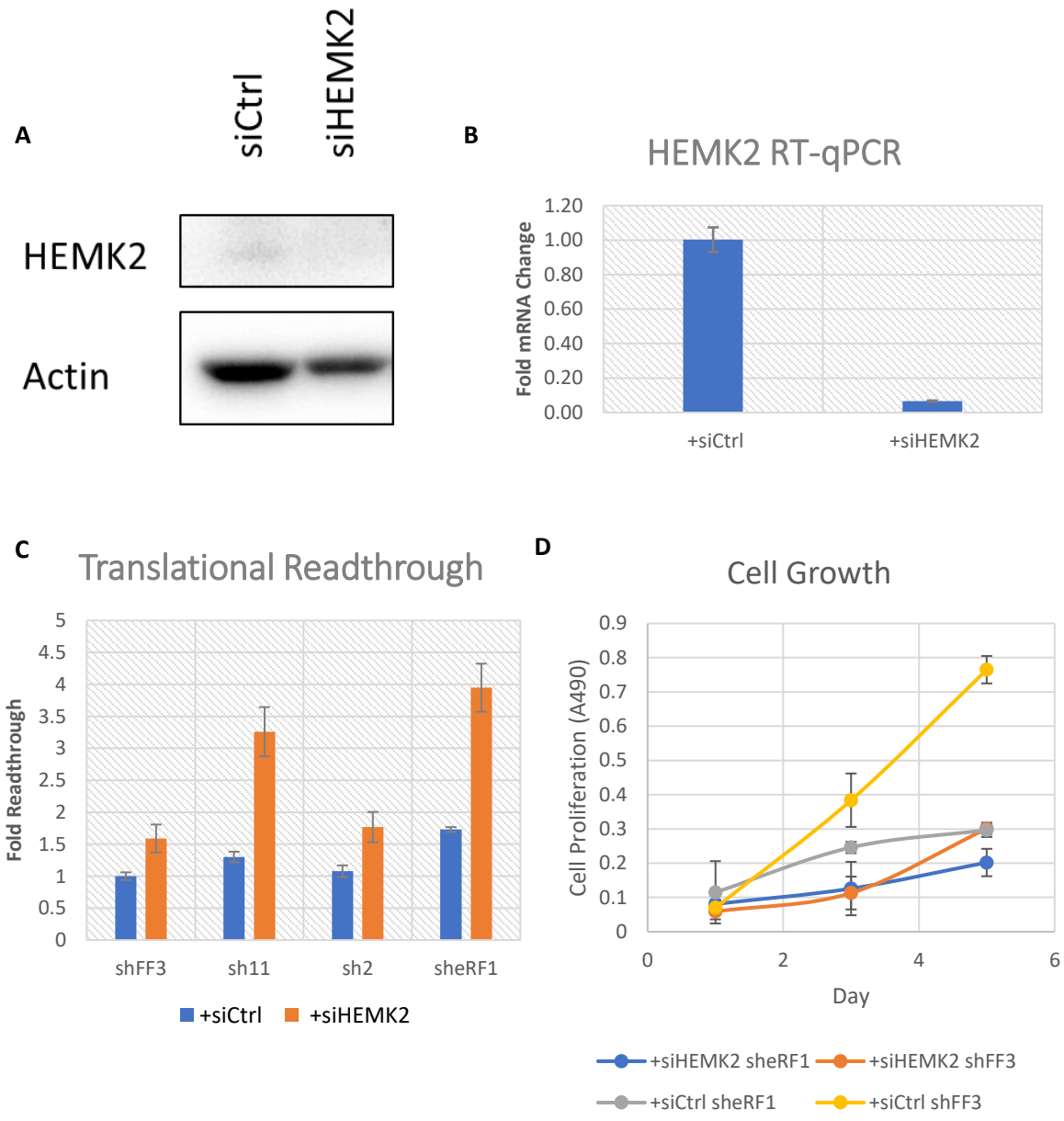


**Figure 3.16: HEMK2 affects translational readthrough and growth.** A) Western Blot shows knockdown of endogenous HEMK2 by HEMK2 siRNA B) RT-qPCR validation of HEMK2 knockdown following HEMK2 siRNA treatment. Performed independently of the western blot. C) U2OS shFF3, sheRF1, shJMJD4#2 (sh2) and shJMJD4#11 (sh11) were treated with Doxycycline for 48h, transfected with HEMK2 or control siRNA and subsequently plated with p2luc reporter plasmid BYDV. D) U2OS shFF3 and sheRF1 were treated with Doxycycline for 48h, transfected with HEMK2 or control siRNA and subsequently transferred to 96 well plates and assayed for proliferation by MTS. Measurements were taken at 3h post addition of MTS. n=3 ± Standard Deviation.

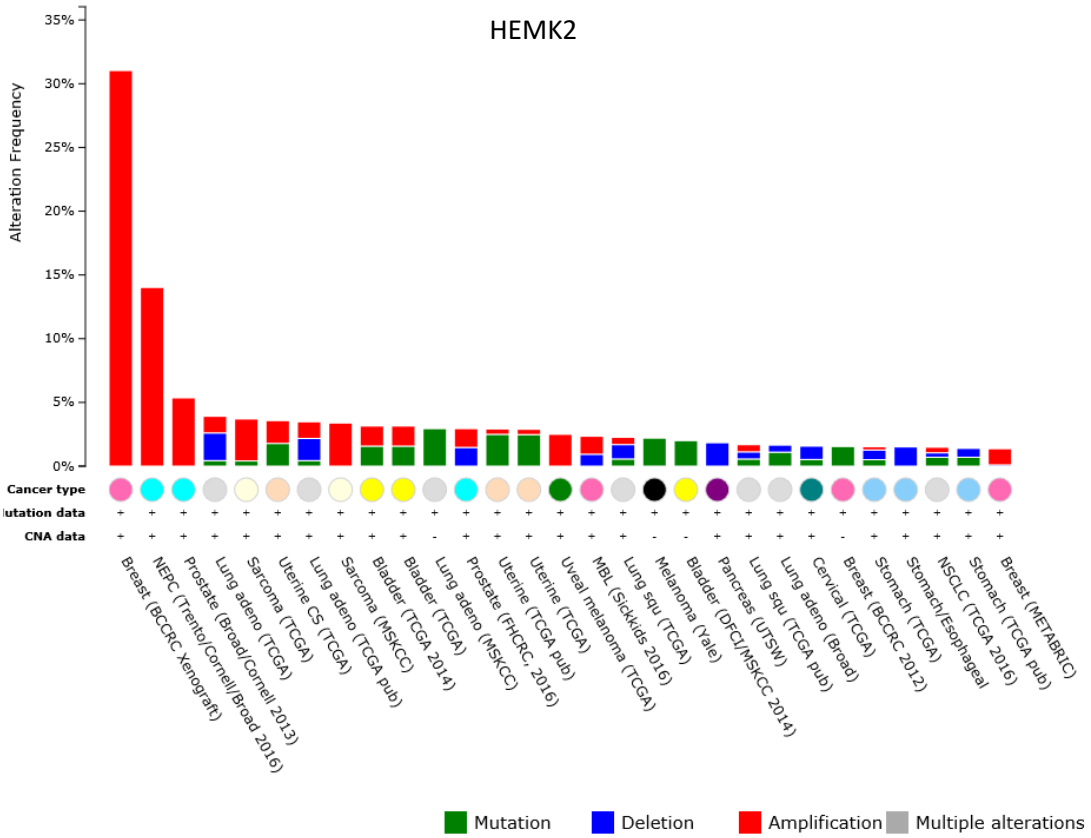


**Figure 3.17: Cancer Genomics of eRF1 methylase HEMK2**: HEMK2 is amplified by up to 30%, principally in breast and neuroendocrine prostate cancers (NEPC). Data obtained through cBioPortal (Gao et al., 2013).

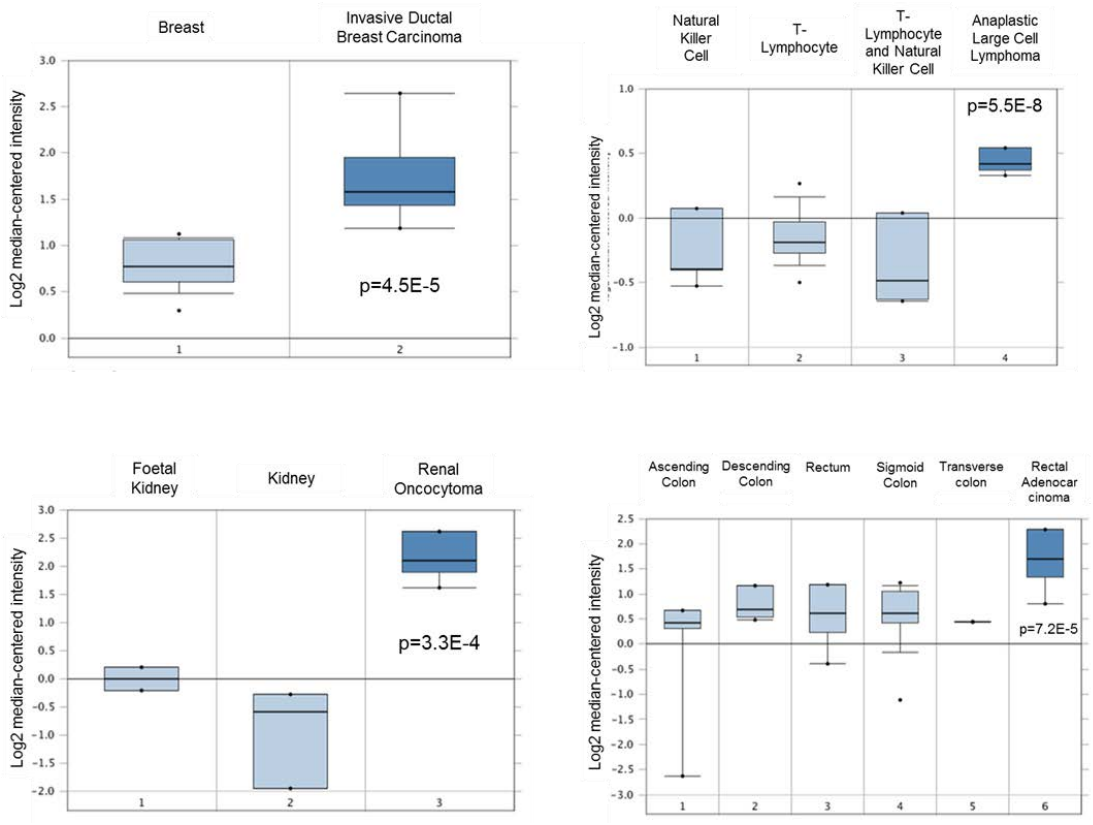


**Figure 3.18: Bioinformatics of HEMK2 gene expression in tumours.** HEMK2 transcript abundance can be shown to be significantly increased in invasive ductal breast carcinoma, anaplastic large cell lymphoma, renal oncocytoma and rectal adenocarcinoma compared to healthy tissue. p=Probability that there is no difference between the populations by two-tailed Student's t-test. Analysis via ONCOMINE (Rhodes et al., 2004).

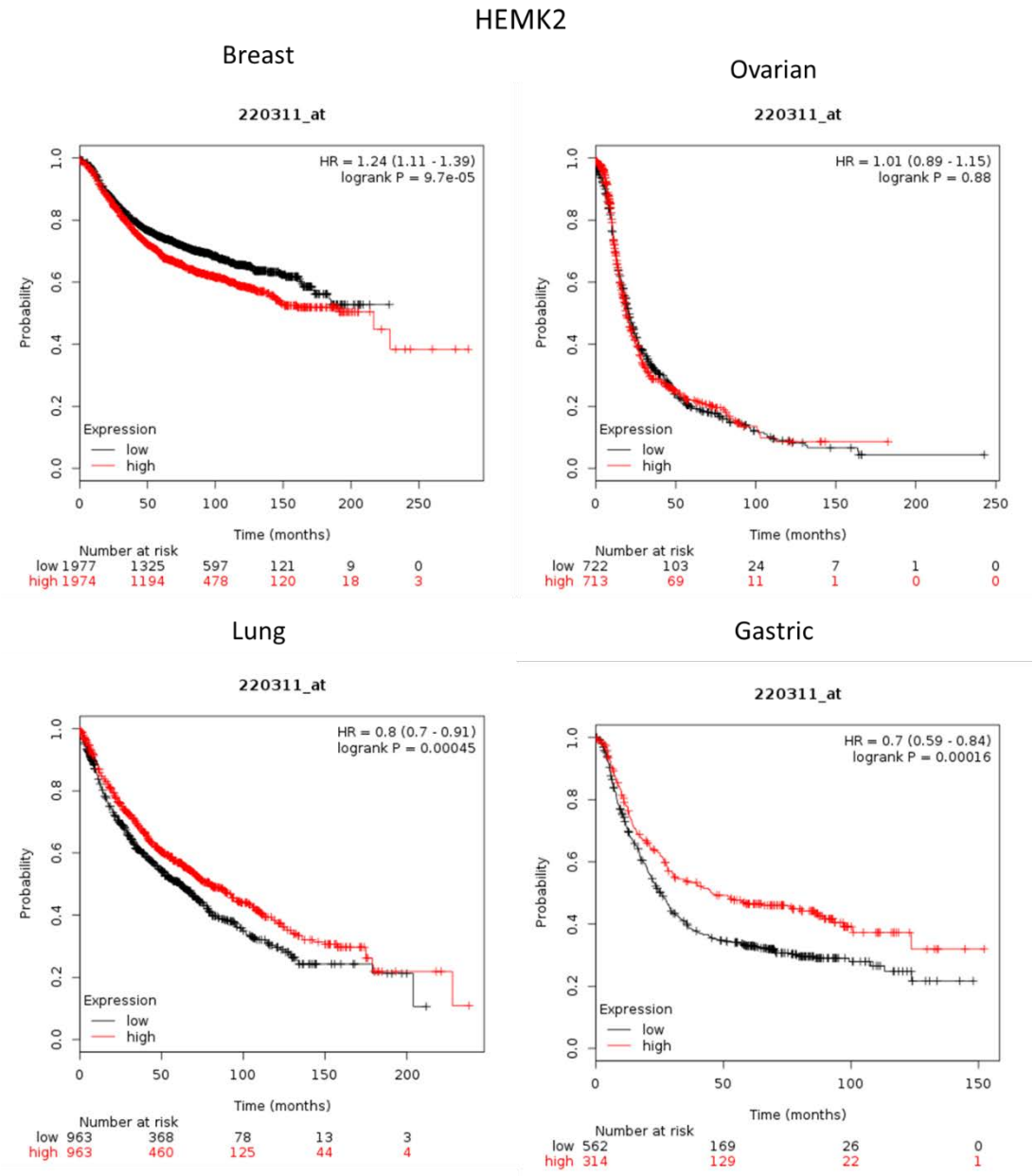


**Figure 3.19: Kaplan-Meier Survival analysis of HEMK2 mRNA expression in Breast, Ovarian, Lung, and Gastric cancers.** The probe identifier is located atop each plot. HR=Hazard Ratio, the ratio at which survival is modified by amplification of the corresponding gene in each cancer type. Logrank P= Probability that the difference between the two groups is significant using the log-rank non-parametric hypothesis test for survival distribution. Probability refers to the percentage probability of survival. Patient numbers in each curve are found below each blot. Analysis via Kaplan Meier Plotter (Szasz et al., 2016).

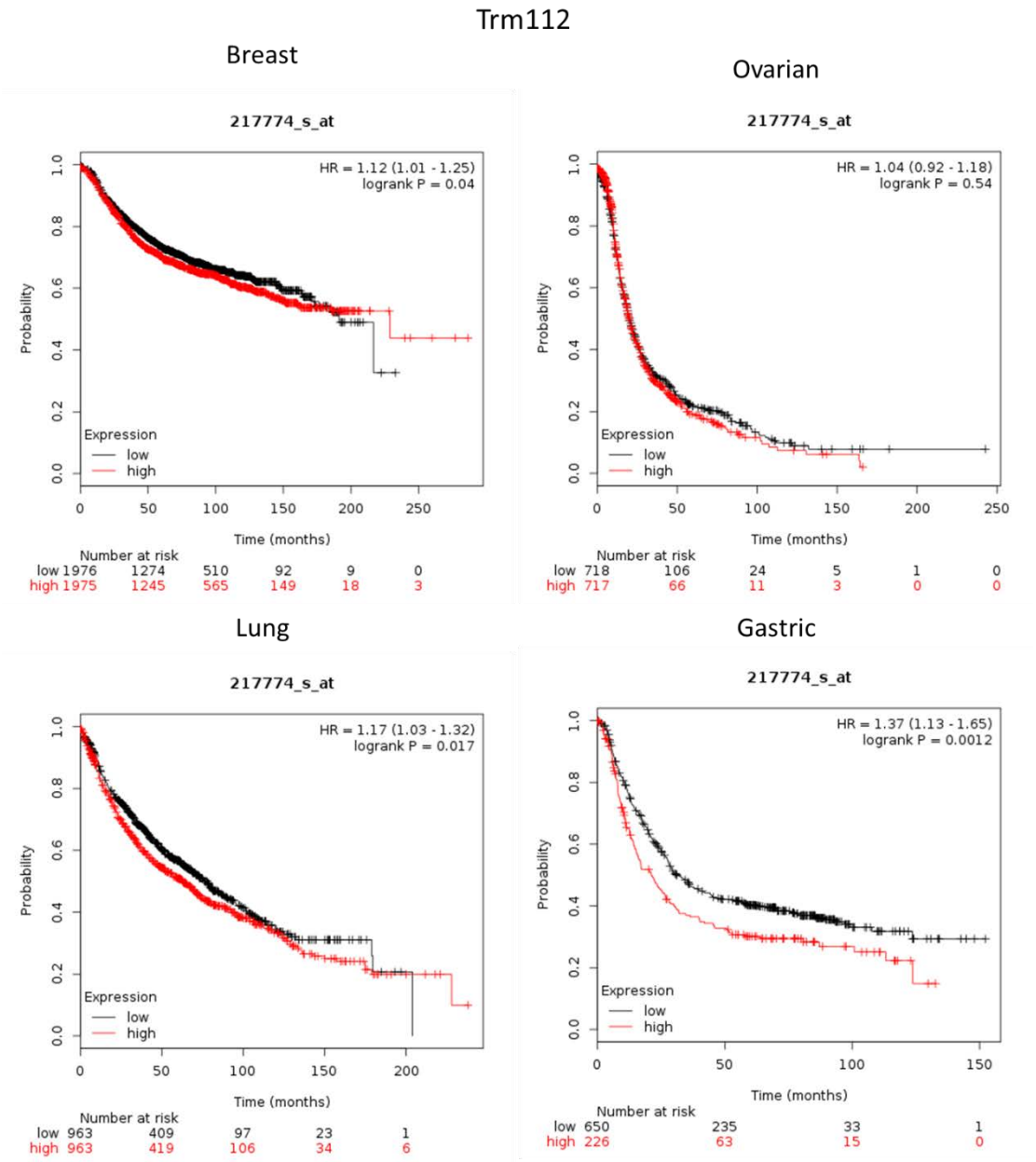


**Figure 3.20: Kaplan-Meier Survival analysis of the HEMK2 transactivator Trm112 RNA expression in Breast, Ovarian, Lung, and Gastric cancers.** The probe identifier is located atop each plot. HR=Hazard Ratio, the ratio at which survival is modified by amplification of the corresponding gene in each cancer type. Logrank P= Probability that the difference between the two groups is significant using the log-rank non-parametric hypothesis test for survival distribution. Probability refers to the percentage probability of survival. Patient numbers in each curve are found below each blot. Analysis via Kaplan Meier Plotter (Szasz et al., 2016).

### 3.2.8 Generation of an siRNA-resistant eRF1 rescue system

Having demonstrated the importance of JMJD4 and HEMK2 in translational readthrough and growth, we wished to explore the role of the corresponding eRF1 modification sites in greater detail. Consequently, a set of eRF1 cDNA sequences were designed containing an N-terminal Hemagglutinin (HA) epitope tag and either i) wildtype eRF1, (ii) ablation of the JMJD4 K63 hydroxylation site in the NIKS motif of eRF1 by mutation to Alanine or iii) mutation of the HEMK2 Q185 methylation site in the GGQ subdomain of eRF1 to Asparagine (as reported in (Seit-Nebi et al., 2001a)). Ideally, the effect of these mutants on growth and translational termination would be studied in the absence of confounding wildtype endogenous eRF1. In order to achieve this, the exogenous eRF1 cDNA sequences were engineered to contain a number of silent mutations in a validated siRNA target site (Figure 3.15). Sufficient mismatches in the exogenous eRF1 cDNA sequences would thus protect them from knockdown under conditions in which the endogenous eRF1 was depleted (Figure 3.21). These eRF1 cDNA sequences were then cloned into a variant pTRIPZ plasmid lacking RFP ('pTIPZ'), to allow conditional and physiological re-expression of eRF1. This system would thus allow for switchable expression of wildtype and mutant eRF1 while being able to selectively knock down the endogenous form.

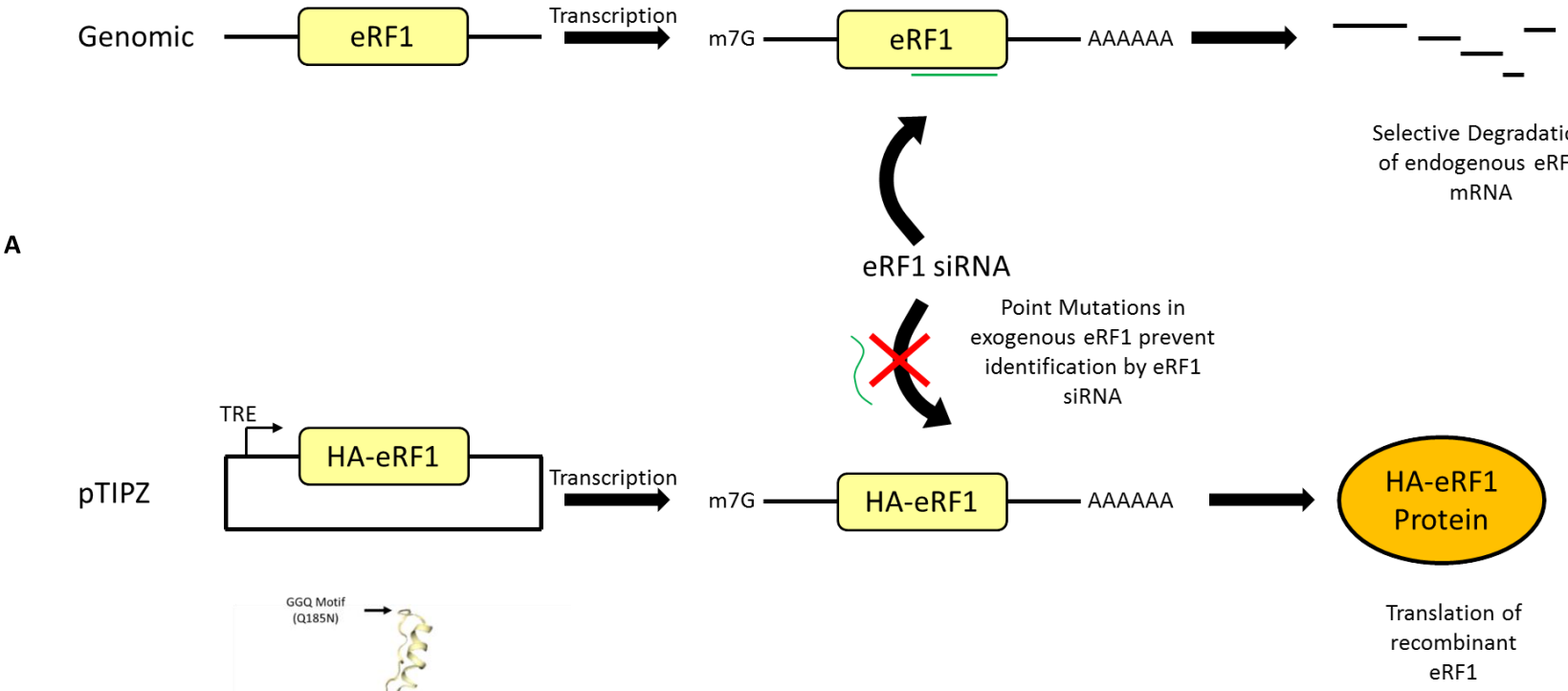


**Figure 3.21: eRF1 Mutations and siRNA/Rescue strategy.** A) Schematic of the eRF1 siRNA/rescue strategy. Induction with doxycycline causes transcription of the introduced HA-eRF1 (WT, K63A or Q185N) under the tetracycline inducible (TRE) promoter. Due to the presence of silent mutations in HA-eRF1, contemporaneous transfection with eRF1 siRNA cannot suppress it, so that only endogenous eRF1 is depleted, leaving the introduced form as the only form of eRF1 in the cell. B) Crystal structure of eRF1 highlighting the NIKS and GGQ motifs, the position of the K63A and Q185N mutations and the location of the HA-tag.

Stable puromycin-resistant U2OS cells were generated following lentiviral delivery of these vectors (as described above for shRNA). Initial validation of this eRF1 siRNA rescue 'structure/function' system was undertaken using 25nM siRNA and 0.1 μg $ml^{-1}$ Doxycycline (Figure 3.22). eRF1 siRNA was found to successfully deplete endogenous eRF1 as indicated by the absence of detectable eRF1 in control pTIPZ cells not expressing HA-eRF1 (designated empty vector, or 'EV').

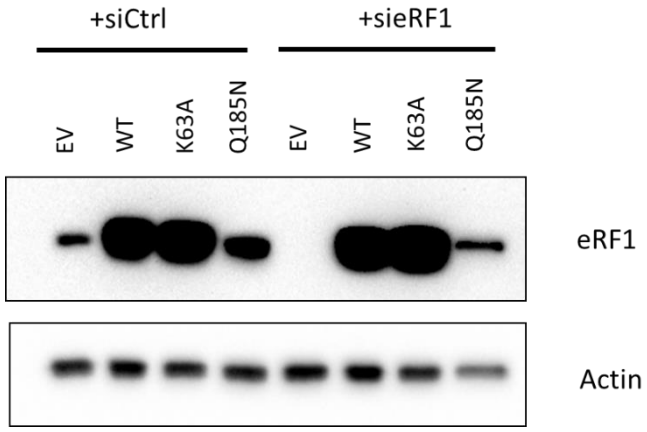


**Figure 3.22: Validation of the generation of an eRF1 rescue cell line system.** Cells were treated with 25nM eRF1 siRNA for 48h with a single dose of Doxycycline at 0.1 μg $ml^{-1}$ during the second day of knockdown. Harvesting occurred 48h after the doxycycline treatment.

Overexpression of eRF1 was readily observed in doxycycline-treated eRF1 wildtype (WT) and K63A mutant pTIPZ cell lines and, as anticipated, this was not affected by eRF1 siRNA treatment. In contrast, the level of re-expression achieved with the Q185N mutant was significantly lower, suggesting that this mutant may be unstable. Unfortunately, the differences in expression between exogenous and endogenous eRF1, and between WT/K63A mutant and Q185N exogenous eRF1 would likely hinder appropriate comparative analyses. Therefore, empirical optimisation of the doxycycline induction protocol was undertaken in order to better equalise eRF1

expression (data not shown). This resulted in doxycycline doses of 0.03 μg $ml^{-1}$ for WT and K63A and 0.5 μg $ml^{-1}$ for Q185N eRF1.

### 3.2.9 Examining the effect of eRF1 re-expression on translational termination and cell proliferation

Following optimisation of eRF1 expression in this system, we proceeded to determine the ability of wildtype and mutant eRF1 to rescue the effects of eRF1 siRNA on translational readthrough and cell growth. EV, WT, K63A and Q185N U2OS cells were treated with 25nM eRF1 or control siRNA along with the relevant optimised doxycycline concentrations. Twenty-four hours after the second siRNA treatment the cells were trypsinised and either reverse transfected with p2luc stop codon readthrough reporters or transferred to 96 well plates for MTS growth assays. Additional samples were taken for western blotting which confirmed successful siRNA knockdown and HA-eRF1 re-expression (Figure 3.23A).

eRF1 siRNA in the control 'EV' U2OS cells resulted in an increase in stop codon readthrough comparable to that seen in the sheRF1 U2OS and sieRF1 HeLa experiments discussed previously (Figure 3.23B). Consistent with an 'on-target' effect of eRF1 siRNA on translation termination, re-expression of WT eRF1 suppressed the majority of stop codon readthrough despite sieRF1 knockdown treatment. Interestingly however, re-expression of K63A completely failed to rescue the stop codon readthrough phenotype, with reporter values similar to those of the EV + sieRF1 treatment group. Similarly, re-expression of Q185N eRF1 completely failed to rescue stop codon readthrough induced by eRF1 siRNA.

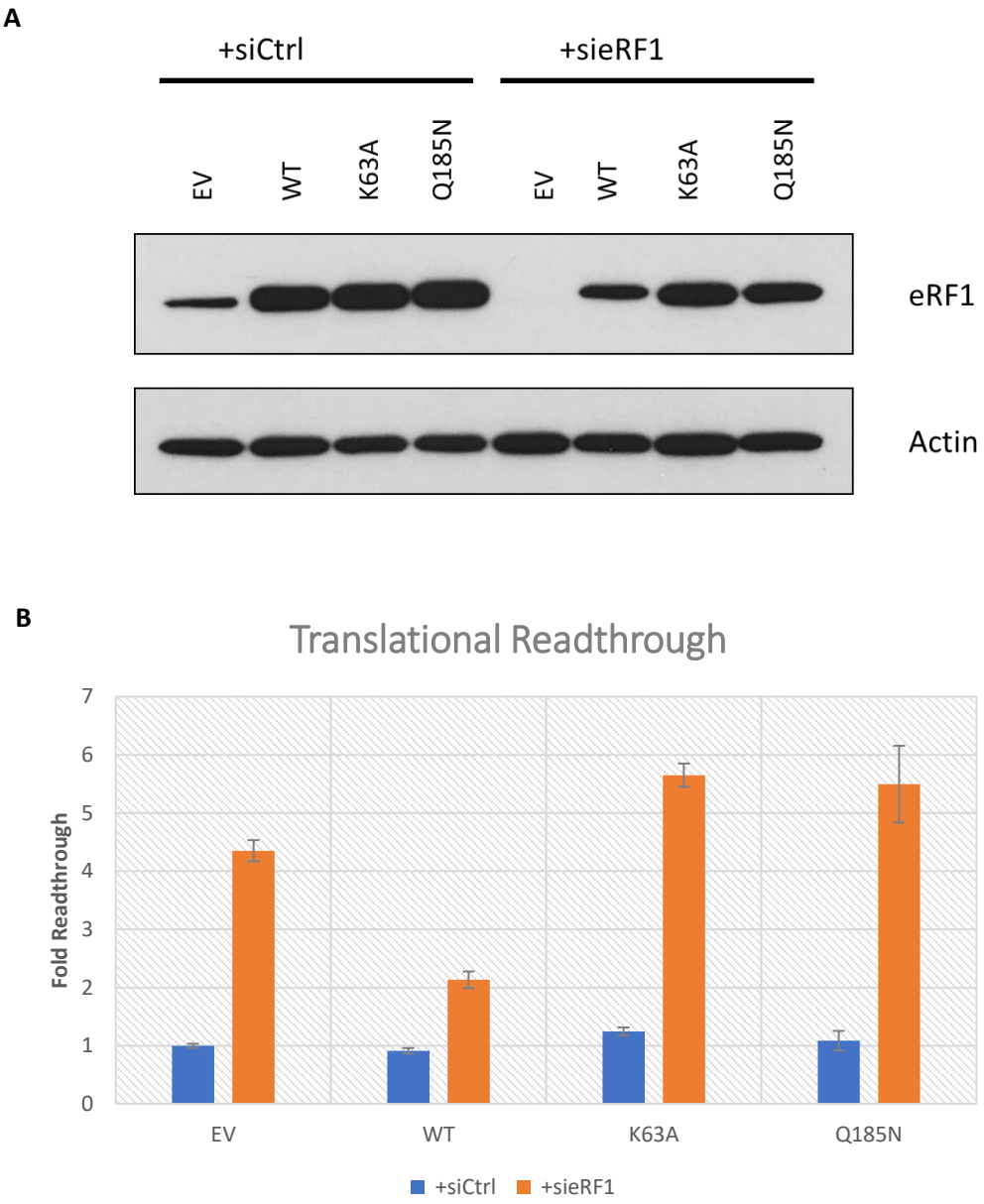


**Figure 3.23: Validation of eRF1 re-expression in U2OS cells inducibly expressing HA-eRF1, HA-eRF1 K63A and HA-eRF1 Q185N.** HA-eRF1, HA-eRF1 K63A were induced with 0.03 µg $ml^{-1}$ and HA-eRF1 Q185N with 0.5 µg $ml^{-1}$ doxycycline for 48h. A) Western Blot of eRF1 expression in the presence or absence of siRNA targeting the endogenous eRF1 only. B) Quantification of the fold translational readthrough during re-expression of the introduced forms of eRF1. n=3 ± Standard Deviation

With regards to cell proliferation (Figure 3.24), eRF1 siRNA led to a profound cytostatic response in the EV control cells, as expected. Reconstitution with siRNA resistant WT-eRF1 completely restored normal growth to comparable levels observed in the control siRNA treated group. Consistent with the stop codon readthrough data, neither K63A nor Q185N mutants were able to restore normal growth control in eRF1 knockdown cells. In the absence of eRF1 knockdown, all cell lines grew at an approximately equal pace, with the notable exception of Q185N: The severe loss of growth in the presence of endogenous eRF1 may indicate that this mutant acts in a dominant negative manner. While the mechanism is unknown, mutation of the GGQ motif to AAQ has previously been used to trap ribosomes in a termination state (Brown et al., 2015). It is therefore possible that Q185N may 'poison' the ribosome, by stalling termination and preventing the release of mature proteins.

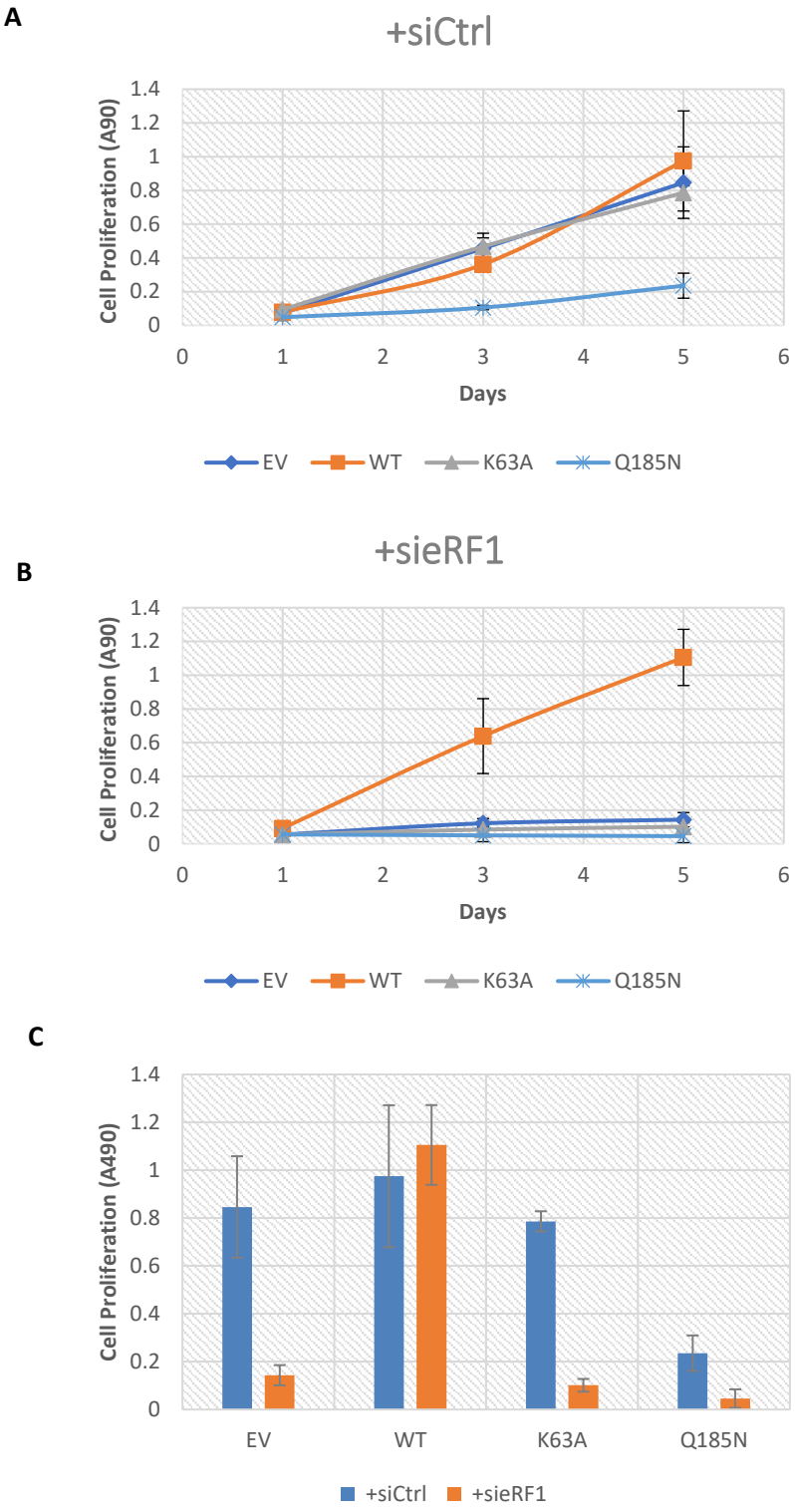


**Figure 3.24: Characterisation of the effect of eRF1 rescue variants on 2D proliferation**. A) Expression of the inducible forms by addition of 0.03 µg $ml^{-1}$ Doxycycline (0.5 µg $ml^{-1}$ for Q185N) for 48h with simultaneous treatment with control siRNA. B) Expression of the inducible forms by addition of 0.03 µg $ml^{-1}$ Doxycycline (0.5 µg $ml^{-1}$ for Q185N) for 48h with simultaneous treatment with eRF1 siRNA. C) Comparison of the +siCtrl and +sieRF1 groups on day 5. n=3± Standard Deviation

## 3.3 Discussion

Previous work describing JMJD4 as a novel termination factor, as well as our observation of its widespread gene amplification in cancer, attracted our interest in how translational termination factors may generally influence cell growth. Here we present evidence that support a role for eRF1, JMJD4 and HEMK2 in translational termination and cell proliferation. We extended these findings using an siRNA resistant eRF1 structure/function system to interrogate the requirement for specific modification sites in normal translational termination and growth control.

Our initial analyses of translational termination factors in cancer initially focused on identifying genetic alterations, particularly amplifications, of the eRF1, JMJD4 and HEMK2 genes using the cBioPortal cancer genome database. This identified that whereas eRF1 and HEMK2 genes were only amplified in a small number of tumour types, JMJD4 was frequently amplified, and in a wide variety of cancers. However, amplification in cancers does not automatically imply a functional role, as copy number alterations are not necessarily associated with increased expression (for instance only 40% of amplified genes in breast cancer are also overexpressed) (Hyman et al., 2002) and may simply be a side effect of chromosomal abnormalities (Tsafrir et al., 2006). Since important cancer genes can be deregulated by multiple mechanisms (Asghar et al., 2015), we therefore also monitored altered expression levels using the online Oncomine transcriptomic database. Using this approach we identified widespread upregulation of eRF1, JMJD4 and HEMK2 mRNA across cancer types, which in some cases was associated with worse patient prognosis. Overall, this preliminary analysis using public ally available data suggested that the

translational termination pathway may be commonly upregulated during tumourigenesis. This would be entirely consistent with evidence that deregulation of translational initiation and elongation factors supports tumourigenesis (Truitt and Ruggero, 2017): Presumably, coordinating the upregulation of the termination process with earlier steps of the translation process is critical in order to maximize protein synthesis rate and fidelity.

To explore the role of termination factors in cell growth we first developed a variety of cell models including transient siRNA, conditional shRNA and an siRNA-resistant 'rescue' system. Prior to their application in growth analyses these systems were first validated using established stop codon readthrough assays based on the dual luciferase p2luc vector described above. These experiments confirmed the anticipated translational termination defects following HEMK2, JMJD4 and eRF1 knockdown. Consistent with this, eRF1 mutants that cannot be modified by JMJD4 or HEMK2 were unable to rescue termination defects when re-expressed in eRF1 knockdown cells.

Interestingly, knockdown experiments indicated that the effect of JMJD4 depletion may not be equal in all termination contexts. In the case of the TMV TGA context JMJD4 knockdown resulted in only 1.5-fold increase in translational readthrough, compared to approximately 3-fold for BYDV and CFW1282* termination contexts (Figure 3.11B).

Context-dependent translational termination has been previously described. For example, several ciliate species utilise a non-standard genetic code lacking termination codons, with the context for termination provided by the mRNA 3' ends (Swart et al., 2016). In a less extreme example, the +1 position following the stop

codon has been shown to influence termination efficiency in viruses, bacteria and mammals (Tate et al., 1995, Li and Rice, 1993, McCaughan et al., 1995), while the bases at positions -1&-2 to the stop codon have also been studied (Cassan and Rousset, 2001).

Additionally, it is of note that siRNA mediated transient knockdown of JMJD4 (Figure 3.15B) resulted in much higher levels of apparent translational readthrough than either of the shJMJD4 cell lines in the same termination context, to levels similar to those obtained by eRF1 knockdown. Since the increase in translational readthrough observed during depletion of eRF1 is similar for sieRF1 and sheRF1 (5-7 fold) the difference is likely specific for JMJD4 rather than dependent on the methodology. There are a number of possible explanations for this. The shJMJD4 cells exhibited significantly reduced levels of JMJD4 even in the absence of doxycycline, so it is likely that habituation to a permanent lack of JMJD4 availability had taken place, resulting in a less dramatic phenotype. Additionally, the reduced JMJD4 baseline in the shJMJD4 cells may have resulted in a lower dynamic range, further impacting measurements.

Concerning the role of termination factors in cell proliferation, we find that JMJD4 or HEMK2 knockdown results in a reduction in cell proliferation, whereas eRF1 depletion results in a strongly cytostatic phenotype. However, growth reduction by JMJD4 siRNA was more pronounced than shRNA, in line with the greater translational readthrough values measured in this approach. Three-dimensional noble agar growth experiments also further supported the idea that JMJD4 and eRF1 have important roles in supporting cell growth, including in more complex conditions designed to mimic physiologically and pathologically relevant micro-environments. Interestingly, our JMJD4 growth data contrasts with a previous study indicating that

JMJD4 appears to be non-essential for mouse embryonic development and may not affect cell growth *in vitro* (Yoo et al., 2016a)**.** Although, the reasons for this discrepancy are unclear at present, it is interesting to note that our study focussed on tumour cells, whereas the study by Yoo *et al* was restricted to non-transformed primary cells. Whether this might highlight a role for eRF1 hydroxylation in specifically supporting tumour cell growth is not clear, but of interest.

Surprisingly, growth reduction following eRF1 or JMJD4 depletion was not associated with specific changes in cell cycle profile. It would appear that affected cells either stop (eRF1) or slow (JMJD4) their progression through each part of the cell cycle equally, rather than activating a single specific cell cycle checkpoint blockade. A similar manner of regulation has been found to occur for the ribosomal proteins RPL5 and RPL11, where their depletion has been shown to result in a reduction of cell cycle proliferation without the induction of checkpoints. Instead, reduced global protein synthesis causes cyclin levels to drop below the minimum threshold for cell cycle progression, causing the cells to halt their cycling rate (Teng et al., 2013). It is likely that a similar mechanism operates during both eRF1 and JMJD4 depletion, and which may therefore be a general cell cycle response to defective translational termination.

The consistent growth and cell cycle phenotype following termination factor knockdown raised questions regarding the molecular mechanism(s) involved. Since other JMJD4 substrates have not (yet) been reported (see also Chapter 2), it is seemingly likely that its role in growth is via modification of eRF1. Beyond its activity as the translation termination factor, eRF1 has been implicated in the formation of a complex with eRF3 and the non-sense mediated decay proteins Upf1 and SMG-1, resulting in the phosphorylation and activation of UPF1 (Kashima et al.,

2006). However, depletion of UPF1 has been shown to result in an early S phase arrest of the cell cycle (Azzalin and Lingner, 2006), while SMG-1 knockdown results in arrest at G2 (Brumbaugh et al., 2004). Consequently, defective eRF1 function in nonsense mediated decay signalling would appear unlikely to explain the characteristics of the growth phenotypes described here. Rather, one could hypothesise that loss of efficient termination would result in nascent polypeptides with abnormally long C-termini, resulting in misfolding and degradation. A number of other potential mechanisms might also occur and contribute to the observed phenotypes. For example, stop codon readthrough can result in extended C-termini that have functional consequences, conferring specific new biological attributes to the protein in question (Loughran et al., 2014, Schueren et al., 2014). Though not yet formally proven, it is also possible that some genes may act as specific termination 'sensors': It has been hypothesised that the expression of transcription factors whose translation is regulated by upstream open reading frames (uORFs) could respond to changes in translational termination efficiency (Ait Ghezala et al., 2012a).

An important caveat of the work presented in this chapter is that the actual eRF1 modifying activity of JMJD4 and HEMK2 were not examined. While knockdown of JMJD4 specifically was tested at the protein level and a translational readthrough phenotype consistent with literature could be observed, its actual level of activity was not measured. This could have been achieved in two ways: presenting cell extracts with JMJD4 peptide substrates *in vitro* and measuring the rate of hydroxylation in order to determine the overall activity of JMJD4 in the samples, and by directly assessing the level of eRF1 hydroxylation within the cells by mass spectrometry. Similarly, following knockdown of eRF1, the level of eRF1 ribosomal occupancy and how it differed from the physiological state was not measured.

In conclusion, eRF1 and its post translational modifiers JMJD4 and HEMK2 appear to play an important role in cell growth, likely mediated by their requirement for efficient translational termination. Exactly how translational termination supports cell growth, and how defects in this fundamental process elicit growth inhibition are not known. The work presented in the chapters that follow aimed to address these questions.

# CHAPTER 4: Characterising the cellular response to defective translational termination using RNA Sequencing

## 4.1 Introduction

In chapter 3, knockdown of translational termination factors was associated with a reduction in cellular proliferation. Combined with the discovery that the reduction in growth was not associated with changes in cell cycle profile, and therefore unlikely to be due to activation of classical cell cycle checkpoints, the question arose how these phenotypes came about. We propose that the observed reduction in growth would be most likely associated with altered cell signalling transduction, the unfolded protein response, other stress-activated pathways, or a combination of these. Such stress and adaptive responses often cause specific transcriptional changes due to the modulation of specific transcription factors (Hetz, 2012). Therefore, in order to begin to understand responses to defective translational termination we proposed an analysis of the transcriptome of cells under eRF1 knockdown. Emphasis was initially placed on solely examining the effects of eRF1 because of the robust phenotypes observed, and limited resources. Using bioinformatic tools, differential expression analyses of the transcriptomes was performed followed by biological pathway analyses.

## 4.2 Results

### 4.2.1 RNASeq

The data presented throughout this chapter were in large part obtained via RNA Sequencing, commonly referred to as RNA-Seq and formally known as whole transcriptome shotgun sequencing. During RNA-Seq, RNA is extracted from cells and its quality assessed through the RNA Integrity Number (RIN) algorithm via capillary gel electrophoresis measurements. Subsequently, the RNA can be further purified to select only specific types, e.g. only mature 3'-polyadenylated mRNAs or to selectively deplete the abundant ribosomal rRNAs. Following the selection stage, the RNA is reverse transcribed into cDNA using random primers and fragmented to create short overlapping sequences. After cDNA synthesis, sequencing adapters are added to the 5' and 3' ends of the short fragments and the results are amplified by PCR prior to sequencing. The results of the sequencing are then typically aligned against the genome of the organism used, the types of RNA expressed are identified and their relative expression quantified (Figure 4.1).

In order to begin to identify the transcriptomic changes associated with defective translational termination, the previously described sheRF1 and shFF3 knockdown cells were used. U2OS sheRF1 and shFF3 were treated with 2 μg $ml^{-1}$ Doxycycline for four days to ensure complete knockdown of eRF1, before being harvested for RNA extraction and Western Blotting. To assess RNA quality the extracts were assayed using a ScreenTape assay, where the 18S/28S rRNA ratio is calculated as a measure of the integrity of total RNA (Figure 4.2). The RNA samples were then

submitted for sequencing using a NeoPrep kit (performed by Dr Celina Whalley, University of Birmingham).

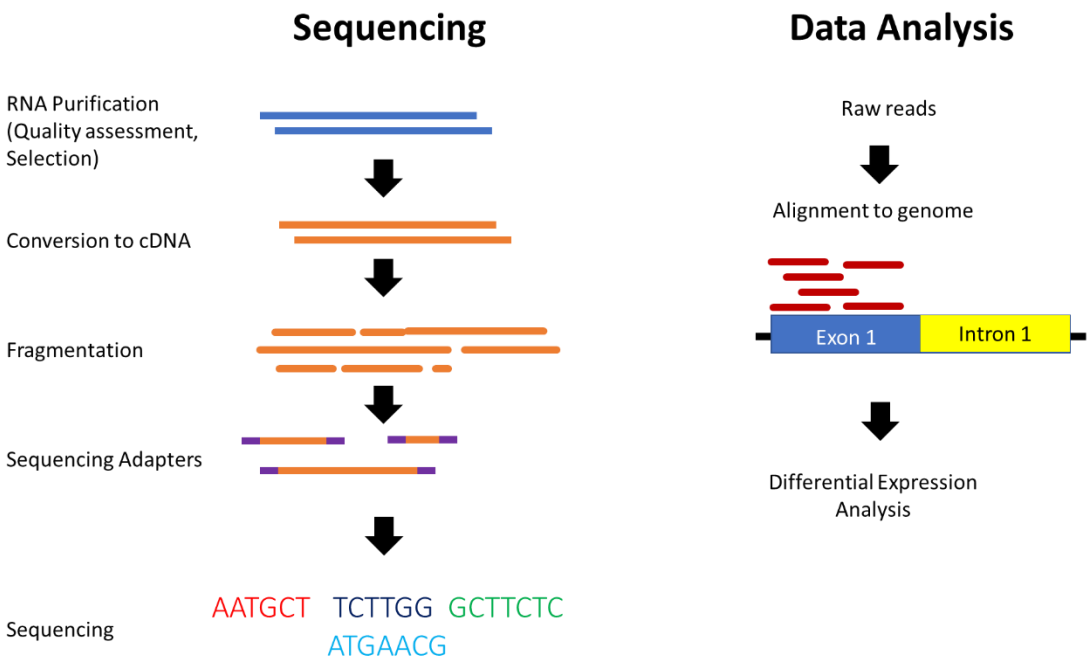


**Figure 4.1: Schematic of a typical RNA-Seq workflow.** Processes have been abbreviated and simplified for clarity. RNA is purified, converted into cDNA and fragmented. The sequence fragments are then ligated to known adapter sequences which are used as the binding site for sequencing primers. The reads are then aligned to the genome of the organism the RNA was isolated from and regulated genes identified based on the level of expression.

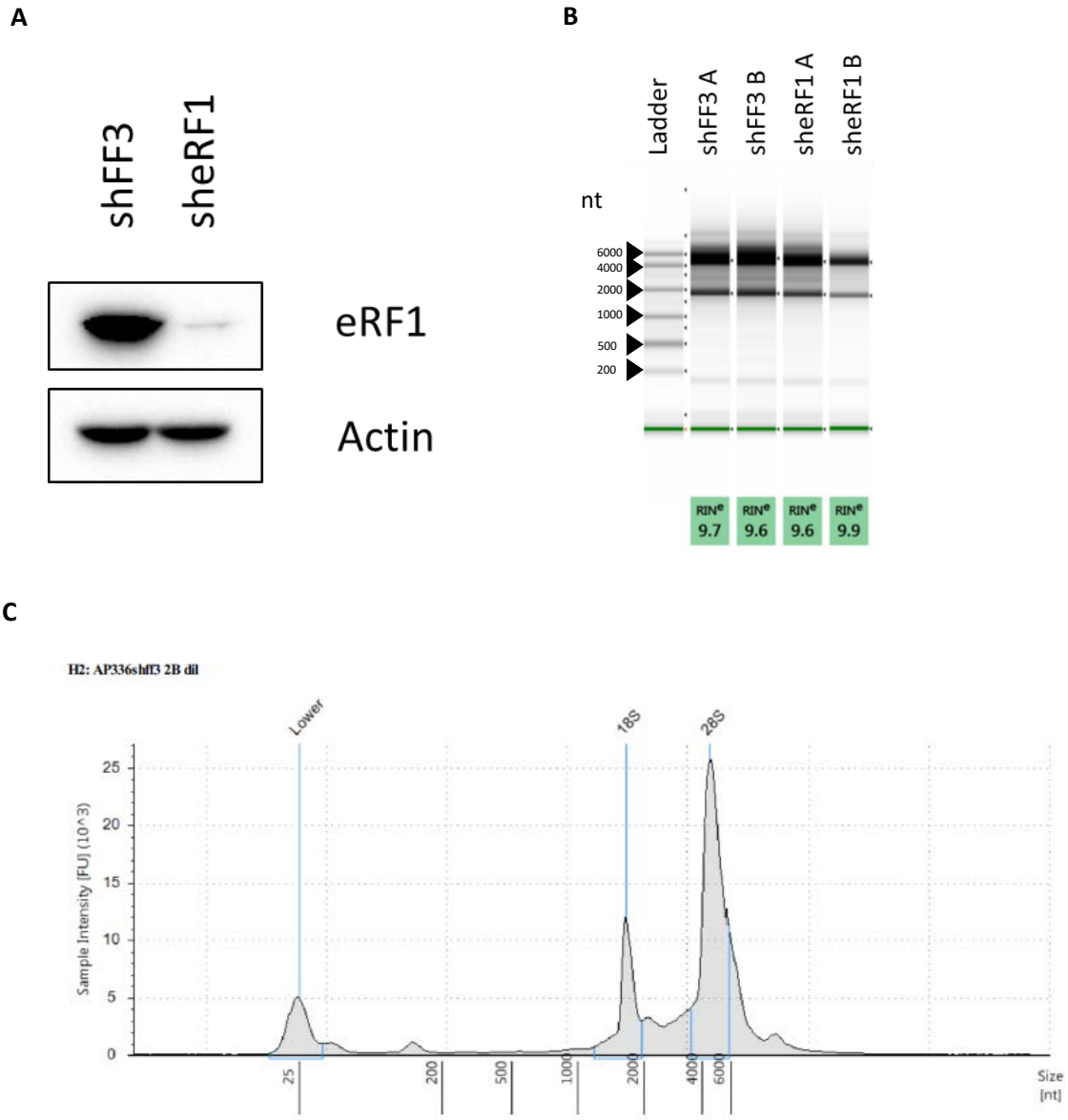


**Figure 4.2: RNA ScreenTape Assay of RNA samples used in the RNASeq and validation of knockdown**. Integrity is evaluated based on the ratio of 18S/28S rRNA and an RNA Integrity (RIN) value assigned on a scale 1-10. Higher RIN values indicate higher RNA integrity, with values >8 being useful for transcriptomic analyses. A) Western blot of the control vs eRF1 knockdown following 96h of 1 µg $ml^{-1}$ doxycycline treatment. B) Gel Image and cumulative Table of RIN values for all samples. C) Representative individual electropherogram validating RNA integrity for each of the samples examined.

Bioinformatic analysis was performed by Dr Robert Hollows (Institute of Cancer and Genomic Sciences, University of Birmingham), as follows. Gene level differential expression analysis of the results was performed by comparing the data from control and sheRF1 cells. RNA-Seq data for the two control replicates and the two eRF1 knockdown replicates were aligned to the hg19 human genome using Rsubread aligner and assigned to individual genes using the featureCounts function. Read counts were then normalised between samples and converted to counts-per-million reads ("cpm") for each gene using the edgeR package in R. Only genes with a cpm of more than 1 in at least 2 samples were considered for subsequent differential expression analysis. Genes were deemed to be differentially expressed between control and knock-out groups if the fold-change (knock-down/control) was greater than 1.5 or less than -1.5 and the probability value was less than 0.05 (Liao et al., 2013).

Based on these criteria, lists of the most upregulated and downregulated genes were compiled. The top 20 most affected genes on each list are catalogued in Figures 4.3 and 4.4, respectively. In 4.4, successful knockdown of the eRF1 gene ETF1 is also validated. The complete gene lists were compared via centroid linkage clustering, demonstrating that the shFF3 and sheRF1 samples clustered independently, a representative example of which is shown in Figure 4.5.

| Gene | Description | PValue | FDR | Fold Change ▼ |
|---|---|---|---|---|
| C2orf80 | chromosome 2 open reading frame 80 | 0 | 0 | 13998.55 |
| IGFBP4 | insulin-like growth factor binding protein 4 | 0 | 0 | 2387.30 |
| MLPH | melanophilin | 9.65E-52 | 5.68E-50 | 759.66 |
| LOC101927697 | uncharacterized LOC101927697 | 5.03E-191 | 3.17E-188 | 645.04 |
| CRYGA | crystallin, gamma A | 5.08E-26 | 1.11E-24 | 419.90 |
| HOXB-AS1 | HOXB cluster antisense RNA 1 | 7.82E-24 | 1.54E-22 | 375.41 |
| CDCA7 | cell division cycle associated 7 | 9.67E-278 | 1.22E-274 | 209.45 |
| CDH11 | cadherin 11, type 2, OB-cadherin (osteoblast) | 7.83E-287 | 1.09E-283 | 152.92 |
| GALNT13 | polypeptide N-acetylgalactosaminyltransferase 13 | 1.30E-80 | 1.54E-78 | 139.40 |
| ALS2CR11 | amyotrophic lateral sclerosis 2 (juvenile) chromosome region, candidate 11 | 1.66E-44 | 7.95E-43 | 130.12 |
| HOXB2 | homeobox B2 | 3.32E-227 | 2.83E-224 | 125.53 |
| SYK | spleen tyrosine kinase | 1.31E-28 | 3.27E-27 | 83.60 |
| C17orf96 | chromosome 17 open reading frame 96 | 1.93E-92 | 2.88E-90 | 76.21 |
| FOXG1 | forkhead box G1 | 3.95E-24 | 7.89E-23 | 69.82 |
| ZNF730 | zinc finger protein 730 | 7.51E-19 | 1.11E-17 | 53.90 |
| ETV1 | ets variant 1 | 1.92E-44 | 9.15E-43 | 53.32 |
| ITGA4 | integrin, alpha 4 | 7.71E-96 | 1.27E-93 | 49.71 |
| GJD3 | gap junction protein, delta 3, 31.9kDa | 3.95E-42 | 1.70E-40 | 39.88 |
| SYCE1L | synaptonemal complex central element protein 1-like | 2.26E-46 | 1.15E-44 | 36.38 |
| ALDH3B2 | aldehyde dehydrogenase 3 family, member B2 | 7.34E-25 | 1.51E-23 | 30.30 |

**Figure 4.3: Gene expression is affected by knockdown of eRF1. Top 20 most upregulated.** Genes identified following bioinformatic analysis of the RNA-Seq data ranked by fold change (high to low). PValue=The probability that the difference between shFF3 and sheRF1 is not real, FDR=False Discovery Rate, the number of anticipated false positives/number of regulated genes. Any value depicted as zero is small enough to be registered as such by the pathway analysis software.

| Symbol | Description | PValue | FDR | Fold Change ▼ |
|---|---|---|---|---|
| MGAT4D | MGAT4 family, member D | 2.57E-89 | 3.60E-87 | -1338.87 |
| CD36 | CD36 molecule (thrombospondin receptor) | 0 | 0 | -678.30 |
| CACNG3 | calcium channel, voltage-dependent, gamma subunit 3 | 1.88E-40 | 7.58E-39 | -554.69 |
| HTN3 | histatin 3 | 8.29E-44 | 3.84E-42 | -138.04 |
| TMPRSS11E | transmembrane protease, serine 11E | 1.86E-161 | 8.47E-159 | -109.80 |
| DNAJC18 | DnaJ (Hsp40) homolog, subfamily C, member 18 | 4.77E-189 | 2.93E-186 | -55.77 |
| SPINK1 | serine peptidase inhibitor, Kazal type 1 | 6.94E-34 | 2.18E-32 | -38.39 |
| HTN1 | histatin 1 | 7.04E-56 | 4.67E-54 | -34.39 |
| PTPN22 | protein tyrosine phosphatase, non-receptor type 22 | 1.14E-32 | 3.39E-31 | -34.37 |
| LINC00861 | long intergenic non-protein coding RNA 861 | 4.55E-268 | 5.01E-265 | -32.86 |
| UGT3A2 | UDP glycosyltransferase 3 family, polypeptide A2 | 1.42E-24 | 2.91E-23 | -32.56 |
| ATP6V0D2 | ATPase, H+ transporting, lysosomal 38kDa, V0 subunit | 6.74E-69 | 6.00E-67 | -32.55 |
| LOC100507351 | uncharacterized LOC100507351 | 4.96E-42 | 2.12E-40 | -30.86 |
| ABCA8 | ATP-binding cassette, sub-family A (ABC1), member 8 | 3.36E-29 | 8.60E-28 | -29.89 |
| CXCL12 | chemokine (C-X-C motif) ligand 12 | 0 | 0 | -29.06 |
| LYPD6B | LY6/PLAUR domain containing 6B | 7.91E-33 | 2.38E-31 | -28.24 |
| LOC101927482 | uncharacterized LOC101927482 | 2.14E-43 | 9.68E-42 | -27.34 |
| CRISP3 | cysteine-rich secretory protein 3 | 3.05E-124 | 8.48E-122 | -26.88 |
| LOC100129520 | testis expressed sequence 13-like | 1.02E-30 | 2.80E-29 | -26.08 |
| ADAM28 | ADAM metallopeptidase domain 28 | 5.48E-165 | 2.73E-162 | -25.74 |
| ETF1 (eRF1) | Eukaryotic Termination Factor 1 | 0 | 0 | -12.15 |

**Figure 4.4: Gene expression is affected by knockdown of eRF1. Top 20 most downregulated.** Genes identified following bioinformatic analysis of the RNA-Seq data ranked by fold change (high to low). PValue=The probability that the difference between shFF3 and sheRF1 is not real, FDR=False Discovery Rate, the number of anticipated false positives/number of regulated genes. Any value depicted as zero is small enough to be registered as such by the pathway analysis software. In the last column, the gene coding for eRF1, ETF1, is presented to validate knockdown.

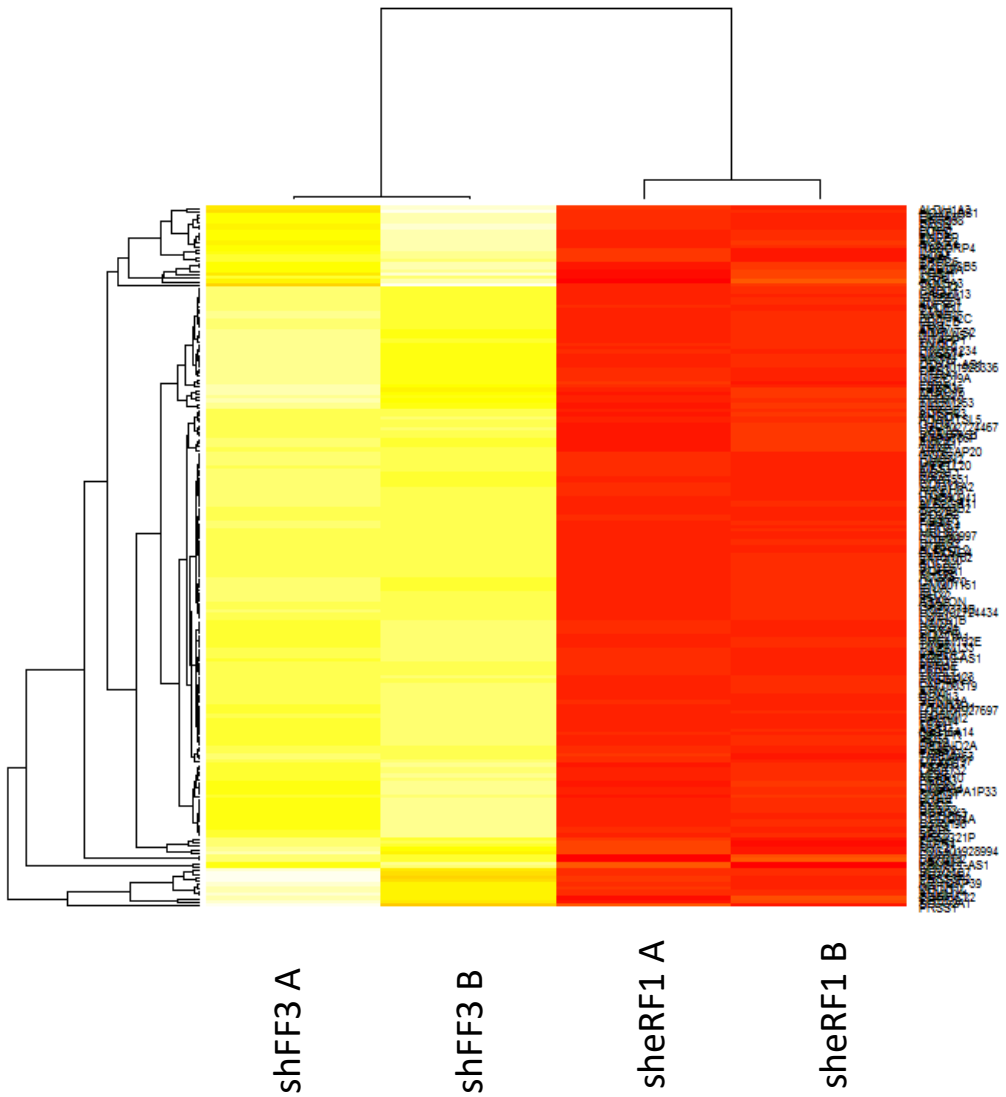


**Figure 4.5: Heatmap of the top 200 upregulated genes.** Genes and samples have been clustered in the heatmap using 1 – (Pearson) correlation (between genes / samples) as the distance measure and using centroid linkage for determining groups. The linkage method determines how the distance between two clusters is defined. With the centroid linkage method, the distance between two clusters is the distance between the cluster centroids or means. The control and eRF1 knockdown samples cluster independently. Graph provided by Dr Robert Hollows, University of Birmingham.

These lists were subsequently further processed through the pathway analysis platform Reactome, in order to determine any pathways which might be significantly regulated at the RNA level. The lists obtained following RNA-Seq were analysed using overrepresentation analysis, an analytic approach in which the abundance of regulated genes is tested against the probability of them being randomly modulated, using a binomial test. The probabilities obtained were further corrected through the Benjamini-Hochberg procedure for multiple testing since the list is compared to every pathway. Pairwise protein-protein interaction data of the European Bioinformatics Institute (EMBL-EBI) database IntAct were included as part of the extended analysis. The results are summarised in Figures 4.6-4.9, along with an explanation of the major metrics involved in their identification. Unfortunately, manual analysis indicated a large degree of overlap in the gene lists by which pathways were identified. Therefore, Reactome pathways were further manually curated so that individual pathways sharing both functional similarity *and* highly similar gene lists have been condensed in broader categories, as indicated in the figures.

A

| Pathway name | #Entities found | #Entities total | Entities ratio | Entities pValue | Entities FDR |
|---|---|---|---|---|---|
| Peptide chain elongation | 27 | 99 | 0.008181818 | 1.71E-04 | 0.127201816 |
| Formation of a pool of free 40S subunits | 28 | 106 | 0.008760331 | 2.88E-04 | 0.127201816 |
| Selenocysteine synthesis | 28 | 116 | 0.009586777 | 8.41E-04 | 0.292192627 |
| Assembly of collagen fibrils and other multimeric structures | 12 | 60 | 0.004958678 | 0.001213744 | 0.292192627 |
| Eukaryotic Translation Termination | 26 | 108 | 0.00892562 | 0.001490779 | 0.292192627 |
| Nonsense Mediated Decay (NMD) independent of the Exon Junction Complex (EJC) | 26 | 102 | 0.008429752 | 0.002685993 | 0.472734742 |
| SRP-dependent cotranslational protein targeting to membrane | 26 | 120 | 0.009917355 | 0.004612677 | 0.678063463 |
| Viral mRNA Translation | 26 | 114 | 0.009421488 | 0.006246058 | 0.843217855 |
| Eukaryotic Translation Elongation | 27 | 104 | 0.008595041 | 0.009712609 | 0.989827197 |
| ECM proteoglycans | 19 | 78 | 0.006446281 | 0.014320201 | 0.989827197 |
| NCAM1 interactions | 13 | 44 | 0.003636364 | 0.015611901 | 0.989827197 |
| GTP hydrolysis and joining of the 60S ribosomal subunit | 28 | 121 | 0.01 | 0.021024448 | 0.989827197 |
| Laminin interactions | 9 | 31 | 0.002561983 | 0.022401032 | 0.989827197 |
| Opsins | 4 | 9 | 7.44E-04 | 0.025806034 | 0.989827197 |
| Formation of the ternary complex, and subsequently, the 43S complex | 12 | 54 | 0.00446281 | 0.037317019 | 0.989827197 |
| ATP sensitive Potassium channels | 3 | 6 | 4.96E-04 | 0.038413148 | 0.989827197 |
| Dopamine receptors | 3 | 6 | 4.96E-04 | 0.038413148 | 0.989827197 |
| Selenoamino acid metabolism | 33 | 188 | 0.01553719 | 0.040475544 | 0.989827197 |
| L13a-mediated translational silencing of Ceruloplasmin expression | 28 | 118 | 0.009752066 | 0.001213744 | 0.292192627 |

B

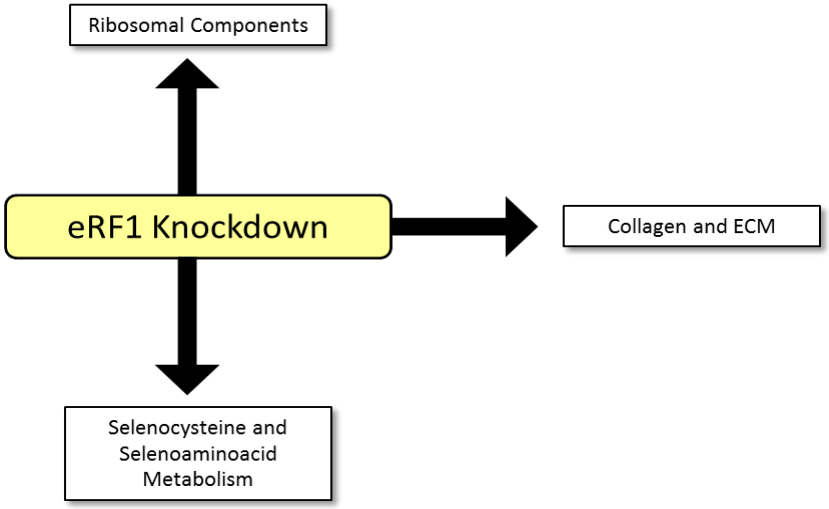


**Figure 4.6: Pathways involving genes upregulated by eRF1 knockdown.** A) List of the 20 pathways most likely to show true regulation based on Reactome Analysis, ranked by probability of being a true positive. *Entities found*: the number of curated and interacting molecules that are common between the submitted data set and the pathway. *Entities total*: The total number of curated and interacting molecules within the pathway. *Entities ratio*: The ratio of entities from this pathway that are molecules vs. all entities of the type selected with Results Type. *Entities Pvalue*: The result of the statistical test for over-representation. *Entities FDR*: False discovery rate, corrected over-representation probability. B) Graphical summary of major pathways associated with genes upregulated as a result of eRF1 knockdown following manual curation. Pathways sharing both functional similarity and highly similar gene lists have been grouped together.

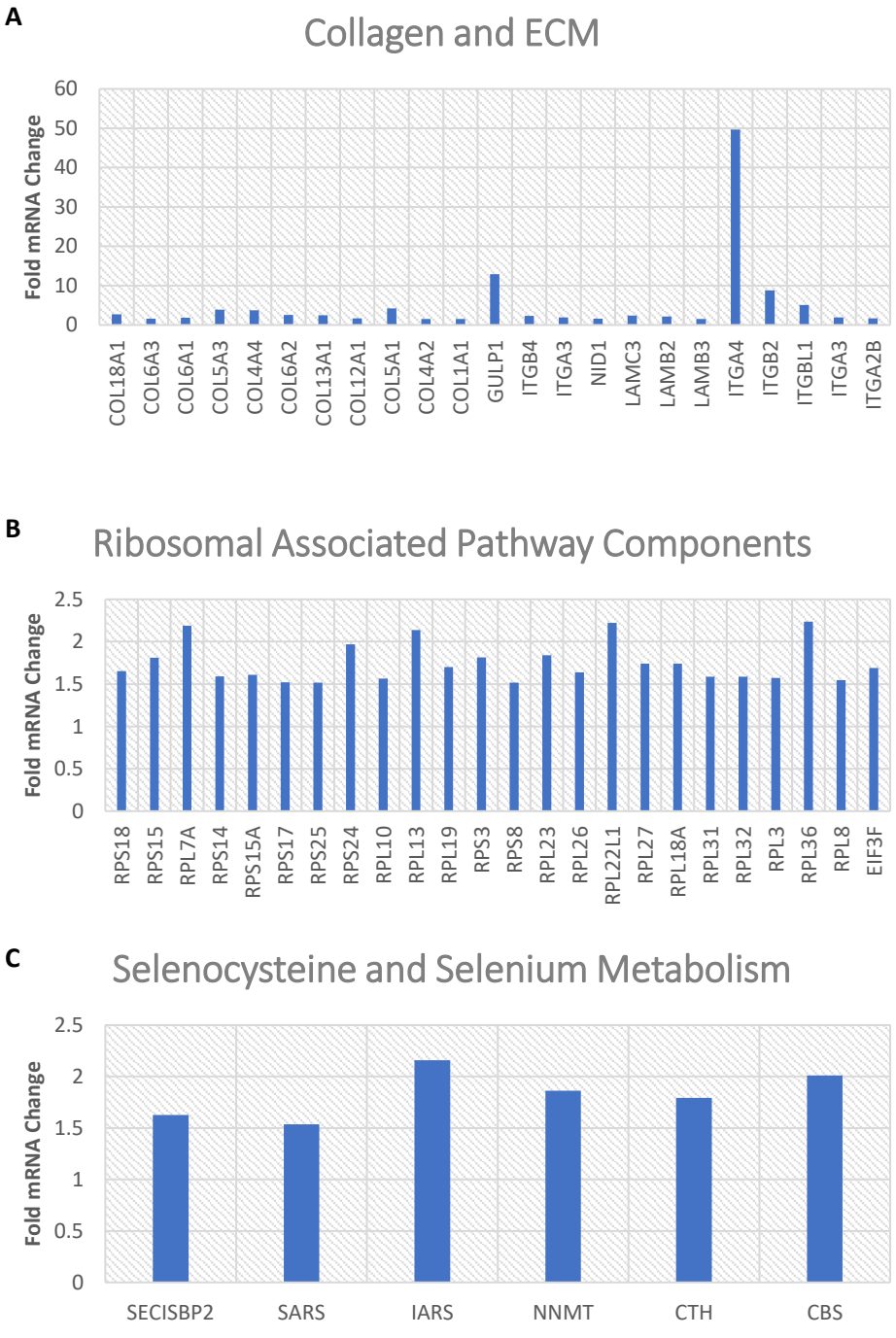


**Figure 4.7: Fold Regulation of genes identified to participate in pathways classified by pathway analysis as upregulated**. Pathways sharing both functional similarity and highly similar gene lists have been grouped together as previously. The composites used are formed of the following pathways: A) *Collagen and ECM*: Assembly of collagen fibrils and other multimeric structures, ECM proteoglycans and laminin interactions B) *Ribosomal Associated Pathway Components*: Formation of a pool of 40s subunits, Eukaryotic Translational Elongation, Eukaryotic Translational Termination, SRP dependent co-translational targeting of proteins to membrane, Viral mRNA Translation and Nonsense mediated Decay. C) *Selenocysteine and Selenium Metabolism*: Selenocysteine synthesis and Selenoaminoacid Metabolism. Genes shared with the ribosomal associated pathway components are not shown.

A

| Pathway name | #Entities found | #Entities total | Entities ratio | Entities pValue | Entities FDR |
|---|---|---|---|---|---|
| Defective B3GALTL causes Peters-plus syndrome (PpS) | 10 | 39 | 0.002913709 | 0.00188957 | 0.971957496 |
| RNA Polymerase I Chain Elongation | 13 | 61 | 0.00455734 | 0.0022049 | 0.971957496 |
| O-glycosylation of TSR domain-containing proteins | 10 | 41 | 0.00306313 | 0.002693705 | 0.971957496 |
| RNA Polymerase I Promoter Opening | 9 | 34 | 0.002540157 | 0.004372806 | 0.971957496 |
| Diseases associated with O-glycosylation of proteins | 14 | 76 | 0.005677998 | 0.006076532 | 0.971957496 |
| Insulin receptor recycling | 7 | 28 | 0.002091894 | 0.009815268 | 0.971957496 |
| PRC2 methylates histones and DNA | 9 | 45 | 0.003361972 | 0.014369678 | 0.971957496 |
| O-linked glycosylation | 20 | 133 | 0.009936496 | 0.016534264 | 0.971957496 |
| DNA methylation | 9 | 37 | 0.002764288 | 0.018437151 | 0.971957496 |
| Nucleosome assembly | 10 | 55 | 0.004109077 | 0.018503623 | 0.971957496 |
| Deposition of new CENPA-containing nucleosomes at the centromere | 10 | 55 | 0.004109077 | 0.018503623 | 0.971957496 |
| Interactions of neurexins and neuroligins at synapses | 13 | 60 | 0.00448263 | 0.032985578 | 0.971957496 |
| Interleukin-20 family signaling | 3 | 9 | 6.72E-04 | 0.040086999 | 0.971957496 |
| Transferrin endocytosis and recycling | 8 | 39 | 0.002913709 | 0.04085912 | 0.971957496 |
| Transcriptional regulation by small RNAs | 13 | 81 | 0.00605155 | 0.044268595 | 0.971957496 |
| Insulin-like Growth Factor-2 mRNA Binding Proteins (IGF2BPs/IMPs/VICKZs) bind RNA | 4 | 13 | 9.71E-04 | 0.054921309 | 0.971957496 |
| Interaction between L1 and Ankyrins | 6 | 33 | 0.002465446 | 0.059792589 | 0.971957496 |
| Gene Silencing by RNA | 16 | 115 | 0.008591707 | 0.065919233 | 0.971957496 |
| Glucagon-like Peptide-1 (GLP1) regulates insulin secretion | 8 | 49 | 0.003660814 | 0.06601782 | 0.971957496 |

B

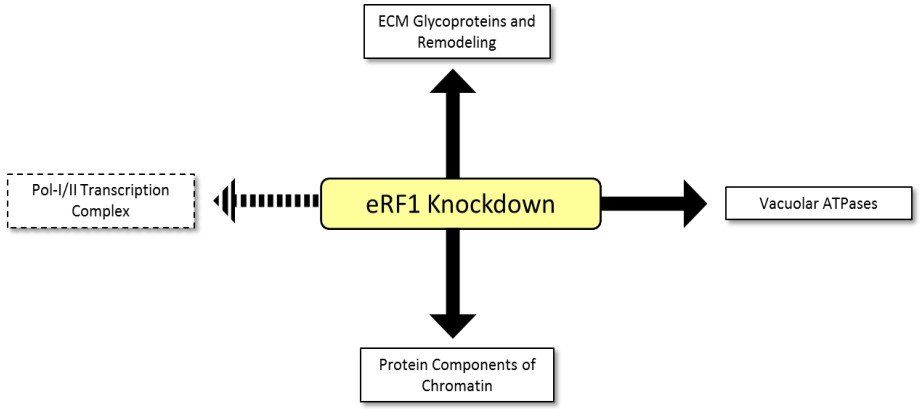


**Figure 4.8: Pathways downregulated during eRF1 knockdown in the RNASeq.** A) List of the 20 pathways most likely to show true regulation based on Reactome Analysis, ranked by probability of being a true positive. *Entities found*: the number of curated and interacting molecules that are common between the submitted data set and the pathway. *Entities total*: The total number of curated and interacting molecules within the pathway. *Entities ratio*: The ratio of entities from this pathway that are molecules vs. all entities of the type selected with Results Type. *Entities Pvalue*: The result of the statistical test for over-representation. *Entities FDR*: False discovery rate, corrected over-representation probability. B) Graphical summary of major pathways associated with genes downregulated as a result of eRF1 knockdown following manual curation. Pathways sharing both functional similarity and highly similar gene lists have been grouped together.

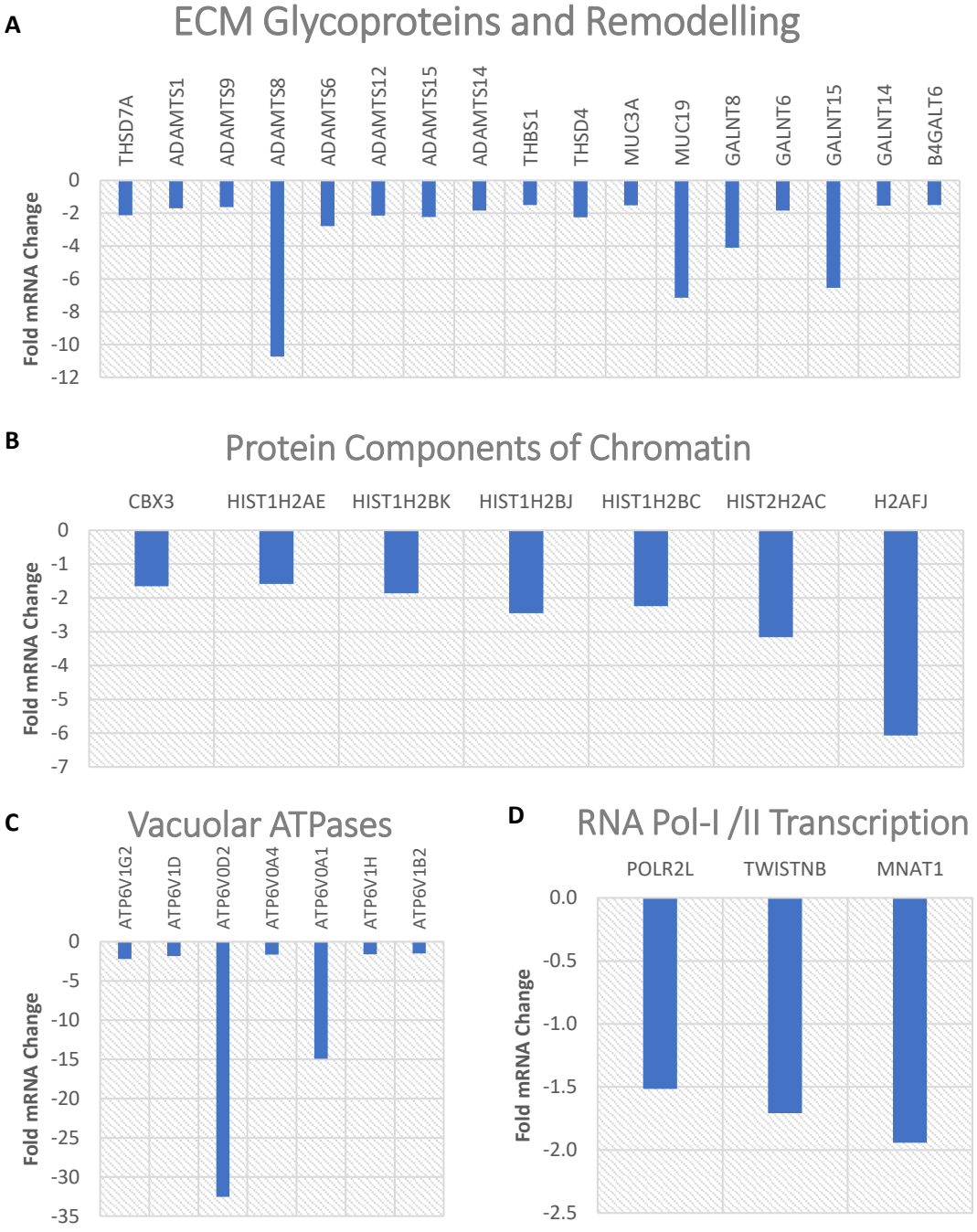


**Figure 4.9: Fold Regulation of genes identified to participate in pathways classified by pathway analysis as upregulated**. Pathways sharing both functional similarity and highly similar gene lists have been grouped together as previously. The composites used are formed of the following pathways: A) *ECM Glycoproteins and Remodelling:* Peter plus Syndrome via BGALTL, O-linked Glycosylation, Diseases associated with O-linked Glycosylation of proteins and O-linked Glycosylation of TSR Domain Containing Proteins B) *Protein Components of Chromatin*: RNA Pol-I chain elongation alone C) *Vacuolar ATPases*: Insulin Receptor Recycling, Glucagon-like Peptide 1 (GPL1) regulating Insulin Secretion, and Insulin-like Growth Factor 2 mRNA binding proteins D) *RNA Pol-I/II Transcription*: RNA Pol-I promoter opening alone.

During shRNA-mediated knockdown of eRF1 in U2OS cells a number of different pathways were found to be affected. Initially, the pathways derived from pathway analysis of genes showing upregulation were examined. Specifically, these pathways were heavily associated with an increase in ribosomal components and translation termination and initiation, extracellular matrix component proteins and selenium metabolism.

The collagen and extracellular matrix (ECM) pathway group is characterised by an abundance of upregulated collagen synthesis genes (COL*), along with laminin (LAM*) and integrin (ITG*) genes. Laminins are a group of ECM glycoproteins involved in structural scaffolding, cell adhesion, migration and signalling (Domogatskaya et al., 2012), while integrins are transmembrane receptors binding to the ECM, including laminins (Nishiuchi et al., 2006). Nidogen-1 (NID1) is another basement membrane glycoprotein, whose function is to connect laminins and collagens (Yurchenco and Patton, 2009). The presence of multiple upregulated pathways for ECM components may indicate a signal towards greater ECM secretion, particularly in relation to collagen.

In the RNA-Seq data, a general upregulation of multiple ribosomal proteins was notable, resulting in the identification of numerous related ribosomal pathways, which have been manually grouped together as the ‘Ribosomal Component’ Pathways. This potential increase in the availability of ribosomal components could be consistent with a cellular response to defects in translation. Although a nonsense mediated decay (NMD) pathway was identified by automatic assignment (Figure 4.6A), all the genes associated with the pathway are actually proteins of the small and large ribosomal subunits, rather than NMD exclusive genes. Therefore, the NMD pathway found here

is most likely a ‘false positive’ pathway assignment and has been folded under the Ribosomal Component Pathway group.

The genes list comprising the Selenocysteine synthesis and metabolism pathway is of interest. Selenocysteine Insertion Sequence Binding Protein 2 (SECISBP2) is responsible for binding to the mRNA to enable insertion of selenocysteine (Fradejas-Villar et al., 2017). Seryl-tRNA Synthetase (SARS) is involved in the first step of the Selenocysteine production pathway (Vincent et al., 1997). Additionally, two further genes closely associated with selenocysteine synthesis could be identified as upregulated by eRF1 depletion, namely Cystathione Beta Synthase (CBS) and Cystathionine Gamma Lyase (CTH), which were upregulated by 2.01 and 1.79-fold, respectively (Aitken et al., 2011). Nicotamide-N-Methyltransferase (NNMT) and Isoleucyl-tRNA Synthetase (IARS) are only peripherally associated with the pathway, but were also upregulated.

Genes that were downregulated resulted in predicted pathways which can be grouped as ECM Glycoproteins and Remodelling, Protein Components of Chromatin, Vacuolar ATPases and potentially Pol-I/II Transcription.

A large number of pathways were identified as participating in O-Glycosylation and Peter-Plus Syndrome (Figure 4.8A) by the automated pathway designation algorithm. However, a detailed manual analysis of the individual genes identified in those pathways resulted in their reassignment and amalgamation as the ‘ECM Glycoproteins and Remodelling’ pathway group. Specifically, comparing the lists for Peter-Plus Syndrome (PpS), a hereditary developmental disorder, and the O-glycosylation pathways, it becomes apparent that the PpS syndrome pathway, despite being rated as the most likely pathway during the analysis, is itself only a subset of

the O-glycosylation associated pathways. In both cases, these pathways are dominated by a decline in the ADAMTS family of matrix metalloproteases, which are responsible for the cleavage of ECM glycoproteins (Figure 4.9A) (Brocker et al., 2009). The other gene family originally pinpointed in the PpS pathway geneset and integrated ECM Glycoproteins and Remodelling into is that of the THS (Thrombospondin) and THDS (THS Domain containing) group of glycoproteins. Of the members identified, at least two have been shown to be involved in cell migration (Kuo et al., 2011, Haviv et al., 2005). The overall O-linked glycosylation pathways identified by Reactome contain all the aforementioned proteins in addition to mucin (MUC) and glycosyltransferases (GALNT) family members. Mucins are important gel forming ECM proteins and the GLNTs are crucial for the first reaction in performing a mucin-type O-linked glycosylation (Bennett et al., 2012) in a possible parallel to the identification of ECM components during pathway analysis of upregulated genes. Consequently, the PpS and O-Glycosylation pathways identified are actually more likely to represent a generalized reduction in both glycosylated ECM components as well as ECM metalloproteases, likely resulting in a reduced rate of ECM remodelling.

Numerous chromatin protein genes were found to be downregulated as part of the analysis. Genes associated with Pol-I promoter opening and chain elongation in the pathway analysis (Figure 4.8) consisted primarily of histone genes, which can be relatively safely dismissed as a 'false positive' and therefore grouped under the manually assigned 'Protein Component of Chromatin' pathway group (Figure 4.9B). The only non-histone component of this group, CBX3 is a heterochromatin participating protein (Ye and Worman, 1996). The reduction in chromatin

components may possibly be the result of the reduction in cell growth phenotype observed.

The manually assigned Vacuolar ATPase pathway group is an aggregation of pathways identified in the automated analysis as part of the Insulin-related signalling pathways (Figure 4.8A). However, as previously, manual assessment reveals that the associated genes contain exclusively subunits of the vacuolar ATPase, a large multiprotein complex which mediates acidification of cellular compartments similar to a reverse ATP Synthase and with a multitude of physiological roles (Finnigan et al., 2012).

Finally, some evidence exists for regulation of RNA Pol-I and Pol-II transcription. POLR2L and TWISTNB are both components of the RNA Pol-I transcribing complex (Acker et al., 1996). Additionally, MNAT is part of the Cyclin Dependent Kinase Activating Complex (CAK), which is responsible for activating RNA Pol-II elongation by phosphorylating the large subunit POLR2A (Eki et al., 1998). Similar to the observed reduction in chromatin components, the downregulation of RNA Pol transcription components could be consistent with effects of eRF1 depletion on growth.

Of the pathways identified, none were clearly associated with a direct role in signalling reduced cell growth. It is possible that the immediate transcriptional responses could be masked by widespread direct and indirect downstream signalling changes as a result of eRF1 depletion. Consequently, we reasoned it would be useful to compare gene lists following eRF1 knockdown to the equivalent transcriptomic data resulting from the depletion of other translational termination factors. Knockdown of the eRF1-associated factor eRF3a has been shown to result in an

increase in the level of readthrough in human cell lines (Chauvin et al., 2005), and a microarray analysis of the transcriptional effects of eRF3a depletion has been reported (Ait Ghezala et al., 2012a) using the HCT116 human colon cancer cell line. Since the latter study utilised the same bioinformatics thresholds as in our analysis (i.e. fold change>1.5, P<0.05, cpm≥1), a direct comparison was possible (Figure 4.10). Among the upregulated genes, only ~4.4% are shared by both eRF1 and eRF3a knockdown. The ratio of shared/total genes upon comparison of the upregulated genes is 20.3% for the eRF3a study however. For downregulated genes the overlap is smaller: the ratio of shared/total genes is ~2.8% for eRF1 and ~8.6% for eRF3a. The list of common genes described in 4.10A subsequently underwent pathway analysis via Reactome using the same assessment criteria as for the datasets earlier. These data are presented in Figures 4.11-12. The list of common downregulated genes was not processed in the same manner as no significant enrichment could be found in these by Fisher's Exact test (Figure 4.10C).

**A**

| | | |
|---|---|---|
| AARS | IARS | STC2 |
| ABCC3 | ITGA3 | SYTL1 |
| ARHGEF37 | JDP2 | TANGO6 |
| ARHGEF6 | KCNG1 | TBC1D5 |
| ARRDC4 | KLF9 | TRAPPC6A |
| ASNS | LAMB3 | TRIB3 |
| ATP6AP1L | LAMP3 | TSC22D3 |
| C14orf78 | LAT2 | TTC18 |
| C2orf15 | LCN2 | UCN |
| C6orf48 | MGEA5 | UPP1 |
| C9orf97 | NBR1 | ZFAND2A |
| CALB2 | PCK2 | ZNF566 |
| CASC2 | PCNXL2 | EXOSC6 |
| CEBPG | PHGDH | |
| CHAC1 | PLAU | |
| DDIT3 | PSAT1 | |
| DDIT4 | PTPDC1 | |
| FAM122A | RBM35A | |
| FAM76B | SARS | |
| FERMT1 | SDSL | |
| FKBP9 | SH3PXD2A | |
| FUT1 | SLC6A9 | |
| GPT2 | SLC7A11 | |
| HDAC4 | SNTB1 | |
| HERPUD1 | SPIN1 | |

**B**

| | |
|---|---|
| AKAP3 | SNRPB2 |
| ASB9 | TMC8 |
| BRMS1L | TMED1 |
| C18orf56 | TMSB15A |
| DMRT1 | TMSB15B |
| FDFT1 | TTC33 |
| FZD9 | |
| GNB3 | |
| GPR3 | |
| H2AFJ | |
| KLHL7 | |
| KLRA1 | |
| LAMA2 | |
| MARCKSL1 | |
| MFAP3L | |
| MLLT11 | |
| NES | |
| NME1 | |
| OXTR | |
| PGM2L1 | |
| PPP2R5D | |
| RAD54B | |
| SKP2 | |
| SLC10A4 | |
| SLC7A8 | |

**Figure 4.10: eRF1 and eRF3a knockdown result in changes in expression of a common list of genes.** The lists of genes upregulated and downregulated by eRF1 knockdown where compared with the equivalent lists caused by eRF3a knockdown in literature. A) List of upregulated genes shared with eRF3a knockdown study by Ghezala *et al*, 2012, performed in HCT116 (human colon cancer) cells B) List of downregulated genes shared with eRF3a knockdown study. (Figure Continued next page)

C

| | Number of UpRegulated Genes | Number of DownRegulated Genes |
|---|---|---|
| eRF1 Total | 1444 | 1148 |
| eRF3a Total | 310 | 374 |
| Number Shared | 63 | 32 |
| %Shared eRF1 | 4.362 | 2.787 |
| %Shared eRF3a | 20.322 | 8.556 |
| **pValue** | **$5.849*10^{-13}$** | **0.05897** |

D

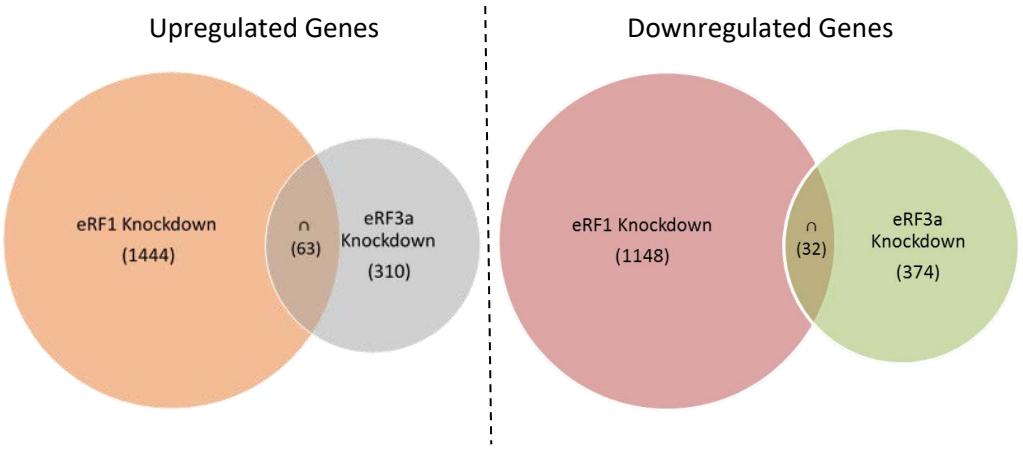


**Figure 4.10 (Continued from previous page): eRF1 and eRF3a knockdown result in changes in expression of a common list of genes.** C) Table of percentage similarity between the two data sets. Statistics for the unique and shared percentages are given for each dataset due to their different size. *eRF1/eRF3a Total*=Total number of genes in each study. *Number Shared*= Number of genes in each study found to be upregulated in the other study as well. *% Shared eRF1/eRF3a*=The percent ratio of Shared/Total genes identified in each list. *pValue*: The probability that the overlap between the two groups is random, through Fisher's Exact test. Only the upregulated gene overlap is significant at P<0.5 E) Venn diagrams of the intersection between the eRF1 and eRF3a knockdown datasets.

A

| Pathway name | #Entities found | #Entities total | Entities ratio | Entities pValue | Entities FDR |
|---|---|---|---|---|---|
| ATF4 activates genes | 6 | 32 | 0.002368265 | 2.12E-06 | 7.85E-04 |
| PERK regulates gene expression | 6 | 38 | 0.002812315 | 4.87E-06 | 9.00E-04 |
| Amino acid synthesis and interconversion (transamination) | 5 | 80 | 0.005920663 | 2.24E-05 | 0.002759684 |
| Serine biosynthesis | 2 | 21 | 0.001554174 | 0.001777121 | 0.260958164 |
| Metabolism of amino acids and derivatives | 7 | 656 | 0.048549438 | 0.006618714 | 0.641434079 |
| Cytosolic tRNA aminoacylation | 3 | 89 | 0.006586738 | 0.006942102 | 0.423468218 |
| Laminin interactions | 2 | 31 | 0.002294257 | 0.00843408 | 0.438572183 |
| Invadopodia formation | 1 | 5 | 3.70E-04 | 0.020494438 | 0.641434079 |
| Basigin interactions | 3 | 26 | 0.001924216 | 0.027771205 | 0.163495086 |
| Activation of AKT2 | 1 | 7 | 5.18E-04 | 0.048492092 | 0.641434079 |
| ATF6 (ATF6-alpha) activates chaperone genes | 2 | 15 | 0.001110124 | 0.057186564 | 0.641434079 |
| MET activates PTK2 signaling | 2 | 32 | 0.002368265 | 0.057186564 | 0.641434079 |
| ATF6 (ATF6-alpha) activates chaperones | 2 | 17 | 0.001258141 | 0.059361996 | 0.641434079 |
| Anchoring fibril formation | 1 | 15 | 0.001110124 | 0.060247983 | 0.641434079 |
| Metal sequestration by antimicrobial proteins | 1 | 13 | 9.62E-04 | 0.064134677 | 0.641434079 |
| G alpha (12/13) signalling events | 2 | 92 | 0.006808763 | 0.064923319 | 0.641434079 |
| tRNA Aminoacylation | 3 | 107 | 0.007918887 | 0.066330539 | 0.641434079 |
| SeMet incorporation into proteins | 1 | 17 | 0.001258141 | 0.068005509 | 0.641434079 |
| MET promotes cell motility | 2 | 45 | 0.003330373 | 0.069493729 | 0.641434079 |

B

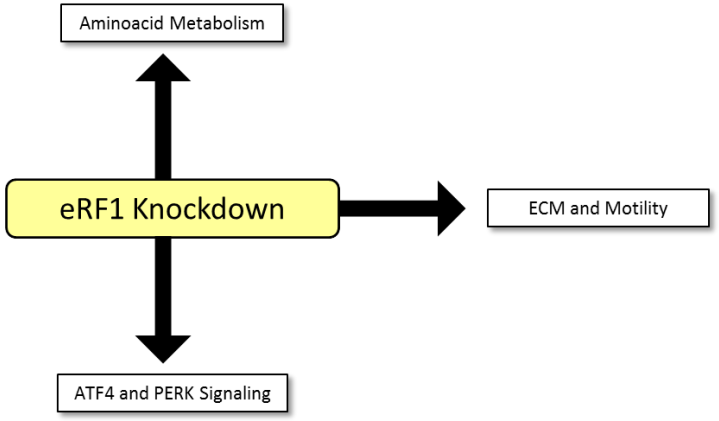


**Figure 4.11: Pathways identified by limiting the search space to targets upregulated during both eRF1 and eRF3a knockdown.** A) List of the 20 pathways most likely to show true regulation based on Reactome Analysis, ranked by probability of being a true positive. *Entities found*: the number of curated and interacting molecules that are common between the submitted data set and the pathway. *Entities total*: The total number of curated and interacting molecules within the pathway. *Entities ratio*: The ratio of entities from this pathway that are molecules vs. all entities of the type selected with Results Type. *Entities Pvalue*: The result of the statistical test for over-representation. *Entities FDR*: False discovery rate, corrected over-representation probability. B) Graphical summary of major pathways associated with genes upregulated as a result of eRF1 knockdown. Pathways sharing both functional similarity and highly similar gene lists have been grouped together.

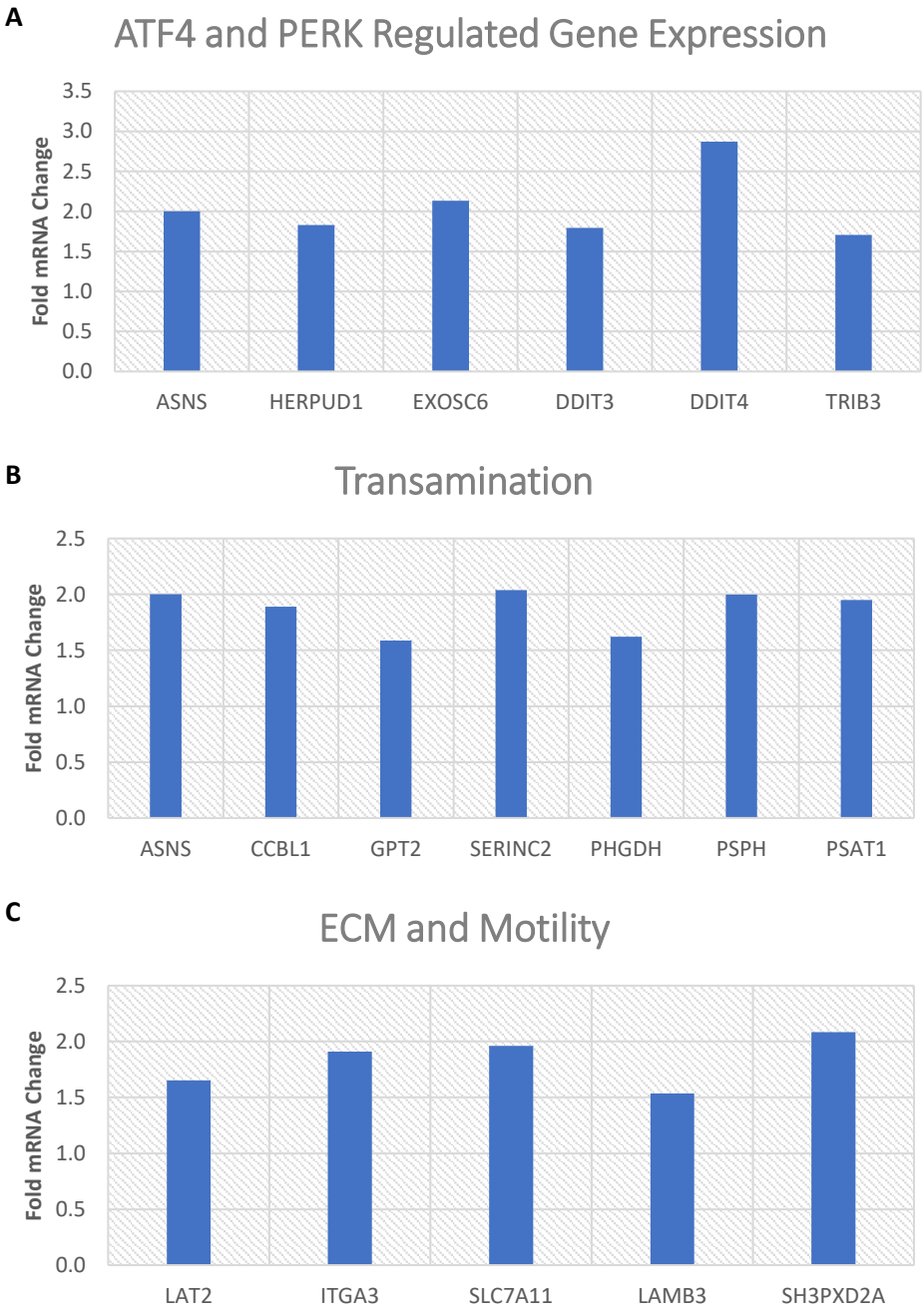


**Figure 4.12: Fold Regulation of genes commonly upregulated between eRF1 and eRF3a knockdown and identified to participate in pathways.** Pathways sharing both functional similarity and highly similar gene lists have been grouped together as previously. The Fold mRNA Change values presented are derived from the eRF1 dataset. The composites used are formed of the following pathways: A) *ATF4 and PERK Regulated Gene Expression*: ATF4 gene activation and PERK regulated gene expression B) *Transamination:* Transamination, Serine Biosynthesis, and Metabolism of aminoacids and derivatives C) *ECM and Motility*: Laminin interactions, Invadopodia formation, Basigin interactions, Anchoring Fibril formation, MET activates PTK2 signalling, and MET promotes cell motility.

We find that a new set of regulated pathways now dominates the list (Figures 4.11-12), most prominently regulation of downstream factors of the Activating Transcription Factor 4 (ATF4), along with PERK regulation of gene expression, transamination, and ECM components.

The gene identity profile for the transamination pathway (Figure 4.12B) is characterised by transaminases (CCBL1, GPT2), a serine phosphotransferase (PSPH), a unique protein incorporating serine into lipid membranes (SERINC2), Asparagine Synthase (ASNS), and a gene believed to code for a phosphoserine aminotransferase (PSAT1). While providing strong evidence for an involvement of transamination in the response to translational termination readthrough, none of the genes listed immediately explain the reduced growth phenotype.

A large number of closely-associated pathways are found concerning the extracellular matrix and motility, similar to the original pathway analysis (Figure 4.12C). Unlike the former however, which was dominated by ECM components and anchoring proteins, only two of these appear here, integrin α3 (ITGA3) and laminin B3 (LAMB3) are co-regulated by both eRF1 and eRF3a knockdown. The other identified proteins have a mix of functions which are associated with EVM and motility. Of these, LAT2 (Linker for Activation of T cells 2) is a transmembrane adaptor protein linking FCER1 and FGER1 signalling by mast and B cells to GRB2 (Brdicka et al., 2002, Tkaczyk et al., 2004). SLC7A11 (Solute Carrier Family 7 Member 11) is a sodium independent anionic aminoacid transporter which exchanges Glu for Cys in the plasma membrane (Gasol et al., 2004). On the other hand, SH3PXD2A, better known as Tsk5, is a member of the Tsk family of adapter proteins, known as Src substrates and binding to a variety of proteins, prominently matrix metaloproteases.

Tsk5 is strongly associated with the formation of invadopodia, degradation of the ECM, and motility in cancer cells (Courtneidge, 2012).

The two categories exhibiting the highest pValue in Figure 4.12A&B, ATF4 and PERK signalling, have been grouped together as part of the ATF4 and PERK signalling pathway (Figure 4.12A). The genes included in the PERK mediated gene activation pathway are a subset of the ones associated with the ATF4 gene activation pathway, which is rated higher in terms of statistical confidence. Since PERK signals upstream of ATF4 (Liu et al., 2015), the specific response seen here is that of ATF4 mediated gene activation. The combined geneset consist of ASNS, also seen in transamination and induced by ATF4 (Ye et al., 2010), three ATF4 downstream factors (DDIT3, DDIT4 and TRIB3), HERPUD1 (which is a protein associated with the Unfolded Protein Response (UPR), and EXOSC6, an mRNA degradation mediating exosome subunit. Overall, these combined analyses indicate that defective translational termination induces the UPR, which could be consistent with stop codon readthrough and the production of misfolded proteins with extended C-termini. Interestingly, with respect to our date on growth control and translational termination, ATF4 has been implicated in cell death and cell cycle progression (Frank et al., 2010).

### 4.2.2 Validation of RNA-Seq Data via qPCR

In order to determine whether the results presented above were reliable, we proceeded to replicate the conditions of the experiment, extracted RNA and then tested a number of candidate regulated genes using Real-Time Quantitative PCR (RT-qPCR). The genes initially selected were based on two factors, either: i) Having been identified as having high levels of inducible expression in the RNA-Seq (e.g. IGFBP4, See Fig. 3.3) upon eRF1 knockdown and/or ii) being a member of one of the major pathways identified in the eRF1 alone or eRF1/eRF3A combined analysis. SYBR-Green RT-qPCR was utilized for these assays. Since this type of assay is potentially sensitive to genomic DNA contamination and non-specific binding to similar sequences, primers were designed to overlap intron-exon sites and preliminary melt curve assays were performed to ensure that only single products existed respectively. Additionally, perfect duplication of any given DNA sequence per cycle cannot be assumed due to differences in binding efficiency of the primers to the target sequence. Consequently, the amplification exponent of each primer was calculated in advance by testing the rate of amplification across a $10^4$ range of dilutions and used in the fold change calculations presented. The empirically derived amplification factors for each primer are listed in Materials and methods, Section 7.3.7. We find that all the genes tested validate as reproducible. Reassuringly, we also find that the level of fold change in the independent replicates closely matches that in the RNA-Seq data (Figure 4.14), with the exception of some very highly upregulated targets, namely IGFBP4, Cadherin 11 and Integrin α4.

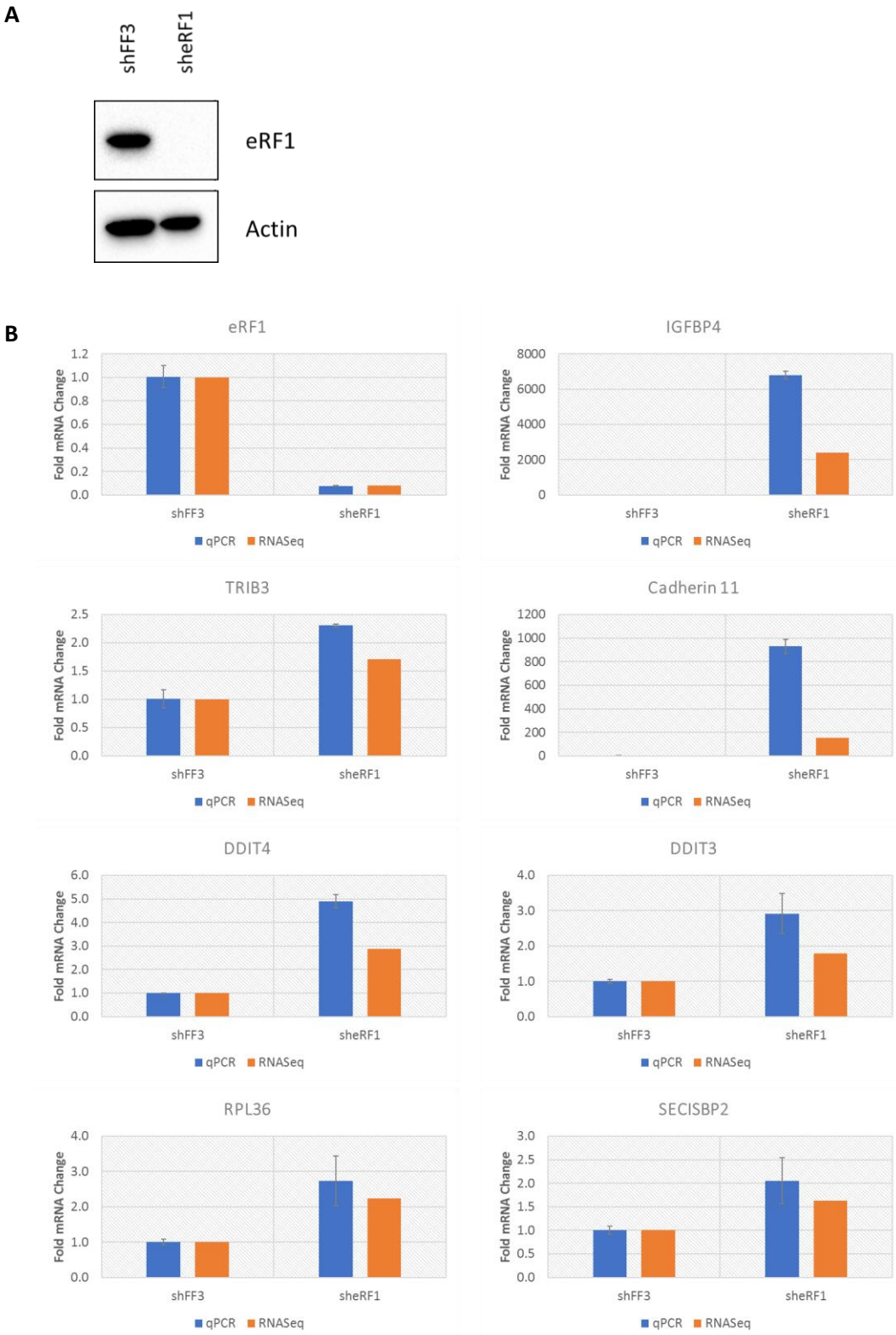


**Figure 4.13: RT-qPCR validation of the shRNA RNA-Seq data.** A) Western Blot validation of ERF1 knockdown following treatment with 1 µg $ml^{-1}$ doxyxyline for 72h. B) The level of fold regulation of each gene obtained in the qPCR is compared to the value obtained by RNA-Seq. n=3±Standard Deviation. The genes included cover eRF1 as a negative control, IGFBP4 and Cadherin 11 due to their observed high upregulation and the ATF4 downstream targets TRIB3, DDIT3 and DDIT4. (Figure Continued on next page)

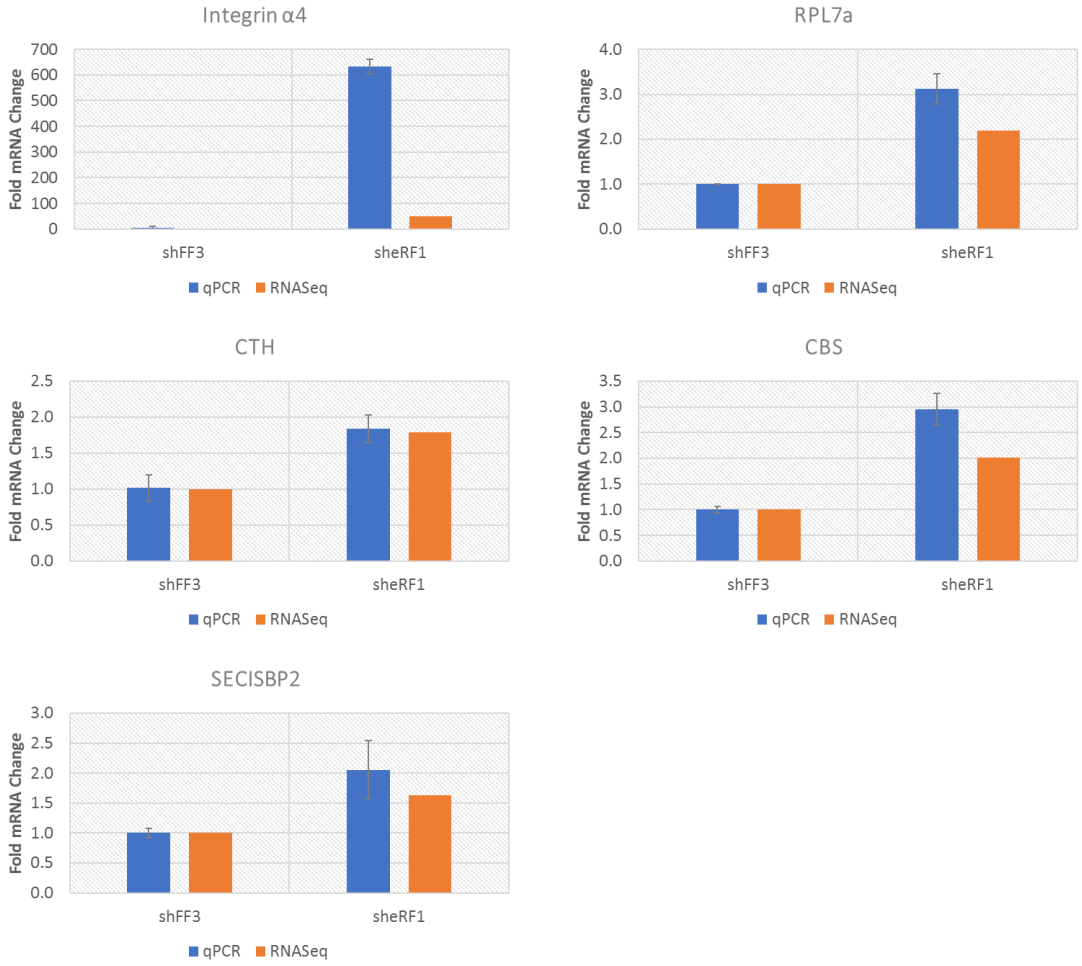


**Figure 4.13: RT-qPCR validation of the shRNA RNA-Seq data (Cont. from previous page).** The level of fold regulation of each gene obtained in the qPCR is compared to the value obtained by RNA-Seq. n=3±Standard Deviation. The genes covered are Integrin α4 as a representative gene from the collagen and ECM group, RPL7a from the ribosomal associated pathways group and CTH, CBS and SECISBP2 for the selenocysteine and selenium metabolism pathway group.

### 4.2.3 Validation of RNA-Seq data with qPCR via siRNA

Thus far, the RNA-Seq data have been validated using independent samples from the U2OS shFF3 and sheRF1 cell models through the use of qPCR. We wished to further validate these findings using an alternative approach, to rule out potential method-specific responses. To this end, parental U2OS were transfected with control or eRF1 siRNA for 48h before being harvested. Subsequently, RNA was purified and reverse transcribed, and utilised to perform RT-qPCR against representative target genes.

We find that several differences are apparent compared to the results from the shRNA qPCR validation (Figure 4.14B). Most notably, IGF4BP and Cadherin 11, both very highly upregulated in the original screen and the RNA-Seq, show little or no differential expression in the siRNA experiment. Of the two other ECM and adhesion gene tested, Integrin α4 and Cadherin 13, only the former demonstrated a modest difference, which is still very substantially smaller than that observed in the RNA-Seq and shRNA knockdown qPCR validation. RPL36 and SECISBP2 both demonstrate an increase of just ~20% compared to control siRNA treatment which, although significant at $p \leq 0.05$, is also substantially less than that observed in the previous experiments. However, all the ATF4 downstream targets tested appear to be upregulated at slightly higher levels than those anticipated by the RNA-Seq and shFF3/sheRF1 qPCR data.

Taken together therefore, the most robust genes induced by eRF1 knockdown were those in common between our dataset and the published eRF3A analysis. These include DDIT3, DDIT4, and TRIB3, all of which are target genes of the transcription factor ATF4.

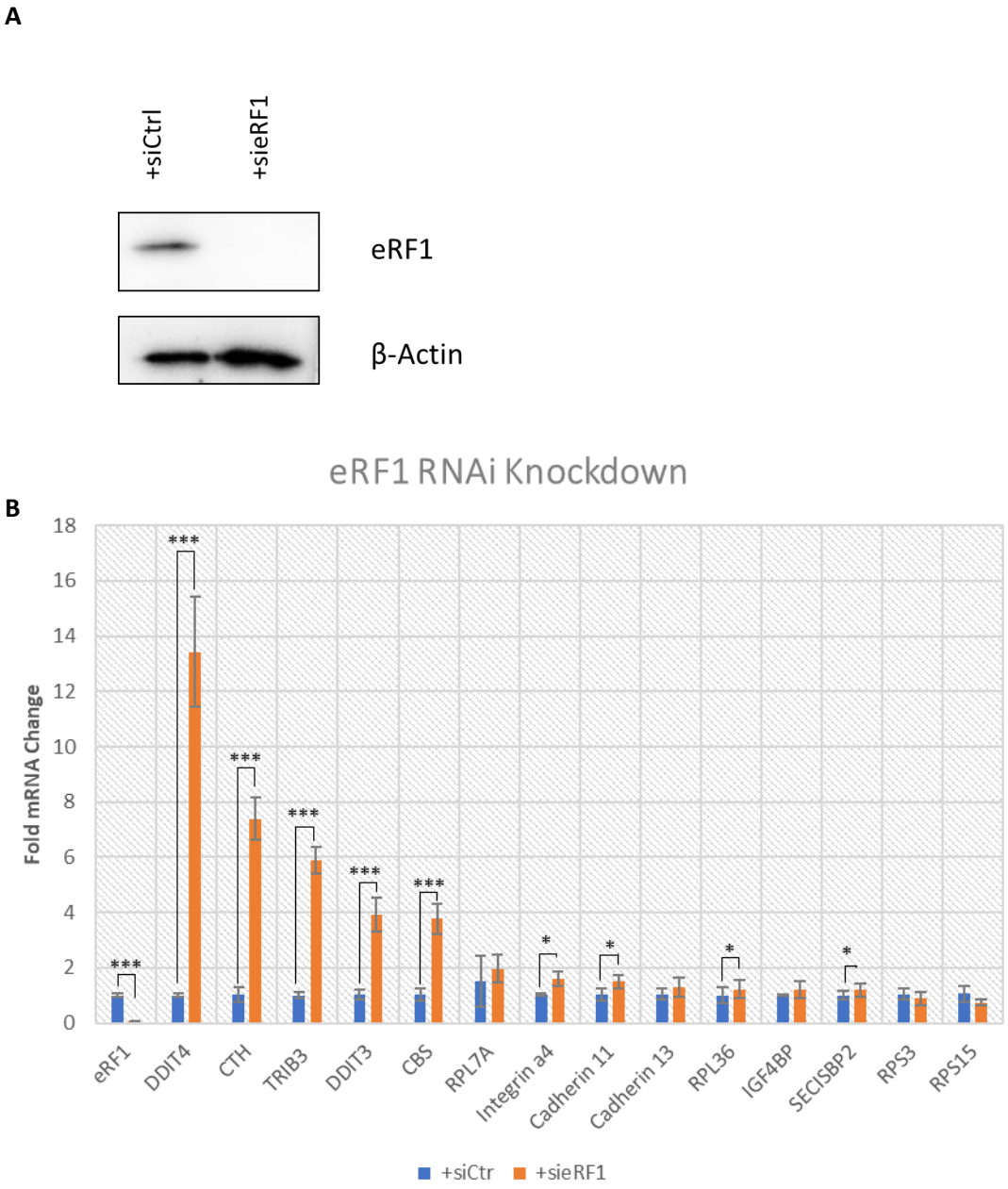


**Figure 4.14: RT-qPCR validation of the siRNA RNA-Seq data.** Parental U2OS cells were treated with 25 nM control or eRF1 siRNA for 48h prior to harvest and qPCR. A) Western Blot validation of eRF1 knockdown. B) Cumulative chart of the changes in fold expression of 8 representative genes tested via RT-qPCR under siRNA mediated knockdown of eRF1. The fold regulation is expressed relative to the control siRNA treatment. n=3±Standard Deviation. Significance testing using student's two-tailed t-test assuming homoscedasticity. ***P<0.001, *P<0.5.

### 4.2.4 eRF1 knockdown potentially promotes cell motility

A major pathway identified as part of the screen was collagen and extracellular matrix involved proteins. This led us to examine the possibility that eRF1 knockdown may affect adherence and motility. In order to test the effect that eRF1 knockdown might have on cell motility, *in vitro* wound healing assays were performed. In this type of assay, a monolayer of the inducible shRNA cell lines was grown, induced for 48 h, scratched and the migration of cells imaged in 8h intervals with brightfield microscopy. Subsequently the area remaining uncovered was measured using ImageJ and the rate of wound healing over time measured and quantified as (Area Free of Cells)/(Area Covered by Cells). We find (Figure 4.17B) that knockdown of eRF1 results in modestly faster migration, a result that appears statistically significant at the 95% confidence level.

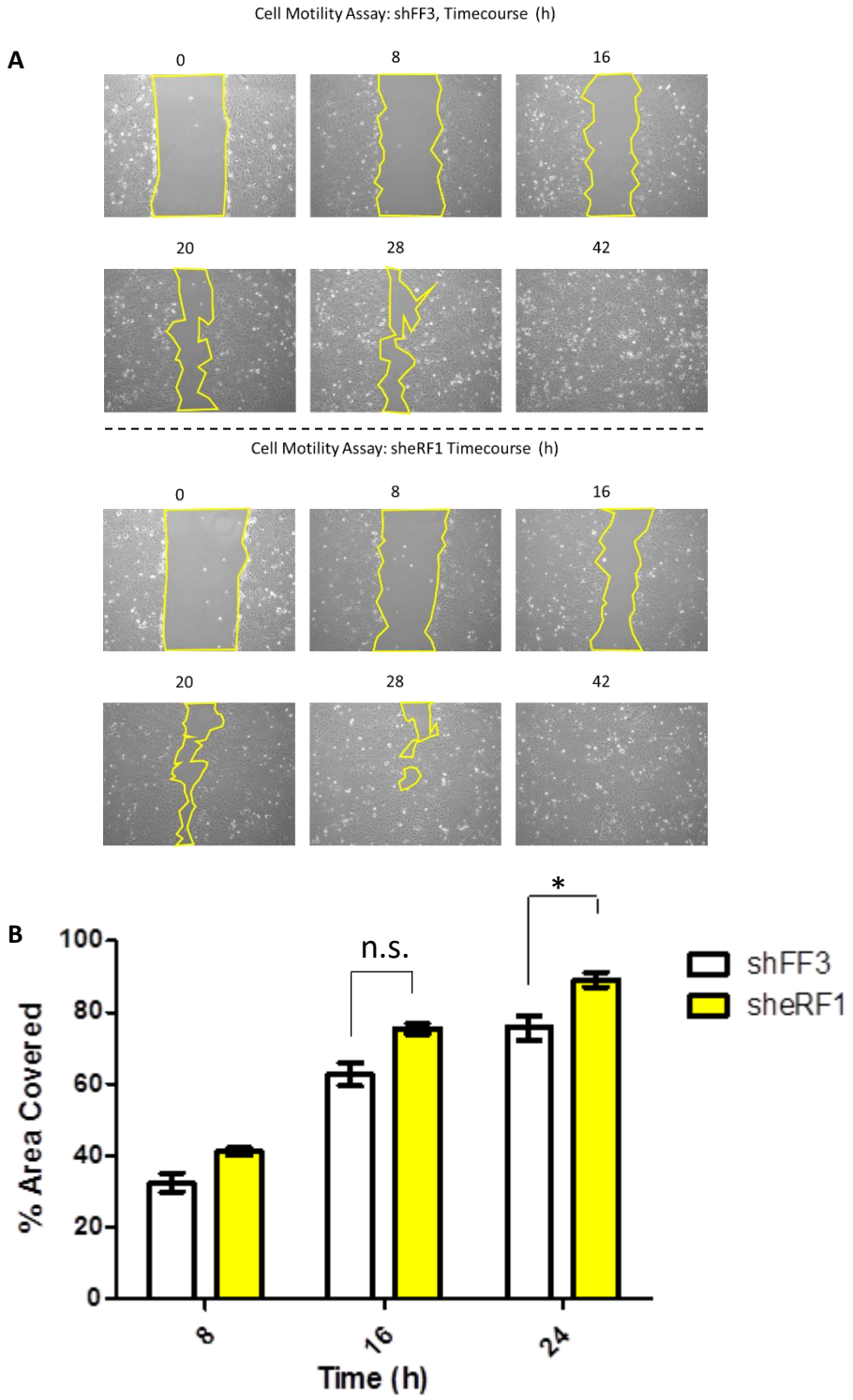


**Figure 4.15: Cell motility may be affected by eRF1 knockdown.** Cells were treated with 1 µg ml$^{-1}$ doxycycline for 72h before the monolayer was scratched. Photos of the wound were taken every 8h afterwards and the area free of cells quantified. A) Representative photos of wound closure experiment, with the converging cells on either side outlined in yellow. B) Quantification of the percentage covered area (Area Covered by Cells/Total Area) as a function of time. n=3±Standard Deviation. * $P<0.05$, n.s.$P>0.05$. Student's two tailed t-test.

## 4.3 Discussion

In this chapter, we have performed whole transcriptome RNA-Sequencing analyses in order to determine the gene expression changes that eRF1 knockdown caused at the mRNA level. These transcriptional changes were subsequently cross-referenced with another study and further validated where appropriate.

Technical assessment of the results of the qPCR revealed two major points of contention: 1) very high-level upregulation of selected genes, that were not subsequently validated, and 2) a high proportion of potential false positives during pathway identification. With regard to the former, a number of genes in the RNA-Seq were found to exhibit very high levels of fold upregulation (Figure 4.3), which could not be observed in the siRNA validation (Figure 4.14). This may potentially indicate that the control shRNA might actually result in mRNA suppression of 'off-targets' as an unintended side effect, rather than eRF1 shRNA-mediated upregulation.

As for the second potential technical issue, during subsequent pathway analysis, a large number of false positive identifications occurred, especially during analysis of the list of downregulated genes (Figures 3.6-3.9). The reason for this is an inherent limitation of the overrepresentation analysis used to determine the relevant pathways. The genes involved in each pathway are not necessarily exclusive to it, so that pathways may appear significantly affected when only components peripheral to it are regulated. For this reason, manual evaluation of the results of the Reactome based

pathway analysis was necessary in order to identify the actual pathways likely regulated. This led to the identification of three upregulated and three downregulated pathways. The former included ribosomal components, Collagen and ECM, and Selenocysteine metabolism.

As might be anticipated from a process which affects protein translation, a general but relatively low-level upregulation of the expression of ribosomal components can easily be identified. Despite those relatively low levels of increase (1.5-2.5 fold), taking into consideration that ribosomal proteins are amongst the most highly expressed proteins in the cell, this increase likely represents a significant increase in the metabolic expenditure of the cell dedicated to translation machinery. Additionally, expression levels of ribosomal components are generally invariant, to the extent they used as controls in gene expression assays in literature. The widespread increase observed here likely implies that the normally high capacity translational machinery is underperforming sufficiently to trigger an attempt by the cell to improve the its translation performance and forms a cautionary tale about the use of ribosomal components as controls in qPCRs. Ribosomal protein expression control has also been shown before in literature to occur during cellular stress, through mTOR and its downstream targets PKA, FHL1 and SFP1 (Martin et al., 2004, Marion et al., 2004), though it results in suppression of ribosomal protein gene transcription in that context. Nevertheless, during qPCR validation using siRNA only RPL36 showed a significant level of increase, so it is possible that this effect may be overestimated in the RNA-Seq and shRNA based qPCR. Whether this pattern holds true in the eRF1 rescue cells needs to be assessed and will be examined in the next chapter.

The inclusion of selenocysteine (Sec) synthesis and selenium metabolism among the regulated pathways was a surprise (Figures 4.6-4.7). Further inspection reveals that

three proteins are unique to this pathway and responsible for the assignment: Selenocysteine Insertion Sequence Binding Protein 2 (SECISBP2), Cystathionine Beta Synthase (CBS) and Cystathionine Gamma Lyase (CTH). The Seryl-tRNA Synthetase (SARS) was also found to be upregulated and it does catalyse the first step in Sec-tRNA synthesis. However, its primary function is the synthesis of Ser-tRNA and a manual sorting through the data reveals several other tRNA synthetases as upregulated (data not shown). Therefore, it is likely that SARS is not upregulated as part of an increase in Sec synthesis but rather a general increase in aminoacyl-tRNA synthesizing enzymes. Among the SECISBP2, CTH and CBS group, CBS and CTH by themselves form the reverse transsulfuration pathway in mammals, critical for the conversion of methionine to cysteine (Aitken et al., 2011). Specifically, CBPS catalyses the reaction of Ser+Homocysteine→Cystathionine, while CTH cleaves Cystathionine into α-Ketobutyrate and Cysteine. Therefore, the critical gene which must be validated for the pathway assignment to be accurate is SECISBP2. While the latter was indeed validated by the shRNA qPCR, in the siRNA qPCR screen only a ~20% increase over control siRNA treatment could be found, below the level of statistical significance. This may imply that either the upregulation of SECISBP2 in the shRNA knockdown cell lines is limited to that specific cell line or experiment set up or possibly the control siRNA used may have resulted in an increase in SECISBP2 compared to the shFF3. If the upregulation of SECISBP2 observed was spurious, then the cells demonstrate an increase in the production of cysteine. If true however, the upregulation of a selenocysteine producing pathway fits unexpectedly elegantly with translational termination defects. Selenoprotein translation in mammals occurs at a UGA, normally a stop codon. Termination at the specific codon however can be avoided in the presence of a selenocysteine insertion sequence (SECIS) located in the

3’ Untranslated Region (3’ UTR) in a process known as translation recoding (Baranov et al., 2002). Following transcription to mRNA, the ~ 60 nucleotides SECIS element adopts a stem-loop structure. The structure of the SECIS element is conserved among eukaryotes, bacteria and archaea, though the sequence itself is not conserved apart from the presence of non-Watson-Crick base pairing 5’-UGAY-3’:5’-UGAU-3’ motifs essential to its structure (Walczak et al., 1996). The SECIS element is bound by SECISBP2 which recruits further factors which result in binding of Sec-tRNA$^{Sec}$ to the ribosome instead of eRF1 and insertion of the selenocysteine. Consequently, it might be the case that in the presence of defective translational termination the cell may be upregulating factors in an attempt to bypass normal termination signals, perhaps in some form of compensation mechanism. While other crucial components of the selenocysteine production pathway such as PSTK [O-phosphoseryl-tRNA[Ser]Sec kinase]) and selenocysteine synthase (Xu et al., 2007) were not found to have been upregulated, it is possible that these pathways may simply not constitute rate limiting steps for the expression of selenoproteins.

Comparison of eRF1 knockdown with eRF3a knockdown data from the literature indicated that the list of upregulated genes shared a statistically significant overlap (Figure 4.10). A single pathway group immediately stood out as in the top two positions by statistical significance (Figure 4.8A). That being the ATF4/PERK gene activation pathway, which was of immediate interest here because of its known roles in growth control and the integrated stress and unfolded protein responses (Jackson et al., 2010). ATF4 is a known regulator of the cytoplasmic stress response and its downstream targets, DDIT3, DDIT4, TRIB3 and ASNS, were upregulated to statistically significant levels in the RNA-Seq, the shRNA qPCR and the siRNA

qPCR, rendering it by far as the most robust and reproducible of the identified pathways.

ATF4 has been implicated as a modulator of cell cycle progression by interaction with CDK4 and $p27^{KIP1}$. However, an increase in ATF4 expression in this context is associated with a $G_1$ cell cycle block (Bagheri-Yarmand et al., 2008), which may not be consistent with the apparent lack of a single cell cycle checkpoint being activated in the cell cycle experiments presented in Chapter 3. Indeed, depletion of eRF3a is also associated with an increase in ATF4 (Ait Ghezala et al., 2012a), but this increase results in a $G_1$ cell cycle arrest through inhibition of the mTOR pathway (Chauvin et al., 2007). Interestingly, upregulation of ATF4 has also been observed as a result of defects in another hydroxylase pathway that targets translation. Knockdown of the prolyl hydroxylase OGFOD1, which hydroxylates the RPS23 ribosomal component protein, results in growth restriction and increased ATF4 activity and expression (Singleton et al., 2014c).

In summary, knockdown of eRF1 has been found by RNA-Seq and subsequent bioinformatic analysis to result in the upregulation of a number of pathways, principal among them those associated with translation, selenocysteine synthesis and collagen and ECM components. Comparison of this data with previous studies additionally indicated an upregulation of the cytoplasmic stress response through ATF4. Validation of the RNA-Seq results through qPCR was in full agreement when performed using the same shFF3-sheRF1 cell lines but less so using siRNA mediated knockdown. How ATF4 activity is induced in response to eRF1 depletion in unclear, but is the focus of the following chapter.

# CHAPTER 5: The Activating Transcription Factor 4 (ATF4) as a response to defective termination

## 5.1 Introduction

In Chapter 4, a comparison of genes upregulated by eRF1 or eRF3a knockdown highlighted downstream targets of the Activating Transcription 4 (ATF4/CREB2) as the pathway upregulated at the highest confidence level by defective translational termination. Subsequent experiments using qPCR further validated the RNA-Seq results, and demonstrated that ATF4 downstream targets were among the most clearly upregulated genes during either shRNA or siRNA-based knockdown of eRF1. However, the mechanism of potential ATF4 activation following eRF1 knockdown was not known.

ATF4 expression is regulated at multiple levels including by transcriptional and post-transcriptional mechanisms. However, analysis of our RNA-Seq data did not support a significant induction of ATF4 transcription: ATF4 mRNA was only induced ~1.4-fold by eRF1 knockdown (data not shown). We felt this change was probably too low to account for the significant upregulation of downstream ATF4 targets observed (3-13 fold). Therefore, subsequent analysis in this Chapter focusses on understanding potential post-transcriptional regulation of ATF4 by eRF1. Importantly, there is substantial precedent in the literature for post-transcriptional control of ATF4 translation in response to stress, as outlined below.

Protein synthesis is tightly regulated in response to diverse cellular stresses. Endoplasmic reticulum stress, e.g. as part of the unfolded protein response, results in activation of the eukaryotic Initiation Factor 2 α (eIF2α) kinase PERK (Ron and Walter, 2007). eIF2α is a subunit of the eukaryotic Initiation Factor 2 (eIF2), which is essential for translational initiation as it forms part of the 43S preinitiation complex along with mRNA and the 40S subunit (Jackson et al., 2010). eIF2α modulates this

process via PERK-mediated S51 phosphorylation, resulting in overall suppression of translation. Specifically, S51 phosphorylated eIF2α binds to, and sequesters, the eIF2B guanidine nucleotide exchange factor, inhibiting its activity and resulting in reduced total eIF2α-GTP availability for formation of preinitiation complexes (Jackson et al., 2010). However, the translation of a specific set of upstream open reading frames (uORFs) located in the 5' region of a number of genes is actually promoted (Vattem and Wek, 2004). The Activating transcription factor 4, a transcription factor that binds to the cAMP Response Element (CRE), and which plays an important role in the integrated stress response, has two such uORFs, uORF1 and uORF2, with uORF2 overlapping the translation start site. Under physiological conditions translation is initiated from uORF1 and uORF2, thus preventing the ATF4 ORF from being translated (See Figure 5.1 for a schematic of this process) (Vattem and Wek, 2004). However, S51 phosphorylation of eIF2α results in inability to recharge the GTP at the downstream uORF, leading to reduced ribosomal ternary complex formation and thus preventing the downstream uORF from being recognised. Instead, the ATF4 ORF is recognised and expressed. Interestingly, eIF2α-*independent* upregulation of ATF4 upon knockdown of eRF3α, a termination factor that stimulates eRF1 activity, has recently been reported (Ait Ghezala et al., 2012a). The proposed mechanism involves ribosomal readthrough of the uORF1 stop codon due to defective translational termination. Given our observations that eRF1 knockdown induces stop codon readthrough (Chapter 3) and an increase in ATF4 target gene expression (Chapter 4), such a mechanism might also apply here.

In this chapter, we provide detailed characterisation of ATF4 regulation by eRF1 knockdown. We demonstrate that increased ATF4 protein expression is controlled at the level of the uORFs, and assess how different mutants of eRF1 affect this response.

Furthermore, we explore the expression of eRF1-regulated and ATF4 target genes using the eRF1 rescue cell lines and describe differential patterns of gene regulation which subsequently implicate specific arms of the UPR in the response to defects in individual eRF1 sub-domains.

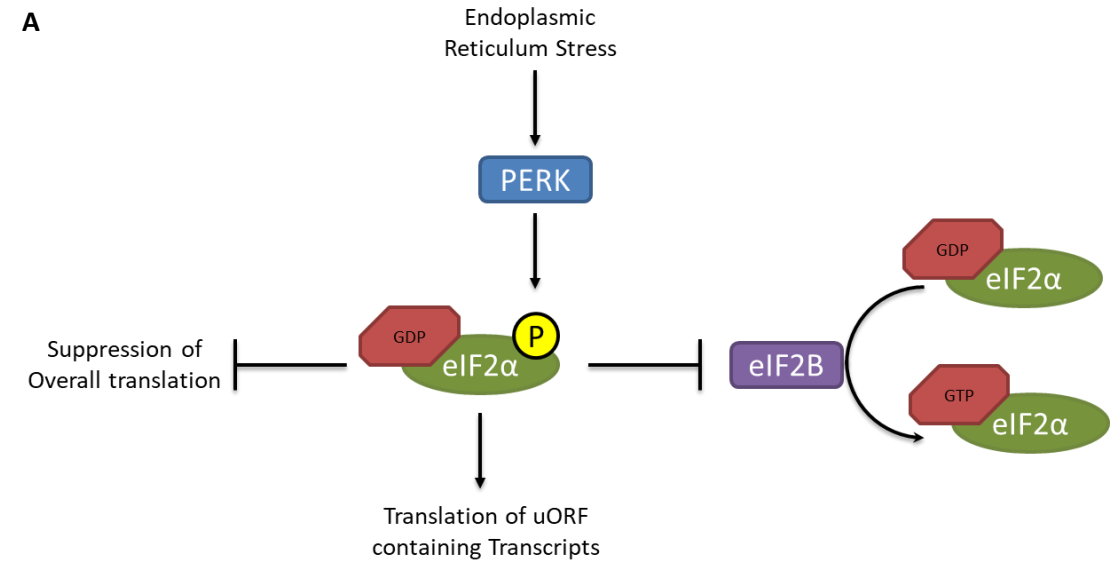
A
Endoplasmic
Reticulum Stress
PERK
GDP
eIF2α
P
Suppression of
Overall translation
eIF2B
GDP
eIF2α
GTP
eIF2α
Translation of uORF
containing Transcripts

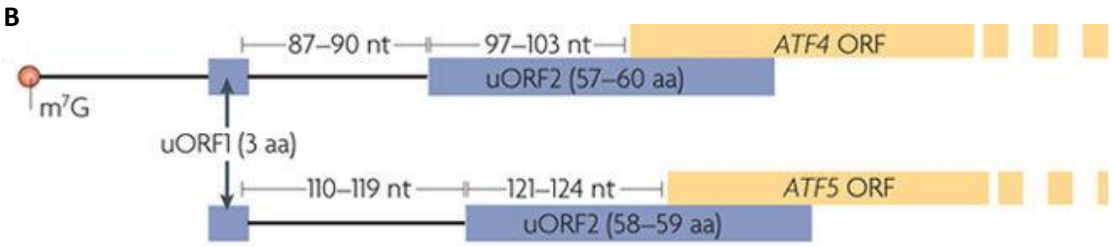
B
87–90 nt
97–103 nt
ATF4 ORF
uORF2 (57–60 aa)
m7G
uORF1 (3 aa)
110–119 nt
121–124 nt
ATF5 ORF
uORF2 (58–59 aa)

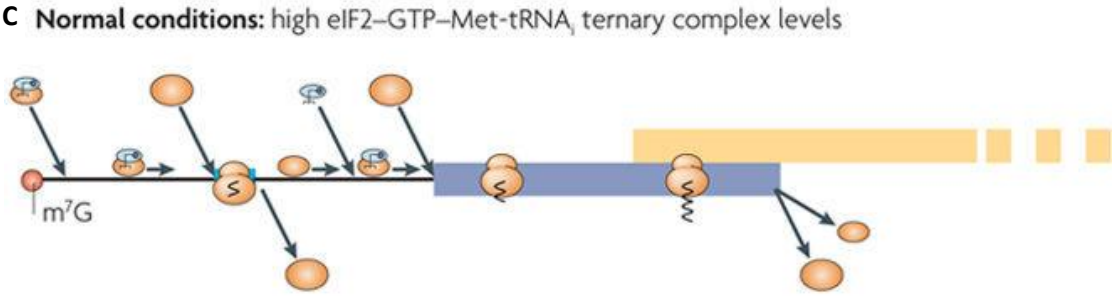
C Normal conditions: high eIF2–GTP–Met-tRNAi ternary complex levels
m7G

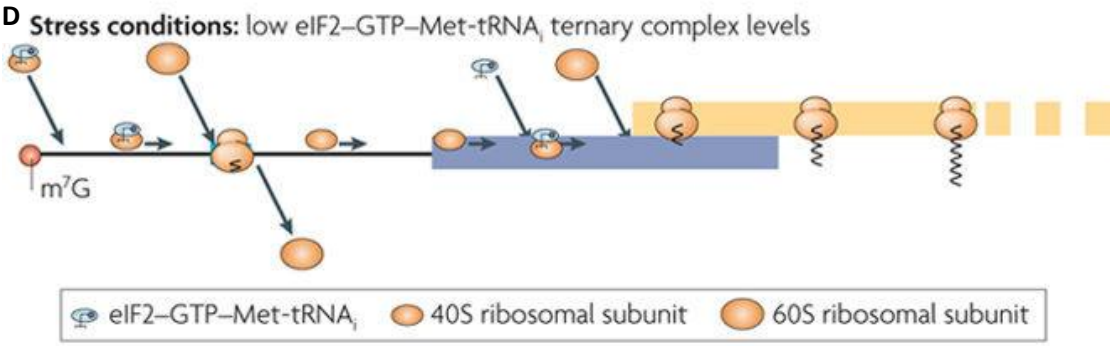
D Stress conditions: low eIF2–GTP–Met-tRNAi ternary complex levels
m7G
eIF2–GTP–Met-tRNAi
40S ribosomal subunit
60S ribosomal subunit

**Figure 5.1 (previous page): Regulation of ATF4 by eIF2α Phosphorylation.** A) Endoplasmic reticulum stress results in the activation of the kinase PERK, which catalyses the phosphorylation of eIF2α on S51. Phosphorylated eIF2α inhibits the eIF2α Guanidine Nucleotide Exchange Factor (GEF), eIF2B, resulting in reduced availability of eIF2α-GTP. This results in suppression of overall translation due to reduced rates of 43S pre-initiation complex assembly. B) The ATF4 ORF is preceded by two upstream ORFs (uORFs), uORF1 and uORF2. The ATF4 ORF is located within the uORF2 reading frame. C) Under normal conditions the ribosome initiates at uORF1, translates a short abortive sequence and then reinitiates at uORF2, thus bypassing the ATF4 ORF. During stress conditions (D), increased phosphorylation of eIF2α results in slower ribosomal assembly, preventing the ribosome from reinitiating at uORF2 and instead allowing ATF4 translation. (Figures B, C and D are reproduced from (Jackson et al., 2010))

## 5.2 Results

### 5.2.1 qPCR validation of target gene induction in eRF1 rescue cell lines

In the previous chapter a consistent and reproducible increase in ATF4 downstream targets was demonstrated using both shRNA and siRNA eRF1 knockdown approaches. To determine whether these effects were 'on-target' and to explore the role of different sub-domains of eRF1, gene expression analyses were performed in the eRF1 'rescue' cell lines described in Chapter 3. Therefore, the expression of genes described in Chapter 4 pathway analyses were tested in this system as follows. U2OS EV, WT, K63A and Q185N eRF1 cell lines were treated with 25 nM of either control or eRF1 siRNA with concurrent doxycycline stimulation (as optimised in Chapter 3) for 48h, followed by extraction of RNA, reverse transcription and SYBR Green qPCR (western blot validation of eRF1 knockdown and rescue is presented in Figure 5.7B). A total of 17 genes were tested across the following manually curated eRF1 response pathways; Ribosomal Components, Selenocysteine and Reverse Trans-sulfuration Components, ECM genes and ATF4 downstream targets.

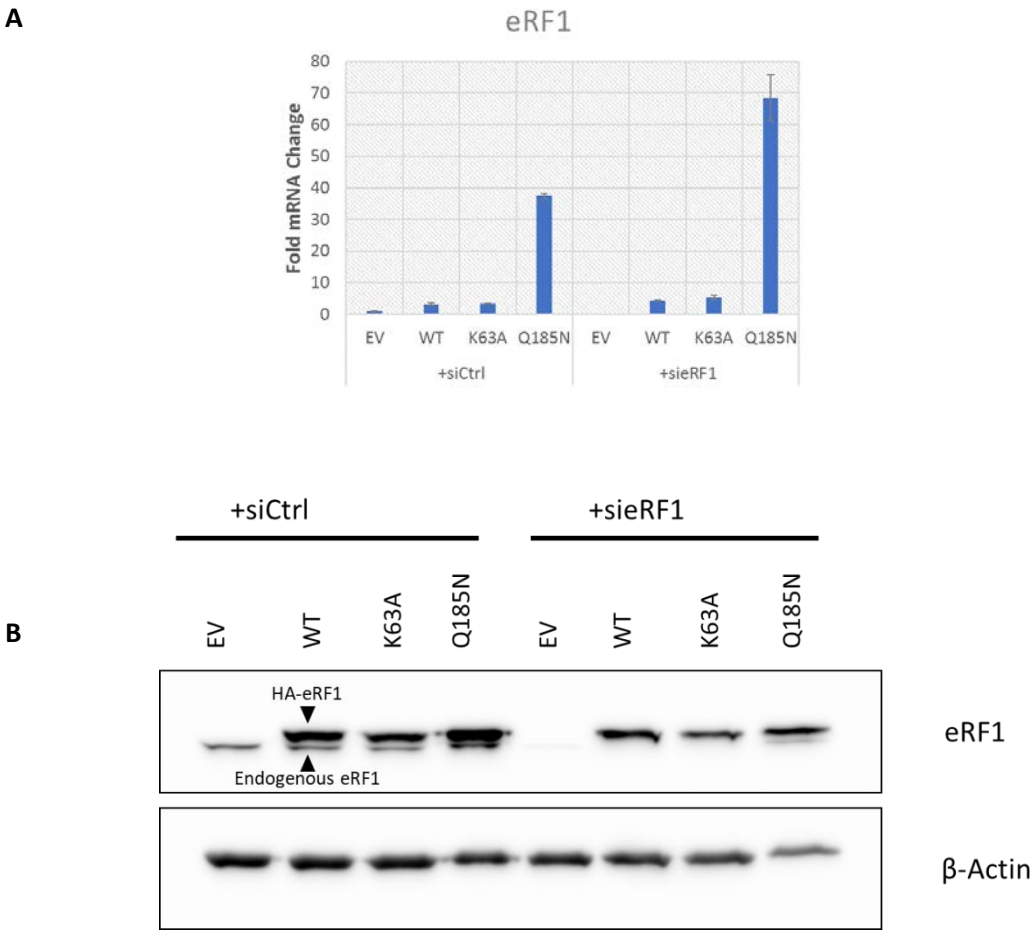


**Figure 5.2: Validation of endogenous eRF1 knockdown and HA-eRF1 expression in the eRF1 rescue cells.** EV, WT and K63A were treated with 0.03 µg $ml^{-1}$ and Q185N with 0.5 µg $ml^{-1}$ doxycycline for 48h. A) qPCR validation of eRF1 mRNA expression. Comparison of the fold change of transcript abundance between control and eRF1 siRNA knockdown (2ΔΔCt, where Ct is the threshold cycle), normalized to the EV+siCtrl sample. n=3±Standard deviation. B) Western blot validation of endogenous eRF1 knockdown and HA-eRF1 expression. The electrophoretic mobilities of endogenous and HA-eRF1 are indicated. The blots presented are the same as in Figure 5.7B.

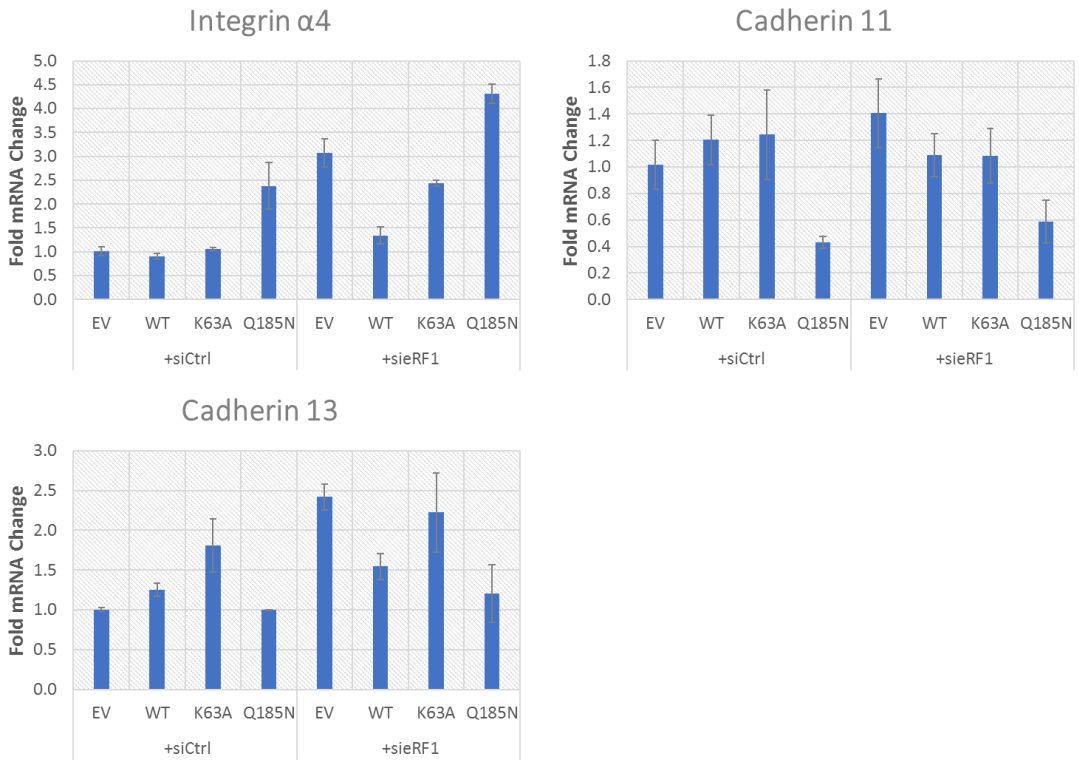


**Figure 5.3: qPCR validation of 'ECM, Adhesion and Motility' associated genes in the eRF1 rescue cells**. Comparison of the fold mRNA change of transcript abundance between control and eRF1 siRNA knockdown, normalized to the EV+siCtrl sample. EV, WT and K63A were treated with 0.03 µg $ml^{-1}$ and Q185N with 0.5 µg $ml^{-1}$ doxycycline for 48h. Genes aligned with the ECM, adhesion and motility pathway group are shown. n=3±Standard deviation.

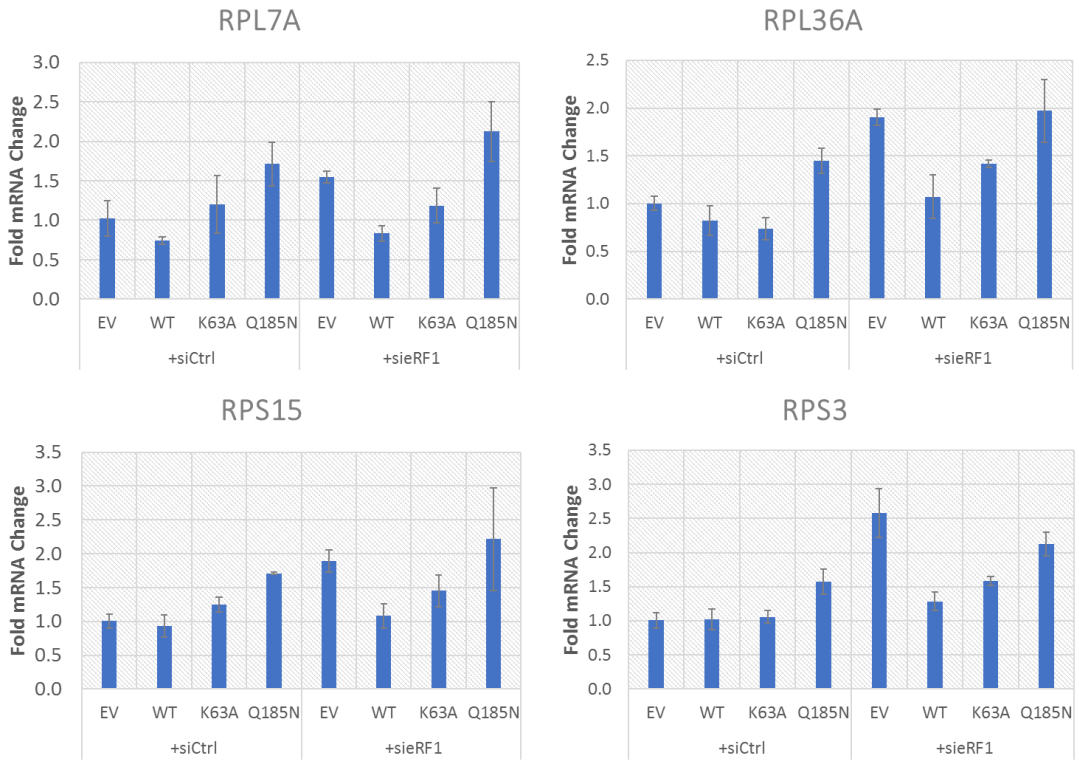


**Figure 5.4: qPCR validation of 'Ribosomal Component Pathway' gene induction in the eRF1 rescue cells**. Comparison of the fold change of transcript abundance between control and eRF1 siRNA knockdown, normalized to the EV+siCtrl sample. EV, WT and K63A were treated with 0.03 µg $ml^{-1}$ and Q185N with 0.5 µg $ml^{-1}$ doxycycline for 48h. Selected genes aligned with the ribosomal component pathway group are shown. n=3±Standard deviation.

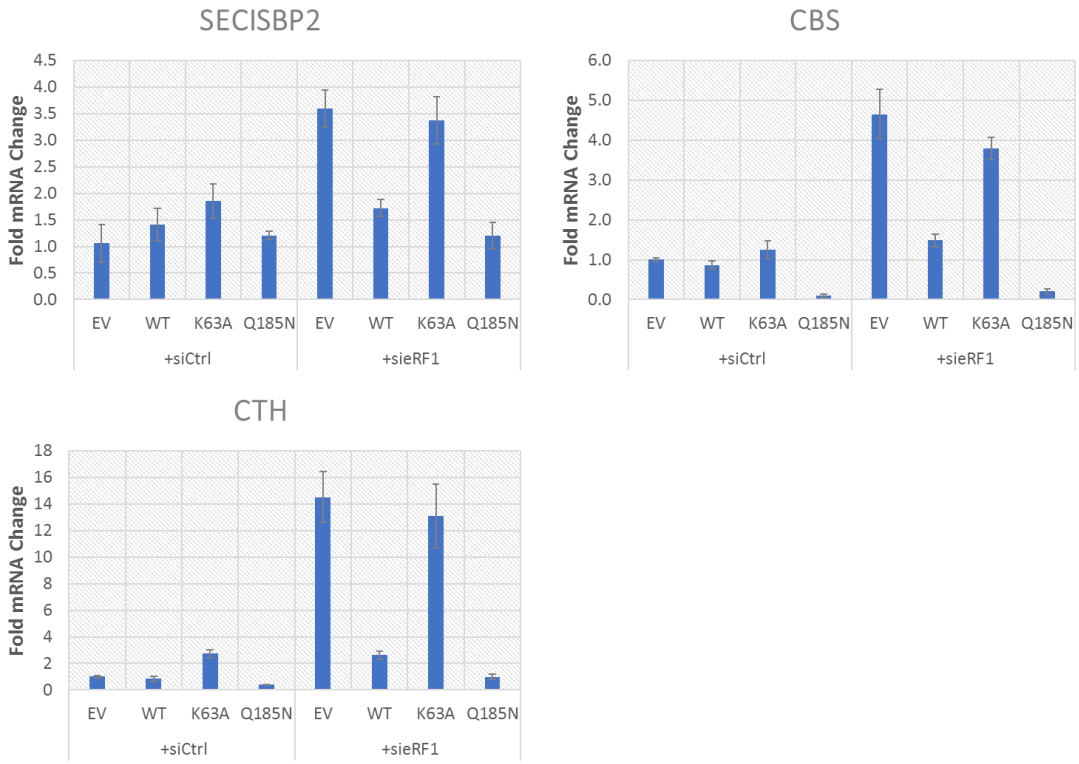


**Figure 5.5: qPCR validation of 'Seleno-aminoacid Metabolism' gene induction in the eRF1 rescue cells**. Comparison of the fold change of transcript abundance between control and eRF1 siRNA knockdown, normalized to the EV+siCtrl sample. EV, WT and K63A were treated with 0.03 µg $ml^{-1}$ and Q185N with 0.5 µg $ml^{-1}$ doxycycline for 48h. Genes aligned with the selenocysteine insertion and selenoaminoacid metabolism pathway group are shown. n=3±Standard deviation.

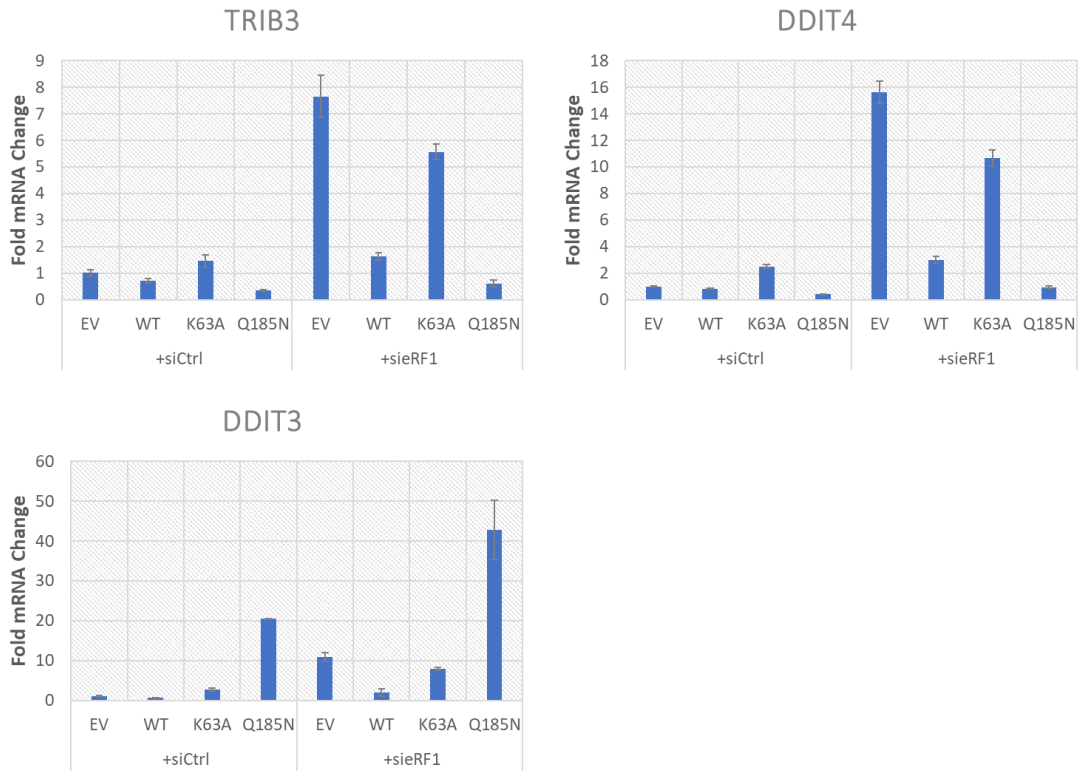


**Figure 5.6: qPCR validation of the induction of 'ATF4 downstream targets' in the eRF1 rescue cells**. Comparison of the fold change of transcript abundance between control and eRF1 siRNA knockdown, normalized to the EV+siCtrl sample. EV, WT and K63A were treated with 0.03 µg $ml^{-1}$ and Q185N with 0.5 µg $ml^{-1}$ doxycycline for 48h. Genes aligned with the ATF4 gene activation pathway group are shown. n=3±Standard deviation.

As anticipated, near complete loss of eRF1 mRNA occurs on eRF1 knockdown in the EV+sieRF1 samples (Figure 5.2). Expression of eRF1 transcript is restored by expression of the WT and K63A eRF1 mutants, demonstrating that they are resistant to sieRF1 knockdown, as expected. Expression of Q185N eRF1 mRNA is much higher than all the other samples in both the siCtrl and sieRF1 treated groups (Figure 5.7). This is presumably due to the higher dose of doxycycline required to induce expression of Q185N eRF1 protein to levels comparable to the WT and other mutants (Chapter 3).

Next we sought to use the eRF1 rescue system to help determine whether or not relatively modestly regulated gene sets identified in Chapter 4 could be confirmed. Therefore, we first analysed the eRF1-responsive cell adhesion proteins Integrin α4, Cadherin 11 and Cadherin 13 (Figure 5.3). Integrin α4 showed the anticipated increase in mRNA expression in response to eRF1 knockdown, which was rescued by WT eRF1 re-expression, but not the K63A mutant. Surprisingly, the expression of the eRF1 Q185N mutant appeared to further induce Integrin α4 mRNA expression. Cadherin 11 remained relatively unaffected by eRF1 knockdown and expression of any of the eRF1 mutants with the exception of Q185N, where its expression dropped to half the normal level in both the control and eRF1 knockdown samples. In contrast, the Cadherin 13 transcript shows a modest 2.4-fold increase in abundance following eRF1 knockdown, which is rescued by WT eRF1 re-expression, but not by K63A, as expected. Surprisingly, Q185N re-expression appeared to rescue normal Cadherin 13 transcript abundance in response to endogenous eRF1 knockdown. However, in light of other data presented below, this likely represents a failure to induce Cadherin 13, rather than a *bona fide* rescue, which would also be at odds with the stop codon readthrough data presented in Chapter 3.

Next we assessed the regulation of ribosomal components by eRF1 knockdown and reconstitution. Consistent with data presented in Chapter 4, eRF1 knockdown resulted in a low-level upregulation of ribosomal components, ranging from 1.5-fold in RPL7a to 2.5-fold in RPS3 (Figure 5.4). Expression of WT eRF1 universally rescued this increase, confirming its eRF1-dependence. However, the effects of eRF1 K63A re-expression were less clear, possibly due to the generally modest levels of regulation. However, Q185N eRF1 expression resulted in approximately 2-fold upregulation under eRF1 knockdown of all four ribosomal components examined, as well as a consistent 1.5-fold increase under control siRNA knockdown. Overall, the changes observed are quite modest. However, the pattern of regulation is unlikely to be stochastic as it is quite consistent among the 4 cell lines and also in line with the previous RNA-Seq data and independent qPCR validation performed in Chapter 4.

In contrast, Selenocysteine and Reverse Trans-sulfuration pathway components demonstrated more striking eRF1-dependent regulation (Figure 5.5). Depletion of eRF1 caused a 4-fold increase in CBS transcript abundance, a 14-fold increase of CTH and a 3-fold increase in SECISBP2. In each case, expression of WT eRF1 fully rescued normal expression, while K63A eRF1 expression completely failed to do so. Interestingly, normal expression appears to be fully restored in response to Q185N re-expression which, similar to its regulation of Cadherin 13, is at odds with its apparent lack of activity in stop codon readthrough assays described in Chapter 3. In fact, Q185N re-expression actually results in a *reduction* in transcript abundance, to levels below that observed in the WT rescue cells. This decline occurs whether endogenous eRF1 is present or not, as it is also present in the samples treated with control siRNA.

Subsequently, the response of the ATF4 target genes TRIB3, DDIT3 and DDIT4 was analysed. Of these, TRIB3 and DDIT4 exhibit a similar pattern of regulation to each

other, with an increase in the EV + sieRF1 cells which is rescued by WT eRF1 expression but not K63A expression, similar to Selenocysteine and Reverse Trans-sulfuration pathway components. Interestingly, the expression of TRIB3 and DDIT4 mRNA also showed a reduction upon Q185N eRF1 expression. DDIT3 is however unique in that while its pattern of regulation is highly similar to the DDIT4 and TRIB3 for the EV, WT and K63A cell lines, the greatest increase in expression appears to occur during Q185N expression in both the control and sieRF1 treated groups. In this respect, regulation of DDIT3 mRNA by eRF1 is more similar to Integrin $\alpha$4.

A

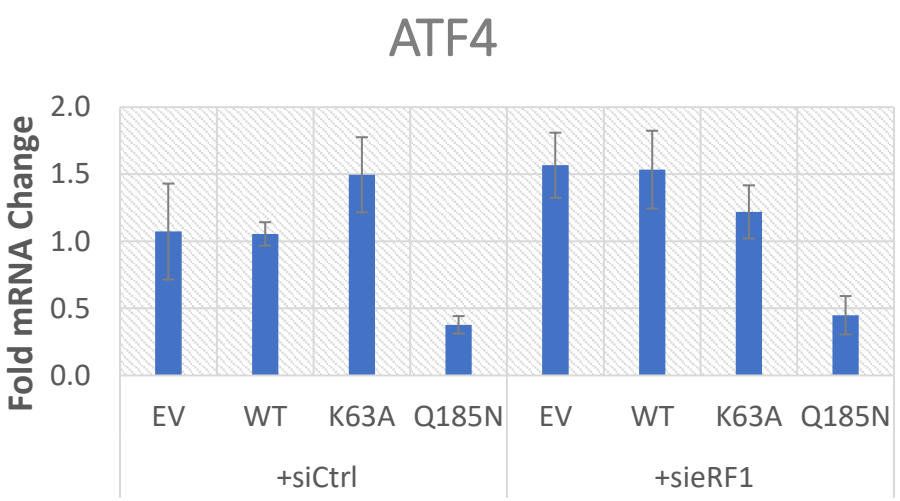


B

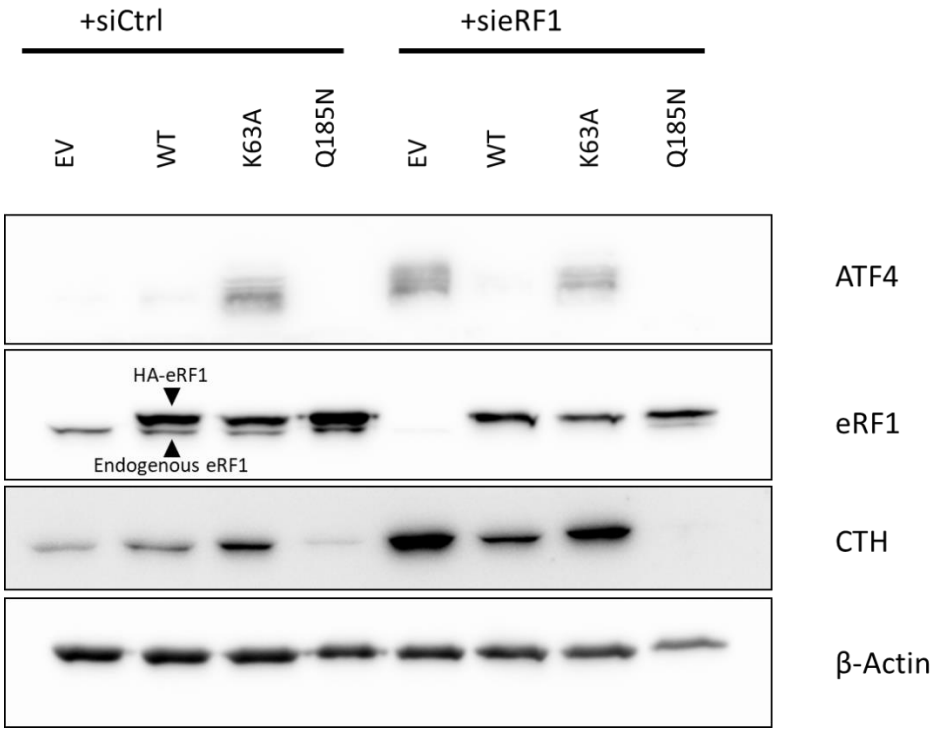


**Figure 5.7: Transcript and protein level expression of ATF4 in the eRF1 rescue cell lines**. EV, WT and K63A were treated with 0.03 µg ml$^{-1}$ and Q185N with 0.5 µg ml$^{-1}$ doxycycline for 48h to induce expression of the recombinant forms A) RT-qPCR of ATF4 mRNA in response to eRF1 knockdown in the eRF1 rescue cells. n=3±Standard deviation. B) Western Blot validation of ATF4 and target gene induction in the eRF1 rescue cells. Comparison of the fold change of protein abundance between control and eRF1 siRNA knockdown. Cystathionine γ-lyase (CTH) was chosen as a representative target gene among those tested in the qPCR analysis above. The electrophoretic mobilities of endogenous and HA-eRF1 are indicated. The eRF1 and β-Actin blots presented were also used in Figure 5.2B.

To further understand the unusual regulation of eRF1-responsive genes by the Q185N mutant, we measured ATF4 mRNA expression in the eRF1 rescue cell lines (Figure 5.7A). Consistent with the RNAseq data (Chapter 4), ATF4 mRNA appears to be slightly upregulated following eRF1 siRNA, although this appeared not to be rescued by WT eRF1 re-expression. Interestingly however, Q185N expression caused a significant reduction in ATF4 mRNA levels, which could perhaps explain the lack of ATF4 target gene regulation under these conditions (Figure 5.6).

To explore whether eRF1 knockdown increases ATF4 protein expression in a 'rescuable' manner, and whether this is suppressed by the expression of eRF1 Q185N, ATF4 protein expression was examined by western blotting (Figure 5.7B). Importantly, abundant ATF4 protein was induced by eRF1 siRNA in EV cells, and in a manner that was suppressed by re-expression of WT eRF1. Consistent with its lack of activity seen in previous Chapters, K63A eRF1 expression failed to suppress ATF4 protein expression. Interestingly, ATF4 protein was also increased in the siCtrl K63A cells, which likely accounts for the low moderate increase in mRNA expression of some of the genes tested via qPCR for those samples (e.g. Figure 5.5/5.6). This would suggest that the K63A mutant has some dominant negative activity with respect to the endogenous wild-type protein. Similar to the ATF4 target gene analyses, Q185N eRF1 appeared to suppress ATF4 protein induction by eRF1 siRNA. However, in light of the reduction in ATF4 mRNA levels seen in Figure 5.7A, this apparent reduction is likely due to a failure to respond to eRF1 siRNA. Overall, the discord between the response of ATF4 mRNA and protein levels to eRF1 depletion highlights some level of post-transcriptional regulation (further explored below).

Next we took the opportunity to further validate our gene expression analyses by testing whether induction of eRF1 responsive genes also result in increased target

protein expression, using a commercially available CTH antibody. Importantly, we find an expression pattern identical to that presented in Figure 5.5. CTH protein abundance was increased in response to eRF1 siRNA and rescued by WT eRF1 but not the K63A mutant. CTH expression was suppressed by expression of the Q185N mutant. Overall, the expression of CTH closely mirrored that of ATF4 protein. Indeed, there is some evidence supporting components of the Selenocysteine and Reverse Trans-sulfuration pathway as ATF4 target genes, including CTH (Dickhout et al., 2012a).

Overall, the data presented in this section suggests that eRF1 knockdown results in post-transcriptional upregulation of ATF4 protein levels, but that this induction is dependent on basal ATF4 transcription (as exemplified by Q185N).

### 5.2.2 eRF1 depletion increases ATF4 protein expression via regulation of upstream open reading frames in the ATF4 5'-UTR

Having validated that increased ATF4 target gene expression following eRF1 knockdown is associated with significantly increased ATF4 protein levels, but not mRNA, we wished to investigate whether this post-transcriptional regulation occurred at the level of its uORFs. In order to achieve this, a specific ATF4 uORF Firefly/*Renilla* based luciferase assay system was used, as obtained from Dr Gavin McNee (University of Birmingham, UK) and described previously (Harding et al., 2000a). Briefly, the *Homo sapiens* uORF1&2 sequences 5' to the ATF4 ORF (and the relevant linker sequences) were inserted upstream of the Firefly luciferase coding gene and driven by a Thymidine Kinase (TK) promoter in a pGL3 plasmid. The resulting vector, termed 'pGL3 ATF4 uORF' positions the luciferase start site in the

same position as the ATF4 start site and is preceded by the same regulatory sequences (Figure 5.8A). Therefore, conditions which result in 'translational expression' of endogenous ATF4 should also control translational expression of the Firefly luciferase. In order to control for differences in transfection efficiency and/or basal transcription, a plasmid expressing *Renilla* luciferase under a constitutive Cystic Megalovirus (CMV) promoter was also co-transfected (pRL-CMV). Therefore, translational regulation of ATF4 can be followed by monitoring the ratio of Firefly/*Renilla* activity (the signals of which can be deconvoluted as discussed in Chapter 3), and normalised to an untreated sample (Figure 5.8B). Therefore, the U2OS eRF1 rescue cell lines EV, WT, K63A and Q185N were treated with their respective optimised Doxycycline concentrations for 48h, with simultaneous transfection of 25 nM control or eRF1 siRNA, before being trypsinised and reverse transfected with the pGL3 ATF4 uORF/pRL-CMV plasmid mixture. The cells were then allowed to rest for 48h before being harvested for luciferase assays and western blots.

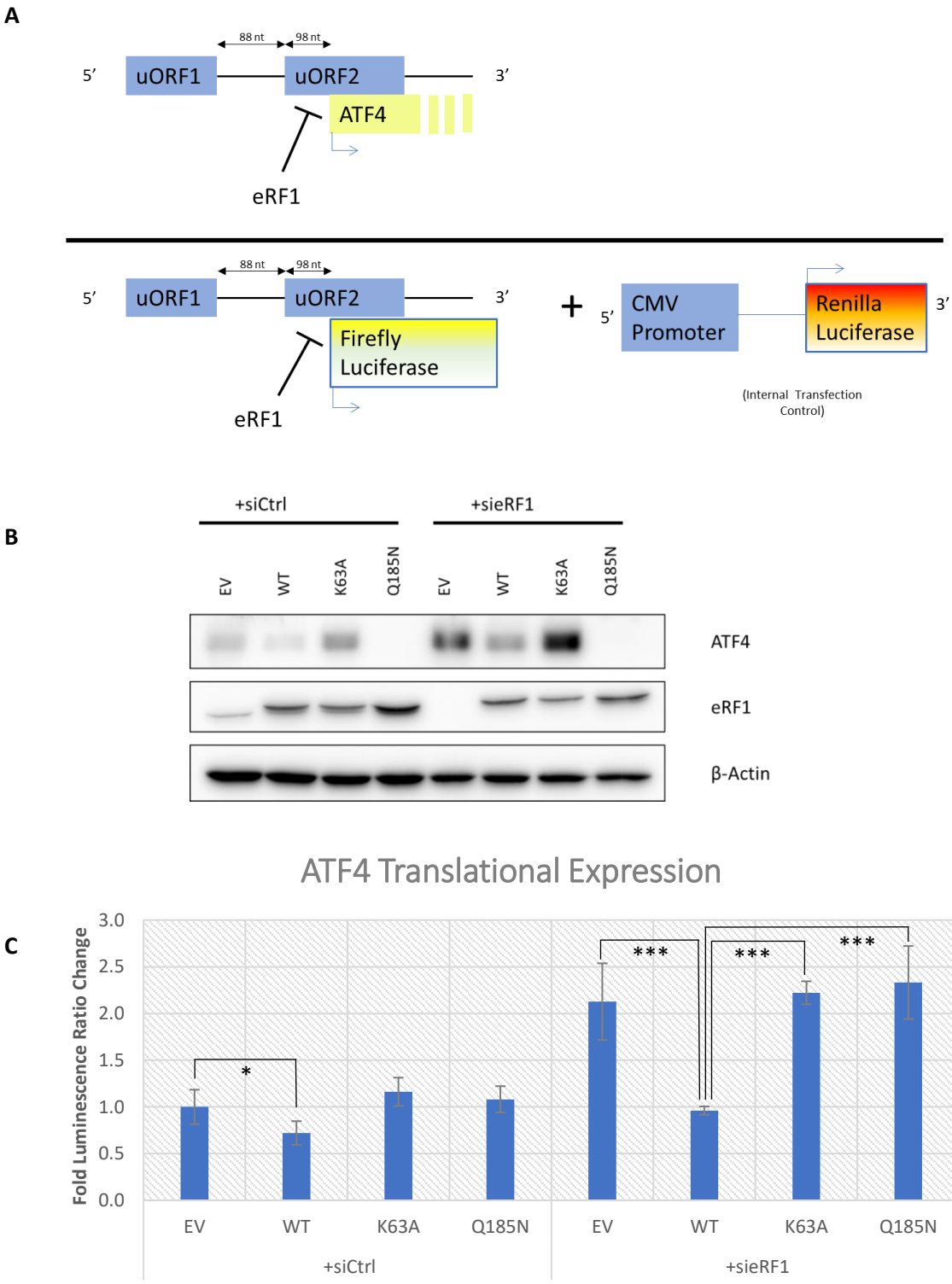


**Figure 5.8: Control of ATF4 expression occurs during translation.** Translational control of eRF1 expression in the eRF1 rescue system A) Assay mechanism**.** B) Western Blot demonstrating knockdown of endogenous eRF1 and expression of the exogenous forms C) Translational control of ATF4 expression in the eRF1 rescue cell lines. Fold Luminescence Change = (Firefly Lum) / (Renilla Lum), normalised to the EV+siCtrl sample. In (B) and (C) EV, WT and K63A were treated with 0.03 µg $ml^{-1}$ and Q185N with 0.5 µg $ml^{-1}$ doxycycline for 48h to induce expression of the recombinant forms of eRF1. n=3, Mean ± StDev. *P<0.05, ***P<0.001. Student's two tailed t-test.

Western blot validation of the eRF1 interventions and ATF4 protein response (Figure 5.8B) were highly similar to those obtained during our initial analysis of ATF4 expression in the eRF1 rescue cells (Figure 5.7). Importantly, under these conditions we observed that eRF1 knockdown in the EV cell line results in an increase in translational expression of ATF4 (Figure 5.8C), as indicated by increased Firefly luciferase activity. Although the observed increase of approximately two-fold was notably lower than might be anticipated based on the western blots in Figure 5.8B, as well as earlier blots of ATF4 (Figure 5.7B), this level of regulation is line with previously published work using this system (Harding et al., 2000a). Importantly, re-expression of WT eRF1 fully rescues the increase in ATF4 translational expression, and actually results in a modest, but statistically significant, reduction in ATF4 translational expression in control knockdown samples. This would suggest that basal ATF4 expression is also under the control of eRF1-dependent uORF regulation, a notion supported by the detection of low levels of ATF4 protein in control cells, and their reduction by eRF1 re-expression (Figure 5.8B). Consistent with the stop codon readthrough analyses (Chapter 3), both the K63A and Q185N mutants were completely inactive, and unable to restore normal translational control of ATF4 protein in response to endogenous eRF1 knockdown. Interestingly, the difference in translational (Figure 5.8C) and transcriptional (Figure 5.7A) regulation of ATF4 by the eRF1 Q185N mutant highlights how the cellular response to this mutant appears to specifically uncouple these steps of ATF4 synthesis.

### 5.2.3 eRF1 knockdown induces eIF2α phosphorylation

Thus far we have demonstrated that eRF1 knockdown is associated with increased uORF-mediated post-transcriptional regulation, elevated ATF4 protein levels, and ATF4 target gene induction. As described earlier, two mechanisms could thus far potentially explain the regulation of ATF4 uORF regulation by eRF1: a) its knockdown activates the UPR, causing an increase in eIF2α phosphorylation which in turn stimulates increased ATF4 translation via its uORFs, or b) eRF1 knockdown increases stop codon readthrough, which causes ribosomes to translate through the uORF1 stop codon, bypassing the uORF2 start site and initiating at the ATF4 ORF.

If the former possibility were correct, then one would expect to observe an increase in eIF2α phosphorylation following eRF1 knockdown. To examine this possibility, a timecourse experiment was designed in which the U2OS shFF3 and sheRF1 knockdown cells were treated with 1 μg $ml^{-1}$doxycycline for a total of 5 days, with protein and RNA samples taken daily. Protein and RNA samples were subsequently analysed to explore the temporal relationship between eRF1 knockdown, ATF4 protein induction, ATF4 target gene activation, and any potential increase in eIF2α phosphorylation.

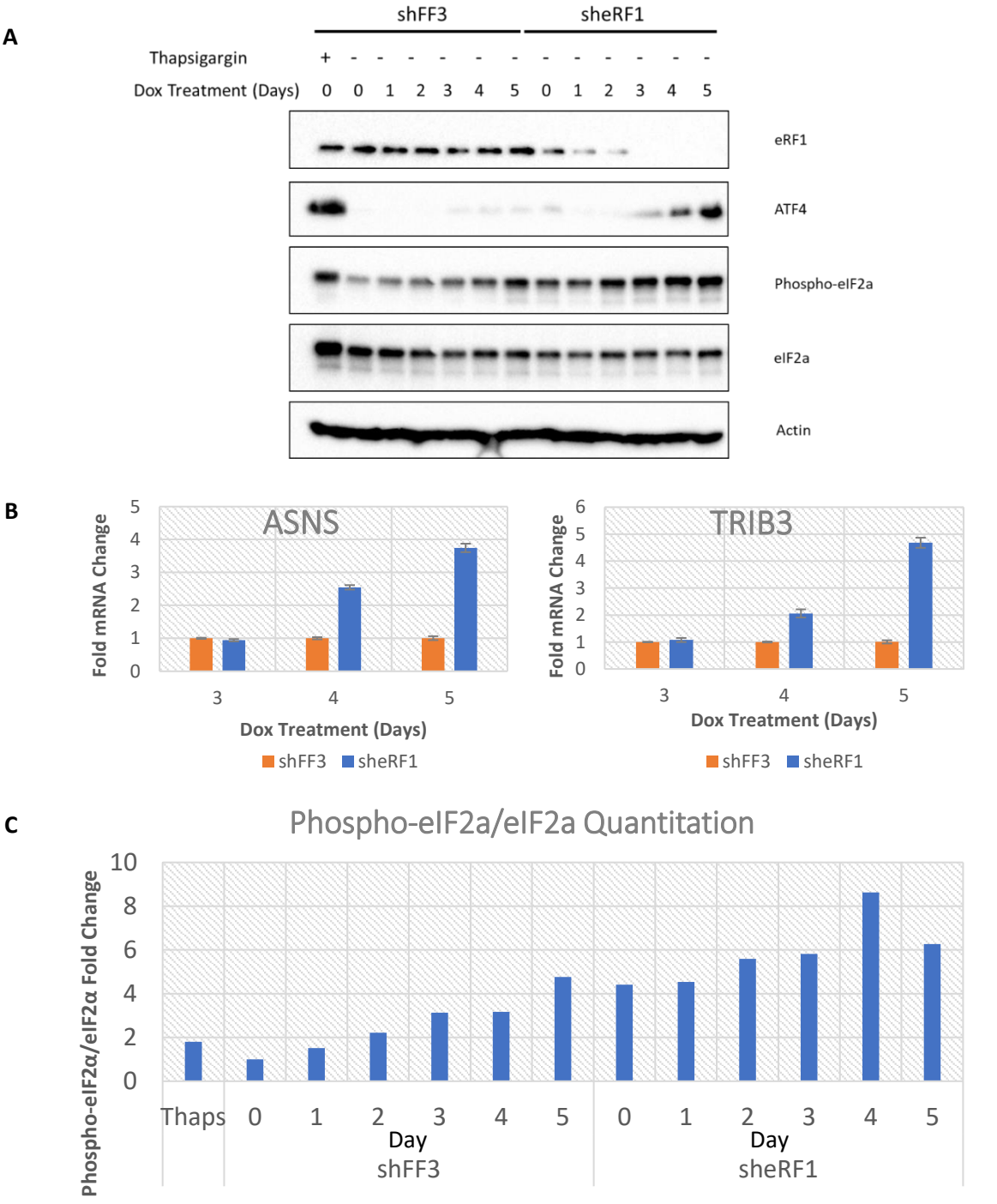


**Figure 5.9: eIF2α phosphorylation and eRF1 knockdown timecourse:** U2OS shFF3 and sheRF1 were treated with 1 μg $ml^{-1}$ doxycycline for a total of 5 days, with protein and RNA samples harvested daily. An additional sample of shFF3 + 0.5 μM of the known ER stress inducer thapsigargin was also prepared**.** A) Western Blot of the timecourse B) RT-qPCR of the ATF4 downstream target genes ASNS and TRIB3 during the timecourse. Values are displayed for days 3-5. No upregulation could be detected before that. n=3 ± Standard Deviation C) Fold change of band intensity in the western blots was quantified by densitometry analysis and normalized to shFF3 Day 0 for that protein. Phospho-eIF2α/eIF2α is the ratio of the phosphorylated-eIF2α to total eIF2α, in turn normalized to the value for that ratio at day 0.

In the associated western blot (Figure 5.9A), complete knockdown of eRF1 occurs after 3 days of continuous doxycycline treatment. That same day is also the first time at which ATF4 protein expression is clearly induced. The expression of ATF4 is not transient, with expression continuing to rise during Days 4 and 5. Importantly, ATF4 target gene expression, as judged by qPCR analyses (Figure 5.9B), was only detected after ATF4 protein induction from Day 4. This increase in ASNS and TRIB3 mRNA increase was also not transient, increasing further from Day 4 to 5, in line with ATF4 levels.

Having determined the timecourse of ATF4 protein and target gene induction following eRF1 knockdown we next assessed the levels of total and phospho-eIF2α (Figure 5.9C). Total eIF2α levels appear mostly unchanged throughout the timecourse for sheRF1 cells, though a slight reduction was observed in the shFF3 cells. In both shFF3 and sheRF1 cells the level of eIF2α phosphorylation appeared to increase throughout the timecourse. Importantly however, eIF2α phosphorylation was greater at every time point in sheRF1 cells than shFF3 control cells. Interestingly, this difference was also apparent at 0 Days, where reduced eRF1 levels were already apparent, possibly reflecting leaky shRNA expression. In order to quantify these changes, western blot signals were measured by densitometry analysis and the ratio of phosphorylated to total eIF2α were calculated for each day (Figure 5.9C). We find that the lowest level of eIF2α phosphorylation occurs in the shFF3 cells at the beginning of the experiment and increases steadily through the timecourse to a 4.5-fold increase by Day 5. Phospho-eIF2α levels in sheRF1 cells start on Day 0 at levels comparable to those of the shFF3 cells on Day 5, and increase steadily to approximately 6-8-fold (relative to Day 0 control cells).

Therefore, while an increase in eIF2α phosphorylation under eRF1 knockdown does occur, an increase also occurs in the control group. However, the overall level of eIF2α phosphorylation is consistently greater in the eRF1 knockdown samples. Whether this would be sufficient to explain the increase in ATF4 protein expression remains unclear. Certainly, the fold change is quite small compared to the level of ATF4 upregulation, and the increase is gradual rather than occurring just beforehand. However, it may be possible that a threshold level of eIF2α phosphorylation is required in order to drive efficient ATF4 translation, and that this threshold is only surpassed in the sheRF1 cells at Days 3-5 of Doxycycline treatment.

To further explore the potential regulation of eIF2α phosphorylation by eRF1 depletion, we turned to the eRF1 rescue model, using the same experimental samples presented in Figure 5.7. Based on the subsequent western blot (Figure 5.10A) and associated densitometry (Figure 5.10B), knockdown of eRF1 via siRNA in the EV cells results in a ~3-fold increase in the phospho-eIF2α/ eIF2α ratio, which is visually confirmed on the western blot. Importantly, expression of siRNA resistant WT, but not K63A, eRF1 rescues this phenotype. Meanwhile the Q185N + sieRF1 sample displays low amounts of phosphorylated eIF2a but also reduced total eIF2α, which is reflected as a high phospho-eIF2α/eIF2α ratio. The presence of incomplete eRF1 knockdown in the latter however makes estimation of the magnitude of the effect more difficult. Overall, the pattern of eIF2a phosphorylation in the eRF1 siRNA group strongly resembles that of the stop codon regulation presented in Chapter 3 and importantly, with respect to the mechanism of ATF4 regulation, the ATF4 translational reporter results presented in Figure 5.8C.

A

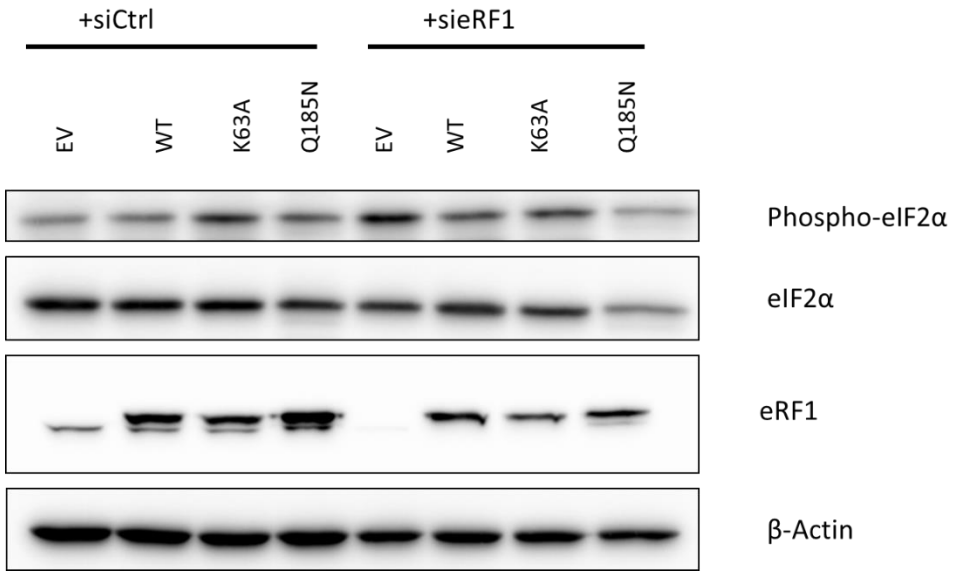


B

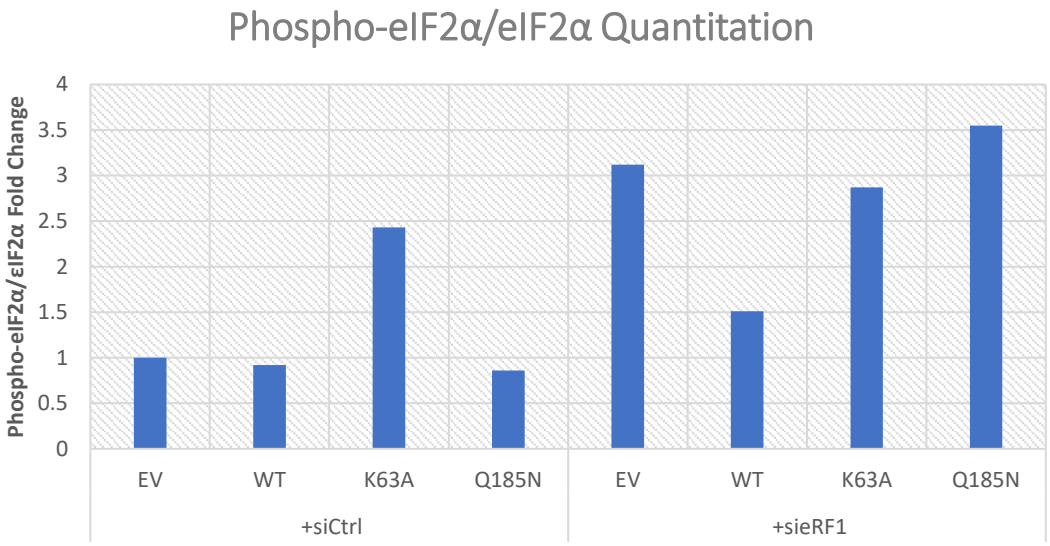


**Figure 5.10: eIF2α phosphorylation in the eRF1 rescue cell lines.** The cells were transfected with 25 nM control or eRF1 siRNA and induced for 48h with 0.03 µg $ml^{-1}$ Doxycycline for EV, WT and K63A and 0.50 µg $ml^{-1}$ for Q185N**.** A) Western Blot of Phospho- and total eIF2α B) Fold change of band intensity in the western blots for phospho-and total eIF2α was quantified by densitometry analysis and normalized to the value for +siCtrl EV.

### 5.2.4 ATF4 induction in response to eRF1 knockdown may be dependent on eIF2α phosphorylation

The data presented above are generally supportive of eIF2α phosphorylation following eRF1 knockdown being associated with ATF4 protein induction. However, this association does not demonstrate that eIF2α phosphorylation is *required* for ATF4 induction. To specifically test this, we aimed to determine whether ATF4 translational expression could still be induce by eRF1 knockdown under conditions in which eIF2α phosphorylation was prevented. To inhibit eIF2α phosphorylation we decided to overexpress GADD34, a largely unstructured protein with two primary sequence features: a series of four (in *H. sapiens*) PEST repeats, which allow binding of eIF2α, and a KVRF sequence close to the C-terminus which is responsible for binding the Ser/Thr phosphatase Protein Phosphatase 1 (PP1) (Rojas et al., 2015). As illustrated in the Figure 5.11, GADD34 acts as an intermediary, allowing PP1 to dephosphorylate eIF2α by binding to both proteins via different domains. Previous studies have established that overexpression of GADD34 results in major loss of eIF2α phosphorylation, presumably by permitting better access of PP1 to eIF2α (Choy et al., 2015). Therefore, GADD34 was cloned into the pCDNA3 expression vector for transient overexpression in cells, with and without eRF1 knockdown. Because this experimental approach was based on transient transfection, where only a fraction of the cells would express GADD34, we considered it appropriate that the 'readout' of the assay would also be limited to the transfected cells (rather than the whole pool, as for western blotting for example). Therefore, we co-transfected GADD34 with the ATF4 uORF translational reporter system described above, where we previously

demonstrated eRF1-dependent regulation (Figure 5.8). U2OS EV cells were transfected with either control or eRF1 siRNA for 48h. Subsequently, they were transfected with an empty pCDNA3 control vector, or pCDNA3-GADD34 in addition to the pGL3-ATF4 and pRL indicator plasmids. Following 48h of transfection and expression, samples were harvested for luciferase activity assays and western blotting.

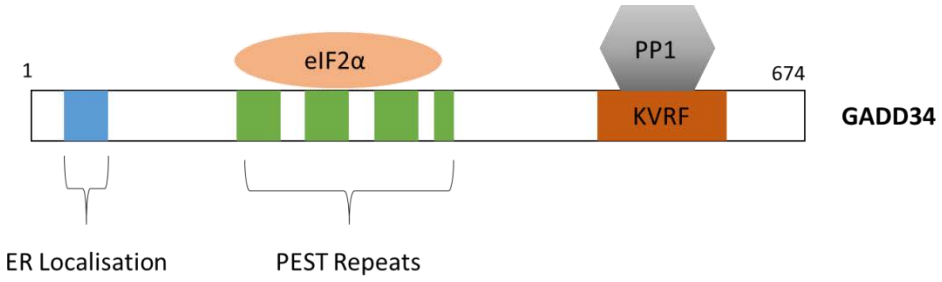


**Figure 5.11: GADD34 domains and function.** GADD34 contains a series of four PEST repeats which allow binding of eIF2α and a KVRF sequence allowing binding of Protein Phosphatase 1 (PP1).

A

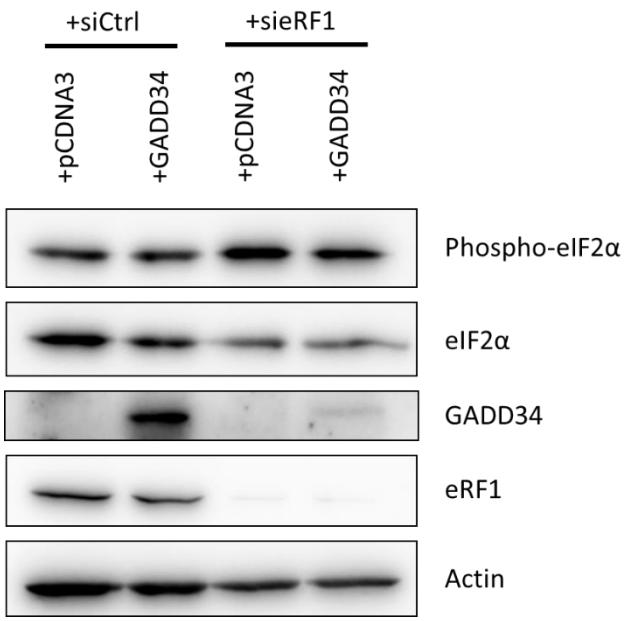


B

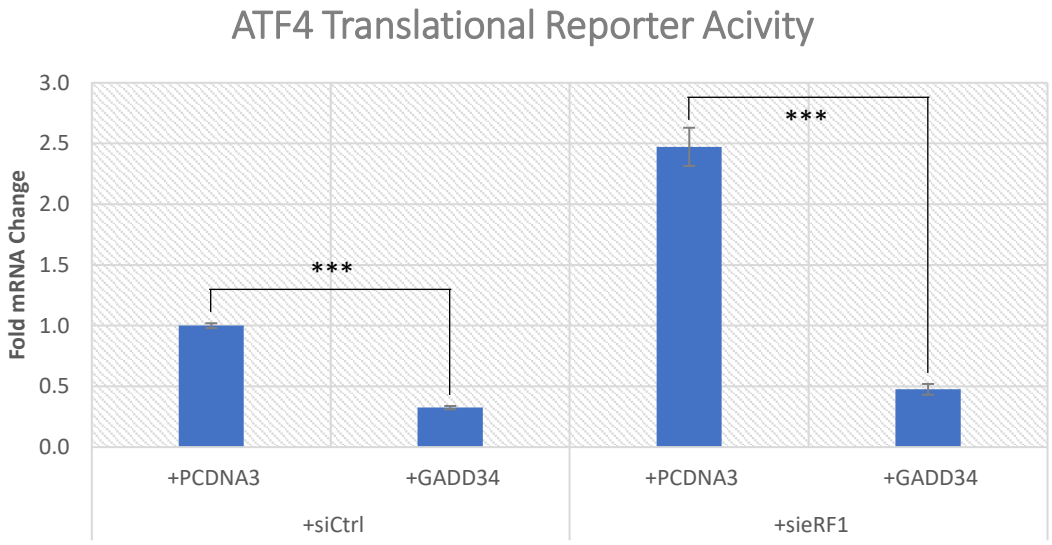


**Figure 5.12: GADD34 overexpression leads to reduction of ATF4 translational expression.** U2OS EV cells were transfected with a pCDNA3 plasmid containing GADD34 under a constitutive promoter, as well as the pGL3/pRL ATF4 translational expression system. A) Western Blot B) ATF4 reporter translational activity. n=3. Mean±St.Dev. ***P<0.001. Student's two-tailed t-test.

The results from the luciferase assay (Figure 5.12B) indicate a 2.5-fold increase in translational expression during eRF1 knockdown (compared to control siRNA treatment) in the absence of GADD34 overexpression, comparable to that observed in the initial ATF4 uORF assays (Figure 5.8). Interestingly, overexpression of GADD34 in control siRNA-treated cells reduced ATF4 uORF reporter activity to only ~30% of the +pCDNA3 control group: This might indicate that ATF4 expression is under the control of eIF2α even under basal conditions. Importantly, overexpression of GADD34 in eRF1 knockdown cells completely rescued the ATF4 translational expression phenotype (despite the reduced GADD34 expression achieved in these cells, Figure 5.12A). This would potentially indicate that expression of ATF4 in response to eRF1 depletion is dependent on eIF2α phosphorylation.

### 5.2.5 Contribution of other arms of the UPR to the eRF1 rescue phenotypes

So far, we have demonstrated that eRF1 depletion results in a robust increase in the expression of ATF4, and provided evidence that this occurs via eIF2α phosphorylation. eIF2α phosphorylation is one arm of a multi-faceted cellular response to misfolded proteins and translational stress known as the Unfolded Protein Response (UPR), which regulates cell survival, apoptosis, and gene expression control (Figure 5.13). Other than ATF4, the transcription factors X-Box Binding Protein 1 (XBP1) and another ATF family member, ATF6, are also heavily involved in the UPR. Whether ATF6 and/or XBP1 are also induced by eRF1 knockdown as part of a general UPR response, or whether eRF1 depletion specifically activates ATF4, is not yet known.

We considered that the unique regulation of DDIT3 and ATF4 mRNA by the eRF1 Q185N mutant in the eRF1 siRNA rescue model might indicate activation of additional arms of the UPR, for the following reasons. While DDIT3 has been well documented to be an ATF4 downstream target (Su and Kilberg, 2008) the increased DDIT3 mRNA expression observed during Q185N eRF1 re-expression (Figure 5.6) cannot be due to ATF4, the activity and expression of which was heavily reduced in those samples (Figures 4.7A&B). Interestingly however, previous literature has suggested that DDIT3 transcription is also regulated by the activated forms of ATF6 and XBP1 (Oyadomari and Mori, 2004).

XBP1 mRNA can be spliced by the Inositol Requiring Enzyme 1α (IRE1α) at the Endoplasmic Reticulum under conditions of stress, resulting in the removal of a 26nt intronic sequence (Figure 5.13 and 5.14A). This produces an alternative reading frame, causing XBP1 that has been spliced in this way to have a different C-terminal sequence (Figure 5.14B). The transcriptional targets also change, and it is the spliced XBP1 which participates in UPR signaling: activation of XBP1 can be assayed by the ratio of spliced to unspliced XBP1. We analysed the expression profile of XBP1 in response to eRF1 knockdown and re-expression: Spliced (i.e. active) XBP1 (henceforth XBP1s) mRNA was quantified by qPCR and gel electrophoresis (Figures 5.14C& 5.15).

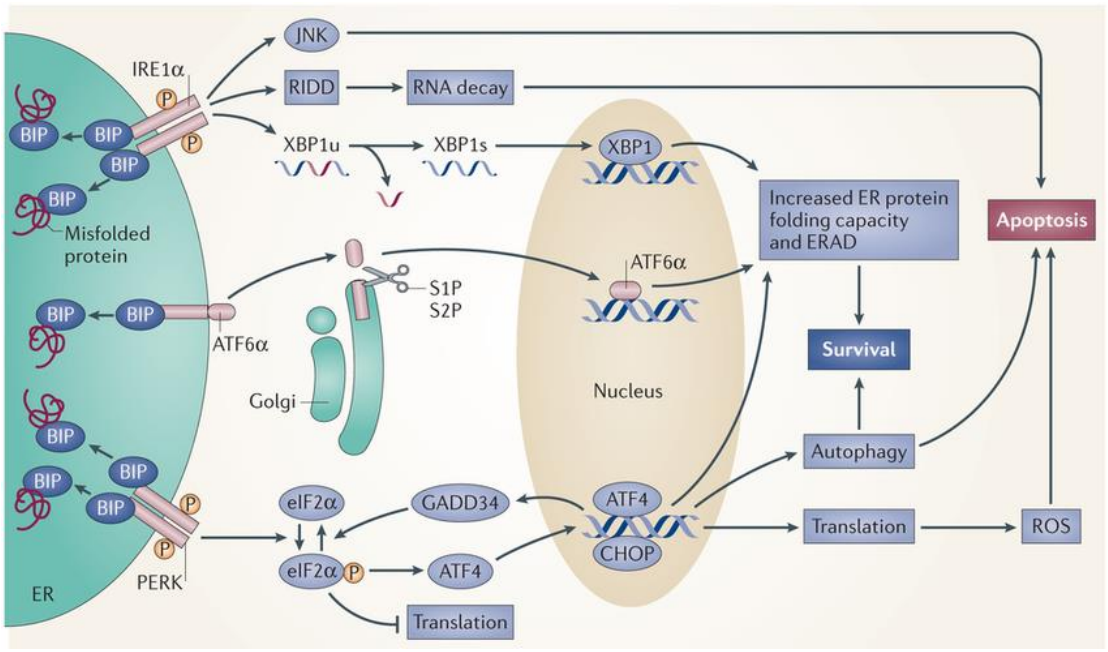


**Figure 5.13: Schematic summary of the Unfolded Protein Response (UPR).** Misfolded proteins in the Endoplasmic Reticulum (ER) as might be caused by defective termination, cause the BiP chaperones to bind to them, triggering three transmembrane signalling cascades. PERK and IRE1α dimerization result in increased eIF2α phosphorylation and splicing of XBP1 to its active form. Meanwhile the transmembrane protein ATF6 translocates to the Golgi where it is cleaved into its activated form by the S1P/S2P proteases. (Figure reproduced from (Wang and Kaufman, 2014)).

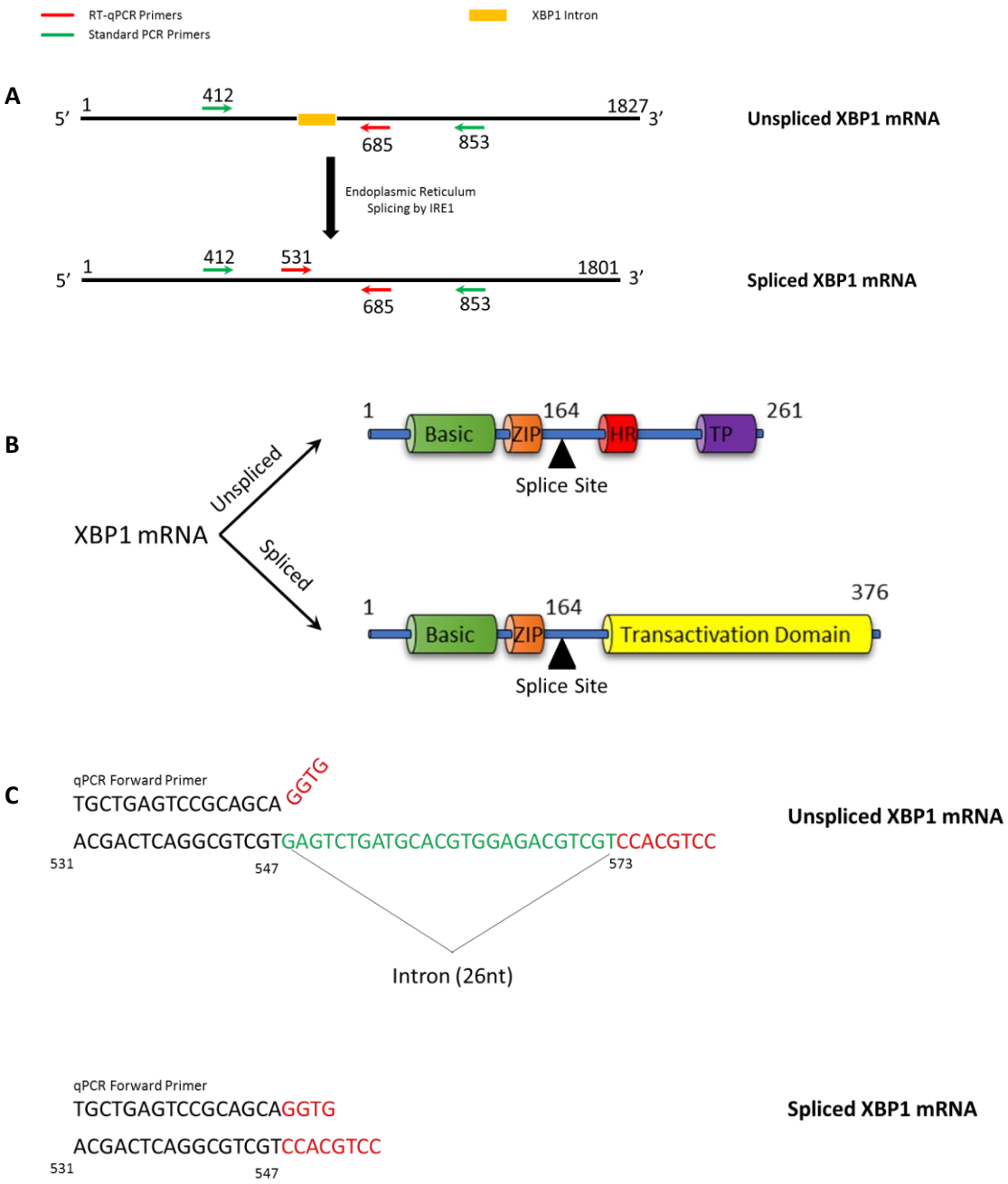


**Figure 5.14: Schematic of XBP1 PCR approach.** Two different approaches for examining the splicing status of XBP1 were utilized, RT-qPCR, and standard PCR followed by gel imaging. A) Positions of the PCR primers used on the XBP1 sequence. The primers for standard PCR will yield two products, one from unspliced XBP1, 441 bp long and one from spliced XBP1 26 bp shorter. Splicing of the intron occurs in the ER by IRE1 under stress conditions. Lengths not to scale. B) ER-Stress mediated splicing of XBP1 results in a frameshift and consequently in a completely different aminoacid sequence post aa 164. The following domains appear: Basic Motif (Basic), Leucine Zipper (ZIP), Hydrophobic Region (HR), Translational Pausing (TP), necessary for pausing of translation and targeting to relevant cell environments, and a Transactivation domain. C) Mechanism of selectivity of the qPCR primers for spliced XBP1. The forward primer contains a sequence (GGTG, highlighted in red) overlapping the splice site, so that amplification can occur only from spliced XBP1 cDNA.

A

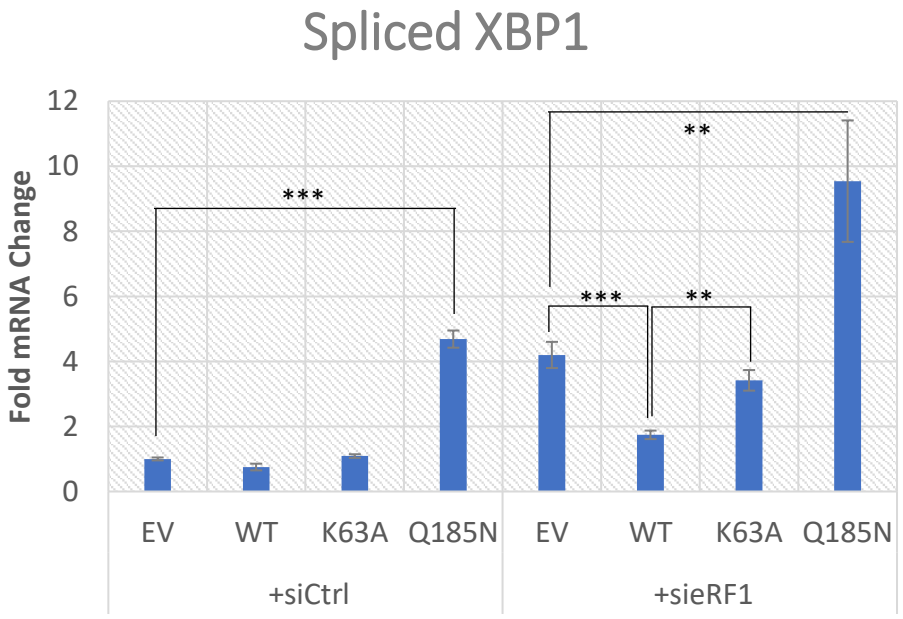


B

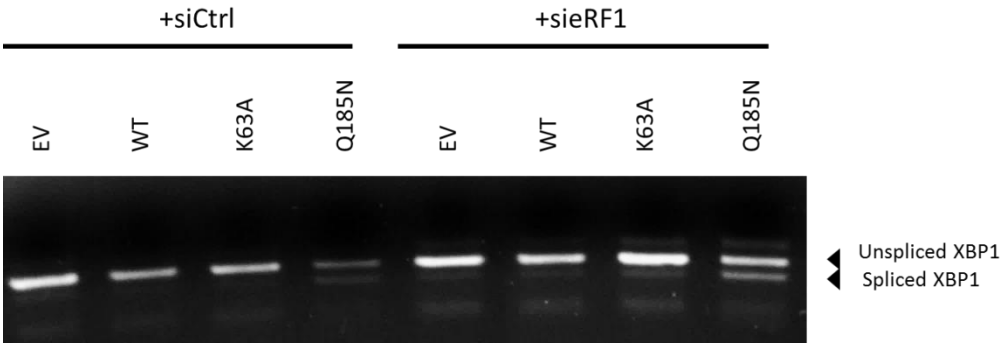


**Figure 5.15: eRF1 depletion induces spliced XBP1 (XBP1s).** EV, WT and K63A were treated with 0.03 µg ml$^{-1}$ and Q185N with 0.5 µg ml$^{-1}$ doxycycline for 48h to induce expression of recombinant eRF1. A) RT-qPCR of XBP1s in the eRF1 rescue cells. The primers used were [Forward: 5′-TGCTGAGTCCGCAGCAGGTG-3′] [Reverse: 5′-GCTGGCAGGCTCTGGGGAAG-3′] n=3, Mean±StDev. ***P<0.001, **P<0.01, *P<0.05. Student's two tailed t-test. B) 3% agarose gel electrophoresis features two bands most prominently in the Q185N cells.

Expression of XBP1s (Figure 5.15A) follows a pattern highly similar to that observed for ATF4 target genes, with the exception of Q185N, which phenocopies that observed for DDIT3 mRNA regulation (Figure 5.6). eRF1 knockdown in control EV cells causes an increase in XBP1s which is suppressed by WT eRF1 re-expression but not the eRF1 K63A mutant. In contrast, re-expression of eRF1 Q185N causes a significant increase in XBP1s levels in both control and eRF1 siRNA treated cells. Visualisation of XBP1 mRNA products by agarose gel electrophoresis further supported this qPCR analysis (Figure 5.15B). Overall, the XBPs analyses would suggest that this arm of the UPR is also activated by eRF1 knockdown, in addition to eIF2α/ATF4, and that re-expression of the Q185N mutant 'super-activates' XBP1s. We postulate that this may, in turn, may play a role in suppressing ATF4 expression and activity (possibly via ATF6).

Taken together, our analysis of eRF1-dependent gene expression control and ATF4 regulation allow us to propose the following model by which eRF1 and its functional sub-domains regulate various branches of the UPR (Figure 5.16). eRF1 knockdown results in activation of both the ATF4 and XBP1s pathways, which is rescued by eRF1 in a K63-dependent manner. In contrast, expression of eRF1 Q185N results in a very significant upregulation of the XBP1s branch of the UPR while resulting in almost complete loss of ATF4 mRNA, protein and activity. Whether ATF6 is also upregulated by eRF1 depletion and Q185N expression is not yet known, but would seem highly likely in light of the results presented here.

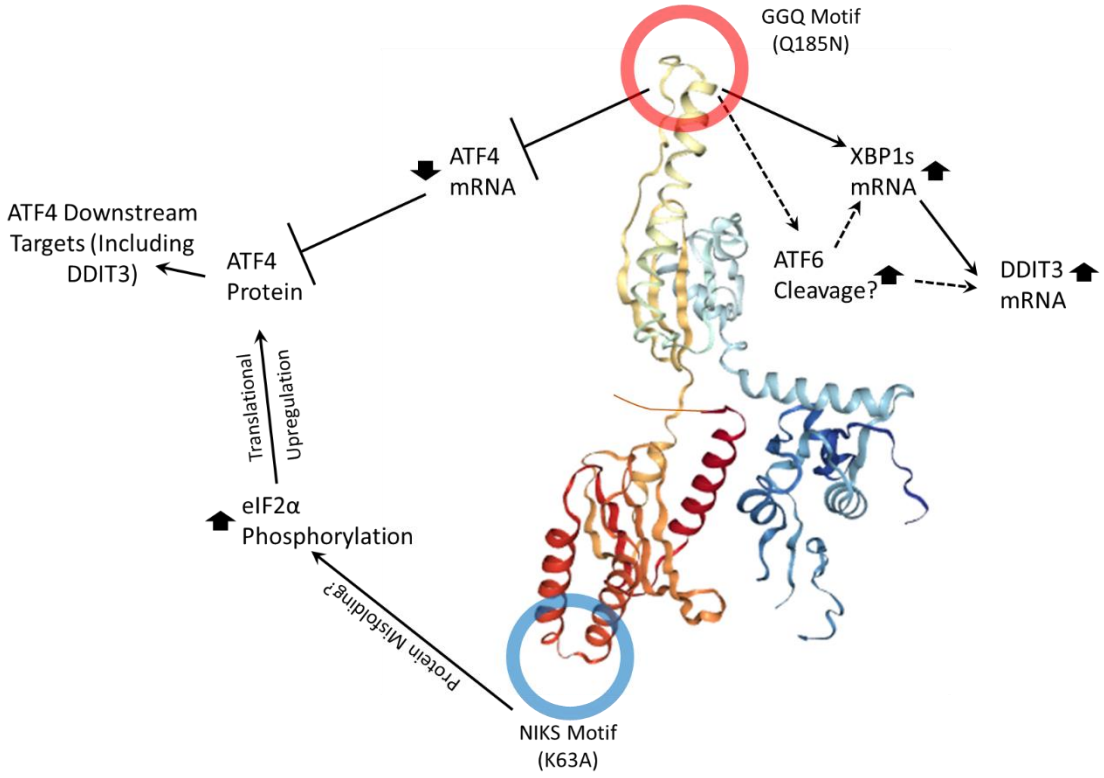


**Figure 5.16: Model of the effect of eRF1 mutations on branches of the Unfolded Protein Response (UPR).** Mutation of K63 to an Ala at the NIKS motif results in an increase in translational readthrough leading to protein misfolding and increased eIF2α phosphorylation. eIF2α phosphorylation results in increased translation at the ATF4 ORF and an increase in ATF4 protein abundance, activating downstream factors such as DDIT3, DDIT4 and TRIB3). Expression of Q185N eRF1 results in a reduction of ATF4 mRNA and consequently of ATF4 protein. Contemporaneously, Q185N eRF1 expression results in stronger upregulation of other components of the UPR, such as spliced XBP1, which results in the upregulation of a number of ATF4 downstream targets such as DDIT3, despite the suppression of ATF4. Though no direct evidence exists of ATF6 cleavage and activation it likely occurs as part of the UPR.

## 5.3 Discussion

*Overview*

In the series of experiments presented in this Chapter, we have further validated the induction of ATF4 following eRF1 knockdown and examined the underlying mechanisms involved. We find that eRF1-dependent regulation of ATF4 expression may be mediated at the level of eIF2α phosphorylation and the uORFs in the ATF4 mRNA 3'UTR. Having also explored the regulation of ATF4 in the eRF1 rescue system, we observed that re-expression of eRF1 Q185N was unique in its control of eRF1-responsive ATF4 target genes, which in turn led to the discovery that eRF1 and its mutants also control other arms of the UPR.

*Validation of eRF1-dependent gene expression using the eRF1 rescue model*

With regard to the gene expression profiles identified by pathway analysis in Chapter 4, we provide further evidence here in this Chapter implicating ATF4 target genes in the response to eRF1 knockdown. qPCRs mRNA analyses of ATF4 downstream target expression generally showed a consistent pattern of regulation characterised by an increase in mRNA in the EV+siERF1 and K63A+sieRF1 samples, and a severe reduction in Q185N eRF1-expressing cells. A strikingly similar pattern of regulation was observed for selected genes with the Selenoaminoacid Metabolism pathway (Figure 5.5): SECISBP2, CTH and CBS all show clear rescue phenotypes, with loss of induction on expression of WT, but not K63A, eRF1. Of these however, only CTH is potentially regulated by ATF4 (Dickhout et al., 2012b)

qPCR analyses of the eRF1 rescue model also appeared to validate the low-level upregulation of multiple Ribosomal Proteins reported in Chapter 4. All four genes

tested were upregulated following eRF1 knockdown, to levels comparable to those seen in the RNA-Seq, and rescued by expression of WT (Figure 5.4). In this case however the response to K63A eRF1 was less clear. Whether the increased abundance of ribosomal protein transcripts observed here leads to increased ribosome biogenesis is not yet known, since unassembled ribosomal proteins have been shown to be targeted for proteasomal degradation (Sung et al., 2016). However, the level of expression of ribosomal proteins can have important implications in growth. For example, two ribosomal proteins, RPL5 and RPL11, are involved in pathways leading to activation of p53, cell cycle arrest and apoptosis (Marechal et al., 1994, Zhang et al., 2003). Rather than a direct signaling role downstream of eRF1 knockdown, the transcriptional response of ribosomal proteins might reflect an indirect adaptive response that primes it for protein synthesis when normal homeostasis is restored.

*Elucidating the mechanism of eRF1-dependent ATF4 regulation*

Using a combination of shRNA and siRNA knockdown models we have shown that eRF1 depletion likely induces eIF2α phosphorylation and ATF4 synthesis, including ATF4 uORF regulation, protein expression and target gene induction. We did not, however, formally demonstrate that increased eIF2α phosphorylation results in ATF4 upregulation at the protein level. Importantly, we show using the eRF1 siRNA rescue model that these phenotypes are 'on-target' and fully suppressed by re-expression of WT eRF1. In contrast, reconstitution with similar levels of an eRF1 NIKS motif mutant, K63A, completely prevented eRF1 from restoring normal eIF2α phosphorylation or ATF4 regulation, thus demonstrating the critical importance of this domain for eRF1 function in cells. Although the importance of the NIKS domain in translational termination is accepted (Brown et al., 2015) (Feng et al., 2014a), those

studies focussed on *in vitro* assays, and its importance in cells, and the physiological consequences of its dysfunction *in vivo*, were not previously explored.

Surprisingly, re-constitution of eRF1 knockdown cells with an siRNA-resistant eRF1 variant with a mutation in the GGQ motif, Q185N, resulted in the complete disappearance of all ATF4 protein and reduced expression of most of the ATF4 target genes analysed. Interestingly, it also led to reduced mRNA expression of other selected eRF1-reponsive genes including CBS, CTH, DDIT4 and TRIB3. Notably however, ATF4 mRNA, largely unaffected in any of the other knockdown and eRF1 mutant combinations, was substantially reduced when the eRF1 Q185N mutant was expressed. Control of ATF4 at the transcriptional level has been indicated before, specifically where ER stress caused by UV irradiation resulted in a reduction in ATF4 mRNA transcription, a well-documented response (Dey et al., 2010, Jiang and Wek, 2005). The reduction in this case was recently shown to proceed via the LIP isoform of the CCAAT/Enhancer-binding Protein β (C/EBPβ), which binds to the ATF4 promoter to suppress its transcription (Dey et al., 2012). However, it is not known whether a similar mechanism is at work during Q185N eRF1 expression.

Surprisingly, Q185N eRF1 expression was also sufficient to *induce* of a sub-set of eRF1 responsive genes, including DDIT3, and integrin α4, even in the absence of eRF1 knockdown (despite this mutant being shown in Chapter 3 to be completely inactive with respect to stop codon readthrough). Potential explanations for this phenomenon, and a detailed discussion of the activation of different arms of the UPR by dysfunction of specific eRF1 sub-domains, are provided in the Final Discussion, Chapter 6.

Overall, we have shown that upregulation of ATF4 and its downstream targets occur via eIF2α phosphorylation in response to depletion of eRF1. This pathway induction is supplemented by at least another branch of the UPR and may be a signal of general UPR induction. eRF1 depletion has been validated to also likely results in upregulation of genes associated with selenocysteine incorporation into proteins, along with potentially ribosomal proteins and at least some ECM, adhesion and motility associated proteins. While they might participate in the reduction of cell proliferation observed during eRF1 depletion, these pathways cannot be exclusively responsible for it, due to differences in the anticipated cell cycle arrest profile. Further research is consequently necessary in order to determine the exact mechanism of proliferation control by defective translational termination, as discussed in the next chapter.

# CHAPTER 6: Discussion and Future Work

## 6.1 Overview

Prior research on JMJD4 identified it as a lysyl hydroxylase with a role in promoting translational termination through hydroxylation of eRF1. However, at this point there had been limited investigation of the physiological roles and potential involvement in pathologies (including cancer) of JMJD4, or indeed other translational termination factors, including eRF1. In this Thesis, we have begun to address this knowledge gap. In Chapter 2, we probed for potentially novel JMJD4 functions by investigating other candidate substrates and binding partners. In Chapter 3, we find that JMJD4, HEMK2 and eRF1 are essential for efficient translational termination and for the growth of cancer cell lines. In Chapter 4, the transcriptional response to defective translational termination was examined and major pathways validated. Finally, in Chapter 5, the most robustly regulated of these pathways, the induction of downstream targets of ATF4, is examined in greater detail and the mechanism of ATF4 regulation explored.

## 6.2 Defective Translational Termination in Growth and Cancer

Here in this Thesis we demonstrate that changes in the abundance of factors essential to translational termination result in concomitant changes in cell growth. Depletion of eRF1 results in almost complete cytostasis, while JMJD4 or HEMK2 knockdown also significantly reduce proliferative capacity (Chapter 3). Whether the effects of JMJD4 and HEMK2 on growth are explained by their modification of eRF1, as opposed to other potential substrates, was not formally proven however. Circumstantial evidence supporting an eRF1-dependent role of JMJD4 in growth includes the similar cell cycle phenotype induced by JMJD4 and eRF1 knockdown (Figure 3.14).

These data are in contrast to those obtained in previous mice studies (Yoo et al., 2016b), where knockout of JMJD4 was not found to result in growth retardation and JMJD4 -/- homozygous mice appeared physiologically typical. However, our research was performed on human cancer cell lines, rather than murine cell cultures or live animals. This implies that a number of different factors may be at play regarding the disparity in observations. Initially, it is possible that JMJD4 plays a more important role in humans compared to mice. While human and murine JMJD4 are highly similar as highlighted in chapter 2, it is possible that the regulatory network surrounding them and the importance of the eRF1 K63 hydroxylation to translational termination differs between mice and humans. Furthermore, it is possible that JMJD4 mediated hydroxylation of eRF1 only acquires an important role in growth in a cancer context. Indeed, all the work presented in this thesis was performed in cancer cell lines, which might explain the observed difference. Certainly, JMJD4 levels can significantly affect outcome in at least some cancers based on bioinformatic analysis as discussed in section 3.2.1. It should be noted here that the Yoo et al, 2016 study only measured JMJD4 knockdown at the transcript level. JMJD4 protein levels, the level of translational readthrough caused by the absence of JMJD4, as well as the level of eRF1 hydroxylation in the cell were not examined and therefore the effective level of JMJD4 activity in the mice is not known.

It is also unclear whether JMJD4 targets any substrate other than eRF1: Our investigation of GTF2I in Chapter 2 suggests that other potential activity-dependent interactors identified in the original JMJD4 proteomic screen are unlikely to be true substrates. Nevertheless, it is important to highlight that other JMJD4 substrates might exist: Expanding the range of conditions in which the substrate proteomics was performed (e.g. different lysis buffers) could yield different results. That being said,

we currently have no evidence that JMJD4 has more than one substrate. Indeed, this possibility would not be without precedent, as other hydroxylases involved in translation generally have only one reported substrate (e.g. NO66), as discussed in the Introduction. It is therefore possible that the results presented here are consistent with a unified role for termination factors in growth control, and possibly cancer: Using publicly available cancer databases we observed that the expression of translational termination factors are generally upregulated in tumours, and that this may be associated with poor patient prognosis in some cases. These observations would be in agreement with extensive work performed in recent years highlighting the important role of translation initiation and elongation factors in tumourigenesis, and the potential for treatments targeting translation in cancer (Bhat et al., 2015, Pelletier et al., 2015). Indeed, it is perhaps unsurprising that termination factors must be upregulated in unison with other steps of protein synthesis pathway in order to maintain sequence fidelity in the context of higher protein synthesis rates. In light of the findings presented in this thesis it may be worthwhile to now consider translational termination as a new target for cancer therapy.

Therapeutic targeting of translational termination could be achieved by developing inhibitors of enzymatic termination factors, such as JMJD4 and/or HEMK2. The suitability of JMJD4 and HEMK2 as medically relevant targets is difficult to assess however, partly due to the small amount of work yet performed. Previous evidence indicates that JMJD4 knockout in normal mouse tissues results in no major phenotype (Yoo et al., 2016a). This, together with our observations that JMJD4 is required for cancer cell line proliferation, might cast it as a potential anti-cancer target with a favourable therapeutic window.

Due to their status as emerging targets for the treatment of a variety of important diseases, 2OG-oxygenases, such as JMJD4, have been the subject of significant medicinal chemistry and translational research. Generic inhibitors of 2OG-oxygenases such as N-oxalylglycine (NOG) and Dimethyloxalylglycine (DMOG) are widely known and were utilised in Chapter 2 to stabilise potential enzyme:substrate complexes. These function as competitive inhibitors by mimicking the structure of 2OG and thus compete with it for the enzyme active site (Rose et al., 2011). Indeed, most 2OG-oxygenase inhibitors under development tend to be competitive inhibitors of 2OG (Rose et al., 2011). For example, *oxalyl* amino acids and other mimics of 2OG such as 2-thioglutarate can function as inhibitors of the HIF prolyl hydroxylases PHD1-3 (Rose et al., 2011). The glycinamide class of compounds has also been shown to bind and inhibit HIF prolyl hydroxylases, with crystal structures of isoquinolinyl glycinamide compounds bound to PHD2 (McDonough et al., 2006) (Yan et al., 2010, Rose et al., 2011). Another class of compounds, the 8-hydroxyquinolines, have been identified in high throughput approaches aimed at identifying inhibitors of histone lysine demethylases (King et al., 2010, Rose et al., 2011). Finally, members of the lysine demethylase family KDM4, contain structural $Zn^{2+}$ ions in their catalytic domains whose removal leads to their permanent inactivation (Labbe et al., 2013), opening the possibility of additional classes of 2OG-oxygenase inhibitors (Sekirnik et al., 2009).

It is perhaps less clear whether HEMK2 has potential as a novel therapeutic target. For example, a recent study suggests that HEMK2 could methylate a range of targets (Kusevic et al., 2016), possibly increasing the potential for off target effects. However, this study relied on candidate peptides tested *in vitro* using recombinant HEMK2 protein, and without subsequent mass spectrometry validation *in vivo*.

Targeting the obligate binding partner of HEMK2, Trm112, would also be a suboptimal approach, as it lacks enzymatic activity, is widely involved in translation, and its depletion is associated with substantial toxicity (Bourgeois et al., 2017).

Therapies targeting translational termination could have advantages in addition to reducing growth potential, by potentially restoring the expression of prematurely terminating (nonsense mutated) tumour suppressor genes. It is known that nonsense mutations result in premature termination of tumour suppressor genes in cancer, and it has been proposed that it may be possible to restore their expression by promoting stop codon readthrough (Bordeira-Carrico et al., 2012, Floquet et al., 2011). This approach could involve JMJD4/HEMK2 inhibitors as discussed above, possibly in combination with established chemical inducers of stop codon readthrough, such as aminoglycoside antibiotics. Aminoglycoside compounds were originally developed as therapeutic agents against gram negative bacteria, capable of binding, often irreversibly, to the ribosome and disrupting translation. The mechanisms of translational disruption differ among specific compounds but generally affect the elongation step (Mingeot-Leclercq et al., 1999), functioning by impairing translational proofreading, resulting in widespread mis-incorporation of near cognate residues, including at stop codons (Fan-Minogue and Bedwell, 2008). Though normally selective for the prokaryotic ribosome, hence their use as antibiotics, certain modified aminoglycoside compounds, such as G418 (Geneticin) and Gentamicin, can also bind to eukaryotic ribosomes (Eustice and Wilhelm, 1984). Such compounds have already been used to partially restore expression of a prematurely terminating protein in mouse models of Proximal spinal muscular atrophy (Heier and DiDonato, 2009). With respect to cancer, aminoglycosides have been used to bypass nonsense mutations in the Adenomatous Polyposis Coli tumour suppressor (Floquet et al.,

2011). However, the efficacy of aminoglycoside treatment can vary greatly (Bidou et al., 2004) and more importantly they tend to be poorly tolerated (Turnidge, 2003), possibly because of the pleiotropic effects on translation. JMJD4 or HEMK2 inhibitors could be considered as more targeted approaches to target translational termination in cancer. Nevertheless, it should be noted that at least with respect to restoration of nonsense mutated disease genes, the efficacy of targeting JMJD4 might depend on the sequence content of the nonsense mutation in question, as readthrough mediated by JMJD4 knockdown appeared dependent on the termination context in Chapter 3. Additionally, whether combining JMJD4 or HEMK2 inhibitors with aminoglycoside antibiotics could enable the dose of the latter to be lowered to more acceptable (non-toxic) levels, is of interest.

### 6.3 The cellular response to defective translational termination

The effective medicinal translation of targeting translational termination would benefit from a greater understanding of the potential cellular responses to such treatment strategies. Indeed, we showed in Chapter 3 that eRF1, JMJD4 or HEMK2 knockdown all cause a significant growth inhibition, but via an unknown mechanism. Therefore, we used gene expression profiling by RNAseq as a means to begin profiling, in an unbiased and genome-wide manner, the cellular response to defective translational termination. Although our analyses identified transcriptional regulation of several cellular processes following eRF1 knockdown, the ATF4 pathway was the most consistently and highly upregulated.

The targets of ATF4 tested in our conditional siRNA-resistant eRF1 reconstitution system included DDIT3, DDIT4 and TRIB3, all of which are known to participate in cellular stress response mechanisms. DDIT3 (DNA-Damage Induced Transcript 3,

also known as CHOP), is a multifunctional transcription factor with roles in cell survival and apoptosis. Normally expressed at low levels but induced by endoplasmic reticulum stress (Ron and Habener, 1992) (Wang et al., 1996), DDIT3 binds to members of the C/EBP family in a dominant negative manner, thereby inhibiting their activity (Jauhiainen et al., 2012). DDIT3 also associates with ATF4 and reduces the efficacy of transcriptional induction of some of its target genes (Su and Kilberg, 2008). Increased DDIT3 expression has also been associated with increased apoptosis (Yamaguchi and Wang, 2004). DDIT4 (also known as REDD1) is another member of the same transcription factor family as DDIT3, but has important roles in the regulation of mTORC1 signaling (Brugarolas et al., 2004). Induction of DDIT4 has been mostly described in the context of energy stress and hypoxia, where it was found to be an important controller of cell size as a result of its effects on mTORC1 (Sofer et al., 2005). TRIB3 is a member of the Tribbles family of pseudokinases which have no detectable catalytic activity, but rather appear to be involved in transcription factor regulation (Eyers et al., 2017). Interestingly, the TRIB3 promoter has binding sites for both DDIT3 and ATF4 and knockdown of either of these results in drastic reduction of TRIB3 expression *in vitro* (Ohoka et al., 2005). This is in agreement with our data, where TRIB3 mRNA failed to be induced in Q185N eRF1 expressing cells, despite the induction of DDIT3, perhaps due to the loss of ATF4 expression (Figures 4.6&4.7). Interestingly, TRIB3 also downregulates the transcriptional activity of both ATF4 and CHOP, thereby creating a negative feedback loop, similar to ATF4/DDIT3 (Jousse et al., 2007). TRIB3 is also reported to have a pro-apoptotic role, and its knockdown increases resistance to tunicamycin (Ohoka et al., 2005). Finally, Asparagine Synthetase (ASNS), which was upregulated following shRNA

knockdown of eRF1 and induction of ATF4 (Figure 5.9B), is required for normal cell growth and its knockdown results in S-phase cell cycle arrest (Yang et al., 2014).

As outlined above, the upregulated ATF4 target genes characterised in response to eRF1 knockdown are generally implicated in cell growth and survival, and may therefore contribute to the observed decreased in cell proliferation observed under such conditions. It would seem that the ATF4 response is unlikely to entirely explain the growth response to defective translational termination however, as the associated cell cycle profile was not restricted to a single phase: The unfolded protein response, eIF2α phosphorylation, and ATF4 upregulation, generally cause a $G_1$ cell cycle arrest (Brewer and Diehl, 2000, Hamanaka et al., 2005). Therefore, in addition to the ATF4 pathway, other additional mechanisms are also likely to contribute to the cellular adaptive response to defective translational termination.

### 6.4 eRF1-dependent ATF4 regulation

In Chapter 5 we showed that eRF1 controls ATF4 protein synthesis via eIF2α phosphorylation. This is in contrast to the eRF1-associated termination factor eRF3a, the knockdown of which is reported to increase ATF4 expression through an increase in stop codon readthrough of an ATF4 mRNA uORF (Ait Ghezala et al., 2012b). While our GADD34 overexpression data indicate that inhibiting eIF2α phosphorylation is sufficient to prevent ATF4 translational expression in response to eRF1 knockdown, we did not directly test whether stop codon readthrough of the uORFs occurred and whether it contributed to ATF4 protein synthesis. Overall however, our results probably suggest that the major mechanism of eRF1-dependent ATF4 regulation is likely to proceed via activation of the UPR. In the future it could be possible to determine whether eRF1 knockdown stimulates stop codon readthrough

of the ATF4 mRNA uORFs using a technique known as Ribosomal Footprinting. In this approach, mRNA bound to translating ribosomes is treated with nucleases in the presence of translation inhibitors or translation-incompetent lysis conditions, causing the degradation of the parts of the mRNA sequence not protected by the ribosome (the ribosomal "footprint"). The free mRNA fragments are subsequently purified and reverse transcribed. Their sequence is then deduced in a manner quite similar to RNA-Seq, providing a snapshot of the total population of translating ribosomes within the cells and their position on the mRNAs (Ingolia et al., 2009). The appearance of a ribosomal population between the ATF4 uORF1 and uORF2 could therefore indicate that stop codon readthrough of uORF1 had occurred following eRF1 knockdown

It remains possible that eRF3a depletion also induces ATF4, at least partly, via activation of the UPR and eIF2α phosphorylation. Importantly, the dependence of the eRF3a phenotype on eIF2α phosphorylation was not formally tested (e.g. by GADD34 overexpression, as in Chapter 5) (Ait Ghezala et al., 2012b). Rather the absence of an increase in eIF2α phosphorylation at three time points was noted. It is possible that eRF3a depletion induces transient activation of eIF2α phosphorylation and ATF4 expression, which is sufficient to induce ATF4 target gene expression. However, other differences in the response to eRF3a depletion could be consistent with alternative stress signaling downstream of these two termination factors. For example, eRF3a knockdown is associated with a $G_1$ cell cycle arrest, as opposed to eRF1 knockdown where a single checkpoint appeared not to be activated (Chauvin et al., 2007). As discussed in Chapter 3, a similar cell cycle response to eRF1 and JMJD4 knockdown has been reported following RPL5 and RPL11 depletion, which was found to proceed by reduced global translation preventing the accumulation of Cyclins (Teng et al., 2013). Whether the similar growth arrest phenotype of eRF1 and

JMJD4 knockdown cells is due to reduced global protein synthesis is not yet known, but of interest. There is some evidence to support a reduction in protein synthesis following eRF1 depletion: Previous polysome analyses (Feng *et al*, 2014, PhD Thesis) indicated that eRF1 knockdown results in a translation phenotype, with an increase in the abundance of free 60S and 40S subunits, and a simultaneous reduction in translating polysomes (data not shown). Additionally, during our stop codon readthrough experiments, the expression of both luciferases, including the constitutively expressed *Renilla*, were consistently much lower in eRF1 or JMJD4 knockdown samples (data not shown), potentially consistent with reduced global protein synthesis rates.

Our cell models have relied on RNA interference as a loss-of-function approached to study the cellular consequences of defective translational termination. However, an important question that then arises is whether changes in eRF1 expression, or modulation of the release factor activity of eRF1, might also occur physiologically. Interestingly, we observed that only a very modest increase in eRF1 levels, such as in the induction of WT eRF1 in control siRNA samples, was sufficient to suppress basal ATF4 translational expression and ATF4 protein synthesis (Chapter 5, Figure 5.8B). This might potentially indicate that translational termination efficiency is poised to regulate the UPR under physiological conditions, potentially making eRF1 availability and/or activity a major determinant of ATF4 expression. However, there are few examples of mechanisms that regulate eRF1 function. Phosphorylation of eRF1 has been reported in *S. cerevisiae,* but it does not appear to affect the efficiency of translational termination or disrupt binding to the ribosome (Kallmeyer et al., 2006). Furthermore, eRF1 expression levels appear to be fairly constant and ubiquitous in healthy cells, and are normally invariant throughout the cell cycle, as is

the case with eRF3a (Chauvin et al., 2007). Thus far, the only reports of functional control of eRF1 activity are by JMJD4 and HEMK2. In the future it will be necessary to determine whether depletion of these termination factors phenocopies eRF1 knockdown, particularly with respect to the regulation of ATF4 expression and activity. Some evidence supporting this possibility is provided by the discovery that K63A and Q185N eRF1 mutants completely fail to restore normal eRF1 translational termination activity and ATF4 regulation.

An initial step in the direction of future research would be to examine whether knockdown of JMJD4 or HEMK2 replicates the transcriptional phenotype observed in the RNA-Seq, ideally by performing additional RNA-Seq experiments. Assuming that the common set of upregulated genes shared by eRF1 and eRF3a knockdown is indeed due to an increase in translational readthrough, JMJD4 and potentially HEMK2 knockdown should result in a broadly similar response. Any affected pathways not shared with those identified by eRF1 knockdown could therefore be unique to JMJD4 and HEMK2 and independent from their activity as eRF1 modifiers. Even in the absence of additional RNA-Seq experiments, the validated set of eRF1 knockdown downstream genes can be tested in the JMJD4 and HEMK2 knockdown cells to illuminate whether JMJD4/HEMK2 and eRF1 knockdown share downstream targets. Additionally, measuring the level of ATF4 translational expression *via* the system described in 5.2.2 using the pGL3 ATF4 uORF plasmid, accompanied by RT-qPCR of ATF4 mRNA, should indicate whether knockdown of JMJD4 or HEMK2 phenocopy eRF1 knockdown in resulting in an increase in translational but not transcriptional expression of ATF4. These results can then be validated using the anti-JMJD4 antibody already in place to directly assess ATF4 protein levels. Finally, epistatic experiments to determine which phenotypes supersede each other would be

useful in determining whether the ATF4 response is contingent to eRF1 or its post-translational modifications. This could be performed by, for instance, combined JMJD4/eRF1 knockdown or HEMK2/eRF1 knockdown and assessing the resultant growth, readthrough, transcriptional and ATF4 expression phenotypes.

### 6.5 The cellular response to eRF1 Q185N

As discussed, we employed a 'structure-function' approach to investigate the role of critical sub-domains or eRF1 targeted by JMJD4 and HEMK2 by introducing missense mutations known to inhibit their function (and prevent their post-translational modification). Whereas the K63A NIKS mutant eRF1 variant behaved as expected, being inactive with respect to translational termination, and unable to restore normal growth and ATF4 regulation following endogenous eRF1 knockdown, the Q185N GGQ eRF1 variant produced a variety of unexpected effects. We find that expression of Q185N eRF1 fails to rescue stop codon readthrough resulting from eRF1 knockdown, as expected, but has a dominant negative phenotype with respect to growth (Chapter 3). Interestingly, modifications to the convergently evolved GGQ motif on bacterial RF1 and RF2 to are also associated with significant reduction in growth (Mora et al., 2003).

Interestingly, human Q185N eRF1 expression completely suppressed ATF4 protein expression, despite the level of ATF4 translational expression (as indicated by the uORF reporter) being induced similarly to EV and K63A eRF1 expressing cells (Chapter 5). This disparity appears to be due to a significant reduction in ATF4 mRNA levels, by an unknown mechanism. It is unlikely however that this mechanism operates exclusively through a general increase in stop codon readthrough, as it would

then be expected to phenocopy the EV and K63A eRF1 results. We considered two other explanations which might account for it however. Firstly, it may be possible for Q185N to affect termination of stop codons in specific contexts, resulting in signaling independent of the broader stop codon readthrough response. Alternatively, it is possible that Q185N results in the ribosome stalling at the stop codon. The latter mechanism would be supported by the use of eRF1 GGQ mutants (e.g. eRF1$^{AAQ}$) to capture the translating complex at the termination step for structural studies (Brown et al., 2015).

### 6.6 Regulation of the Unfolded Protein Response by eRF1 depletion

Through our work on the eRF1 Q185N variant, evidence accumulated to suggest a more widespread response of the UPR to defective termination. Specifically, it appeared that induction of eRF1 Q185N was associated with an increase in other transcription factors, notably spliced XBP1. Interestingly, the regulation of XBP1s by eRF1 depletion and Q185N expression correlated with the unusual regulation of a sub-set of eRF1-responsive genes, including DDIT3. ATF4 and XBP1s form two of the three major signaling arms of the UPR, in addition to ATF6. While we were not able to also investigate potential regulation of ATF6 by eRF1, due to a lack of reagents, it would seem likely ATF6 is also activated, as all three arms of the UPR share the same upstream signaling mechanism via the chaperone BiP (Wang and Kaufman, 2014).

The question then arises as to how eRF1 depletion and Q185N expression activate the various arms of the UPR. Defective termination might result in the accumulation of misfolded proteins in the ER due to stop codon readthrough producing proteins with extended and disordered C-termini. Misfolded proteins would in turn be bound by BiP

chaperones and sequester them, resulting in the upregulation of IRE1α and PERK activity, splicing XBP1 mRNA to its active isoform and phosphorylating eIF2α at Ser51, respectively (Figure 5.13) (Somers et al., 2013). Testing this hypothesis would involve assaying the extent of protein misfolding in the ER, for which several techniques exist, primarily through Green Fluorescent Protein (GFP) tags attached to constitutively expressed indicator proteins (Waldo et al., 1999) or enzymatic indicators e.g. chloramphenicol acetyltransferase (Maxwell et al., 1999). Furthermore, assays for the determination of PERK and IRE1 activity are well known (Yan et al., 2002, Hikiji et al., 2015) and could be easily performed to test this hypothesis.

Overall, the UPR appears to be at least one major adaptive response that cells mount in the face of defective translational termination. The UPR is likely contributing to adaptation and survival of the cells (Harding et al., 2000b) and is known to affect cellular proliferation and differentiation (Tsang et al., 2010), in addition to varied pro-proliferative roles in tumorigenesis (Zanetti et al., 2016). It is plausible to consider that cells treated with inhibitors targeting translational termination could become 'addicted' to activation of the UPR, potentially creating an opportunity for combined therapies.

## 6.7 Conclusions

The work presented in this Thesis has highlighted a potential role for translational termination as an important factor affecting cell growth and stress, and that it has potential as a novel target for cancer therapy. Future efforts are necessary to better understand the mechanism by which JMJD4, HEMK2 and eRF1 knockdown cause reduced cell growth, particularly exploring the impact of global protein synthesis

inhibition. Finally, future work should also aim to understand the molecular mechanism(s) by which defective translation termination signals to the UPR, and how inhibiting the function of eRF1 in peptidyl-tRNA hydrolysis (e.g. by Q185N mutation) leads to the unique regulation of eRF1-responsive genes and XBP1 splicing.

# CHAPTER 7: Materials and Methods

## 7.1 Reagents

Where not specified, reagents were purchased from Sigma-Aldrich. Common laboratory solvents (e.g. ethanol, methanol) were purchased from Thermo-Fisher-Scientific.

### 7.1.1 Solutions

**Phosphate Buffered Saline (PBS; 10X):** 1.37 M NaCl, 27 mM KCl, 43 mM $Na_2HPO_4$, 14 mM $KH_2PO_4$, pH adjusted to 7.4. 1X PBS was prepared by diluting 10X concentrated stock with ultrapurified water. 1X PBS-Tween (PBST) was prepared by adding 0.1 % Tween-20 (v/v) to 1X PBS.

**Tris-Borate-EDTA (TBE) Buffer:** 1X TBE running buffer was prepared by diluting 10X TBE concentrated stock with ultrapurified water to a final concentration of 89 mM Tris-borate and 2 mM EDTA, pH 8.3.

**SDS-PAGE Resolving Gel Buffer (4X):** 1.5 M Tris-HCl pH 8.8, 0.4 % (w/v) SDS.

**SDS-PAGE Stacking Gel Buffer (4X):** 0.5 M Tris-HCl pH 6.8, 0.4 % (w/v) SDS.

**Laemmli SDS-PAGE loading buffer (6X):** 350 mM Tris-HCl pH 6.8, 10 % (w/v) SDS, 50 % (v/v) glycerol, 0.6 M dithiothreitol (DTT), 0.1 % (w/v) bromophenol blue.

**JIES Lysis Buffer:** 20 mM Tris-HCl pH 7.4, 100 mM NaCl, 5 mM MgCl2, 0.5 % (v/v) NP-40. Protease inhibitor (Sigma-Aldrich) and phosphatase inhibitor (Roche) cocktails were added immediately prior to cell lysis.

**RIPA Lysis buffer:** 150 mM NaCl , 5 mM EDTA, 50 mM Tris, 1 % (v/v) NP-40, 0.5 % (v/v) Sodium Deoxycholate, 0.1 % (v/v) SDS.

**Passive Lysis Buffer (PLB):** 1X passive lysis buffer was prepared from 5X Passive Lysis Buffer (Promega, from Dual Luciferase Kit, Cat. # E1910) diluted with 4 volumes ultrapurified water.

**3-(4,5-dimethyl-2-yl)-5-(3-carboxymethoxyphenyl)-2-(4-sulfophenyl)-2H-tetrazolium, inner salt (MTS) solution:** In a dark environment, 42 mg of CellTiter 96® AQueous MTS reagent powder (Promega) were dissolved in 21 ml of Dulbecco's PBS and the pH adjusted to 6-6.5. Subsequently, it was filtered through a 0.2µm pore opening filter, aliquoted and stored at -20°C in an opaque container.

**Phenazine methosulfate (PMS) solution**: In a dark environment, 9.2 mg of PMS was dissolved in 10 ml of Dulbecco's PBS and vortexed until fully dissolved. The solution was subsequently filtered through a 0.2 µm pore opening filter, aliquoted and stored at -20°C in an opaque container.

## 7.2 Bacterial Techniques

### 7.2.1 Media and Reagents

**Luria-Bertani media:** Luria-Bertani (LB) media were prepared by diluting LB granules (Invitrogen, Cat.# 12780029) 1:50 w/v in ultrapure water, followed by autoclaving at 121 °C, 100 kPa. LB agar plates were prepared by addition of $15:10^3$ agar powder, followed by autoclaving as above. For antibiotic addition, the agar was melted, mixed and antibiotics added at ~50 °C.

**SOC Media**: SOC (Super Optimal Broth + 20 mM Glucose) media was purchased from New England Biolabs (NEB) (Cat.# B9020S).

**Ampicillin:** For selection purposes 100 μg $ml^{-1}$ Ampicillin was added to LB and LB agar were appropriate.

**Bacterial Strains:** All bacteria used were NEB® 5-alpha Competent E. coli (High Efficiency) (Cat.# C2987I)

### 7.2.2 Transformation

Competent *E. coli* were thawed on ice and ligation mix was diluted in bacteria at a ratio of 1:10, or 50-100 μg of plasmid DNA were added. The tube was flicked to ensure even mixing, followed by a 30 minute on-ice incubation. Subsequently, the bacteria were heat shocked at 42 °C for 30 sec, followed by an additional 5 min recovery on ice. The bacteria were then added to 450 μl SOC media and incubated at 37 °C for 1 hour. Cultures intended for plasmid extraction were then added to an appropriate volume of LB and incubated overnight in a shaking incubator at 220 rpm, 37 °C. Cultures intended for LB plating were centrifuged at 3000 rpm until a pellet formed. The supernatant was removed and the bacteria resuspended in 50 μL LB and spread onto an agar plate. Incubation occurred for 12-16 hours h at 37 °C or until colonies were visible.

### 7.2.3 Plasmid DNA Isolation and Purification

Small scale plasmid preparation (Miniprep) was performed using a GenElute™ Plasmid Miniprep Kit (Sigma, Cat.#PLN70) following manufacturer's instructions. Briefly, bacterial cultures were centrifuged, subjected to alkaline lysis and then precipitated. The DNA in the supernatant was bound in a silica binding column, washed and then extracted using ultrapure water or the kit's own extraction buffer, dependent on downstream applications. Large scale preparations were performed

using a GeneJet Plasmid Maxiprep kit (ThermoFisher Scientific, Cat.# K0491), the process being broadly similar to the above.

## 7.3 Nucleic Acid Techniques

### 7.3.1 DNA/RNA Quantification

DNA and RNA quantification was performed using a NanoDrop (ThermoFisher Scientific) tabletop Microvolume Spectrophotometers and Fluorometer using a 1 µl volume of liquid. Quality of DNA was considered acceptable when A260/A280 ratio was ≥1.8 and the RNA A260/A280 ratio ≥2.0

### 7.3.2 Polymerase Chain Reaction (PCR)

PCR mixes were prepared in 25/50 µL reaction volume containing 0.5 µM primers and Phusion High-Fidelity PCR Master Mix with HF Buffer (NEB, Cat.# F531S) at half of the total reaction volume. DNA amplification was performed using a T100 Thermal Cycler (BioRad). Cycling conditions had to be adjusted for individual products but were typically [Initial denaturation temp: 98 (30sec), then 35 cycles of: [Denature 98 °C (10 s), Annealing 58 °C (10 s), Extension time 72 °C (15-30 s/1kbp of amplified DNA)] with Final extension 72 °C (10 min) x35 cycles.

### 7.3.3 Site Directed Mutagenesis (SDM)

SDM was performed through the use of specific primers designed to contain mismatches coding for the intended amino acid, with the PCR protocol as above. Following amplification samples were treated with *DpnI* for 1 hour at 37 °C.

### 7.3.4 Plasmid Engineering

Restriction digest was performed on 500-1000 ng of plasmid using High Fidelity Restriction Endonucleases (NEB) at manufacturer recommended amounts in the presence of 1x High Fidelity Restriction Buffer (NEB), at 37 °C, for 30 min-1 h. The plasmid DNA was further treated with Calf Intestinal Phosphatase (10-20 U) at 37 °C for 1 h in order to dephosphorylate plasmid ends and prevent reannealing during subsequent ligation. Ligation of the plasmid was achieved using T4 DNA ligase (NEB, Cat.# M0202S) for 10 min at 16°C, followed by a denaturation of the ligase enzyme at 65°C for 10 minutes, at insert:plasmid molar ratios of 3:1, 6:1 and 9:1.

### 7.3.5 DNA Sequencing

All plasmid DNA sequencing was performed by Eurofins Genomic Services using plasmid specific primers.

### 7.3.6 RNA extraction and cDNA Synthesis

RNA extraction was performed using the GenElute Mammalian Total RNA Miniprep Kit (Sigma-Aldrich, Cat.#TRN70). Briefly, cells were lysed in a solution containing guanidine isothiocyanate and 2-mercaptoethanol, inactivating RNAses. Subsequently, cellular debris and DNA shearing occurs via column centrifugation and RNA in the eluate bound to a silica column, followed by washes and elution with a low salt buffer and quantified as described in 7.3.1.

cDNA synthesis took place with the use of the High Capacity cDNA Reverse Transcription kit (Applied Biosystems, Cat.# 4368814). A typical reaction contained 1 μg RNA template, 2 μl 10X Reverse Transcription buffer, 4 mM dNTPs, 2 μl 10X random primers, 50 U MultiScribe Reverse Transcriptase, 20 U RNAse inhibitor, topped to 20 μl with nuclease-Free water. The PCR machine used was a T100

Thermal Cycler (BioRad) set to the following program: 25 °C (10 min), 37 °C (120 min), 85 °C (5 min).

### 7.3.7 Real-Time Quantitative PCR (RT-qPCR)

In order to quantify transcript abundance in the cells, RT-qPCR was performed using custom primers and SYBR Green. For each gene to be examined, a search was performed on Primer-BLAST (National Centre for Biotechnology Information) using the following criteria: PCR product size 90-150 nt, Tm 60 °C, spans an intron-exon junction. Amplification efficiency for each primer set was calculated by performing RT-qPCR using the primers across four orders of magnitude of substrate (cDNA) concentration, 0.1, 1, 10 and 100 ng/µL and producing a graph plotting $\log_{10}$cDNA vs the Threshold Cycle (Ct) of the RT-qPCR. The slope of the graph can be used to assess replication efficiency as: Amplification Efficiency = [10(-1/slope)] – 1. In order to confirm that only single melt peaks could be observed, i.e. no confounding unintended primer targets existed, a Melt Curve was obtained by increasing the temperature of the mix in 5 °C increments, up to 90 °C, every 3 min.

Reactions were performed as follows: 200 mM in 1 ul of each forward and reverse primer were mixed with 10 µl SYBR Green qPCR Mastermix (Thermo-Fisher Scientific, Cat.# 4309155), followed by the addition of 1 ng of template cDNA and nuclease-free water to a Vtot=20µl. All samples were pipetted onto a 96 well qPCR plate. RT-qPCR amplification and measurements were performed using a Bio-Rad iQ5 Real Time PCR detection System (BioRad). Cycling conditions were 95 °C (10 min), [60 °C (1 min)] x50 cycles, followed by obtaining a melt curve as described

above. Preliminary data analysis was performed using the iQ5 proprietary software to determine raw Ct values, with all further analysis performed in Excel (Microsoft).

| Name | Primer (5'-3') |
|---|---|
| RPL36A_F | GGGCCCTCAAATTTATCAAGA |
| RPL36A_R | GTCTTTCTTGGCAGCAGCTT |
| RPL7A_F | CACACAGGTGAACTCGGAAG |
| RPL7A_R | ACATTGCCACCCCAGTGA |
| RPS3_F | AGGTGGCCACTAGAGGTCTG |
| RPS3_R | CATGATGAACCGCAGCAC |
| RPS15_F | TTCTGAGGATCCGGCAAG |
| RPS15_R | CATCAGCTGCTCGTAGGACAT |
| Cadherin 11_F | ACGGCCAATGGACCAAGATT |
| Cadherin 11_R | TACAAGTCCTGCTTCTGCCG |
| Cadherin 13_F | GAATTCCAAAGTGGACTGCAA |
| Cadherin 13_R | CAGACGTCAGGAGTTCTCACA |
| Integrin α4_F | CCGGCCATCCATTTTAGA |
| Integrin α4_R | CCTTGTTTAGTTCAATTACTCTTGGA |
| SECISBP2_F | CGCCCCACTGATGAAGAA |
| SECISBP2_R | TGCTTTCTCTCTTGCCGTTC |
| CBS_F | AAACAGATCCGCCTCACG |
| CBS_R | TCCCGGTGCTGTGGTACT |
| CTH_F | AAGCTTTGAAGGCAGCACA |
| CTH_R | TGGTCCATTTAATTACTCAGGAAGAT |
| IGFBP4_F | CCTCTACATCATCCCCATCC |
| IGFBP4_R | GGTCCACACACCAGCACTT |
| DDIT3_F | AAGGCACTGAGCGTATCATGT |
| DDIT3_R | TGAAGATACACTTCCTTCTTGAACAC |
| TRIB3_F | CCGTCTTGGGCCCTATGT |
| TRIB3_R | CTTCCTGGACGGGGTACA |
| DDIT4_F | CAGGCACTGAGTATACCTGCAA |
| DDIT4_R | GTACCAGCCAGGACCTCAGT |
| ATF4_F | CTGGAGAGCTCGGACTGC |
| ATF4_R | CATCCAGGTAAGCCGTGTCT |
| XBP1_F (from van Schadewijk et al, 2012) | GGTCAGTCCCTCCAACAACA |
| XBP1_R (from van Schadewijk et al, 2012) | CTATACCCAACAGGGCATCC |
| eRF1_F | TGAGATATGTTCTTCATTGCCAAG |
| eRF1_R | CATGTTCCTGTCCGGTCTC |
| Human beta actin _F | CTCTTCCAGCCTTCCTTCCT |
| Human beta actin _R | GGATGTCCACGTCACACTTC |
| GADD34_F | CGGTGTCCTACGTCAGAGC |
| GADD34_R | GCCATCTTCTCGCCTCCT |
| JMJD4_F | CACCTACTGGAAAGAGTACATACAGG |
| JMJD4_R | GGGTGAAAACGTCCTCCA |
| HEMK2_F | GCTTCTGGCAGACCGAAC |
| HEMK2_R | GTAGCCTGATGGGGTGCTT |

**Figure 7.1 (previous Page): Table of all RT-qPCR oligonucleotide primer sequences utilised.**

| Gene Name | Amplification Factor |
|---|---|
| RPL36A | 1.98 |
| RPL7A | 2.01 |
| RPS3 | 1.99 |
| RPS15 | 1.90 |
| Cadherin 11 | 1.93 |
| Cadherin 13 | 2.02 |
| Integrin α4 | 1.89 |
| SECISBP2 | 1.97 |
| CBS | 1.93 |
| CTH | 1.95 |
| IGFBP4 | 1.96 |
| DDIT3 | 1.96 |
| TRIB3 | 2.10 |
| DDIT4 | 1.92 |
| ATF4 | 1.95 |
| XBP1 (from van Schadewijk et al, 2012) | 1.93 |
| eRF1 | 1.94 |
| Human beta actin | 1.97 |
| JMJD4 | 1.96 |

**Figure 7.2: Table of empirically derived amplification factors for each primer pair used to calculate fold change in the RT-qPCRs.** Any values > 2 were rounded to 2 in the calculations.

### 7.3.8 Agarose Gel Electrophoresis

Agarose gels were prepared by suspending 1 % (w/v) agarose (Sigma Aldrich) in TBE buffer. The colloidal suspension was then heated in a microwave oven until fully homogeneous and 1:20000 (v/v) of SYBR Safe DNA Gel Stain (Thermo-Fisher Scientific, Cat.# S33102) was added as an in-gel DNA stain. The liquid agarose was then cooled under water and poured into a casting tray until fully solid. Electrophoresis of all gels took place at 150 V current. For the XBP1 gels a 3 % agarose gel was prepared to permit better separation between bands. Any bands to be extracted for downstream use were removed with a steel scalpel under UV light to visualized the DNA.

### 7.3.9 RNA-Seq

Dr Celina Whalley (Institute of Cancer and Genomics, University of Birmingham) performed the library prep and operated the NextSeq sequencer described below. Analysis of the raw data was performed by Dr Robert Hollows to obtain the lists of regulated genes.

A 4200 TapeStation (Agilent) was used to determine RNA quality of the samples to be used downstream by calculation of the RNA Integrity Number (RIN) as described in chapter 5 following quantification by NanoDrop and QuBit (Thermo-Fisher Scientific). RNA samples were then diluted to 6 ng/µl in ultrapure nuclease-free water and submitted for analysis. Library Preparation was performed using a v1 TrueSeq Neoprep mRNA kit (Illumina, Cat.# NP-202-1001). Briefly, poly-A containing RNAs were precipitated using oligo-dT RPB2 RNA purification beads and loaded onto a library card, after which they underwent thermal cycling, cDNA synthesis and adaptor binding. Sequencing was performed using a NextSeq 500 Sequencer (Illumina), set to

use single indexing and paired-end reads (i.e. sequencing each transcript from both ends).

RNA-Seq data for the two control replicates and the two eRF1 knockdown replicates were aligned to the hg19 human genome using Rsubread aligner and assigned to individual genes using the featureCounts function. Read counts were then normalized between samples and converted to counts-per-million reads ("cpm") for each gene using the edgeR package in R. Only genes with a cpm of more than 1 in at least 2 samples were considered for subsequent differential expression analysis. Genes were deemed to be differentially expressed between control and knockdown groups if the fold-change (knockdown / control) was greater than 1.5 or less than -1.5 and the probability value was less than 0.05. Further manipulation of the data was performed in Microsoft Excel 2013.

## 7.4 Mammalian Cell Culture Techniques

### 7.4.1 Cell Culture

All cells were cultured in Dulbecco's Modified Eagle Media (DMEM) with 10 % fetal calf serum, 2 mM L-Glutamine and 1 % penicillin and streptomycin at 37°C at 5% $CO_2$ in a humidified incubator. Stable inducible shRNA cell lines were cultured with an additional 1 $\mu g\ ml^{-1}$ Puromycin to maintain the selection.

### 7.4.2 Cell Lysis

Cells were washed with ice-cold PBS, drained and then samples were lysed in RIPA buffer with the addition of 1X cOmplete Protease Inhibitor (Roche, Prod. No. 04693116001) and 1x Halt Phosphatase Inhibitor Cocktail (Thermo Scientific, Catalog No. 78440).

### 7.4.3 Sub-cellular Fractionation

Sub-cellular fractionation was performed using the NE-PER Nuclear and Cytoplasmic Extraction Reagent kit (Thermo Scientific, Prod. No. 78833) and associated protocol.

## 7.4.4 2D Growth Assays

Cells were seeded in triplicates or quadriplicates in 96 well plates at $4x10^3$ cells/well in 100 µl Vtot and their proliferation assayed over 5 days using either MTS ((3-(4,5-dimethylthiazol-2-yl)-5-(3-carboxymethoxyphenyl)-2-(4-sulfophenyl)-2H-tetrazolium)) (CellTiter 96® $AQ_{ueous}$ MTS Reagent Powder – Promega G1112, G11) and Phenazine methosulfate (PMS, Sigma P9625) or CyQuant™ NF Direct Cell Proliferation Assay (Life Technologies, Cat. #C35006). For the MTS+PMS approach, 20 µl of an 20:1 (v/v) MTS:PMS (individual solutions prepared as described in 7.1.1) mix were added into each well and following 1 h of incubation at 37˚C its 490nm absorbance was measured. For CyQuant assay manufacturer instructions were followed and fluorescence 508/527 was measured. All measurements were taken using on an EnSight Multimode Plate Reader (Perkin Elmer).

### 7.4.5 3D Growth Assays

Noble agar (Sigma-Aldrich, Cat.#A5431) was prepared at a 2 % (w/v) stock solution and maintained at 4˚C for up to 2 months. Prior to the experiment an appropriate volume was melted at 42˚C and mixed with cell culture media as described in section 7.4.1 with an additional 20 % FBS to prepare a 0.6 % (w/v) nobal agar solution. 100 µl of this solution was aliquoted into each well of a 96 well plate and allowed to solidify. Another solution of 0.6 % (w/v) noble agar solution with an equal volume of media+cells was mixed to produce a 0.3 % (w/v) noble agar: media + cells mix. 200 µl of this mix was added on top of the 100 µl 0.6 % layer in each well and allowed to

solidify at room temperature. Once set, they were returned to a humidified incubator at normal cell culture conditions. Following this, 20 µl of cell culture media was added to the cells every 72 h until cell colonies were clearly visible under the microscope. The mass of cell colonies was quantified by adding 100 µl of Alamar Blue cell indicator. After 1 h of incubation the Alamar Blue supernatant was moved to a new 96 well plate and fluorescence at 590 nm was measured.

### 7.4.6 Plasmid Transfection

All plasmid transfections took place using the FuGene6 transfection reagent (Promega, Cat. #E2691), as per the manufacturer's protocol. The optimal conditions for 1ml of cells in a 12-well plate were found to be 0.5 µg of plasmid DNA added to 50 µl of reduced serum media, Optimem (Thermo-Fisher Scientific, Cat.#31985070), followed by addition of 1.5 µl FuGene6. The solution was mixed on a benchtop vortex and incubated at room temperature. After 30 minutes the solution was added to the cells, this protocol was scaled accordingly for larger preparations. Two different types of transfections were performed: In plasmid transfections of p2luc and pGL3 plasmids described above, the DNA-media-transfection reagent mix was added to the well before the cells, a technique known as reverse transfection. This was used to simultaneously knockdown the endogenous gene, while inducing expression of the rescue and luciferase gene. In all other cases forward transfection was used, where the transfection mix was added to adherent cells when reaching ~30% confluence, ~24 h post seeding.

### 7.4.7 siRNA mediated Knockdown

The procedure described has been optimised for transfection of single 6 cm plate containing 5 ml of media, with single cells at 30% confluence. 5 µl of 50 mM siRNA is added to 1233 µl Optimem in an Eppendorf tube and the mixture briefly vortexed. In a separate tube, 87 µl Optimem is added to 13 µl of Oligofectamine Transfection Reagent (Cat. #12252011) and the tube briefly vortexed. Both tubes are left to form complexes for 5 min at room temperature, after which they are mixed together and left to incubate for an additional 45 min. Following that, the siRNA transfection mix is pipetted into the cell media and mixed in by gentle agitation, resulting in 25 nM final siRNA concentration. After 24 h, the media was changed and the treatment repeated in order to maximise knockdown.

**A**

| Target transcript | siRNA description | Sequence start position |
|---|---|---|
| Negative Control | MISSION siRNA Universal Negative Control # 1 | Not Applicable |
| JMJD4 (NM_001161465) | MISSION siRNA SASI_Hs01_00053631 | 475 |
| eRF1 (NM_001256302.1) | MISSION siRNA SASI_Hs01_00015827 | 396 |

**B**

| Target transcript | shRNA Sequence |
|---|---|
| shFF3 (Control) | 5' GGGCTCGGTGCGAATCTATTAtcaagagTAATAGATTCGCACCGAGCCC 3' |
| JMJD4 | 5' GTCCGACTGGCTGAATGAGTTtcaagagACTCATTCAGCCAGTCGGAC 3' |
| eRF1 | 5' GAACTGCATCTAACATTAAGTtcaagagCTTAATGTTAGATGCAGTTC 3' |

**Figure 7.3: List of siRNAs and shRNAs used in this thesis.** A) siRNAs: NM_[X] indicates the RefSeq entry on which this sequence is based. Sequence start site indicates the position of the first nucleotide on the target sequence recognised by the siRNA B) shRNAs: The hairpin loop sequence is in lowercase.

### 7.4.8 Stop Codon Readthrough

Knockdown was achieved using protocol from section 7.4.5 with 25 nM of JMJD4/eRF1 siRNA. After 48 hours of knockdown, the cells were trypsinised and seeded into 12-well plates at $2x10^5$ cells/well, 1 ml/well, where they were reverse transfected with 50 ng of p2luc promoter plasmid. After 24 h the media in the wells were changed to fresh. 48/72 h after the seeding in 12 well plates the cells were washed with ice cold PBS, drained and lysed with 50 µl of 1x PLB on a rocker for 15 min. The lysates were then either used directly for analysis or frozen for later use.

During examination of the eRF1 rescue cell lines, an additional step to the aforementioned was the addition of doxycycline at empirically determined amounts (described per cell line in Chapter 4) during the second siRNA knockdown of eRF1. That concentration of doxycycline was then maintained throughout the experiment.

Stop codon readthrough was assayed using the Dual Luciferase Reporter Assay System (Promega, E1910), as described in the kit with the following modifications: 10 µl of sample/well and 50 µl of LARII and Stop&Glo were used respectively, in an "Opti-Plate 96" white, opaque bottom 96 well plate (Perkin Elmer, Cat.# 6005290). Additionally, measurements for Firefly were taken first for the entire plate before the Renilla results were acquired to prevent contamination by luminescence of nearby wells. All samples were taken in biological triplicates. An EnSight Multimode plate reader was used to assess luminescence. After the addition of each substrate Luminescence was measured over 12 seconds at 0.5 sec intervals. A focal height of 10 mm was used for scanning the plate and the sum of the values was used in downstream calculations as described in chapter 4.

P2luc reporter plasmids were kindly donated by Dr Penny Feng (Wellcome Trust Institute, Oxford). The sequences cloned into the recording window were:

| Name | Sequence (5'-3') |
|---|---|
| **TMV R** | CAGGAACACAACAGCAATTACAG |
| **TMV TGA** | CAGGAACACAATGACAATTACAG |
| **TMV TAA** | CAGGAACACAATAACAATTACAG |
| **BYDV** | ACGTCTCCCAAAUGAGUAGAC |
| **CFW1282*** | ACTTTGCAACAGTGAAGGAAAGCCTTT |

**Figure 7.4: Termination contexts used in the stop codon readthrough assays.** TMVR: Tobacco Mosaic Virus replicase termination context where the wild type UAG stop codon has been substituted with a sense codon. TMV TGA: Tobacco Mosaic Virus replicase termination context where the UAG stop codon has been substituted with a UGA stop codon. TMV TAA: Tobacco Mosaic Virus replicase termination context where the UAG stop codon has been substituted with a UAA stop codon BYDV: Barley Dward Virus PAV Coat Protein Readthrough Termination Context. CFW1282* :Nonsense Mutation in the CTFR of a number of Cystic Fibrosis patients.

### 7.4.9 ATF4 Translational Reporter Assay

U2OS cells were siRNA transfected twice over 48 h with 25 nM eRF1 siRNA in 6 cm plates at 30 % confluence prior to trypsinisation and reseeded into 12 well plates (1 ml/well at $10^5$ cells $ml^{-1)}$. Concurrently, they were reverse transfected with 50 µl Optimem containing 450 ng of pGL3-ATF4 uORF plasmid, a reporter incorporating the uORF1/uORF2 motif in the ATF4 promoter coupled to the Firefly Luciferase gene, and 50 ng of pRL-CMV plasmid, a Renilla Luciferase containing plasmid coupled to a CMV constitutive promoter. The following day the media was removed and replaced with fresh. 48 h after transfection the cells were washed with ice-cold PBS, drained and lysed in 1x PLB. The Renilla and Firefly luciferase activities were then assayed as in the stop codon readthrough assay. Both plasmids used were kindly

donated by Dr Gavin McNee. The same process as for stop codon readthrough assays was used to obtain measurements and analyse the Firefly/Renilla ratio.

### 7.4.10 Establishment of stable cell lines

Parental HEK293T cells were seeded into 6 well plates, 2 ml/well and transfected with the following transfection mix (per well): 100 µl Optimem, 500 ng lentiviral vector (pTIPZ), 150 ng pMD2 plasmid, 350 ng psPAX2 plasmid and 3 µl FuGene. The pMD2 and psPAX2 plasmids encode components of the viral capsid, allowing the transfected cells to package the lentiviral vector into viral particles. After incubation for 48 h, the supernatant containing the viral particles was diluted 1:2 with fresh media and sterilised through a 0.2 µm filter directly before adding to wells containing sub-confluent U2OS cells. After 48 h the media was changed to fresh media containing 1 µg $ml^{-1}$ Puromycin and antibiotic selection took place.

### 7.4.11 Cell Microscopy

The images in Figure 3.7 were obtained using a Nikon Eclipse TE200 Inverted Fluorescence Phase Contrast Microscope. The cells in Figure 3.8 were imaged using an EVOS AMB fluorescence microscope.

## 7.5 Protein Techniques

### 7.5.1 Western Blotting

Samples were electrophoresed on homemade 12 % polyacrylamide gels and transferred to PVDF membranes using wet transfer cassettes (320 mA, 25 min/membrane). For gels with over 14 samples Criterion TGX precast gradient gels were used and transferred to PVDF membranes using the TransBlot Turbo Semi Dry Transfer System (BioRad). The membranes were blocked using PBS-Tween with 5 % (w/v) milk for 1 h and immunoblotted with the intended antibodies. For phospho-sensitive blots 5 % BSA in TBST was instead used for blocking and antibody dilutions. Blots were imaged using a Vilber Lourmat Chemilluminescence/Fluorescence GelDoc System.

A

| Antigen | Antibody | Source | Cat. # | Dilution |
|---|---|---|---|---|
| **eRF1** | Mouse Polyclonal | Santa Cruz Biotech | sc-365653 | 1:1000 |
| **JMJD4** | Mouse Monoclonal | University of Oxford (Produced by Dr Helen Turley) | N/A | 1:50 |
| **ATF4** | Rabbit Monoclonal | Cell Signalling | 11815 | 1:1000 |
| **β-Actin** | Mouse Monoclonal | Abcam | ab8227 | 1:20000 |
| **FLAG** | Mouse Monoclonal | Sigma-Aldrich | F3165 | 1:3000 |
| **HA** | Mouse Polyclonal | Roche | 12CA5 | 1:10000 |
| **CTH** | Rabbit Monoclonal | Santa Cruz Biotech | sc-374249 | 1:1000 |
| **TCP1-γ** | Rabbit Polyclonal | Santa Cruz Biotech | sc-33145 | 1:1000 |
| **eIF2a** | Rabbit Monoclonal | Cell Signalling | 9722 | 1:1000 |
| **Phospho-eIF2a** | Rabbit Monoclonal | Cell Signalling | 9721 | 1:1000 |
| **GTF2I** | Rabbit Polyclonal | Bethyl Laboratories | A301-330A | 1:1000 |
| **HEMK2** | Rabbit Polyclonal | GeneTex | GTX32649 | 1:200 |

B

| Antibody | Source | Cat. # | Dilution |
|---|---|---|---|
| **Goat anti-Rabbit IgG, HRP-linked** | Cell Signalling | 7074 | 1:2000 |
| **Horse anti-Mouse IgG, HRP-linked** | Cell Signalling | 7076 | 1:2000 |

**Figure 7.5: List of antibodies used in this thesis.** A) Primary Antibodies B) Secondary antibodies

### 7.5.2 Immunoprecipitation

**i.** FLAG-tagged JMJD4: The procedure was performed on cells from 6 well plates for overexpression experiments and 15 cm plates for endogenous interactions. Cell cultures were washed using cold PBS and harvested with ice cold JIES lysis buffer containing 1 mM N-oxalylglycine (NOG) and protease inhibitors. The samples were then centrifuged at 4 °C for 5 min at 14000 rpm on a Micro200R Hettich centrifuge, an aliquot of the supernatant was retained and Laemmli sample buffer added. M2 anti-FLAG magnetic beads were washed 4 times with 1 ml cold JIES using a magnetic stand and incubated with the remaining supernatant on a rotating wheel overnight at 4 °C. The supernatant was discarded and the samples washed 4x with 1 ml JIES + NOG + protease inhibitors and then boiled with 2x Laemmli buffer for 5 min.

ii. HA-Tagged JMJD4/V5-Tagged GTF2I: the procedure was as above with the substitution of α-HA and α-V5 beads, respectively, with additional centrifugation steps since the beads used were not magnetic.

### 7.5.3 *In vitro* Transcription/Translation

In vitro Transcription/Translation (IVTT) was performed using the TNT Quick Coupled Transcription/Translation kit (Promega, Cat.# L1170) as per the manufacturer's instructions. The plasmids used were pCDNA3 expressing full length *M. musculus* V5-GTF2I and pCDNA3 expressing *H. sapiens* isoform 2 V5-GTF2I.

### 7.5.4 Mass Spectrometry

Operation of the Instrument was performed by Dr Cleidiane Zampronio (Advanced Mass Spectrometry Facility, University of Birmingham) for determination of band identity in the TCP1-γ experiments and Dr Rebecca Konietzny (Proteomic Group, University of Oxford) for the GTF2I mass-spectrometry based PTM identification.

#### 7.5.4.1 Protein ID by LC-MS/MS analysis (Gel sample)

*Protease digestion*

Samples from HEK293T cells modified to stably contain and express pIPZ Empty Vector, pIPZ FLAG-JMJD4 and pIPZ FLAG-JMJD4 H189A were immunoprecipitated using M2 Magnetic anti-FLAG resin, and the resulting samples electrophoresed on an 8-16% NuView polyacrylamide gradient gel. The gel was then stained with Coomassie, relevant bands identified, excised and sent for identification to the Birmingham Proteomics Facility. The total amount of protein used for the digestion was 100 μg, corresponding to ~10μl of sample volume. To that, 40 μl of 100 mM ammonium bicarbonate (pH 8) were added. Following ammonium bicarbonate addition 50 μL 10 mM dithiothreitol (DTT) were further added and the samples incubated at 56 °°C for 30 mins. Samples were then cooled to room temperature and 50 μl of 50 mM iodoacetamide was added in order to alkylate cysteines, after which the samples were incubated at room temperature in the dark for 30 mins. Finally, 25 μl of 6 ng/μl Trypsin Gold (Promega) or Elastase (Promega) were added to each sample, followed by 37 °C overnight incubation.

*LC-MS/MS Experiment*

After having undergone tryptic digest, the peptide samples were separated and concentrated using a Dionex UltiMate 3000 Ultra Performance Liquid Chromatography. The purified samples were subsequently bound on a Dionex uPrecolumn Cartridge (Acclaim PepMap 100 C18, 5 µm, 100 Å 300 µm i.d. x 5 mm) and gradient separated using a 75 µm Nano Series™ Standard Columns (75 µm i.d. x 15 cm, packed with C18 PepMap100, 3 µm, 100 Å pore size) (Dionex) by eluting with a 3.2 % to 44 % ratio of 0.1 % methanoic acid in acetonitrile solvent for 30 min. A Triversa Nanomate nanospray source (Advion Biosciences) was used to directly elute peptides into an LTQ Orbitrap Elite ETD mass spectrometer (ThermoFisher Scientific) at a flow rate of 350 nL $min^{-1}$. Following an initial full FT-MS scan between m/z 380 – 1800), the top 7 peptides were subsequently selected and analysed via collision-induced dissociation (CID) MS/MS. The Xcalibur 2.1 software package was utilised for analysis of the raw scanning data.

#### 7.5.4.2 Post-Translational Modification via MS

Following tryptic or elastase digest, desalted samples were analyzed by nLC-MS/MS. A Dionex UltiMate 3000 Ultra Performance Liquid Chromatography (UPLC) system (250 nl/min flowrate) (Thermo-Fisher Scientific) was used as frontend separation. Peptides were separated using a PepMAP C18 column (75 μm × 500 mm, 2 μm particle size) and a one-hour gradient of 2-35 % Acetonitrile in 5 % DMSO/0.1 % formic acid. The MS and MS/MS scan modes were FT-ICR/Orbitrap in both cases, using an ESI (nanospray) ion source and CID/CAD fragmentation mode.

The PEAKS 7.0 (Bioinformatics Solutions) engine was used to search for PTMs, set to parent Mass Error Tolerance of 10.0 parts per million (ppm) and a fragment Mass Error Tolerance of 0.05 Da. Precursor Mass Search Type was set as monoisotopic. Deamidation, carbamidomethylation, ubiquitination and hydroxylation were all recorded but only hydroxylation is presented here. Of these, Carbamidomethylation on Cysteine was selected as a fixed modification, while Oxidation (M), Deamidation (N, Q) and Hydroxylation (P, K, D, N, R, Y) were selected as variable modifications for the database search. The peptide false discovery rate was set to 1 % as part of a target/decoy fusion approach. Peptide abundance was measured as accumulated ion counts after extraction of the chromatographic elution profile of the precursor mass of interest using Qual Browser, Xcalibur 3.0.63 (Thermo-Fisher Scientific).

# CHAPTER 8: References

ACKER, J., MURRONI, O., MATTEI, M. G., KEDINGER, C. & VIGNERON, M. 1996. The gene (POLR2L) encoding the hRPB7.6 subunit of human RNA polymerase. *Genomics,* 32**,** 86-90.

AIK, W., MCDONOUGH, M. A., THALHAMMER, A., CHOWDHURY, R. & SCHOFIELD, C. J. 2012. Role of the jelly-roll fold in substrate binding by 2-oxoglutarate oxygenases. *Current Opinion in Structural Biology,* 22**,** 691-700.

AIT GHEZALA, H., JOLLES, B., SALHI, S., CASTRILLO, K., CARPENTIER, W., CAGNARD, N., BRUHAT, A., FAFOURNOUX, P. & JEAN-JEAN, O. 2012a. Translation termination efficiency modulates ATF4 response by regulating ATF4 mRNA translation at 5' short ORFs. *Nucleic Acids Res,* 40**,** 9557-70.

AIT GHEZALA, H., JOLLES, B., SALHI, S., CASTRILLO, K., CARPENTIER, W., CAGNARD, N., BRUHAT, A., FAFOURNOUX, P. & JEAN-JEAN, O. 2012b. Translation termination efficiency modulates ATF4 response by regulating ATF4 mRNA translation at 5' short ORFs. *Nucleic acids research,* 40**,** 9557-70.

AITKEN, S. M., LODHA, P. H. & MORNEAU, D. J. 2011. The enzymes of the transsulfuration pathways: active-site characterizations. *Biochim Biophys Acta,* 1814**,** 1511-7.

AKRAM, M. 2014. Citric acid cycle and role of its intermediates in metabolism. *Cell Biochem Biophys,* 68**,** 475-8.

ALKALAEVA, E. Z., PISAREV, A. V., FROLOVA, L. Y., KISSELEV, L. L. & PESTOVA, T. V. 2006. In vitro reconstitution of eukaryotic translation reveals cooperativity between release factors eRF1 and eRF3. *Cell,* 125**,** 1125-36.

ARABI, A., WU, S., RIDDERSTRALE, K., BIERHOFF, H., SHIUE, C., FATYOL, K., FAHLEN, S., HYDBRING, P., SODERBERG, O., GRUMMT, I., LARSSON, L. G. & WRIGHT, A. P. 2005. c-Myc associates with ribosomal DNA and activates RNA polymerase I transcription. *Nat Cell Biol,* 7**,** 303-10.

ASGHAR, U., WITKIEWICZ, A. K., TURNER, N. C. & KNUDSEN, E. S. 2015. The history and future of targeting cyclin-dependent kinases in cancer therapy. *Nat Rev Drug Discov,* 14**,** 130-46.

ASHWORTH, T. & ROY, A. L. 2007. Cutting Edge: TFII-I controls B cell proliferation via regulating NF-kappaB. *J Immunol,* 178**,** 2631-5.

ATKINSON, G. C., BALDAUF, S. L. & HAURYLIUK, V. 2008. Evolution of nonstop, no-go and nonsense-mediated mRNA decay and their termination factor-derived components. *BMC Evol Biol,* 8**,** 290.

AZZALIN, C. M. & LINGNER, J. 2006. The human RNA surveillance factor UPF1 is required for S phase progression and genome stability. *Curr Biol,* 16**,** 433-9.

BAGHERI-YARMAND, R., HUNT, K. K. & KEYOMARSI, K. 2008. Activating transcription factor 4 is a novel regulator of the cell cycle through direct interaction with p27<sup>kip1 </sup>and cdk4 in breast cancer. *Cancer Research,* 68**,** 5078-5078.

BARANOV, P. V., GESTELAND, R. F. & ATKINS, J. F. 2002. Recoding: translational bifurcations in gene expression. *Gene,* 286**,** 187-201.

BEEMON, K. & KEITH, J. 1977. Localization of N6-methyladenosine in the Rous sarcoma virus genome. *J Mol Biol,* 113**,** 165-79.

BELIN, S., BEGHIN, A., SOLANO-GONZALEZ, E., BEZIN, L., BRUNET-MANQUAT, S., TEXTORIS, J., PRATS, A. C., MERTANI, H. C., DUMONTET, C. & DIAZ, J. J. 2009. Dysregulation of ribosome biogenesis and translational capacity is associated with tumor progression of human breast cancer cells. *PLoS One,* 4**,** e7147.

BENNETT, E. P., MANDEL, U., CLAUSEN, H., GERKEN, T. A., FRITZ, T. A. & TABAK, L. A. 2012. Control of mucin-type O-glycosylation: a classification of the polypeptide GalNAc-transferase gene family. *Glycobiology,* 22**,** 736-56.

BERRY, W. L. & JANKNECHT, R. 2013a. KDM4/JMJD2 histone demethylases: epigenetic regulators in cancer cells. *Cancer research,* 73**,** 2936-42.

BERRY, W. L. & JANKNECHT, R. 2013b. KDM4/JMJD2 histone demethylases: epigenetic regulators in cancer cells. *Cancer Res,* 73**,** 2936-42.
BHAT, M., ROBICHAUD, N., HULEA, L., SONENBERG, N., PELLETIER, J. & TOPISIROVIC, I. 2015. Targeting the translation machinery in cancer. *Nat Rev Drug Discov,* 14**,** 261-78.
BI, M., NACZKI, C., KORITZINSKY, M., FELS, D., BLAIS, J., HU, N., HARDING, H., NOVOA, I., VARIA, M., RALEIGH, J., SCHEUNER, D., KAUFMAN, R. J., BELL, J., RON, D., WOUTERS, B. G. & KOUMENIS, C. 2005. ER stress-regulated translation increases tolerance to extreme hypoxia and promotes tumor growth. *EMBO J,* 24**,** 3470-81.
BIDOU, L., HATIN, I., PEREZ, N., ALLAMAND, V., PANTHIER, J. J. & ROUSSET, J. P. 2004. Premature stop codons involved in muscular dystrophies show a broad spectrum of readthrough efficiencies in response to gentamicin treatment. *Gene Ther,* 11**,** 619-27.
BLACK, J. C., VAN RECHEM, C. & WHETSTINE, J. R. 2012. Histone lysine methylation dynamics: establishment, regulation, and biological impact. *Molecular cell,* 48**,** 491-507.
BLANCHET, S., ROWE, M., VON DER HAAR, T., FABRET, C., DEMAIS, S., HOWARD, M. J. & NAMY, O. 2015. New insights into stop codon recognition by eRF1. *Nucleic Acids Research,* 43**,** 3298-3308.
BOKAR, J. A., SHAMBAUGH, M. E., POLAYES, D., MATERA, A. G. & ROTTMAN, F. M. 1997. Purification and cDNA cloning of the AdoMet-binding subunit of the human mRNA (N6-adenosine)-methyltransferase. *RNA,* 3**,** 1233-47.
BONETTI, B., FU, L., MOON, J. & BEDWELL, D. M. 1995. The efficiency of translation termination is determined by a synergistic interplay between upstream and downstream sequences in Saccharomyces cerevisiae. *J Mol Biol,* 251**,** 334-45.
BORDEIRA-CARRICO, R., PEGO, A. P., SANTOS, M. & OLIVEIRA, C. 2012. Cancer syndromes and therapy by stop-codon readthrough. *Trends Mol Med,* 18**,** 667-78.
BOSE, J., GRUBER, A. D., HELMING, L., SCHIEBE, S., WEGENER, I., HAFNER, M., BEALES, M., KONTGEN, F. & LENGELING, A. 2004. The phosphatidylserine receptor has essential functions during embryogenesis but not in apoptotic cell removal. *Journal of biology,* 3**,** 15.
BOURGEOIS, G., LETOQUART, J., VAN TRAN, N. & GRAILLE, M. 2017. Trm112, a Protein Activator of Methyltransferases Modifying Actors of the Eukaryotic Translational Apparatus. *Biomolecules,* 7.
BRACKLEY, K. I. & GRANTHAM, J. 2009. Activities of the chaperonin containing TCP-1 (CCT): implications for cell cycle progression and cytoskeletal organisation. *Cell Stress & Chaperones,* 14**,** 23-31.
BRAMEIER, M., KRINGS, A. & MACCALLUM, R. M. 2007. NucPred--predicting nuclear localization of proteins. *Bioinformatics,* 23**,** 1159-60.
BRASS, N., UKENA, I., REMBERGER, K., MACK, U., SYBRECHT, G. W. & MEESE, E. U. 1996. DNA amplification on chromosome 3q26.1-q26.3 in squamous cell carcinoma of the lung detected by reverse chromosome painting. *Eur J Cancer,* 32A**,** 1205-8.
BRDICKA, T., IMRICH, M., ANGELISOVA, P., BRDICKOVA, N., HORVATH, O., SPICKA, J., HILGERT, I., LUSKOVA, P., DRABER, P., NOVAK, P., ENGELS, N., WIENANDS, J., SIMEONI, L., OSTERREICHER, J., AGUADO, E., MALISSEN, M., SCHRAVEN, B. & HOREJSI, V. 2002. Non-T cell activation linker (NTAL): a transmembrane adaptor protein involved in immunoreceptor signaling. *J Exp Med,* 196**,** 1617-26.
BREWER, J. W. & DIEHL, J. A. 2000. PERK mediates cell-cycle exit during the mammalian unfolded protein response. *Proc Natl Acad Sci U S A,* 97**,** 12625-30.
BROCKER, C. N., VASILIOU, V. & NEBERT, D. W. 2009. Evolutionary divergence and functions of the ADAM and ADAMTS gene families. *Hum Genomics,* 4**,** 43-55.

BROWN, A., SHAO, S., MURRAY, J., HEGDE, R. S. & RAMAKRISHNAN, V. 2015. Structural basis for stop codon recognition in eukaryotes. *Nature,* 524**,** 493-496.

BRUGAROLAS, J., LEI, K., HURLEY, R. L., MANNING, B. D., REILING, J. H., HAFEN, E., WITTERS, L. A., ELLISEN, L. W. & KAELIN, W. G., JR. 2004. Regulation of mTOR function in response to hypoxia by REDD1 and the TSC1/TSC2 tumor suppressor complex. *Genes Dev,* 18**,** 2893-904.

BRUMBAUGH, K. M., OTTERNESS, D. M., GEISEN, C., OLIVEIRA, V., BROGNARD, J., LI, X., LEJEUNE, F., TIBBETTS, R. S., MAQUAT, L. E. & ABRAHAM, R. T. 2004. The mRNA surveillance protein hSMG-1 functions in genotoxic stress response pathways in mammalian cells. *Mol Cell,* 14**,** 585-98.

BULYGIN, K. N., KHAIRULINA, Y. S., KOLOSOV, P. M., VEN'YAMINOVA, A. G., GRAIFER, D. M., VOROBJEV, Y. N., FROLOVA, L. Y., KISSELEV, L. L. & KARPOVA, G. G. 2010. Three distinct peptides from the N domain of translation termination factor eRF1 surround stop codon in the ribosome. *RNA,* 16**,** 1902-14.

CASSAN, M. & ROUSSET, J. P. 2001. UAG readthrough in mammalian cells: effect of upstream and downstream stop codon contexts reveal different signals. *BMC Mol Biol,* 2**,** 3.

CHANG, B., CHEN, Y., ZHAO, Y. & BRUICK, R. K. 2007. JMJD6 Is a Histone Arginine Demethylase. *Science,* 318**,** 444-447.

CHAUVIN, C., SALHI, S. & JEAN-JEAN, O. 2007. Human eukaryotic release factor 3a depletion causes cell cycle arrest at G1 phase through inhibition of the mTOR pathway. *Mol Cell Biol,* 27**,** 5619-29.

CHAUVIN, C., SALHI, S., LE GOFF, C., VIRANAICKEN, W., DIOP, D. & JEAN-JEAN, O. 2005. Involvement of human release factors eRF3a and eRF3b in translation termination and regulation of the termination complex formation. *Mol Cell Biol,* 25**,** 5801-11.

CHAVATTE, L., SEIT-NEBI, A., DUBOVAYA, V. & FAVRE, A. 2002. The invariant uridine of stop codons contacts the conserved NIKSR loop of human eRF1 in the ribosome. *The EMBO journal,* 21**,** 5302-11.

CHEN, B., YU, M., CHANG, Q., LU, Y., THAKUR, C., MA, D., YI, Z. & CHEN, F. 2013a. Mdig de-represses H19 large intergenic non-coding RNA (lincRNA) by down-regulating H3K9me3 and heterochromatin. *Oncotarget,* 4**,** 1427-37.

CHEN, C., STEVENS, B., KAUR, J., SMILANSKY, Z., COOPERMAN, B. S. & GOLDMAN, Y. E. 2011. Allosteric vs. spontaneous exit-site (E-site) tRNA dissociation early in protein synthesis. *Proc Natl Acad Sci U S A,* 108**,** 16980-5.

CHEN, G. & BURGER, M. M. 2004. p150 overexpression in gastric carcinoma: the association with p53, apoptosis and cell proliferation. *Int J Cancer,* 112**,** 393-8.

CHEN, Q., CHEN, Y., BIAN, C., FUJIKI, R. & YU, X. 2013b. TET2 promotes histone O-GlcNAcylation during gene transcription. *Nature,* 493**,** 561-4.

CHENG, Z., SAITO, K., PISAREV, A. V., WADA, M., PISAREVA, V. P., PESTOVA, T. V., GAJDA, M., ROUND, A., KONG, C., LIM, M., NAKAMURA, Y., SVERGUN, D. I., ITO, K. & SONG, H. 2009. Structural insights into eRF3 and stop codon recognition by eRF1. *Genes Dev,* 23**,** 1106-18.

CHOWDHURY, R., SEKIRNIK, R., BRISSETT, N. C., KROJER, T., HO, C.-H., NG, S. S., CLIFTON, I. J., GE, W., KERSHAW, N. J., FOX, G. C., MUNIZ, J. R. C., VOLLMAR, M., PHILLIPS, C., PILKA, E. S., KAVANAGH, K. L., VON DELFT, F., OPPERMANN, U., MCDONOUGH, M. A., DOHERTY, A. J. & SCHOFIELD, C. J. 2014a. Ribosomal oxygenases are structurally conserved from prokaryotes to humans. *Nature,* 510**,** 422.

CHOWDHURY, R., SEKIRNIK, R., BRISSETT, N. C., KROJER, T., HO, C. H., NG, S. S., CLIFTON, I. J., GE, W., KERSHAW, N. J., FOX, G. C., MUNIZ, J. R., VOLLMAR, M., PHILLIPS, C., PILKA, E. S., KAVANAGH, K. L., VON DELFT, F., OPPERMANN, U., MCDONOUGH, M. A., DOHERTY, A. J. & SCHOFIELD, C. J. 2014b. Ribosomal oxygenases are structurally conserved from prokaryotes to humans. *Nature,* 510**,** 422-6.

CHOWDHURY, R., SEKIRNIK, R., BRISSETT, N. C., KROJER, T., HO, C. H., NG, S. S., CLIFTON, I. J., GE, W., KERSHAW, N. J., FOX, G. C., MUNIZ, J. R. C., VOLLMAR, M., PHILLIPS, C., PILKA, E. S., KAVANAGH, K. L., VON DELFT, F., OPPERMANN, U., MCDONOUGH, M. A., DOHERTY, A. J. & SCHOFIELD, C. J. 2014c. Ribosomal oxygenases are structurally conserved from prokaryotes to humans. *Nature,* 510**,** 422-426.

CHOY, M. S., YUSOFF, P., LEE, I. C., NEWTON, J. C., GOH, C. W., PAGE, R., SHENOLIKAR, S. & PETI, W. 2015. Structural and Functional Analysis of the GADD34:PP1 eIF2alpha Phosphatase. *Cell Rep,* 11**,** 1885-91.

CORY, A. H., OWEN, T. C., BARLTROP, J. A. & CORY, J. G. 1991. Use of an aqueous soluble tetrazolium/formazan assay for cell growth assays in culture. *Cancer Commun,* 3**,** 207-12.

COURTNEIDGE, S. A. 2012. Cell migration and invasion in human disease: the Tks adaptor proteins. *Biochem Soc Trans,* 40**,** 129-32.

DEL RIZZO, P. A., KRISHNAN, S. & TRIEVEL, R. C. 2012. Crystal structure and functional analysis of JMJD5 indicate an alternate specificity and function. *Molecular and cellular biology,* 32**,** 4044-52.

DERENZINI, M., CECCARELLI, C., SANTINI, D., TAFFURELLI, M. & TRERE, D. 2004. The prognostic value of the AgNOR parameter in human breast cancer depends on the pRb and p53 status. *J Clin Pathol,* 57**,** 755-61.

DERENZINI, M. & TRERE, D. 1991. Importance of interphase nucleolar organizer regions in tumor pathology. *Virchows Arch B Cell Pathol Incl Mol Pathol,* 61**,** 1-8.

DEVER, T. E. & GREEN, R. 2012. The elongation, termination, and recycling phases of translation in eukaryotes. *Cold Spring Harb Perspect Biol,* 4**,** a013706.

DEY, S., BAIRD, T. D., ZHOU, D., PALAM, L. R., SPANDAU, D. F. & WEK, R. C. 2010. Both transcriptional regulation and translational control of ATF4 are central to the integrated stress response. *J Biol Chem,* 285**,** 33165-74.

DEY, S., SAVANT, S., TESKE, B. F., HATZOGLOU, M., CALKHOVEN, C. F. & WEK, R. C. 2012. Transcriptional repression of ATF4 gene by CCAAT/enhancer-binding protein beta (C/EBPbeta) differentially regulates integrated stress response. *J Biol Chem,* 287**,** 21936-49.

DHAR, S. S., ALAM, H., LI, N., WAGNER, K. W., CHUNG, J., AHN, Y. W. & LEE, M. G. 2014. Transcriptional repression of histone deacetylase 3 by the histone demethylase KDM2A is coupled to tumorigenicity of lung cancer cells. *The Journal of biological chemistry,* 289**,** 7483-96.

DICKHOUT, J. G., CARLISLE, R. E., JEROME, D. E., MOHAMMED-ALI, Z., JIANG, H., YANG, G., MANI, S., GARG, S. K., BANERJEE, R., KAUFMAN, R. J., MACLEAN, K. N., WANG, R. & AUSTIN, R. C. 2012a. Integrated stress response modulates cellular redox state via induction of cystathionine gamma-lyase: cross-talk between integrated stress response and thiol metabolism. *J Biol Chem,* 287**,** 7603-14.

DICKHOUT, J. G., CARLISLE, R. E., JEROME, D. E., MOHAMMED-ALI, Z., JIANG, H., YANG, G., MANI, S., GARG, S. K., BANERJEE, R., KAUFMAN, R. J., MACLEAN, K. N., WANG, R. & AUSTIN, R. C. 2012b. Integrated Stress Response Modulates Cellular Redox State via Induction of Cystathionine γ-Lyase: CROSS-TALK BETWEEN INTEGRATED STRESS RESPONSE AND THIOL METABOLISM. *The Journal of Biological Chemistry,* 287**,** 7603-7614.

DIMITROVA, E., TURBERFIELD, A. H. & KLOSE, R. J. 2015. Histone demethylases in chromatin biology and beyond. *EMBO Rep,* 16**,** 1620-39.

DO, R., BAILEY, S. D., DESBIENS, K., BELISLE, A., MONTPETIT, A., BOUCHARD, C., PERUSSE, L., VOHL, M. C. & ENGERT, J. C. 2008. Genetic variants of FTO influence adiposity, insulin sensitivity, leptin levels, and resting metabolic rate in the Quebec Family Study. *Diabetes,* 57**,** 1147-50.

DOMOGATSKAYA, A., RODIN, S. & TRYGGVASON, K. 2012. Functional diversity of laminins. *Annu Rev Cell Dev Biol,* 28**,** 523-53.
DONG, Z. & ZHANG, J. T. 2006. Initiation factor eIF3 and regulation of mRNA translation, cell growth, and cancer. *Crit Rev Oncol Hematol,* 59**,** 169-80.
DONZE, O., JAGUS, R., KOROMILAS, A. E., HERSHEY, J. W. & SONENBERG, N. 1995. Abrogation of translation initiation factor eIF-2 phosphorylation causes malignant transformation of NIH 3T3 cells. *EMBO J,* 14**,** 3828-34.
DUBOURG, C., TOUTAIN, B., HELIAS, C., HENRY, C., LESSARD, M., LE GALL, J. Y., LE TREUT, A. & GUENET, L. 2002. Evaluation of ETF1/eRF1, mapping to 5q31, as a candidate myeloid tumor suppressor gene. *Cancer Genet Cytogenet,* 134**,** 33-7.
DUNCAN, T., TREWICK, S. C., KOIVISTO, P., BATES, P. A., LINDAHL, T. & SEDGWICK, B. 2002. Reversal of DNA alkylation damage by two human dioxygenases. *Proc Natl Acad Sci U S A,* 99**,** 16660-5.
DURAN, R. V., MACKENZIE, E. D., BOULAHBEL, H., FREZZA, C., HEISERICH, L., TARDITO, S., BUSSOLATI, O., ROCHA, S., HALL, M. N. & GOTTLIEB, E. 2013. HIF-independent role of prolyl hydroxylases in the cellular response to amino acids. *Oncogene,* 32**,** 4549-56.
EKI, T., OKUMURA, K., ABE, M., KAGOTANI, K., TAGUCHI, H., MURAKAMI, Y., PAN, Z. Q. & HANAOKA, F. 1998. Mapping of the human genes encoding cyclin H (CCNH) and the CDK-activating kinase (CAK) assembly factor MAT1 (MNAT1) to chromosome bands 5q13.3-q14 and 14q23, respectively. *Genomics,* 47**,** 115-20.
EL YACOUBI, B., BAILLY, M. & DE CRECY-LAGARD, V. 2012. Biosynthesis and function of posttranscriptional modifications of transfer RNAs. *Annu Rev Genet,* 46**,** 69-95.
ELKINS, J. M., HEWITSON, K. S., MCNEILL, L. A., SEIBEL, J. F., SCHLEMMINGER, I., PUGH, C. W., RATCLIFFE, P. J. & SCHOFIELD, C. J. 2003. Structure of factor-inhibiting hypoxia-inducible factor (HIF) reveals mechanism of oxidative modification of HIF-1 alpha. *J Biol Chem,* 278**,** 1802-6.
EPSTEIN, A. C., GLEADLE, J. M., MCNEILL, L. A., HEWITSON, K. S., O'ROURKE, J., MOLE, D. R., MUKHERJI, M., METZEN, E., WILSON, M. I., DHANDA, A., TIAN, Y. M., MASSON, N., HAMILTON, D. L., JAAKKOLA, P., BARSTEAD, R., HODGKIN, J., MAXWELL, P. H., PUGH, C. W., SCHOFIELD, C. J. & RATCLIFFE, P. J. 2001a. C. elegans EGL-9 and mammalian homologs define a family of dioxygenases that regulate HIF by prolyl hydroxylation. *Cell,* 107**,** 43-54.
EPSTEIN, A. C. R., GLEADLE, J. M., MCNEILL, L. A., HEWITSON, K. S., O'ROURKE, J., MOLE, D. R., MUKHERJI, M., METZEN, E., WILSON, M. I., DHANDA, A., TIAN, Y.-M., MASSON, N., HAMILTON, D. L., JAAKKOLA, P., BARSTEAD, R., HODGKIN, J., MAXWELL, P. H., PUGH, C. W., SCHOFIELD, C. J. & RATCLIFFE, P. J. 2001b. C. elegans EGL-9 and Mammalian Homologs Define a Family of Dioxygenases that Regulate HIF by Prolyl Hydroxylation. *Cell,* 107**,** 43-54.
EUBANK, T. D., RODA, J. M., LIU, H., O'NEIL, T. & MARSH, C. B. 2011. Opposing roles for HIF-1alpha and HIF-2alpha in the regulation of angiogenesis by mononuclear phagocytes. *Blood,* 117**,** 323-32.
EUSTICE, D. C. & WILHELM, J. M. 1984. Mechanisms of action of aminoglycoside antibiotics in eucaryotic protein synthesis. *Antimicrobial Agents and Chemotherapy,* 26**,** 53-60.
EYERS, P. A., KEESHAN, K. & KANNAN, N. 2017. Tribbles in the 21st Century: The Evolving Roles of Tribbles Pseudokinases in Biology and Disease. *Trends Cell Biol,* 27**,** 284-298.
EYLER, D. E. & GREEN, R. 2011. Distinct response of yeast ribosomes to a miscoding event during translation. *RNA,* 17**,** 925-32.
FAN-MINOGUE, H. & BEDWELL, D. M. 2008. Eukaryotic ribosomal RNA determinants of aminoglycoside resistance and their role in translational fidelity. *RNA,* 14**,** 148-57.

FAN, M., HE, X. & XU, X. 2015. Restored expression levels of TET1 decrease the proliferation and migration of renal carcinoma cells. *Mol Med Rep,* 12**,** 4837-42.

FENG, T., YAMAMOTO, A., WILKINS, S. E., SOKOLOVA, E., YATES, L. A., MUNZEL, M., SINGH, P., HOPKINSON, R. J., FISCHER, R., COCKMAN, M. E., SHELLEY, J., TRUDGIAN, D. C., SCHODEL, J., MCCULLAGH, J. S., GE, W., KESSLER, B. M., GILBERT, R. J., FROLOVA, L. Y., ALKALAEVA, E., RATCLIFFE, P. J., SCHOFIELD, C. J. & COLEMAN, M. L. 2014a. Optimal translational termination requires C4 lysyl hydroxylation of eRF1. *Mol Cell,* 53**,** 645-54.

FENG, T., YAMAMOTO, A., WILKINS, SARAH E., SOKOLOVA, E., YATES, LUKE A., MÜNZEL, M., SINGH, P., HOPKINSON, RICHARD J., FISCHER, R., COCKMAN, MATTHEW E., SHELLEY, J., TRUDGIAN, DAVID C., SCHÖDEL, J., MCCULLAGH, JAMES S. O., GE, W., KESSLER, BENEDIKT M., GILBERT, ROBERT J., FROLOVA, LUDMILA Y., ALKALAEVA, E., RATCLIFFE, PETER J., SCHOFIELD, CHRISTOPHER J. & COLEMAN, MATHEW L. 2014b. Optimal Translational Termination Requires C4 Lysyl Hydroxylation of eRF1. *Molecular cell*.

FIGARO, S., SCRIMA, N., BUCKINGHAM, R. H. & HEURGUE-HAMARD, V. 2008. HemK2 protein, encoded on human chromosome 21, methylates translation termination factor eRF1. *FEBS Lett,* 582**,** 2352-6.

FINNIGAN, G. C., HANSON-SMITH, V., STEVENS, T. H. & THORNTON, J. W. 2012. Evolution of increased complexity in a molecular machine. *Nature,* 481**,** 360-4.

FLAVIN, R., C SMYTH, P., FINN, S., LAIOS, A., O'TOOLE, S., BARRETT, C., RING, M., M DENNING, K., LI, J., AHERNE, S., A AZIZ, N., ALHADI, A., SHEPPARD, B., LODA, M., MARTIN, C., SHEILS, O. & J O'LEARY, J. 2008. *Altered eIF6 and Dicer expression is associated with clinicopathological features in ovarian serous carcinoma patients*.

FLOQUET, C., ROUSSET, J. P. & BIDOU, L. 2011. Readthrough of premature termination codons in the adenomatous polyposis coli gene restores its biological activity in human cancer cells. *PLoS One,* 6**,** e24125.

FRADEJAS-VILLAR, N., SEEHER, S., ANDERSON, C. B., DOENGI, M., CARLSON, B. A., HATFIELD, D. L., SCHWEIZER, U. & HOWARD, M. T. 2017. The RNA-binding protein Secisbp2 differentially modulates UGA codon reassignment and RNA decay. *Nucleic Acids Res,* 45**,** 4094-4107.

FRANK, C. L., GE, X., XIE, Z., ZHOU, Y. & TSAI, L. H. 2010. Control of activating transcription factor 4 (ATF4) persistence by multisite phosphorylation impacts cell cycle progression and neurogenesis. *J Biol Chem,* 285**,** 33324-37.

FREDRIKSSON, R., HAGGLUND, M., OLSZEWSKI, P. K., STEPHANSSON, O., JACOBSSON, J. A., OLSZEWSKA, A. M., LEVINE, A. S., LINDBLOM, J. & SCHIOTH, H. B. 2008. The obesity gene, FTO, is of ancient origin, up-regulated during food deprivation and expressed in neurons of feeding-related nuclei of the brain. *Endocrinology,* 149**,** 2062-71.

FROLOVA, L., LE GOFF, X., RASMUSSEN, H. H., CHEPEREGIN, S., DRUGEON, G., KRESS, M., ARMAN, I., HAENNI, A. L., CELIS, J. E., PHILIPPE, M. & ET AL. 1994. A highly conserved eukaryotic protein family possessing properties of polypeptide chain release factor. *Nature,* 372**,** 701-3.

FROLOVA, L., LE GOFF, X., ZHOURAVLEVA, G., DAVYDOVA, E., PHILIPPE, M. & KISSELEV, L. 1996. Eukaryotic polypeptide chain release factor eRF3 is an eRF1- and ribosome-dependent guanosine triphosphatase. *RNA,* 2**,** 334-41.

FROLOVA, L. Y., MERKULOVA, T. I. & KISSELEV, L. L. 2000. Translation termination in eukaryotes: polypeptide release factor eRF1 is composed of functionally and structurally distinct domains. *RNA,* 6**,** 381-90.

FROLOVA, L. Y., TSIVKOVSKII, R. Y., SIVOLOBOVA, G. F., OPARINA, N. Y., SERPINSKY, O. I., BLINOV, V. M., TATKOV, S. I. & KISSELEV, L. L. 1999. Mutations in the highly

conserved GGQ motif of class 1 polypeptide release factors abolish ability of human eRF1 to trigger peptidyl-tRNA hydrolysis. *RNA,* 5**,** 1014-20.
FU, Y., DAI, Q., ZHANG, W., REN, J., PAN, T. & HE, C. 2010a. The AlkB Domain of Mammalian ABH8 Catalyzes Hydroxylation of 5-Methoxycarbonylmethyluridine at the Wobble Position of tRNA. *Angewandte Chemie International Edition,* 49**,** 8885-8888.
FU, Y., DAI, Q., ZHANG, W., REN, J., PAN, T. & HE, C. 2010b. The AlkB domain of mammalian ABH8 catalyzes hydroxylation of 5-methoxycarbonylmethyluridine at the wobble position of tRNA. *Angew Chem Int Ed Engl,* 49**,** 8885-8.
FUJII, T., SHIMADA, K., ANAI, S., FUJIMOTO, K. & KONISHI, N. 2013. ALKBH2, a novel AlkB homologue, contributes to human bladder cancer progression by regulating MUC1 expression. *Cancer science,* 104**,** 321-7.
FUJIMURA, K., WRIGHT, T., STRNADEL, J., KAUSHAL, S., METILDI, C., LOWY, A. M., BOUVET, M., KELBER, J. A. & KLEMKE, R. L. 2014. A hypusine-eIF5A-PEAK1 switch regulates the pathogenesis of pancreatic cancer. *Cancer Res,* 74**,** 6671-81.
GAO, J., AKSOY, B. A., DOGRUSOZ, U., DRESDNER, G., GROSS, B., SUMER, S. O., SUN, Y., JACOBSEN, A., SINHA, R., LARSSON, E., CERAMI, E., SANDER, C. & SCHULTZ, N. 2013. Integrative analysis of complex cancer genomics and clinical profiles using the cBioPortal. *Sci Signal,* 6**,** pl1.
GARCIA-CLOSAS, M., COUCH, F. J., LINDSTROM, S., MICHAILIDOU, K., SCHMIDT, M. K., BROOK, M. N., ORR, N., RHIE, S. K., RIBOLI, E., FEIGELSON, H. S., LE MARCHAND, L., BURING, J. E., ECCLES, D., MIRON, P., FASCHING, P. A., BRAUCH, H., CHANG-CLAUDE, J., CARPENTER, J., GODWIN, A. K., NEVANLINNA, H., GILES, G. G., COX, A., HOPPER, J. L., BOLLA, M. K., WANG, Q., DENNIS, J., DICKS, E., HOWAT, W. J., SCHOOF, N., BOJESEN, S. E., LAMBRECHTS, D., BROEKS, A., ANDRULIS, I. L., GUENEL, P., BURWINKEL, B., SAWYER, E. J., HOLLESTELLE, A., FLETCHER, O., WINQVIST, R., BRENNER, H., MANNERMAA, A., HAMANN, U., MEINDL, A., LINDBLOM, A., ZHENG, W., DEVILLEE, P., GOLDBERG, M. S., LUBINSKI, J., KRISTENSEN, V., SWERDLOW, A., ANTON-CULVER, H., DORK, T., MUIR, K., MATSUO, K., WU, A. H., RADICE, P., TEO, S. H., SHU, X. O., BLOT, W., KANG, D., HARTMAN, M., SANGRAJRANG, S., SHEN, C. Y., SOUTHEY, M. C., PARK, D. J., HAMMET, F., STONE, J., VEER, L. J., RUTGERS, E. J., LOPHATANANON, A., STEWART-BROWN, S., SIRIWANARANGSAN, P., PETO, J., SCHRAUDER, M. G., EKICI, A. B., BECKMANN, M. W., DOS SANTOS SILVA, I., JOHNSON, N., WARREN, H., TOMLINSON, I., KERIN, M. J., MILLER, N., MARME, F., SCHNEEWEISS, A., SOHN, C., TRUONG, T., LAURENT-PUIG, P., KERBRAT, P., NORDESTGAARD, B. G., NIELSEN, S. F., FLYGER, H., MILNE, R. L., PEREZ, J. I., MENENDEZ, P., MULLER, H., ARNDT, V., STEGMAIER, C., LICHTNER, P., LOCHMANN, M., JUSTENHOVEN, C., et al. 2013. Genome-wide association studies identify four ER negative-specific breast cancer risk loci. *Nature genetics,* 45**,** 392-8, 398e1-2.
GASOL, E., JIMENEZ-VIDAL, M., CHILLARON, J., ZORZANO, A. & PALACIN, M. 2004. Membrane topology of system xc- light subunit reveals a re-entrant loop with substrate-restricted accessibility. *J Biol Chem,* 279**,** 31228-36.
GE, W., WOLF, A., FENG, T., HO, C.-H., SEKIRNIK, R., ZAYER, A., GRANATINO, N., COCKMAN, M. E., LOENARZ, C., LOIK, N. D., HARDY, A. P., CLARIDGE, T. D. W., HAMED, R. B., CHOWDHURY, R., GONG, L., ROBINSON, C. V., TRUDGIAN, D. C., JIANG, M., MACKEEN, M. M., MCCULLAGH, J. S., GORDIYENKO, Y., THALHAMMER, A., YAMAMOTO, A., YANG, M., LIU-YI, P., ZHANG, Z., SCHMIDT-ZACHMANN, M., KESSLER, B. M., RATCLIFFE, P. J., PRESTON, G. M., COLEMAN, M. L. & SCHOFIELD, C. J. 2012a. Oxygenase-catalyzed ribosome hydroxylation occurs in prokaryotes and humans. *Nat Chem Biol,* 8**,** 960-962.
GE, W., WOLF, A., FENG, T., HO, C. H., SEKIRNIK, R., ZAYER, A., GRANATINO, N., COCKMAN, M. E., LOENARZ, C., LOIK, N. D., HARDY, A. P., CLARIDGE, T. D. W., HAMED, R. B.,

CHOWDHURY, R., GONG, L., ROBINSON, C. V., TRUDGIAN, D. C., JIANG, M., MACKEEN, M. M., MCCULLAGH, J. S., GORDIYENKO, Y., THALHAMMER, A., YAMAMOTO, A., YANG, M., LIU-YI, P., ZHANG, Z., SCHMIDT-ZACHMANN, M., KESSLER, B. M., RATCLIFFE, P. J., PRESTON, G. M., COLEMAN, M. L. & SCHOFIELD, C. J. 2012b. Oxygenase-catalyzed ribosome hydroxylation occurs in prokaryotes and humans. *Nat Chem Biol,* 8**,** 960-962.

GERKEN, T., GIRARD, C. A., TUNG, Y. C., WEBBY, C. J., SAUDEK, V., HEWITSON, K. S., YEO, G. S., MCDONOUGH, M. A., CUNLIFFE, S., MCNEILL, L. A., GALVANOVSKIS, J., RORSMAN, P., ROBINS, P., PRIEUR, X., COLL, A. P., MA, M., JOVANOVIC, Z., FAROOQI, I. S., SEDGWICK, B., BARROSO, I., LINDAHL, T., PONTING, C. P., ASHCROFT, F. M., O'RAHILLY, S. & SCHOFIELD, C. J. 2007. The obesity-associated FTO gene encodes a 2-oxoglutarate-dependent nucleic acid demethylase. *Science (New York, N.Y.),* 318**,** 1469-72.

GERLINGER M, ROWAN AJ, HORSWELL S, LARKIN J, ENDESFELDER D, GRONROOS E , ET AL. 2012. Intratumor heterogeneity and branched evolution revealed by multiregion sequencing. N Engl J Med ;366:883-92

GETZ, M. J., ELDER, P. K., BENZ, E. W., JR., STEPHENS, R. E. & MOSES, H. L. 1976. Effect of cell proliferation on levels and diversity of poly(A)-containing mRNA. *Cell,* 7**,** 255 -65.

GINGRAS, A. C., RAUGHT, B. & SONENBERG, N. 1999. eIF4 initiation factors: effectors of mRNA recruitment to ribosomes and regulators of translation. *Annu Rev Biochem,* 68**,** 913-63.

GOH, S. H., HONG, S. H., LEE, B.-C., JU, M. H., JEONG, J. S., CHO, Y. R., KIM, I. H. & LEE, Y. S. 2011. *EIF3m expression influences the regulation of tumorigenesis-related genes in human colon cancer*.

GOLDSTEIN, J. L., BEAUDET, A. L. & CASKEY, C. T. 1970. Peptide chain termination with mammalian release factor. *Proc Natl Acad Sci U S A,* 67**,** 99-106.

GOODARZI, H., NGUYEN, H. C. B., ZHANG, S., DILL, B. D., MOLINA, H. & TAVAZOIE, S. F. 2016. Modulated Expression of Specific tRNAs Drives Gene Expression and Cancer Progression. *Cell,* 165**,** 1416-1427.

GRENTZMANN, G., GESTELAND, R. F. & ATKINS, J. F. 2000. Dual-luciferase reporter system. Google Patents.

GU, Y. Z., MORAN, S. M., HOGENESCH, J. B., WARTMAN, L. & BRADFIELD, C. A. 1998. Molecular characterization and chromosomal localization of a third alpha-class hypoxia inducible factor subunit, HIF3alpha. *Gene Expr,* 7**,** 205-13.

GUO, J. U., SU, Y., ZHONG, C., MING, G. L. & SONG, H. 2011. Hydroxylation of 5-methylcytosine by TET1 promotes active DNA demethylation in the adult brain. *Cell,* 145**,** 423-434.

HAAG, S., SLOAN, K. E., RANJAN, N., WARDA, A. S., KRETSCHMER, J., BLESSING, C., HUBNER, B., SEIKOWSKI, J., DENNERLEIN, S., REHLING, P., RODNINA, M. V., HOBARTNER, C. & BOHNSACK, M. T. 2016. NSUN3 and ABH1 modify the wobble position of mt-tRNAMet to expand codon recognition in mitochondrial translation. *EMBO J,* 35**,** 2104-2119.

HAMANAKA, R. B., BENNETT, B. S., CULLINAN, S. B. & DIEHL, J. A. 2005. PERK and GCN2 Contribute to eIF2α Phosphorylation and Cell Cycle Arrest after Activation of the Unfolded Protein Response Pathway. *Molecular Biology of the Cell,* 16**,** 5493-5501.

HARDING, H. P., NOVOA, I., ZHANG, Y., ZENG, H., WEK, R., SCHAPIRA, M. & RON, D. 2000a. Regulated translation initiation controls stress-induced gene expression in mammalian cells. *Mol Cell,* 6**,** 1099-108.

HARDING, H. P., ZHANG, Y., BERTOLOTTI, A., ZENG, H. & RON, D. 2000b. Perk is essential for translational regulation and cell survival during the unfolded protein response. *Mol Cell,* 5**,** 897-904.

HARRIS, M. N., OZPOLAT, B., ABDI, F., GU, S., LEGLER, A., MAWUENYEGA, K. G., TIRADO-GOMEZ, M., LOPEZ-BERESTEIN, G. & CHEN, X. 2004. Comparative proteomic analysis of all-trans-retinoic acid treatment reveals systematic posttranscriptional control mechanisms in acute promyelocytic leukemia. *Blood,* 104**,** 1314-23.

HAVIV, F., BRADLEY, M. F., KALVIN, D. M., SCHNEIDER, A. J., DAVIDSON, D. J., MAJEST, S. M., MCKAY, L. M., HASKELL, C. J., BELL, R. L., NGUYEN, B., MARSH, K. C., SURBER, B. W., UCHIC, J. T., FERRERO, J., WANG, Y. C., LEAL, J., RECORD, R. D., HODDE, J., BADYLAK, S. F., LESNIEWSKI, R. R. & HENKIN, J. 2005. Thrombospondin-1 mimetic peptide inhibitors of angiogenesis and tumor growth: design, synthesis, and optimization of pharmacokinetics and biological activities. *J Med Chem,* 48**,** 2838-46.

HE, J., NGUYEN, A. T. & ZHANG, Y. 2011a. *KDM2b/JHDM1b, an H3K36me2-specific demethylase, is required for initiation and maintenance of acute myeloid leukemia*.

HE, Y.-F., LI, B.-Z., LI, Z., LIU, P., WANG, Y., TANG, Q., DING, J., JIA, Y., CHEN, Z., LI, L., SUN, Y., LI, X., DAI, Q., SONG, C.-X., ZHANG, K., HE, C. & XU, G.-L. 2011b. Tet-Mediated Formation of 5-Carboxylcytosine and Its Excision by TDG in Mammalian DNA. *Science,* 333**,** 1303-1307.

HEIDBREDER, M., QADRI, F., JOHREN, O., DENDORFER, A., DEPPING, R., FROHLICH, F., WAGNER, K. F. & DOMINIAK, P. 2007. Non-hypoxic induction of HIF-3alpha by 2-deoxy-D-glucose and insulin. *Biochem Biophys Res Commun,* 352**,** 437-43.

HEIER, C. R. & DIDONATO, C. J. 2009. Translational readthrough by the aminoglycoside geneticin (G418) modulates SMN stability in vitro and improves motor function in SMA mice in vivo. *Hum Mol Genet,* 18**,** 1310-22.

HEISS, N. S., KNIGHT, S. W., VULLIAMY, T. J., KLAUCK, S. M., WIEMANN, S., MASON, P. J., POUSTKA, A. & DOKAL, I. 1998. X-linked dyskeratosis congenita is caused by mutations in a highly conserved gene with putative nucleolar functions. *Nat Genet,* 19**,** 32-8.

HETZ, C. 2012. The unfolded protein response: controlling cell fate decisions under ER stress and beyond. *Nat Rev Mol Cell Biol,* 13**,** 89-102.

HIKIJI, T., NORISADA, J., HIRATA, Y., OKUDA, K., NAGASAWA, H., ISHIGAKI, S., SOBUE, G., KIUCHI, K. & OH-HASHI, K. 2015. A highly sensitive assay of IRE1 activity using the small luciferase NanoLuc: Evaluation of ALS-related genetic and pathological factors. *Biochem Biophys Res Commun,* 463**,** 881-7.

HONG, X., ZANG, J., WHITE, J., WANG, C., PAN, C. H., ZHAO, R., MURPHY, R. C., DAI, S., HENSON, P., KAPPLER, J. W., HAGMAN, J. & ZHANG, G. 2010a. Interaction of JMJD6 with single-stranded RNA. *Proc Natl Acad Sci U S A,* 107**,** 14568-72.

HONG, X., ZANG, J., WHITE, J., WANG, C., PAN, C. H., ZHAO, R., MURPHY, R. C., DAI, S., HENSON, P., KAPPLER, J. W., HAGMAN, J. & ZHANG, G. 2010b. Interaction of JMJD6 with single-stranded RNA. *Proceedings of the National Academy of Sciences of the United States of America,* 107**,** 14568-72.

HORTON, J. R., UPADHYAY, A. K., QI, H. H., ZHANG, X., SHI, Y. & CHENG, X. 2010. Enzymatic and structural insights for substrate specificity of a family of jumonji histone lysine demethylases. *Nat Struct Mol Biol,* 17**,** 38-43.

HSIA, D. A., TEPPER, C. G., POCHAMPALLI, M. R., HSIA, E. Y., IZUMIYA, C., HUERTA, S. B., WRIGHT, M. E., CHEN, H. W., KUNG, H. J. & IZUMIYA, Y. 2010. KDM8, a H3K36me2 histone demethylase that acts in the cyclin A1 coding region to regulate cancer cell proliferation. *Proceedings of the National Academy of Sciences of the United States of America,* 107**,** 9671-6.

HU, Y.-J. & IMBALZANO, A. N. 2016. Global gene expression profiling of JMJD6- and JMJD4-depleted mouse NIH3T3 fibroblasts. *Scientific Data,* 3**,** 160022.

HU, Z., GOMES, I., HORRIGAN, S. K., KRAVARUSIC, J., MAR, B., ARBIEVA, Z., CHYNA, B., FULTON, N., EDASSERY, S., RAZA, A. & WESTBROOK, C. A. 2001. A novel nuclear

protein, 5qNCA (LOC51780) is a candidate for the myeloid leukemia tumor suppressor gene on chromosome 5 band q31. *Oncogene,* 20**,** 6946-54.

HUANG, J., ZHAO, Q., MOONEY, S. M. & LEE, F. S. 2002. Sequence determinants in hypoxia-inducible factor-1alpha for hydroxylation by the prolyl hydroxylases PHD1, PHD2, and PHD3. *J Biol Chem,* 277**,** 39792-800.

HYMAN, E., KAURANIEMI, P., HAUTANIEMI, S., WOLF, M., MOUSSES, S., ROZENBLUM, E., RINGNER, M., SAUTER, G., MONNI, O., ELKAHLOUN, A., KALLIONIEMI, O. P. & KALLIONIEMI, A. 2002. Impact of DNA amplification on gene expression patterns in breast cancer. *Cancer Res,* 62**,** 6240-5.

ILES, M. M., LAW, M. H., STACEY, S. N., HAN, J., FANG, S., PFEIFFER, R., HARLAND, M., MACGREGOR, S., TAYLOR, J. C., ABEN, K. K., AKSLEN, L. A., AVRIL, M. F., AZIZI, E., BAKKER, B., BENEDIKTSDOTTIR, K. R., BERGMAN, W., SCARRA, G. B., BROWN, K. M., CALISTA, D., CHAUDRU, V., FARGNOLI, M. C., CUST, A. E., DEMENAIS, F., DE WAAL, A. C., DEBNIAK, T., ELDER, D. E., FRIEDMAN, E., GALAN, P., GHIORZO, P., GILLANDERS, E. M., GOLDSTEIN, A. M., GRUIS, N. A., HANSSON, J., HELSING, P., HOCEVAR, M., HOIOM, V., HOPPER, J. L., INGVAR, C., JANSSEN, M., JENKINS, M. A., KANETSKY, P. A., KIEMENEY, L. A., LANG, J., LATHROP, G. M., LEACHMAN, S., LEE, J. E., LUBINSKI, J., MACKIE, R. M., MANN, G. J., MARTIN, N. G., MAYORDOMO, J. I., MOLVEN, A., MULDER, S., NAGORE, E., NOVAKOVIC, S., OKAMOTO, I., OLAFSSON, J. H., OLSSON, H., PEHAMBERGER, H., PERIS, K., GRASA, M. P., PLANELLES, D., PUIG, S., PUIG-BUTILLE, J. A., RANDERSON-MOOR, J., REQUENA, C., RIVOLTINI, L., RODOLFO, M., SANTINAMI, M., SIGURGEIRSSON, B., SNOWDEN, H., SONG, F., SULEM, P., THORISDOTTIR, K., TUOMINEN, R., VAN BELLE, P., VAN DER STOEP, N., VAN ROSSUM, M. M., WEI, Q., WENDT, J., ZELENIKA, D., ZHANG, M., LANDI, M. T., THORLEIFSSON, G., BISHOP, D. T., AMOS, C. I., HAYWARD, N. K., STEFANSSON, K., BISHOP, J. A. & BARRETT, J. H. 2013. A variant in FTO shows association with melanoma risk not due to BMI. *Nature genetics,* 45**,** 428-32, 432e1.

INAGAKI, Y., BLOUIN, C., DOOLITTLE, W. F. & ROGER, A. J. 2002. Convergence and constraint in eukaryotic release factor 1 (eRF1) domain 1: the evolution of stop codon specificity. *Nucleic Acids Res,* 30**,** 532-44.

INGOLIA, N. T., GHAEMMAGHAMI, S., NEWMAN, J. R. & WEISSMAN, J. S. 2009. Genome-wide analysis in vivo of translation with nucleotide resolution using ribosome profiling. *Science,* 324**,** 218-23.

ISHIZAKI, H., YANO, H., TSUNEOKA, M., OGASAWARA, S., AKIBA, J., NISHIDA, N., KOJIRO, S., FUKAHORI, S., MORIYA, F., MATSUOKA, K. & KOJIRO, M. 2007. Overexpression of the myc target gene Mina53 in advanced renal cell carcinoma. *Pathol Int,* 57**,** 672-80.

JAAKKOLA, P. M. & RANTANEN, K. 2013. The regulation, localization, and functions of oxygen-sensing prolyl hydroxylase PHD3. *Biol Chem,* 394**,** 449-57.

JACKSON, R. J., HELLEN, C. U. & PESTOVA, T. V. 2010. The mechanism of eukaryotic translation initiation and principles of its regulation. *Nat Rev Mol Cell Biol,* 11**,** 113-27.

JACOBSSON, J. A., KLOVINS, J., KAPA, I., DANIELSSON, P., SVENSSON, V., RIDDERSTRALE, M., GYLLENSTEN, U., MARCUS, C., FREDRIKSSON, R. & SCHIOTH, H. B. 2008. Novel genetic variant in FTO influences insulin levels and insulin resistance in severely obese children and adolescents. *Int J Obes (Lond),* 32**,** 1730-5.

JAO, D. L. & CHEN, K. Y. 2006. Tandem affinity purification revealed the hypusine-dependent binding of eukaryotic initiation factor 5A to the translating 80S ribosomal complex. *J Cell Biochem,* 97**,** 583-98.

JAUHIAINEN, A., THOMSEN, C., STROMBOM, L., GRUNDEVIK, P., ANDERSSON, C., DANIELSSON, A., ANDERSSON, M. K., NERMAN, O., RORKVIST, L., STAHLBERG, A. &

AMAN, P. 2012. Distinct cytoplasmic and nuclear functions of the stress induced protein DDIT3/CHOP/GADD153. *PLoS One,* 7**,** e33208.
JIA, G., FU, Y., ZHAO, X., DAI, Q., ZHENG, G., YANG, Y., YI, C., LINDAHL, T., PAN, T., YANG, Y.-G. & HE, C. 2011. N6-Methyladenosine in nuclear RNA is a major substrate of the obesity-associated FTO. *Nat Chem Biol,* 7**,** 885-887.
JIANG, H.-Y. & WEK, RONALD C. 2005. GCN2 phosphorylation of eIF2α activates NF-κB in response to UV irradiation. *Biochemical Journal,* 385**,** 371-380.
JOHANNESSEN, T. C., PRESTEGARDEN, L., GRUDIC, A., HEGI, M. E., TYSNES, B. B. & BJERKVIG, R. 2013. The DNA repair protein ALKBH2 mediates temozolomide resistance in human glioblastoma cells. *Neuro-oncology,* 15**,** 269-78.
JOHANSSON, C., TUMBER, A., CHE, K., CAIN, P., NOWAK, R., GILEADI, C. & OPPERMANN, U. 2014. The roles of Jumonji-type oxygenases in human disease. *Epigenomics,* 6**,** 89-120.
JOHNSON, L. F., LEVIS, R., ABELSON, H. T., GREEN, H. & PENMAN, S. 1976. Changes in RNA in relation to growth of the fibroblast. IV. Alterations in theproduction and processing of mRNA and rRNA in resting and growing cells. *J Cell Biol,* 71**,** 933-8.
JOUSSE, C., DEVAL, C., MAURIN, A. C., PARRY, L., CHERASSE, Y., CHAVEROUX, C., LEFLOCH, R., LENORMAND, P., BRUHAT, A. & FAFOURNOUX, P. 2007. TRB3 inhibits the transcriptional activation of stress-regulated genes by a negative feedback on the ATF4 pathway. *J Biol Chem,* 282**,** 15851-61.
KALLMEYER, A. K., KEELING, K. M. & BEDWELL, D. M. 2006. Eukaryotic Release Factor 1 Phosphorylation by CK2 Protein Kinase Is Dynamic but Has Little Effect on the Efficiency of Translation Termination in Saccharomyces cerevisiae. *Eukaryotic Cell,* 5**,** 1378-1387.
KANDOTH, C., MCLELLAN, M. D., VANDIN, F., YE, K., NIU, B., LU, C., XIE, M., ZHANG, Q., MCMICHAEL, J. F., WYCZALKOWSKI, M. A., LEISERSON, M. D. M., MILLER, C. A., WELCH, J. S., WALTER, M. J., WENDL, M. C., LEY, T. J., WILSON, R. K., RAPHAEL, B. J. & DING, L. 2013. Mutational landscape and significance across 12 major cancer types. *Nature,* 502**,** 333-339.
KANEKO, S., BONASIO, R., SALDANA-MEYER, R., YOSHIDA, T., SON, J., NISHINO, K., UMEZAWA, A. & REINBERG, D. 2014. Interactions between JARID2 and noncoding RNAs regulate PRC2 recruitment to chromatin. *Molecular cell,* 53**,** 290-300.
KASHIMA, I., YAMASHITA, A., IZUMI, N., KATAOKA, N., MORISHITA, R., HOSHINO, S., OHNO, M., DREYFUSS, G. & OHNO, S. 2006. Binding of a novel SMG-1-Upf1-eRF1-eRF3 complex (SURF) to the exon junction complex triggers Upf1 phosphorylation and nonsense-mediated mRNA decay. *Genes Dev,* 20**,** 355-67.
KATO, M., ARAISO, Y., NOMA, A., NAGAO, A., SUZUKI, T., ISHITANI, R. & NUREKI, O. 2011a. Crystal structure of a novel JmjC-domain-containing protein, TYW5, involved in tRNA modification. *Nucleic Acids Res,* 39**,** 1576-85.
KATO, M., ARAISO, Y., NOMA, A., NAGAO, A., SUZUKI, T., ISHITANI, R. & NUREKI, O. 2011b. Crystal structure of a novel JmjC-domain-containing protein, TYW5, involved in tRNA modification. *Nucleic acids research,* 39**,** 1576-85.
KEVIL, C. G., DE BENEDETTI, A., PAYNE, D. K., COE, L. L., LAROUX, F. S. & ALEXANDER, J. S. 1996. Translational regulation of vascular permeability factor by eukaryotic initiation factor 4E: implications for tumor angiogenesis. *Int J Cancer,* 65**,** 785-90.
KIM, J. H., LEE, S. M., LEE, J. H., CHUN, S., KANG, B. H., KWAK, S., ROE, J. S., KIM, T. W., KIM, H., KIM, W. H., CHO, E. J. & YOUN, H. D. 2015. OGFOD1 is required for breast cancer cell proliferation and is associated with poor prognosis in breast cancer. *Oncotarget,* 6**,** 19528-41.
KIM, J. Y., KIM, K. B., EOM, G. H., CHOE, N., KEE, H. J., SON, H. J., OH, S. T., KIM, D. W., PAK, J. H., BAEK, H. J., KOOK, H., HAHN, Y., KOOK, H., CHAKRAVARTI, D. & SEO, S. B. 2012.

KDM3B is the H3K9 demethylase involved in transcriptional activation of lmo2 in leukemia. *Molecular and cellular biology,* 32**,** 2917-33.

KING, O. N., LI, X. S., SAKURAI, M., KAWAMURA, A., ROSE, N. R., NG, S. S., QUINN, A. M., RAI, G., MOTT, B. T., BESWICK, P., KLOSE, R. J., OPPERMANN, U., JADHAV, A., HEIGHTMAN, T. D., MALONEY, D. J., SCHOFIELD, C. J. & SIMEONOV, A. 2010. Quantitative high-throughput screening identifies 8-hydroxyquinolines as cell-active histone demethylase inhibitors. *PLoS One,* 5**,** e15535.

KLOSE, R. J., KALLIN, E. M. & ZHANG, Y. 2006. JmjC-domain-containing proteins and histone demethylation. *Nat Rev Genet,* 7**,** 715-27.

KNOWLES, H. J., RAVAL, R. R., HARRIS, A. L. & RATCLIFFE, P. J. 2003. Effect of ascorbate on the activity of hypoxia-inducible factor in cancer cells. *Cancer Res,* 63**,** 1764-8.

KO, M., HUANG, Y., JANKOWSKA, A. M., PAPE, U. J., TAHILIANI, M., BANDUKWALA, H. S., AN, J., LAMPERTI, E. D., KOH, K. P., GANETZKY, R., LIU, X. S., ARAVIND, L., AGARWAL, S., MACIEJEWSKI, J. P. & RAO, A. 2010. Impaired hydroxylation of 5-methylcytosine in myeloid cancers with mutant TET2. *Nature,* 468**,** 839-43.

KOHLI, R. M. & ZHANG, Y. 2013. TET enzymes, TDG and the dynamics of DNA demethylation. *Nature,* 502**,** 472-479.

KOIKE, K., UEDA, Y., HASE, H., KITAE, K., FUSAMAE, Y., MASAI, S., INAGAKI, T., SAIGO, Y., HIRASAWA, S., NAKAJIMA, K., OHSHIO, I., MAKINO, Y., KONISHI, N., YAMAMOTO, H. & TSUJIKAWA, K. 2012. anti-tumor effect of AlkB homolog 3 knockdown in hormone-independent prostate cancer cells. *Current cancer drug targets,* 12**,** 847-56.

KOLOSOV, P., FROLOVA, L., SEIT-NEBI, A., DUBOVAYA, V., KONONENKO, A., OPARINA, N., JUSTESEN, J., EFIMOV, A. & KISSELEV, L. 2005. Invariant amino acids essential for decoding function of polypeptide release factor eRF1. *Nucleic Acids Res,* 33**,** 6418-25.

KOMIYA, K., SUEOKA-ARAGANE, N., SATO, A., HISATOMI, T., SAKURAGI, T., MITSUOKA, M., SATO, T., HAYASHI, S., IZUMI, H., TSUNEOKA, M. & SUEOKA, E. 2010. Expression of Mina53, a novel c-Myc target gene, is a favorable prognostic marker in early stage lung cancer. *Lung Cancer,* 69**,** 232-8.

KONECKI, D. S., AUNE, K. C., TATE, W. & CASKEY, C. T. 1977. Characterization of reticulocyte release factor. *J Biol Chem,* 252**,** 4514-20.

KONONENKO, A. V., MITKEVICH, V. A., DUBOVAYA, V. I., KOLOSOV, P. M., MAKAROV, A. A. & KISSELEV, L. L. 2008. Role of the individual domains of translation termination factor eRF1 in GTP binding to eRF3. *Proteins,* 70**,** 388-93.

KOOISTRA, S. M. & HELIN, K. 2012a. Molecular mechanisms and potential functions of histone demethylases. *Nature reviews. Molecular cell biology,* 13**,** 297-311.

KOOISTRA, S. M. & HELIN, K. 2012b. Molecular mechanisms and potential functions of histone demethylases. *Nat Rev Mol Cell Biol,* 13**,** 297-311.

KOROMILAS, A. E. 2015. Roles of the translation initiation factor eIF2alpha serine 51 phosphorylation in cancer formation and treatment. *Biochim Biophys Acta,* 1849**,** 871-80.

KOROMILAS, A. E. & MOUNIR, Z. 2013. Control of oncogenesis by eIF2alpha phosphorylation: implications in PTEN and PI3K-Akt signaling and tumor treatment. *Future Oncol,* 9**,** 1005-15.

KOZAK, M. 1991. Structural features in eukaryotic mRNAs that modulate the initiation of translation. *J Biol Chem,* 266**,** 19867-70.

KUO, M. W., WANG, C. H., WU, H. C., CHANG, S. J. & CHUANG, Y. J. 2011. Soluble THSD7A is an N-glycoprotein that promotes endothelial cell migration and tube formation in angiogenesis. *PLoS One,* 6**,** e29000.

KUSEVIC, D., KUDITHIPUDI, S. & JELTSCH, A. 2016. Substrate Specificity of the HEMK2 Protein Glutamine Methyltransferase and Identification of Novel Substrates. *J Biol Chem,* 291**,** 6124-33.

LABBE, R. M., HOLOWATYJ, A. & YANG, Z. Q. 2013. Histone lysine demethylase (KDM) subfamily 4: structures, functions and therapeutic potential. *Am J Transl Res,* 6**,** 1-15.

LAI, M. D. & XU, J. 2007. Ribosomal proteins and colorectal cancer. *Curr Genomics,* 8**,** 43-9.

LANDAU, G., BERCOVICH, Z., PARK, M.-H. & KAHANA, C. 2010. *The Role of Polyamines in Supporting Growth of Mammalian Cells Is Mediated through Their Requirement for Translation Initiation and Elongation*.

LAZARIS-KARATZAS, A. & SONENBERG, N. 1992. The mRNA 5' cap-binding protein, eIF-4E, cooperates with v-myc or E1A in the transformation of primary rodent fibroblasts. *Mol Cell Biol,* 12**,** 1234-8.

LEE, A. S., KRANZUSCH, P. J. & CATE, J. H. 2015. eIF3 targets cell-proliferation messenger RNAs for translational activation or repression. *Nature,* 522**,** 111-4.

LEE, D. H., JIN, S. G., CAI, S., CHEN, Y., PFEIFER, G. P. & O'CONNOR, T. R. 2005a. Repair of methylation damage in DNA and RNA by mammalian AlkB homologues. *The Journal of biological chemistry,* 280**,** 39448-39459.

LEE, D. H., JIN, S. G., CAI, S., CHEN, Y., PFEIFER, G. P. & O'CONNOR, T. R. 2005b. Repair of methylation damage in DNA and RNA by mammalian AlkB homologues. *The Journal of biological chemistry,* 280**,** 39448-59.

LEE, Y. F., MILLER, L. D., CHAN, X. B., BLACK, M. A., PANG, B., ONG, C. W., SALTO-TELLEZ, M., LIU, E. T. & DESAI, K. V. 2012. JMJD6 is a driver of cellular proliferation and motility and a marker of poor prognosis in breast cancer. *Breast cancer research : BCR,* 14**,** R85.

LI, B. D., LIU, L., DAWSON, M. & DE BENEDETTI, A. 1997. Overexpression of eukaryotic initiation factor 4E (eIF4E) in breast carcinoma. *Cancer,* 79**,** 2385-90.

LI, G. & RICE, C. M. 1993. The signal for translational readthrough of a UGA codon in Sindbis virus RNA involves a single cytidine residue immediately downstream of the termination codon. *J Virol,* 67**,** 5062-7.

LI, P., GAO, S., WANG, L., YU, F., LI, J., WANG, C., LI, J. & WONG, J. 2013. ABH2 couples regulation of ribosomal DNA transcription with DNA alkylation repair. *Cell Rep,* 4**,** 817-29.

LI, Z., WENG, H., SU, R., WENG, X., ZUO, Z., LI, C., HUANG, H., NACHTERGAELE, S., DONG, L., HU, C., QIN, X., TANG, L., WANG, Y., HONG, G. M., HUANG, H., WANG, X., CHEN, P., GURBUXANI, S., ARNOVITZ, S., LI, Y., LI, S., STRONG, J., NEILLY, M. B., LARSON, R. A., JIANG, X., ZHANG, P., JIN, J., HE, C. & CHEN, J. 2017. FTO Plays an Oncogenic Role in Acute Myeloid Leukemia as a N6-Methyladenosine RNA Demethylase. *Cancer Cell,* 31**,** 127-141.

LIAO, Y., SMYTH, G. K. & SHI, W. 2013. The Subread aligner: fast, accurate and scalable read mapping by seed-and-vote. *Nucleic Acids Res,* 41**,** e108.

LISY, K. & PEET, D. J. 2008. Turn me on: regulating HIF transcriptional activity. *Cell Death Differ,* 15**,** 642-9.

LIU, F., CLARK, W., LUO, G., WANG, X., FU, Y., WEI, J., WANG, X., HAO, Z., DAI, Q., ZHENG, G., MA, H., HAN, D., EVANS, M., KLUNGLAND, A., PAN, T. & HE, C. 2016. ALKBH1-Mediated tRNA Demethylation Regulates Translation. *Cell,* 167**,** 1897.

LIU, P., NIE, S., LI, B., YANG, Z. Q., XU, Z. M., FEI, J., LIN, C., ZENG, R. & XU, G. L. 2010. Deficiency in a glutamine-specific methyltransferase for release factor causes mouse embryonic lethality. *Mol Cell Biol,* 30**,** 4245-53.

LIU, Z., LV, Y., ZHAO, N., GUAN, G. & WANG, J. 2015. Protein kinase R-like ER kinase and its role in endoplasmic reticulum stress-decided cell fate. *Cell Death Dis,* 6**,** e1822.

LOENARZ, C. & SCHOFIELD, C. J. 2011. Physiological and biochemical aspects of hydroxylations and demethylations catalyzed by human 2-oxoglutarate oxygenases. *Trends Biochem Sci,* 36**,** 7-18.

LOENARZ, C., SEKIRNIK, R., THALHAMMER, A., GE, W., SPIVAKOVSKY, E., MACKEEN, M. M., MCDONOUGH, M. A., COCKMAN, M. E., KESSLER, B. M., RATCLIFFE, P. J., WOLF, A. & SCHOFIELD, C. J. 2014. Hydroxylation of the eukaryotic ribosomal decoding center affects translational accuracy. *Proceedings of the National Academy of Sciences,* 111**,** 4019-4024.

LOUGHRAN, G., CHOU, M. Y., IVANOV, I. P., JUNGREIS, I., KELLIS, M., KIRAN, A. M., BARANOV, P. V. & ATKINS, J. F. 2014. Evidence of efficient stop codon readthrough in four mammalian genes. *Nucleic Acids Res,* 42**,** 8928-38.

LU, Y., CHANG, Q., ZHANG, Y., BEEZHOLD, K., ROJANASAKUL, Y., ZHAO, H., CASTRANOVA, V., SHI, X. & CHEN, F. 2009. Lung cancer-associated JmjC domain protein mdig suppresses formation of tri-methyl lysine 9 of histone H3. *Cell Cycle,* 8**,** 2101-9.

LUNDGREN DH, HWANG SI, WU L, HAN DK. 2010. Role of spectral counting in quantitative proteomics. *Expert Rev Proteomics*. 7, 39–53.

MAKINO, Y., CAO, R., SVENSSON, K., BERTILSSON, G., ASMAN, M., TANAKA, H., CAO, Y., BERKENSTAM, A. & POELLINGER, L. 2001. Inhibitory PAS domain protein is a negative regulator of hypoxia-inducible gene expression. *Nature,* 414**,** 550-4.

MAKINO, Y., KANOPKA, A., WILSON, W. J., TANAKA, H. & POELLINGER, L. 2002. Inhibitory PAS domain protein (IPAS) is a hypoxia-inducible splicing variant of the hypoxia-inducible factor-3alpha locus. *J Biol Chem,* 277**,** 32405-8.

MAKINO, Y., UENISHI, R., OKAMOTO, K., ISOE, T., HOSONO, O., TANAKA, H., KANOPKA, A., POELLINGER, L., HANEDA, M. & MORIMOTO, C. 2007. Transcriptional up-regulation of inhibitory PAS domain protein gene expression by hypoxia-inducible factor 1 (HIF-1): a negative feedback regulatory circuit in HIF-1-mediated signaling in hypoxic cells. *J Biol Chem,* 282**,** 14073-82.

MALTA-VACAS, J., CHAUVIN, C., GONCALVES, L., NAZARE, A., CARVALHO, C., MONTEIRO, C., BAGREL, D., JEAN-JEAN, O. & BRITO, M. 2009a. eRF3a/GSPT1 12-GGC allele increases the susceptibility for breast cancer development. *Oncol Rep,* 21**,** 1551-8.

MALTA-VACAS, J., NOLASCO, S., MONTEIRO, C., SOARES, H. & BRITO, M. 2009b. *Translation termination and protein folding pathway genes are not correlated in gastric cancer*.

MANTRI, M., WEBBY, C. J., LOIK, N. D., HAMED, R. B., NIELSEN, M. L., MCDONOUGH, M. A., MCCULLAGH, J. S. O., BOTTGER, A., SCHOFIELD, C. J. & WOLF, A. 2012a. Self-hydroxylation of the splicing factor lysyl hydroxylase, JMJD6. *MedChemComm,* 3**,** 80-85.

MANTRI, M., ZHANG, Z., MCDONOUGH, M. A. & SCHOFIELD, C. J. 2012b. Autocatalysed oxidative modifications to 2-oxoglutarate dependent oxygenases. *FEBS J,* 279**,** 1563-75.

MARECHAL, V., ELENBAAS, B., PIETTE, J., NICOLAS, J. C. & LEVINE, A. J. 1994. The ribosomal L5 protein is associated with mdm-2 and mdm-2-p53 complexes. *Mol Cell Biol,* 14**,** 7414-20.

MARINTCHEV, A. & WAGNER, G. 2004. Translation initiation: structures, mechanisms and evolution. *Q Rev Biophys,* 37**,** 197-284.

MARION, R. M., REGEV, A., SEGAL, E., BARASH, Y., KOLLER, D., FRIEDMAN, N. & O'SHEA, E. K. 2004. Sfp1 is a stress- and nutrient-sensitive regulator of ribosomal protein gene expression. *Proc Natl Acad Sci U S A,* 101**,** 14315-22.

MARTIN, D. E., SOULARD, A. & HALL, M. N. 2004. TOR regulates ribosomal protein gene expression via PKA and the Forkhead transcription factor FHL1. *Cell,* 119**,** 969-79.

MASSON, N., APPELHOFF, R. J., TUCKERMAN, J. R., TIAN, Y.-M., DEMOL, H., PUYPE, M., VANDEKERCKHOVE, J., RATCLIFFE, P. J. & PUGH, C. W. 2004. The HIF prolyl

hydroxylase PHD3 is a potential substrate of the TRiC chaperonin. *FEBS Letters,* 570**,** 166-170.

MATHEWS, M. B. & HERSHEY, J. W. 2015. The translation factor eIF5A and human cancer. *Biochim Biophys Acta,* 1849**,** 836-44.

MAUER, J., LUO, X., BLANJOIE, A., JIAO, X., GROZHIK, A. V., PATIL, D. P., LINDER, B., PICKERING, B. F., VASSEUR, J. J., CHEN, Q., GROSS, S. S., ELEMENTO, O., DEBART, F., KILEDJIAN, M. & JAFFREY, S. R. 2017. Reversible methylation of m6Am in the 5' cap controls mRNA stability. *Nature,* 541**,** 371-375.

MAXWELL, K. L., MITTERMAIER, A. K., FORMAN-KAY, J. D. & DAVIDSON, A. R. 1999. A simple in vivo assay for increased protein solubility. *Protein Sci,* 8**,** 1908-11.

MAYNARD, M. A., QI, H., CHUNG, J., LEE, E. H., KONDO, Y., HARA, S., CONAWAY, R. C., CONAWAY, J. W. & OHH, M. 2003. Multiple splice variants of the human HIF-3 alpha locus are targets of the von Hippel-Lindau E3 ubiquitin ligase complex. *J Biol Chem,* 278**,** 11032-40.

MCCAUGHAN, K. K., BROWN, C. M., DALPHIN, M. E., BERRY, M. J. & TATE, W. P. 1995. Translational termination efficiency in mammals is influenced by the base following the stop codon. *Proc Natl Acad Sci U S A,* 92**,** 5431-5.

MCDONOUGH, M. A., LI, V., FLASHMAN, E., CHOWDHURY, R., MOHR, C., LIENARD, B. M., ZONDLO, J., OLDHAM, N. J., CLIFTON, I. J., LEWIS, J., MCNEILL, L. A., KURZEJA, R. J., HEWITSON, K. S., YANG, E., JORDAN, S., SYED, R. S. & SCHOFIELD, C. J. 2006. Cellular oxygen sensing: Crystal structure of hypoxia-inducible factor prolyl hydroxylase (PHD2). *Proc Natl Acad Sci U S A,* 103**,** 9814-9.

MCDONOUGH, M. A., LOENARZ, C., CHOWDHURY, R., CLIFTON, I. J. & SCHOFIELD, C. J. 2010. Structural studies on human 2-oxoglutarate dependent oxygenases. *Curr Opin Struct Biol,* 20**,** 659-72.

MEMIN, E., HOQUE, M., JAIN, M. R., HELLER, D. S., LI, H., CRACCHIOLO, B., HANAUSKE-ABEL, H. M., PE'ERY, T. & MATHEWS, M. B. 2014. Blocking eIF5A modification in cervical cancer cells alters the expression of cancer-related genes and suppresses cell proliferation. *Cancer Res,* 74**,** 552-62.

MENG, Q. B., KANG, W. M., YU, J. C., LIU, Y. Q., MA, Z. Q., ZHOU, L., CUI, Q. C. & ZHOU, W. X. 2015. Overexpression of eukaryotic translation initiation factor 5A2 (EIF5A2) correlates with cell aggressiveness and poor survival in gastric cancer. *PLoS One,* 10**,** e0119229.

MILUZIO, A., BEUGNET, A., VOLTA, V. & BIFFO, S. 2009. *Eukaryotic initiation factor 6 mediates a continuum between 60S ribosome biogenesis and translation*.

MINGEOT-LECLERCQ, M. P., GLUPCZYNSKI, Y. & TULKENS, P. M. 1999. Aminoglycosides: activity and resistance. *Antimicrob Agents Chemother,* 43**,** 727-37.

MONTANARO, L., CALIENNI, M., BERTONI, S., ROCCHI, L., SANSONE, P., STORCI, G., SANTINI, D., CECCARELLI, C., TAFFURELLI, M., CARNICELLI, D., BRIGOTTI, M., BONAFÈ, M., TRERÉ, D. & DERENZINI, M. 2010. Novel Dyskerin-Mediated Mechanism of p53 Inactivation through Defective mRNA Translation. *Cancer Research,* 70**,** 4767-4777.

MORA, L., HEURGUE-HAMARD, V., CHAMP, S., EHRENBERG, M., KISSELEV, L. L. & BUCKINGHAM, R. H. 2003. The essential role of the invariant GGQ motif in the function and stability in vivo of bacterial release factors RF1 and RF2. *Mol Microbiol,* 47**,** 267-75.

MOSMANN, T. 1983. Rapid colorimetric assay for cellular growth and survival: application to proliferation and cytotoxicity assays. *J Immunol Methods,* 65**,** 55-63.

MOTTAGUI-TABAR, S., TUITE, M. F. & ISAKSSON, L. A. 1998. The influence of 5' codon context on translation termination in Saccharomyces cerevisiae. *Eur J Biochem,* 257**,** 249-54.

MYLLYHARJU, J. 2003. Prolyl 4-hydroxylases, the key enzymes of collagen biosynthesis. *Matrix Biol,* 22**,** 15-24.

NAKAMURA, Y. & ITO, K. 1998. How protein reads the stop codon and terminates translation. *Genes Cells,* 3**,** 265-78.

NANDAL, A., RUIZ, JULIO C., SUBRAMANIAN, P., GHIMIRE-RIJAL, S., SINNAMON, RUTH A., STEMMLER, TIMOTHY L., BRUICK, RICHARD K. & PHILPOTT, CAROLINE C. Activation of the HIF Prolyl Hydroxylase by the Iron Chaperones PCBP1 and PCBP2. *Cell Metabolism,* 14**,** 647-657.

NERI, F., DETTORI, D., INCARNATO, D., KREPELOVA, A., RAPELLI, S., MALDOTTI, M., PARLATO, C., PALIOGIANNIS, P. & OLIVIERO, S. 2015. TET1 is a tumour suppressor that inhibits colon cancer growth by derepressing inhibitors of the WNT pathway. *Oncogene,* 34**,** 4168-76.

NG, S. S., KAVANAGH, K. L., MCDONOUGH, M. A., BUTLER, D., PILKA, E. S., LIENARD, B. M., BRAY, J. E., SAVITSKY, P., GILEADI, O., VON DELFT, F., ROSE, N. R., OFFER, J., SCHEINOST, J. C., BOROWSKI, T., SUNDSTROM, M., SCHOFIELD, C. J. & OPPERMANN, U. 2007. Crystal structures of histone demethylase JMJD2A reveal basis for substrate specificity. *Nature,* 448**,** 87-91.

NIERHAUS, K. H. 1990. The allosteric three-site model for the ribosomal elongation cycle: features and future. *Biochemistry,* 29**,** 4997-5008.

NISHIUCHI, R., TAKAGI, J., HAYASHI, M., IDO, H., YAGI, Y., SANZEN, N., TSUJI, T., YAMADA, M. & SEKIGUCHI, K. 2006. Ligand-binding specificities of laminin-binding integrins: a comprehensive survey of laminin-integrin interactions using recombinant alpha3beta1, alpha6beta1, alpha7beta1 and alpha6beta4 integrins. *Matrix Biol,* 25**,** 189-97.

NISHIZAWA, Y., NISHIDA, N., KONNO, M., KAWAMOTO, K., ASAI, A., KOSEKI, J., TAKAHASHI, H., HARAGUCHI, N., NISHIMURA, J., HATA, T., MATSUDA, C., MIZUSHIMA, T., SATOH, T., DOKI, Y., MORI, M. & ISHII, H. 2017. Clinical Significance of Histone Demethylase NO66 in Invasive Colorectal Cancer. *Ann Surg Oncol,* 24**,** 841-849.

NOSKE, A., LINDENBERG, J. L., DARB-ESFAHANI, S., WEICHERT, W., BUCKENDAHL, A. C., ROSKE, A., SEHOULI, J., DIETEL, M. & DENKERT, C. 2008. Activation of mTOR in a subgroup of ovarian carcinomas: correlation with p-eIF-4E and prognosis. *Oncol Rep,* 20**,** 1409-17.

NOVINA, C. D., KUMAR, S., BAJPAI, U., CHERIYATH, V., ZHANG, K., PILLAI, S., WORTIS, H. H. & ROY, A. L. 1999. Regulation of nuclear localization and transcriptional activity of TFII-I by Bruton's tyrosine kinase. *Mol Cell Biol,* 19**,** 5014-24.

OHOKA, N., YOSHII, S., HATTORI, T., ONOZAKI, K. & HAYASHI, H. 2005. TRB3, a novel ER stress-inducible gene, is induced via ATF4-CHOP pathway and is involved in cell death. *EMBO J,* 24**,** 1243-55.

OKAMOTO, M., VAN STRY, M., CHUNG, L., KOYANAGI, M., SUN, X., SUZUKI, Y., OHARA, O., KITAMURA, H., HIJIKATA, A., KUBO, M. & BIX, M. 2009. Mina, an Il4 repressor, controls T helper type 2 bias. *Nat Immunol,* 10**,** 872-9.

OYADOMARI, S. & MORI, M. 2004. Roles of CHOP/GADD153 in endoplasmic reticulum stress. *Cell Death Differ,* 11**,** 381-9.

PARK, S. J., LEE, B. R., KIM, H. S., JI, Y. R., SUNG, Y. H., SHIKCHOI, K., PARK, H. D., KIM, S. H., KIM, M. O. & RYOO, Z. Y. 2016. Inhibition of Migration and Invasion by Tet-1 Overexpression in Human Lung Carcinoma H460 Cells. *Oncol Res,* 23**,** 89-98.

PASINI, D., CLOOS, P. A., WALFRIDSSON, J., OLSSON, L., BUKOWSKI, J. P., JOHANSEN, J. V., BAK, M., TOMMERUP, N., RAPPSILBER, J. & HELIN, K. 2010. JARID2 regulates binding of the Polycomb repressive complex 2 to target genes in ES cells. *Nature,* 464**,** 306-310.

PATEL, J., LANDERS, K., MORTIMER, R. H. & RICHARD, K. 2010. Regulation of hypoxia inducible factors (HIF) in hypoxia and normoxia during placental development. *Placenta,* 31**,** 951-7.

PAULIN, F. E., CAMPBELL, L. E., O'BRIEN, K., LOUGHLIN, J. & PROUD, C. G. 2001. Eukaryotic translation initiation factor 5 (eIF5) acts as a classical GTPase-activator protein. *Curr Biol,* 11**,** 55-9.

PAVELIC, Z. P., SLOCUM, H. K., RUSTUM, Y. M., CREAVEN, P. J., NOWAK, N. J., KARAKOUSIS, C., TAKITA, H. & MITTELMAN, A. 1980. Growth of cell colonies in soft agar from biopsies of different human solid tumors. *Cancer Res,* 40**,** 4151-8.

PELLETIER, J., GRAFF, J., RUGGERO, D. & SONENBERG, N. 2015. Targeting the eIF4F translation initiation complex: a critical nexus for cancer development. *Cancer Res,* 75**,** 250-63.

PERSHING, N. L., LAMPSON, B. L., BELSKY, J. A., KALTENBRUN, E., MACALPINE, D. M. & COUNTER, C. M. 2015. Rare codons capacitate Kras-driven de novo tumorigenesis. *J Clin Invest,* 125**,** 222-33.

PESTOVA, T. V. & KOLUPAEVA, V. G. 2002. The roles of individual eukaryotic translation initiation factors in ribosomal scanning and initiation codon selection. *Genes Dev,* 16**,** 2906-22.

PETROVA, A., KIKTEV, D., ASKINAZI, O., CHABELSKAYA, S., MOSKALENKO, S., ZEMLYANKO, O. & ZHOURAVLEVA, G. 2015. The translation termination factor eRF1 (Sup45p) of Saccharomyces cerevisiae is required for pseudohyphal growth and invasion. *FEMS Yeast Res,* 15**,** fov033.

PFEIFFER, S., KRÜGER, J., MAIERHOFER, A., BÖTTCHER, Y., KLÖTING, N., HAJJ, N., SCHLEINITZ, D., SCHÖN, M., DIETRICH, A., FASSHAUER, M., LOHMANN, T., DREßLER, M., STUMVOLL, M., HAAF, T., BLÜHER, M. & KOVACS, P. 2016. *Hypoxia-inducible factor 3A gene expression and methylation in adipose tissue is related to adipose tissue dysfunction*.

PINCHEIRA, R., CHEN, Q. & ZHANG, J. T. 2001. Identification of a 170-kDa protein over-expressed in lung cancers. *Br J Cancer,* 84**,** 1520-7.

PISAREVA, V. P., PISAREV, A. V., HELLEN, C. U., RODNINA, M. V. & PESTOVA, T. V. 2006. Kinetic analysis of interaction of eukaryotic release factor 3 with guanine nucleotides. *J Biol Chem,* 281**,** 40224-35.

PLOUMAKIS, A. & COLEMAN, M. L. 2015. OH, the Places You'll Go! Hydroxylation, Gene Expression, and Cancer. *Mol Cell,* 58**,** 729-41.

POLEVODA, B., SPAN, L. & SHERMAN, F. 2006. The yeast translation release factors Mrf1p and Sup45p (eRF1) are methylated, respectively, by the methyltransferases Mtq1p and Mtq2p. *J Biol Chem,* 281**,** 2562-71.

POLLARD, P., LOENARZ, C., R MOLE, D., MCDONOUGH, M., GLEADLE, J., J SCHOFIELD, C. & RATCLIFFE, P. 2008. *Regulation of Jumonji-domain-containing histone demethylases by hypoxia-inducible factor (HIF)-1??*

POOLE, E. S., BROWN, C. M. & TATE, W. P. 1995. The identity of the base following the stop codon determines the efficiency of in vivo translational termination in Escherichia coli. *EMBO J,* 14**,** 151-8.

RANGANATHAN, A. C., OJHA, S., KOURTIDIS, A., CONKLIN, D. S. & AGUIRRE-GHISO, J. A. 2008. Dual function of pancreatic endoplasmic reticulum kinase in tumor cell growth arrest and survival. *Cancer Res,* 68**,** 3260-8.

RATCLIFFE, P. J. 2013. Oxygen sensing and hypoxia signalling pathways in animals: the implications of physiology for cancer. *J Physiol,* 591**,** 2027-42.

RHODES, D. R., YU, J., SHANKER, K., DESHPANDE, N., VARAMBALLY, R., GHOSH, D., BARRETTE, T., PANDEY, A. & CHINNAIYAN, A. M. 2004. ONCOMINE: a cancer microarray database and integrated data-mining platform. *Neoplasia,* 6**,** 1-6.

RINGVOLL, J., MOEN, M. N., NORDSTRAND, L. M., MEIRA, L. B., PANG, B., BEKKELUND, A., DEDON, P. C., BJELLAND, S., SAMSON, L. D., FALNES, P. O. & KLUNGLAND, A. 2008. AlkB homologue 2-mediated repair of ethenoadenine lesions in mammalian DNA. *Cancer research,* 68**,** 4142-9.

RODNINA, M. V. & WINTERMEYER, W. 2009. Recent mechanistic insights into eukaryotic ribosomes. *Curr Opin Cell Biol,* 21**,** 435-43.

ROJAS, M., VASCONCELOS, G. & DEVER, T. E. 2015. An eIF2alpha-binding motif in protein phosphatase 1 subunit GADD34 and its viral orthologs is required to promote dephosphorylation of eIF2alpha. *Proc Natl Acad Sci U S A,* 112**,** E3466-75.

RON, D. & HABENER, J. F. 1992. CHOP, a novel developmentally regulated nuclear protein that dimerizes with transcription factors C/EBP and LAP and functions as a dominant-negative inhibitor of gene transcription. *Genes Dev,* 6**,** 439-53.

RON, D. & WALTER, P. 2007. Signal integration in the endoplasmic reticulum unfolded protein response. *Nat Rev Mol Cell Biol,* 8**,** 519-29.

ROSE, N. R., MCDONOUGH, M. A., KING, O. N., KAWAMURA, A. & SCHOFIELD, C. J. 2011. Inhibition of 2-oxoglutarate dependent oxygenases. *Chem Soc Rev,* 40**,** 4364-97.

ROSENWALD, I. B., CHEN, J.-J., WANG, S., SAVAS, L., LONDON, I. M. & PULLMAN, J. 1999. Upregulation of protein synthesis initiation factor eIF-4E is an early event during colon carcinogenesis. *Oncogene,* 18**,** 2507.

ROSSI, D., KUROSHU, R., ZANELLI, C. F. & VALENTINI, S. R. 2014. eIF5A and EF-P: two unique translation factors are now traveling the same road. *Wiley Interdiscip Rev RNA,* 5**,** 209-22.

ROSSO MD, P., CORTESINA MD, G., SANVITO MD, F., PIER CARLO MARCHISIO MD, P., ROSSO, P., CORTESINA, G., SANVITO, F., DONADINI, A., DI BENEDETTO, B., BIFFO, S. & MARCHISIO, P. 2004. *Overexpression of p27BBP in head and neck carcinomas and their lymph node metastases*.

ROY, A. L. 2012. Biochemistry and biology of the inducible multifunctional transcription factor TFII-I: 10 years later. *Gene,* 492**,** 32-41.

SAINI, P., EYLER, D. E., GREEN, R. & DEVER, T. E. 2009. Hypusine-containing protein eIF5A promotes translation elongation. *Nature,* 459**,** 118-21.

SANVITO, F., VIVOLI, F., GAMBINI, S., SANTAMBROGIO, G., CATENA, M., VIALE, E., VEGLIA, F., DONADINI, A., BIFFO, S. & MARCHISIO, P. C. 2000. Expression of a highly conserved protein, p27BBP, during the progression of human colorectal cancer. *Cancer Res,* 60**,** 510-6.

SAVITSKI, M. F. & SAVITSKI, M. M. 2010. Unbiased detection of posttranslational modifications using mass spectrometry. *Methods Mol Biol,* 673**,** 203-10.

SCHNEIDER-POETSCH, T., USUI, T., KAIDA, D. & YOSHIDA, M. 2010. Garbled messages and corrupted translations. *Nat Chem Biol,* 6**,** 189-198.

SCHODEL, J., MOLE, D. R. & RATCLIFFE, P. J. 2013. Pan-genomic binding of hypoxia-inducible transcription factors. *Biol Chem,* 394**,** 507-17.

SCHOFIELD, C. J. & RATCLIFFE, P. J. 2004. Oxygen sensing by HIF hydroxylases. *Nat Rev Mol Cell Biol,* 5**,** 343-54.

SCHUEREN, F., LINGNER, T., GEORGE, R., HOFHUIS, J., DICKEL, C., GARTNER, J. & THOMS, S. 2014. Peroxisomal lactate dehydrogenase is generated by translational readthrough in mammals. *Elife,* 3**,** e03640.

SEDGWICK, B. 2004. Repairing DNA-methylation damage. *Nature reviews. Molecular cell biology,* 5**,** 148-57.

SEIT-NEBI, A., FROLOVA, L., JUSTESEN, J. & KISSELEV, L. 2001a. Class-1 translation termination factors: invariant GGQ minidomain is essential for release activity and ribosome binding but not for stop codon recognition. *Nucleic Acids Res,* 29**,** 3982-7.

SEIT-NEBI, A., FROLOVA, L., JUSTESEN, J. & KISSELEV, L. 2001b. Class-1 translation termination factors: invariant GGQ minidomain is essential for release activity and ribosome binding but not for stop codon recognition. *Nucleic Acids Research,* 29**,** 3982-3987.

SEKIRNIK, R., ROSE, N. R., THALHAMMER, A., SEDEN, P. T., MECINOVIC, J. & SCHOFIELD, C. J. 2009. Inhibition of the histone lysine demethylase JMJD2A by ejection of structural Zn(II). *Chem Commun (Camb)***,** 6376-8.

SEMENZA, G. L. 2003. Targeting HIF-1 for cancer therapy. *Nat Rev Cancer,* 3**,** 721-32.

SEMENZA, G. L. 2010. Defining the role of hypoxia-inducible factor 1 in cancer biology and therapeutics. *Oncogene,* 29**,** 625-34.

SHAFI, R., IYER, S. P., ELLIES, L. G., O'DONNELL, N., MAREK, K. W., CHUI, D., HART, G. W. & MARTH, J. D. 2000. The O-GlcNAc transferase gene resides on the X chromosome and is essential for embryonic stem cell viability and mouse ontogeny. *Proceedings of the National Academy of Sciences of the United States of America,* 97**,** 5735-9.

SHEN, C. & KAELIN, W. G., JR. 2013. The VHL/HIF axis in clear cell renal carcinoma. *Semin Cancer Biol,* 23**,** 18-25.

SHEN, F., HUANG, W., HUANG, J. T., XIONG, J., YANG, Y., WU, K., JIA, G. F., CHEN, J., FENG, Y. Q., YUAN, B. F. & LIU, S. M. 2015. Decreased N(6)-Methyladenosine in Peripheral Blood RNA From Diabetic Patients Is Associated With FTO Expression Rather Than ALKBH5. *J Clin Endocrinol Metab,* 100**,** E148-54.

SHIMADA, K., FUJII, T., TSUJIKAWA, K., ANAI, S., FUJIMOTO, K. & KONISHI, N. 2012. ALKBH3 contributes to survival and angiogenesis of human urothelial carcinoma cells through NADPH oxidase and tweak/Fn14/VEGF signals. *Clinical cancer research : an official journal of the American Association for Cancer Research,* 18**,** 5247-55.

SHIMADA, K., NAKAMURA, M., ANAI, S., DE VELASCO, M., TANAKA, M., TSUJIKAWA, K., OUJI, Y. & KONISHI, N. 2009. A novel human AlkB homologue, ALKBH8, contributes to human bladder cancer progression. *Cancer research,* 69**,** 3157-3164.

SILVERA, D., ARJU, R., DARVISHIAN, F., LEVINE, P. H., ZOLFAGHARI, L., GOLDBERG, J., HOCHMAN, T., FORMENTI, S. C. & SCHNEIDER, R. J. 2009. Essential role for eIF4GI overexpression in the pathogenesis of inflammatory breast cancer. *Nat Cell Biol,* 11**,** 903-8.

SINGLETON, R. S., LIU-YI, P., FORMENTI, F., GE, W., SEKIRNIK, R., FISCHER, R., ADAM, J., POLLARD, P. J., WOLF, A., THALHAMMER, A., LOENARZ, C., FLASHMAN, E., YAMAMOTO, A., COLEMAN, M. L., KESSLER, B. M., WAPPNER, P., SCHOFIELD, C. J., RATCLIFFE, P. J. & COCKMAN, M. E. 2014a. OGFOD1 catalyzes prolyl hydroxylation of RPS23 and is involved in translation control and stress granule formation. *Proceedings of the National Academy of Sciences of the United States of America,* 111**,** 4031-6.

SINGLETON, R. S., LIU-YI, P., FORMENTI, F., GE, W., SEKIRNIK, R., FISCHER, R., ADAM, J., POLLARD, P. J., WOLF, A., THALHAMMER, A., LOENARZ, C., FLASHMAN, E., YAMAMOTO, A., COLEMAN, M. L., KESSLER, B. M., WAPPNER, P., SCHOFIELD, C. J., RATCLIFFE, P. J. & COCKMAN, M. E. 2014b. OGFOD1 catalyzes prolyl hydroxylation of RPS23 and is involved in translation control and stress granule formation. *Proceedings of the National Academy of Sciences of the United States of America,* 111**,** 4031-4036.

SINGLETON, R. S., LIU-YI, P., FORMENTI, F., GE, W., SEKIRNIK, R., FISCHER, R., ADAM, J., POLLARD, P. J., WOLF, A., THALHAMMER, A., LOENARZ, C., FLASHMAN, E., YAMAMOTO, A., COLEMAN, M. L., KESSLER, B. M., WAPPNER, P., SCHOFIELD, C. J., RATCLIFFE, P. J. & COCKMAN, M. E. 2014c. OGFOD1 catalyzes prolyl hydroxylation of RPS23 and is involved in translation control and stress granule formation. *Proc Natl Acad Sci U S A,* 111**,** 4031-6.

SINHA, K. M., YASUDA, H., COOMBES, M. M., DENT, S. Y. & DE CROMBRUGGHE, B. 2010a. Regulation of the osteoblast-specific transcription factor Osterix by NO66, a Jumonji family histone demethylase. *The EMBO journal,* 29**,** 68-79.

SINHA, K. M., YASUDA, H., COOMBES, M. M., DENT, S. Y. & DE CROMBRUGGHE, B. 2010b. Regulation of the osteoblast-specific transcription factor Osterix by NO66, a Jumonji family histone demethylase. *EMBO J,* 29**,** 68-79.

SOFER, A., LEI, K., JOHANNESSEN, C. M. & ELLISEN, L. W. 2005. Regulation of mTOR and cell growth in response to energy stress by REDD1. *Mol Cell Biol,* 25**,** 5834-45.

SOMERS, J., POYRY, T. & WILLIS, A. E. 2013. A perspective on mammalian upstream open reading frame function. *Int J Biochem Cell Biol,* 45**,** 1690-700.

SONENBERG, N. & HINNEBUSCH, A. G. 2009. Regulation of translation initiation in eukaryotes: mechanisms and biological targets. *Cell,* 136**,** 731-45.

SONG, H., MUGNIER, P., DAS, A. K., WEBB, H. M., EVANS, D. R., TUITE, M. F., HEMMINGS, B. A. & BARFORD, D. 2000. The crystal structure of human eukaryotic release factor eRF1--mechanism of stop codon recognition and peptidyl-tRNA hydrolysis. *Cell,* 100**,** 311-21.

SORRELLS, D. L., JR., GHALI, G. E., DE BENEDETTI, A., NATHAN, C. O. & LI, B. D. 1999. Progressive amplification and overexpression of the eukaryotic initiation factor 4E gene in different zones of head and neck cancers. *J Oral Maxillofac Surg,* 57**,** 294-9.

SPILKA, R., ERNST, C., MEHTA, A. K. & HAYBAECK, J. 2013. Eukaryotic translation initiation factors in cancer development and progression. *Cancer Lett,* 340**,** 9-21.

STANSFIELD, I., JONES, K. M., KUSHNIROV, V. V., DAGKESAMANSKAYA, A. R., POZNYAKOVSKI, A. I., PAUSHKIN, S. V., NIERRAS, C. R., COX, B. S., TER-AVANESYAN, M. D. & TUITE, M. F. 1995. The products of the SUP45 (eRF1) and SUP35 genes interact to mediate translation termination in Saccharomyces cerevisiae. *EMBO J,* 14**,** 4365-73.

SU, N. & KILBERG, M. S. 2008. C/EBP homology protein (CHOP) interacts with activating transcription factor 4 (ATF4) and negatively regulates the stress-dependent induction of the asparagine synthetase gene. *J Biol Chem,* 283**,** 35106-17.

SUNG, M. K., REITSMA, J. M., SWEREDOSKI, M. J., HESS, S. & DESHAIES, R. J. 2016. Ribosomal proteins produced in excess are degraded by the ubiquitin-proteasome system. *Mol Biol Cell,* 27**,** 2642-52.

SUZUKI, C., TAKAHASHI, K., HAYAMA, S., ISHIKAWA, N., KATO, T., ITO, T., TSUCHIYA, E., NAKAMURA, Y. & DAIGO, Y. 2007a. Identification of Myc-associated protein with JmjC domain as a novel therapeutic target oncogene for lung cancer. *Molecular cancer therapeutics,* 6**,** 542-551.

SUZUKI, C., TAKAHASHI, K., HAYAMA, S., ISHIKAWA, N., KATO, T., ITO, T., TSUCHIYA, E., NAKAMURA, Y. & DAIGO, Y. 2007b. Identification of Myc-associated protein with JmjC domain as a novel therapeutic target oncogene for lung cancer. *Mol Cancer Ther,* 6**,** 542-51.

SWART, E. C., SERRA, V., PETRONI, G. & NOWACKI, M. 2016. Genetic Codes with No Dedicated Stop Codon: Context-Dependent Translation Termination. *Cell,* 166**,** 691-702.

SZASZ, A. M., LANCZKY, A., NAGY, A., FORSTER, S., HARK, K., GREEN, J. E., BOUSSIOUTAS, A., BUSUTTIL, R., SZABO, A. & GYORFFY, B. 2016. Cross-validation of survival associated biomarkers in gastric cancer using transcriptomic data of 1,065 patients. *Oncotarget,* 7**,** 49322-49333.

TAHILIANI, M., KOH, K. P., SHEN, Y., PASTOR, W. A., BANDUKWALA, H., BRUDNO, Y., AGARWAL, S., IYER, L. M., LIU, D. R., ARAVIND, L. & RAO, A. 2009a. Conversion of 5-methylcytosine to 5-hydroxymethylcytosine in mammalian DNA by MLL partner TET1. *Science,* 324**,** 930-5.

TAHILIANI, M., KOH, K. P., SHEN, Y., PASTOR, W. A., BANDUKWALA, H., BRUDNO, Y., AGARWAL, S., IYER, L. M., LIU, D. R., ARAVIND, L. & RAO, A. 2009b. Conversion of 5-methylcytosine to 5-hydroxymethylcytosine in mammalian DNA by MLL partner TET1. *Science (New York, N.Y.),* 324**,** 930-935.

TANIKAWA, M., WADA-HIRAIKE, O., NAKAGAWA, S., SHIRANE, A., HIRAIKE, H., KOYAMA, S., MIYAMOTO, Y., SONE, K., TSURUGA, T., NAGASAKA, K., MATSUMOTO, Y., IKEDA, Y., SHOJI, K., ODA, K., FUKUHARA, H., NAKAGAWA, K., KATO, S., YANO, T. & TAKETANI, Y. 2011. Multifunctional transcription factor TFII-I is an activator of BRCA1 function. *Br J Cancer,* 104**,** 1349-55.

TAO, Y., WU, M., ZHOU, X., YIN, W., HU, B., DE CROMBRUGGHE, B., SINHA, K. M. & ZANG, J. 2013. Structural insights into histone demethylase NO66 in interaction with osteoblast-specific transcription factor osterix and gene repression. *J Biol Chem,* 288**,** 16430-7.

TARHONSKAYA, H., SZÖLLÖSSI, A., LEUNG, I. K. H., BUSH, J. T., HENRY, L., CHOWDHURY, R., IQBAL, A., CLARIDGE, T. D. W., SCHOFIELD, C. J. & FLASHMAN, E. 2014. Studies on Deacetoxycephalosporin C Synthase Support a Consensus Mechanism for 2-Oxoglutarate Dependent Oxygenases. *Biochemistry,* 53**,** 2483-2493.

TATE, W. P., POOLE, E. S., HORSFIELD, J. A., MANNERING, S. A., BROWN, C. M., MOFFAT, J. G., DALPHIN, M. E., MCCAUGHAN, K. K., MAJOR, L. L. & WILSON, D. N. 1995. Translational termination efficiency in both bacteria and mammals is regulated by the base following the stop codon. *Biochem Cell Biol,* 73**,** 1095-103.

TENG, T., MERCER, C. A., HEXLEY, P., THOMAS, G. & FUMAGALLI, S. 2013. Loss of tumor suppressor RPL5/RPL11 does not induce cell cycle arrest but impedes proliferation due to reduced ribosome content and translation capacity. *Mol Cell Biol,* 33**,** 4660-71.

TENG, Y., GAO, M., WANG, J., KONG, Q., HUA, H., LUO, T. & JIANG, Y. 2014. Inhibition of eIF2alpha dephosphorylation enhances TRAIL-induced apoptosis in hepatoma cells. *Cell Death Dis,* 5**,** e1060.

THAKUR, C., LU, Y., SUN, J., YU, M., CHEN, B. & CHEN, F. 2014. Increased expression of mdig predicts poorer survival of the breast cancer patients. *Gene,* 535**,** 218-24.

THALHAMMER, A., BENCOKOVA, Z., POOLE, R., LOENARZ, C., ADAM, J., O'FLAHERTY, L., SCHODEL, J., MOLE, D., GIASLAKIOTIS, K., SCHOFIELD, C. J., HAMMOND, E. M., RATCLIFFE, P. J. & POLLARD, P. J. 2011. Human AlkB homologue 5 is a nuclear 2-oxoglutarate dependent oxygenase and a direct target of hypoxia-inducible factor 1alpha (HIF-1alpha). *PLoS One,* 6**,** e16210.

THIENPONT, B., STEINBACHER, J., ZHAO, H., D'ANNA, F., KUCHNIO, A., PLOUMAKIS, A., GHESQUIÈRE, B., VAN DYCK, L., BOECKX, B., SCHOONJANS, L., HERMANS, E., AMANT, F., KRISTENSEN, V. N., PENG KOH, K., MAZZONE, M., COLEMAN, M., CARELL, T., CARMELIET, P. & LAMBRECHTS, D. 2016. Tumor hypoxia causes DNA hypermethylation by reducing TET activity. *Nature,* 537**,** 63-68.

TKACZYK, C., HOREJSI, V., IWAKI, S., DRABER, P., SAMELSON, L. E., SATTERTHWAITE, A. B., NAHM, D. H., METCALFE, D. D. & GILFILLAN, A. M. 2004. NTAL phosphorylation is a pivotal link between the signaling cascades leading to human mast cell degranulation following Kit activation and Fc epsilon RI aggregation. *Blood,* 104**,** 207-14.

TRUITT, M. L. & RUGGERO, D. 2017. New frontiers in translational control of the cancer genome. *Nat Rev Cancer,* 17**,** 332.

TSAFRIR, D., BACOLOD, M., SELVANAYAGAM, Z., TSAFRIR, I., SHIA, J., ZENG, Z., LIU, H., KRIER, C., STENGEL, R. F., BARANY, F., GERALD, W. L., PATY, P. B., DOMANY, E. & NOTTERMAN, D. A. 2006. Relationship of gene expression and chromosomal abnormalities in colorectal cancer. *Cancer Res,* 66**,** 2129-37.

TSAI, Y. P., CHEN, H. F., CHEN, S. Y., CHENG, W. C., WANG, H. W., SHEN, Z. J., SONG, C., TENG, S. C., HE, C. & WU, K. J. 2014. TET1 regulates hypoxia-induced epithelial-mesenchymal transition by acting as a co-activator. *Genome biology,* 15**,** 513.

TSANG, K. Y., CHAN, D., BATEMAN, J. F. & CHEAH, K. S. 2010. In vivo cellular adaptation to ER stress: survival strategies with double-edged consequences. *J Cell Sci,* 123**,** 2145-54.

TU, L., LIU, Z., HE, X., HE, Y., YANG, H., JIANG, Q., XIE, S., XIAO, G., LI, X., YAO, K. & FANG, W. 2010. Over-expression of eukaryotic translation initiation factor 4 gamma 1 correlates with tumor progression and poor prognosis in nasopharyngeal carcinoma. *Mol Cancer,* 9**,** 78.

TURNIDGE, J. 2003. *Pharmacodynamic and dosing of aminoglycosides*.

VAKOC, C. R., MANDAT, S. A., OLENCHOCK, B. A. & BLOBEL, G. A. 2005. Histone H3 lysine 9 methylation and HP1gamma are associated with transcription elongation through mammalian chromatin. *Molecular cell,* 19**,** 381-91.

VAN DER MEULEN, J., SPELEMAN, F. & VAN VLIERBERGHE, P. 2014. The H3K27me3 demethylase UTX in normal development and disease. *Epigenetics,* 9**,** 658-68.

VATTEM, K. M. & WEK, R. C. 2004. Reinitiation involving upstream ORFs regulates ATF4 mRNA translation in mammalian cells. *Proc Natl Acad Sci U S A,* 101**,** 11269-74.

VESTERGAARD, B., VAN, L. B., ANDERSEN, G. R., NYBORG, J., BUCKINGHAM, R. H. & KJELDGAARD, M. 2001. Bacterial polypeptide release factor RF2 is structurally distinct from eukaryotic eRF1. *Mol Cell,* 8**,** 1375-82.

VINCENT, C., TARBOURIECH, N. & HARTLEIN, M. 1997. Genomic organization, cDNA sequence, bacterial expression, and purification of human seryl-tRNA synthase. *Eur J Biochem,* 250**,** 77-84.

WALDO, G. S., STANDISH, B. M., BERENDZEN, J. & TERWILLIGER, T. C. 1999. Rapid protein-folding assay using green fluorescent protein. *Nat Biotechnol,* 17**,** 691-5.

WANG, C., ZHANG, Q., HANG, T., TAO, Y., MA, X., WU, M., ZHANG, X. & ZANG, J. 2015. Structure of the JmjC domain-containing protein NO66 complexed with ribosomal protein Rpl8. *Acta Crystallographica Section D: Biological Crystallography,* 71**,** 1955-1964.

WANG, F. W., CAI, M. Y., MAI, S. J., CHEN, J. W., BAI, H. Y., LI, Y., LIAO, Y. J., LI, C. P., TIAN, X. P., KUNG, H. F., GUAN, X. Y. & XIE, D. 2014. Ablation of EIF5A2 induces tumor vasculature remodeling and improves tumor response to chemotherapy via regulation of matrix metalloproteinase 2 expression. *Oncotarget,* 5**,** 6716-33.

WANG, H., ZHOU, X., WU, M., WANG, C., ZHANG, X., TAO, Y., CHEN, N. & ZANG, J. 2013. Structure of the JmjC-domain-containing protein JMJD5. *Acta crystallographica. Section D, Biological crystallography,* 69**,** 1911-20.

WANG SS, GU YF, WOLFF N, STEFANIUS K, CHRISTIE A, DEY A , ET AL. 2014. Bap1 is essential for kidney function and cooperates with Vhl in renal tumorigenesis. Proc Natl Acad Sci U S A ;111:16538-43

WANG, M. & KAUFMAN, R. J. 2014. The impact of the endoplasmic reticulum protein-folding environment on cancer development. *Nat Rev Cancer,* 14**,** 581-97.

WANG, X. Z., LAWSON, B., BREWER, J. W., ZINSZNER, H., SANJAY, A., MI, L. J., BOORSTEIN, R., KREIBICH, G., HENDERSHOT, L. M. & RON, D. 1996. Signals from the stressed endoplasmic reticulum induce C/EBP-homologous protein (CHOP/GADD153). *Mol Cell Biol,* 16**,** 4273-80.

WEBBY, C. J., WOLF, A., GROMAK, N., DREGER, M., KRAMER, H., KESSLER, B., NIELSEN, M. L., SCHMITZ, C., BUTLER, D. S., YATES, J. R., 3RD, DELAHUNTY, C. M., HAHN, P., LENGELING, A., MANN, M., PROUDFOOT, N. J., SCHOFIELD, C. J. & BOTTGER, A. 2009. Jmjd6 catalyses lysyl-hydroxylation of U2AF65, a protein associated with RNA splicing. *Science (New York, N.Y.),* 325**,** 90-3.

WEI, C. M. & MOSS, B. 1977. Nucleotide sequences at the N6-methyladenosine sites of HeLa cell messenger ribonucleic acid. *Biochemistry,* 16**,** 1672-6.

WESTBYE, M. P., FEYZI, E., AAS, P. A., VAGBO, C. B., TALSTAD, V. A., KAVLI, B., HAGEN, L., SUNDHEIM, O., AKBARI, M., LIABAKK, N. B., SLUPPHAUG, G., OTTERLEI, M. & KROKAN, H. E. 2008. Human AlkB homolog 1 is a mitochondrial protein that demethylates 3-methylcytosine in DNA and RNA. *J Biol Chem,* 283**,** 25046-56.

WONG, L. E., LI, Y., PILLAY, S., FROLOVA, L. & PERVUSHIN, K. 2012. Selectivity of stop codon recognition in translation termination is modulated by multiple conformations of GTS loop in eRF1. *Nucleic Acids Res,* 40**,** 5751-65.

WU, B. K. & BRENNER, C. 2014. Suppression of TET1-Dependent DNA Demethylation Is Essential for KRAS-Mediated Transformation. *Cell Rep,* 9**,** 1827-40.

XU, X. M., CARLSON, B. A., MIX, H., ZHANG, Y., SAIRA, K., GLASS, R. S., BERRY, M. J., GLADYSHEV, V. N. & HATFIELD, D. L. 2007. Biosynthesis of selenocysteine on its tRNA in eukaryotes. *PLoS Biol,* 5**,** e4.

YAMAGUCHI, H. & WANG, H. G. 2004. CHOP is involved in endoplasmic reticulum stress-induced apoptosis by enhancing DR5 expression in human carcinoma cells. *J Biol Chem,* 279**,** 45495-502.

YAN, L., COLANDREA, V. J. & HALE, J. J. 2010. Prolyl hydroxylase domain-containing protein inhibitors as stabilizers of hypoxia-inducible factor: small molecule-based therapeutics for anemia. *Expert Opin Ther Pat,* 20**,** 1219-45.

YAN, W., FRANK, C. L., KORTH, M. J., SOPHER, B. L., NOVOA, I., RON, D. & KATZE, M. G. 2002. Control of PERK eIF2α kinase activity by the endoplasmic reticulum stress-induced molecular chaperone P58(IPK). *Proceedings of the National Academy of Sciences of the United States of America,* 99**,** 15920-15925.

YANG, H., HE, X., ZHENG, Y., FENG, W., XIA, X., YU, X. & LIN, Z. 2014. Down-regulation of asparagine synthetase induces cell cycle arrest and inhibits cell proliferation of breast cancer. *Chem Biol Drug Des,* 84**,** 578-84.

YANG, X., ONGUSAHA, P. P., MILES, P. D., HAVSTAD, J. C., ZHANG, F., SO, W. V., KUDLOW, J. E., MICHELL, R. H., OLEFSKY, J. M., FIELD, S. J. & EVANS, R. M. 2008a. Phosphoinositide signalling links O-GlcNAc transferase to insulin resistance. *Nature,* 451**,** 964-969.

YANG, X., ONGUSAHA, P. P., MILES, P. D., HAVSTAD, J. C., ZHANG, F., SO, W. V., KUDLOW, J. E., MICHELL, R. H., OLEFSKY, J. M., FIELD, S. J. & EVANS, R. M. 2008b. Phosphoinositide signalling links O-GlcNAc transferase to insulin resistance. *Nature,* 451**,** 964-9.

YE, J., KUMANOVA, M., HART, L. S., SLOANE, K., ZHANG, H., DE PANIS, D. N., BOBROVNIKOVA-MARJON, E., DIEHL, J. A., RON, D. & KOUMENIS, C. 2010. The GCN2-ATF4 pathway is critical for tumour cell survival and proliferation in response to nutrient deprivation. *EMBO J,* 29**,** 2082-96.

YE, Q. & WORMAN, H. J. 1996. Interaction between an integral protein of the nuclear envelope inner membrane and human chromodomain proteins homologous to Drosophila HP1. *J Biol Chem,* 271**,** 14653-6.

YI, J., SHEN, H. F., QIU, J. S., HUANG, M. F., ZHANG, W. J., DING, J. C., ZHU, X. Y., ZHOU, Y., FU, X. D. & LIU, W. 2017. JMJD6 and U2AF65 co-regulate alternative splicing in both JMJD6 enzymatic activity dependent and independent manner. *Nucleic Acids Res,* 45**,** 3503-3518.

YIN, Y., MORGUNOVA, E., JOLMA, A., KAASINEN, E., SAHU, B., KHUND-SAYEED, S., DAS, P. K., KIVIOJA, T., DAVE, K., ZHONG, F., NITTA, K. R., TAIPALE, M., POPOV, A., GINNO, P. A., DOMCKE, S., YAN, J., SCHUBELER, D., VINSON, C. & TAIPALE, J. 2017. Impact of cytosine methylation on DNA binding specificities of human transcription factors. *Science,* 356.

YOO, H., SON, D., LEE, Y. J. & HONG, K. 2016a. Mouse JMJD4 is dispensable for embryogenesis. *Mol Reprod Dev,* 83**,** 588-93.
YOO, H., SON, D., LEE, Y. J. & HONG, K. 2016b. Mouse JMJD4 is dispensable for embryogenesis. *Molecular Reproduction and Development,* 83**,** 588-593.
YOUN, M. Y., YOKOYAMA, A., FUJIYAMA-NAKAMURA, S., OHTAKE, F., MINEHATA, K., YASUDA, H., SUZUKI, T., KATO, S. & IMAI, Y. 2012. JMJD5, a Jumonji C (JmjC) domain-containing protein, negatively regulates osteoclastogenesis by facilitating NFATc1 protein degradation. *The Journal of biological chemistry,* 287**,** 12994-3004.
YUE, Y., LIU, J. & HE, C. 2015. RNA N6-methyladenosine methylation in post-transcriptional gene expression regulation. *Genes Dev,* 29**,** 1343-55.
YURCHENCO, P. D. & PATTON, B. L. 2009. Developmental and pathogenic mechanisms of basement membrane assembly. *Curr Pharm Des,* 15**,** 1277-94.
ZANETTI, M., RODVOLD, J. J. & MAHADEVAN, N. R. 2016. The evolving paradigm of cell-nonautonomous UPR-based regulation of immunity by cancer cells. *Oncogene,* 35**,** 269-78.
ZETTERBERG, A., LARSSON, O. & WIMAN, K. G. 1995. What is the restriction point? *Curr Opin Cell Biol,* 7**,** 835-42.
ZHAI, W. & COMAI, L. 2000. Repression of RNA polymerase I transcription by the tumor suppressor p53. *Mol Cell Biol,* 20**,** 5930-8.
ZHANG, L., PAN, X. & HERSHEY, J. W. 2007. Individual overexpression of five subunits of human translation initiation factor eIF3 promotes malignant transformation of immortal fibroblast cells. *J Biol Chem,* 282**,** 5790-800.
ZHANG, S., XIE, Y., CAO, H. & WANG, H. 2017. *Common microRNA–mRNA interactions exist among distinct porcine iPSC lines independent of their metastable pluripotent states*.
ZHANG, Y., WHITE WOLF, G., BHAT, K., JIN, A., ALLIO, T., BURKHART, W. A. & XIONG, Y. 2003. Ribosomal Protein L11 Negatively Regulates Oncoprotein MDM2 and Mediates a p53-Dependent Ribosomal-Stress Checkpoint Pathway. *Molecular and Cellular Biology,* 23**,** 8902-8912.
ZHAO, J., DU, F., SHEN, G., ZHENG, F. & XU, B. 2015. The role of hypoxia-inducible factor-2 in digestive system cancers. *Cell Death Dis,* 6**,** e1600.
ZHENG, G., DAHL, JOHN A., NIU, Y., FEDORCSAK, P., HUANG, C.-M., LI, CHARLES J., VÅGBØ, CATHRINE B., SHI, Y., WANG, W.-L., SONG, S.-H., LU, Z., BOSMANS, RALPH P. G., DAI, Q., HAO, Y.-J., YANG, X., ZHAO, W.-M., TONG, W.-M., WANG, X.-J., BOGDAN, F., FURU, K., FU, Y., JIA, G., ZHAO, X., LIU, J., KROKAN, HANS E., KLUNGLAND, A., YANG, Y.-G. & HE, C. ALKBH5 Is a Mammalian RNA Demethylase that Impacts RNA Metabolism and Mouse Fertility. *Molecular cell,* 49**,** 18-29.
ZHONG, S., LI, H., BODI, Z., BUTTON, J., VESPA, L., HERZOG, M. & FRAY, R. G. 2008. MTA Is an Arabidopsis Messenger RNA Adenosine Methylase and Interacts with a Homolog of a Sex-Specific Splicing Factor. *The Plant Cell,* 20**,** 1278-1288.
ZHOURAVLEVA, G., FROLOVA, L., LE GOFF, X., LE GUELLEC, R., INGE-VECHTOMOV, S., KISSELEV, L. & PHILIPPE, M. 1995. Termination of translation in eukaryotes is governed by two interacting polypeptide chain release factors, eRF1 and eRF3. *The EMBO Journal,* 14**,** 4065-4072.
ZHU, W., CAI, M.-Y., TONG, Z.-T., DONG, S.-S., MAI, S.-J., LIAO, Y.-J., BIAN, X.-W., LIN, M. C., KUNG, H.-F., ZENG, Y.-X., GUAN, X.-Y. & XIE, D. 2012. Overexpression of EIF5A2 promotes colorectal carcinoma cell aggressiveness by upregulating MTA1 through C-myc to induce epithelial–mesenchymaltransition. *Gut,* 61**,** 562-575.
ZHU, X. X., YAN, Y. W., AI, C. Z., JIANG, S., XU, S. S., NIU, M., WANG, X. Z., ZHONG, G. S., LU, X. F., XUE, Y., TIAN, S., LI, G., TANG, S. & JIANG, Y. Z. 2017. Jarid2 is essential for the maintenance of tumor initiating cells in bladder cancer. *Oncotarget,* 8**,** 24483-24490.

ZHUANG, Q., FENG, T. & COLEMAN, M. L. 2015. Modifying the maker: Oxygenases target ribosome biology. *Translation (Austin),* 3**,** e1009331.